University of Alberta
Department of Civil Engineering

Structural Engineering Report No. 81

Tests of Wall Segments From Reactor Containments Volume 1

by

S.H. Simmonds

S.H. Rizkalla

and

J.G. MacGregor

November, 1979

The University of Alberta

Department of Civil Engineering

TESTS OF WALL SEGMENTS FROM REACTOR CONTAINMENTS

by

S.H. Simmonds, S.H. Rizkalla,

and

J.G. MacGregor

A Technical Report to the
Atomic Energy Control Board
Nuclear Plant Licensing Directorate
P.O. Box 1046
Ottawa, Canada
K1P 5S9

November, 1979

DISCLAIMER

The interpretation of the technical data and any opinions or conclusions arising in this report are those of the authors only and do not necessarily reflect those of the cooperating agencies.

ABSTRACT

Twelve prestressed concrete wall segments simulating portions of the walls of secondary containment vessels were loaded by uniaxial or biaxial tensile loads to obtain load-deformation and cracking behavior. During the tests the loads, strains and crack widths, were measured. This report describes the test specimens, loading apparatus, test procedures and presents the reduced data and load-deformation response. The crack data is analyzed and discussed in another report.

Table of Contents

List of Tables

List of Figures

NOTATION AND TERMINOLOGY

E_c - modulus of elasticity of concrete

f'_c - compressive strength of 6 by 12 in. cylinder at time of test, psi

$\sqrt{f'_c}$ - a measure of the tensile strength of the concrete, psi

f_t - split cylinder tensile strength, psi

H - horizontal load in test

V - vertical load in test

ε - strain

ΔL - change in length

ν - Poisson's Ratio

σ - stress

Demec Readings - Strain measurements made with a mechanical strain gage having a gage length of 2 or 5 in.

Face A - Side of specimen which was on top during casting and on south side during testing.

Face B - Opposite side of specimen.

1. INTRODUCTION

1.1 Introduction

The nuclear reactors in Canadian nuclear power plants of the Gentilly-2 type are housed in circular prestressed concrete containment structures. Such a structure, shown schematically in Fig. 1.1 consists of a heavy concrete base, a cylindrical wall, a ring beam and a spherical dome. Each element contains a grid of conventional reinforcement and prestressing tendons.

In the event of a malfunction, pressurized gases or steam may be discharged. The function of the secondary containment vessel is to prevent such gases from escaping into the atmosphere. The containment is designed to have zero tensile stress under 1.15 times the design basis accident (DBA) pressure of 18.5 psi which is the maximum pressure attained if a secondary steam line ruptures and the water dousing system acts to condense the steam.

In the extremely unlikely event that a secondary steam line fails and the dousing system also fails to act, internal pressures may reach several times the DBA pressure. This would result in the walls and dome of the containment being stressed in biaxial tension. The response of the containment structure to this overpressure is the purpose of a comprehensive study undertaken at the University of Alberta and for which this report is a part.

In order to obtain data on the response of the structural components to biaxial tension a series of 14 wall segments representative of construction details in the containment were tested. The relationship between a typical segment and the containment is shown in

Fig. 1.1. Twelve of these wall segments were tested to obtain load-deflection and cracking behavior of the structure. This report describes the tests of these segments.

1.2 Objective of Wall Segment Tests

The wall segment tests have two main purposes: firstly, to investigate the load-deflection and cracking behavior of wall sections of the containment under large biaxial tension forces; and secondly, to provide data for use in calibrating and extending the scope of the inelastic analyses which form a part of the analytical phase of this research program. In particular, the formation and propagation of cracks in the concrete was noted carefully in order to develop techniques to predict the number and width of cracks in the containment structure with increasing internal pressure.

All wall segments in the test program are planar rather than curved since the results of planar segments are more readily interpreted and adequately represent the biaxial loading state of the wall segments to meet these objectives.

1.3 Scope of this Report

Several reports in the overall study are based on the experimental results from the wall segment tests. This report presents detailed information about the wall segment tests including test variables, specimen fabrication, material properties, testing procedures and instrumentation and the load-strain response for each segment. The

readings of load and strain recorded during testing are contained in Appendix A which is printed as Volume 2 of this report.

The data obtained from the tests reported herein has been used in the derivation of constitutive relationships for use in the analytical studies. This derivation of material properties and a comparison of the predicted response from the analysis to the observed test results is given in Reference (1). The interpretation of the crack data is given in Reference (2). The results of the two segments used to determine the rates of leakage of air through the wall segments at different stages of cracking is given in Reference (3).

A description of the wall segment specimens is given in Chapter 2. Chapter 3 contains a description of the material properties used in fabricating the specimens. The instrumentation and procedures used in data reduction are described in Chapter 4. The principal results of each of the segment tests are given in Chapter 5.

1.4 Acknowledgements

The research project "Study of Concrete Containment Structures under Overpressure Conditions" was sponsored at the University of Alberta by the Atomic Energy Control Board of Canada and was under the general supervision of Dr. W.D. Smythe and Dr. F. Campbell of AECB. Principal investigators at the University of Alberta, Department of Civil Engineering were Drs. J.G. MacGregor, D.W. Murray and S.H. Simmonds. Initially, Mr. Declan Whelan served as technical liaison between AECB and the project directors, however, since the summer of 1977, Dr. G.J.K. Asmis has served in this capacity.

The progress of the project has been reviewed from time to time by an Advisory Committee with representatives from the Atomic Energy Control Board, Atomic Energy of Canada Limited, Canatom Limited, Hydro Quebec and Ontario Hydro. The project directors wish to thank the members of this committee for the help and guidance received during this work.

Testing was carried out at the I.F. Morrison Structural Engineering Laboratory at the University of Alberta, Edmonton, Canada. Dr. S. Rizkalla was in charge of laboratory work and was assisted by Cheung Wong and Larp Chitnuyanondh.

2. DESCRIPTION OF SEGMENT SPECIMENS

2.1 Concept of Wall Segments

The purpose of the segment tests was to obtain data on load-deformation response and crack initiation and propagation that is representative of that which would occur in the walls of the prototype containment in the event that they were subject to an internal over-pressure. To achieve this goal it is essential that the properties of the materials used in the segments, the construction details, particularly in regard to reinforcement, prestress tendons, duct size and grouting techniques, and the restraint or boundary conditions of the segment under load resemble as closely as possible in behavior these items existing in the walls of the prototype. This establishes certain requirements for the segment scale and loading procedures.

Due to the axisymmetric nature of an internal pressure loading for a structure consisting of shells of revolution, the surfaces of the containment are required to resist primarily tensile membrane forces both along and across their meridians. Essentially there is no restraint to the corresponding deformations or significant bending moments except near the base and ring beam. For this reason and the magnitude of the radius of curvature it was felt that the objectives of the segment tests could be achieved using planar specimens rather than curved surfaces. This substitution greatly facilitates the fabrication, testing and interpretation of results.

To simulate the loading condition existing in a segment of containment wall it is necessary to be able to transmit large tensile

forces into the specimens while leaving the edges free to expand as cracks develop. Since a series of segments were to be tested, a simple mechanical connection between segment and loading frame was required. Load transfer to the segments was accomplished by pulling on the reinforcing bars and prestress tendons which were extended beyond the edges of the segment. Details of the loading apparatus are given in Chapter 4. Thus each segment specimen may be considered as a portion of the containment wall isolated from the remainder of the wall by four pre-existing cracks.

A total of fourteen reinforced and prestressed segments measuring 31.5 inches square and, with one exception, 10.5 inches thick were tested. Twelve of these segments (Segments 1 to 9 and 11 to 13) were used to determine load-deformation and cracking behavior and are fully described in this report. Two additional specimens, Segments 10 and 14, were identical in fabriaction details to Segments 1 and 5, respectively, but in addition to the tensile loading a differential air pressure was applied to one face of the segment and the rate of leakage through the segment at different crack levels was measured. The results of these leakage tests are given in a companion report (3).

2.2 Selection of Specimen Scale

A minimum specimen size is dictated by the need to reproduce deformations and cracking that are representative of the large concrete surfaces in the prototype structure. On the other hand a maximum size is dictated by the magnitude of the largest tensile forces that can be applied to the speicmen in the laboratory.

The segment thickness must be sufficient to accommodate prestressing strand enclosed in ducts that will permit prestressing in two perpendicular directions and two layers of standard reinforcement in each face. To achieve prestressing in two directions without introducing bending moments into the segment requires a minimum of three layers of strand.

The prototype containment was built using the Canadian BBR prestressing system and the same system was adopted for the segments. The smallest size of tendon duct manufactured by Canadian BBR is almost exactly one-fourth the size of the similar ducts used in the prototype containment. While most of the segments used #3 (3/8 inch diam.) reinforcement some segments used #4 (1/2 inch diam.) reinforcement with 0.5 inch clear cover on the faces. To accommodate the tendon ducts and fittings and reinforcement with spacings through the wall comparable to those in the prototype, a wall thickness of 10.5 inches was chosen. This corresponds to quarter scale for the prototype.

The lateral dimensions of the segments were restricted by the total lateral force that could be applied in the laboratory. It was expected that through the wall cracks would occur with a spacing approximately equal to the thickness. In addition, it was assumed that a region of approximately half of the thickness at each edge of the segment would serve as a load introduction zone. To allow for this zone and the formation of more than one through the wall crack, a lateral dimension of three times the wall thickness or 31.5 inches was chosen, a dimension just within the capacity of the horizontal jacks.

2.3 Selection of Segment Variables

The main parameters varied were the ratio of prestressing in two directions, the ratio of applied tensile forces, amount of concrete cover and bar spacing for non-prestressed and prestressed segments, use of bar splices and combined applied axial force and bending moment. The values of these parameters for each segment are given in Table 2.1. This section contains a discussion of the factors which led to the selection of the variables considered. Detailed variables for each specimen are given in Section 2.4.

(a) Ratio of Prestressing and Loading

With internal pressure loading the membrane stresses in the cylindrical portion of the containment in the hoop or circumferential direction (σ_1 in Fig. 1.1(a)) are twice the stresses in the longitudinal or meridian direction (σ_2 in Fig. 1.1(a)). In the dome portion, however, these stresses are equal in magnitude. In the prototype containment the prestress forces essentially correspond to these stresses although some differences occur in the dome near the edge beam due to the geometry of the net of prestressing tendons.

For the segments prestressed in two directions the prestress corresponding to the σ_2 or meridian direction was obtained using 3 six wire tendons placed at mid-thickness of the segment. To obtain the greater prestress required in the perpendicular direction without introducing bending moments into the segment, 4 seven wire strands were used, two on either side of the 3 six wire strands. The location of the prestressing strands are shown in Fig. 2.1 and 2.2.

The four tendon direction represents the circumferential direction in the prototype. In the prototype these tendons are located near the outer quarter point of the wall thickness and, due to the curvature of the wall, produce a uniform compressive hoop stress through the wall. In the wall segments the centre two of these tendons are placed adjacent to one face to simulate actual cover and spacing of these tendons in the protytype containment while the remaining two are placed near the opposite face to obtain a uniform state of prestress through the segment thickness.

To obtain corresponding ratios of prestress as exist in the prototype cylindrical wall sections the tendons in the three tendon directions were stressed to approximately 48 kips per tendon and in the four tendon direction to 64 kips per tendon. All segments prestressed in two directions had identical tendon layouts and initial prestress forces regardless of the applied load ratios.

The ratio of load applied to each segment in the two directions is also given in Table 2.1. The ratio H/V given in this table refers to the ratio horizontal to vertical loads as applied during the test which is a rotation of 90° from that existing in the prototype (see Fig. 1.1(b)). The reason for this rotation of orientation for testing is that greater forces could be applied in the vertical direction with the testing apparatus available as explained in detail in Chapter 4.

(b) Variations in Cover and Bar Spacing

In any existing theory for predicting the crack width and crack spacing in reinforced concrete, the major parameters are the concrete cover over the reinforcing bars and the bar spacing. To

ascertain the effects of these quantities when combined with prestressing, the bar size and spacing as well as the concrete cover were varied.

The percentage of reinforcement used in the segments was chosen so that cracking in the concrete would occur before the reinforcement transmitting the load into the concrete would yield. This resulted in a percentage of reinforcement representative of segments taken from near the top of the wall of the prototype structure since sections at mid-height were more lightly reinforced. To approximate bar spacing to thickness ratios in the prototype the standard reinforcement in each direction in each face was No. 3 (3/8 in. diam.) reinforcement at 3 in. spacing. When larger bars were substituted the ratio of bar spacing to bar diameter of 8 was maintained which resulted in larger percentages of reinforcement with the larger bars.

(c) Lapped Splices

In the prototype structure the non-prestressed reinforcement is spliced by lapping. To study the effects of the splice on the cracking and deformation characteristics, two segments were tested which contained lapped splices.

(d) Combined Axial Tension and Bending Moment

Near the base and ring beam the surfaces of the prototype structure are loaded by both axial tensile forces and bending moments. This causes a non-uniform stress distribution across the thickness. To examine the effects of this distribution on the formation and propagation of the cracks, two segments were loaded to simulate combined axial load and bending by applying eccentric tension forces to the protruding reinforcement.

2.4 Details of Individual Segment Specimens

One of the purposes of the study was to develop analytical techniques which would permit the prediction of the load-deformation and cracking response of any concrete containment structure loaded with high internal pressure. When selecting the detailed variables for each segment it was decided that a variety of parameters that would permit evaluating the analytical techniques was more important than attempting to model specific portions of the prototype structure. One result of this decision is the use of several segments which have either no prestressing or were loaded with axial force in one direction only, conditions that do not exist in a containment structure but do allow evaluation of the range of applicability of the predictive procedures. Another result is that the number of segments tested was kept to a minimum.

A summary of the major variables and loading for each segment is given in Table 2.1. Fig. 2.1 and 2.2 indicate the positions of prestress tendons and reinforcement for all segments except Segments 4 to 7 inclusive, hence, these are considered the standard details from which variations in reinforcement are referred. The concrete cover for all typically reinforced segments is 0.5 in. except for Segment 8 which has a concrete cover of 1.25 in.

In describing the segments in this report the word "face" refers to the 31.5 inch square surfaces. "Face A" is the surface that was on top during casting of the concrete and is the south face during testing. "Face B" is the other side. In all cases the two center

tendons in the four tendon direction (Section AA, Fig. 2.2) were adjacent to Face A. The word "edge" refers to the four 31.5 x 10.5 inch surfaces through which the reinforcement extends. During testing these edges are conveniently designated as top and bottom.

Segments 1 and 2 are identical and represent the only replication of segments in the test program. These segments represent the prestressing conditions and loading that would be anticipated in the cylindrical wall portion of the prototype structure. The reinforcement size and spacing is also representiatve of segments near the upper portion of the wall. Hence the load-deformation and cracking characteristics of these segments should best represent the behavior of the prototype structure.

Segment 3 is identical in construction to Segments 1 and 2 but the ratio of loading in the two directions was made equal, representative of the loading, conditions in the dome portion. It should be recalled that the degree of prestressing in all segments prestressed in two directions is the same regardless of the ratio of applied loads.

To obtain the effects of prestressing in only one direction Segment 5 is identical in construction to Segment 1 except that prestressing tendons were placed in the three tendon direction only. Segment 6 is identical to Segment 5 except that the non-prestressed reinforcement was changed from ten #3 @ 3 in. to eight #4 @ 4 in. Both Segments 5 and 6 were loaded only in the three tendon direction.

To further determine the effects of prestressing on crack formation and to evaluate crack prediction capabilities, two segments, Segments 4 and 7 were fabricated with no prestressing tendons. The reinforcement for Segment 4 corresponded to that in Segment 6, however, Segment 4 was loaded equally in two directions.

Segment 7 permits the evaluation of scale effects. Similar to Segment 4, the overall thickness was increased 1.5 times to 15.75 in. (1/3 scale) and the reinforcement size, spacing and cover increased proportionally. Segment 7 was also loaded equally in two directions to facilitate comparison with Segment 4.

Segment 8 is identical to Segment 1 except that the concrete cover was increased to 1.25 inches compared to 0.5 in., which permits a direct evaluation of the effects of concrete cover on cracking.

Segments 9 and 11, which were used to evaluate effects of lapped splices, are identical in construction and loading to Segment 1 except for the lapped splices. In Segment 9 all of the reinforcing bars in the three tendon direction, that is the inside layer of bars, were lapped spliced for a length of 15 in. (40 bar diameters) centred in the segment. This length corresponds to a Class C splice for a Grade 60 bars in accordance with the ACI code (4). Segment 11 was similar except that only alternate bars in the three tendon direction were spliced.

Segments 12 and 13 were identical in fabrication details to Segment 1. Segment 12 was loaded with eccentric tensile forces in the three-tendon direction only so as to create a stress distribution through the wall corresponding to combined axial force and bending. Segment 13 was loaded eccentrically in both directions.

2.5 Construction of Segment Specimens

The prestressing wires used to post-tension the segments were supplied by the manufacturer in a preassembled unit complete with all fittings and ducts. A complete unit is shown in Fig. 2.3. Depending, on the direction in which the tendon was to be used, each unit consisted of 6 or 7 wires cut to the same length and held in a symmetrical pattern by being passed through threaded end fittings. The ends of all wires were buttoned to provide end anchorage. The unit also consisted of two 5 1/2 in. square plates which were embedded in the concrete and had welded to the inner faces a 1 1/2 in. OD tube to which the grout nipples were welded. These plates provided a bearing transfer of the prestressing force to the concrete surface. A third plate of identical size was located outside the "fixed end" (see Fig. 2.3) and together with one of the embedded plates acted as a bearing plate for the split ring load cell. Two lengths of telescoping ducts were also included in the unit so as to provide a complete sheath prior to placing concrete.

Fabrication of the segments began by placing the electric resistance strain gages and targets for the mechanical strain gages on the steel reinforcement. A plywood form was constructed to fit around the segment edges. This form had slots around both faces of appropriate depth to hold the reinforcement in position as shown in Fig. 2.4. The stressing end of the prestressing tendons were inserted in holes drilled in the form to accommodate the size of the threaded end fitting. At the fixed end the form must fit between two bearing plates. This was accomplished by splitting the forms longitudinally. After all steel had been

placed, as shown in Fig. 2.4, a plywood sheet was placed to form the bottom face and thin sheet metal strips of appropriate width were placed along the edges adjacent to the segment faces to plug the slots holding the reinforcing bars.

Prior to concreting, all joints in the tendon sheaths were sealed with silicone rubber calking compound to prevent concrete from leaking into the sheaths and the plastic grouting tubes attached.

The concrete for a specimen was obtained from a single 9 cu. ft. mix. Approximately 6 cu. ft. of this mix was used for the segment and the balance used in casting test cylinders for use in tension and compression tests on the concrete. Internal vibrators were used to consolidate the concrete with care being taken to avoid overvibration and bleeding of the concrete.

The segment and cylinders were allowed to set and then were covered with wet burlap from 24 to 48 hours, after which time the forms were removed. The segment and cylinders were again covered with wet burlap and allowed to moist cure for one week. Curing in air was continued for approximately another three to six weeks at which time the segments were prestressed.

2.6 Prestressing Concrete Segments

After the curing period the split ring aluminum load cell and sufficient split ring shims were inserted at the fixed end of the tendon assembly as indicated in Fig. 2.3 to make the threaded end fittings of the tendon assembly unit snug against the bearing plates cast in the specimen.

The prestressing force was applied using a centre hole hydraulic ram acting on a rod to which was attached a threaded coupler that fitted onto the threaded end fitting at the stressing end of the tendon assembly. Final force transfer was obtained by adjusting the lock nuts. The stressing sequence was staged to minimize anchorage losses and in the four tendon direction in sufficient steps to avoid cracking of the concrete due to eccentric prestress.

During pulling of the tendons the force was measured using the split ring load cells. These were made from hollow aluminum cylinders, split into two halves so as to be fitted around the tendon. Strains measured using two electric resistance strain gages mounted on each half of the cell were read as a 4-arm bridge and compared to calibration made earlier. The load cell readings were reproduceable to the nearest 0.1 kip. The total force applied to each tendon was 48 kips in the three tendon direction and 64 kips in the four tendon direction.

The loads measured by these load cells were monitored until grouting occurred in an effort to determine prestress losses. Approximately two days after prestressing the end fittings were sealed with epoxy resin and grout was injected through a grout tube at one end of the tendon until pure grout flowed out the tube at the other end. This latter tube was then sealed and the grouting pressure increased to between 30 and 40 psi to ensure complete grouting of the voids inside the tendon sheath. During this operation the load cells became filled with grout and with the tendons bonded to the concrete further readings from the load cells were meaningless.

Various schemes such as gages on the reinforcement and mechanical strain gages on the concrete were used in an attempt to measure prestress losses. However, none of these procedures proved reliable since the strains measured were in the order of 0.00002 in./in. or roughly the accuracy of the measuring devices used.

To obtain some estimate of the likely prestress losses prior to testing the theory proposed by Libby (5) was used. This procedure separates the various strains caused by shrinkage, creep and relaxation for different time intervals between jacking and testing. A computer code was written to facilitate performing the calculations for different segments, and the results of these calculations indicated losses between 10 and 12 percent in the four (7 wire) tendons and between 4 and 6 percent in the three (6 wire) tendons. Due to the very short length of the tendons, however, losses due to creep under end anchorages, which are normally neglected, were of the same magnitude as those due to creep along the length of the member. In addition a short period of expansion (or less rapid shortening) was noted as the expanding grout was curing.

Based on the results of the computations and the measurements made, losses of 12 percent in the four tendon direction and 8 percent in the three tendon direction were assumed for all segments. The prestress in the tendons is listed in Table 2.2.

The effective prestress in the concrete at the time of test was obtained assuming the effective force after losses acted on a transformed cross-section with holes representing the tendon ducts. Although the centroid of the prestressing forces had a slight eccentricity (0.01

to 0.04 in.) relative to the centroid of the concrete, these were neglected in the calculations.

A typical wall segment specimen, in this case Segment 2, completely fabricated and ready for testing is shown in Fig. 2.5.

3. MATERIAL PROPERTIES

3.1 Concrete

3.1.1. Concrete Mix Design

All concrete used in the wall segment tests had a nominal design strength of 4500 psi and was mixed in the laboratory. Normal density aggregates were used with the coarse aggregate obtained from glacial outwash deposits containing quartzite, granite and other silicates. The volume of each batch was 9 cu. ft., the capacity of the mixer, and contained the following quantities:

Water	113 lbs.
Cement (type 1 Portland Cement)	208
Sand	423
3/8 in. gravel	560
Water/cement ratio by weight	0.54

Only one bach was required to cast a wall segment and the accompanying test cylinders except for Segment 7 which required two batches.

3.1.2. Concrete Compressive and Tensile Strengths

With each segment either five or six standard 6 x 12 in. cylinders were cast to determine concrete strengths. These cylinders were cured in the laboratory in the same manner as the segments and were loaded at the same time as the corresponding segment was tested. In general three of these cylinders were tested in compression and the remaining two of three used in split cylinder tensile tests. The results of these tests are summarized in Table 3.1.

Since the compressive cylinder tests were performed at the time of the segment test and were cured with the segment, the values of compressive strength, f'_c, are not so much a measure of the potential of the concrete mix but rather of the compressive strength of the concrete in the segment at the time of testing.

The tensile strengths were obtained using the "Method of Test for Splitting Tensile Strength of Molded Concrete Cylinders", ASTM Specification C496-71. Expressed as functions of the compressive strength the tensile strengths ranged from $4.82\sqrt{f'_c}$ to $7.23\sqrt{f'_c}$ with a mean value of $6.21\sqrt{f'_c}$ and a coefficient of variation of 11 percent. Thus the reliability of the tensile tests are well within the range expected for such tests when compared with published data (6).

3.1.3 Modulus of Elasticity and Poisson's Ratio

Initially it was planned to obtain values of both Poisson's ratio and modulus of elasticity of the concrete directly from measured values on the segments themselves and the generalized Hooke's Law equations. For each load increment the stresses in both directions would be computed by dividing the applied load by the cross-sectional area transformed to all concrete. The corresponding strains would be obtained using 4 inch long SR-4 electric resistance strain gages mounted perpendicularly at the mid-height of the segments. That portion of the loading corresponding with the unloading of the precompression stresses and extending into the tensile region prior to first cracking would be used.

For the two segments tested in uniaxial tension, Segments 5 and 6, values of Poissons ratio could be obtained directly as a ratio of measured strains. For these two segments the value of Poisson's ratio obtained was 0.19.

For those segments tested in biaxial tension values of modulus of elasticity and Poisson's ratio were to be obtained from a solution of Hooke's Law as follows.

1. Assuming a value of Poisson's, ν, ratio equal to 0.2, plots of $(\sigma_V - \nu\sigma_H)$ vs ε_V and $(\sigma_H - \nu\sigma_V)$ vs ε_H were prepared. The slopes of the best fit lines as determined by regression analysis correspond to values of the modulus of elasticity, E_c, in the vertical and horizontal directions.

2. Using the average of these values of E_c, plots of $(\sigma_V - E_c\ \varepsilon_V)$ vs σ_H and $(\sigma_H - E_c\ \varepsilon_H)$ vs σ_V were prepared. The slopes of these plots represent values if ν in the two directions.

3. Using the average value of ν obtained in step 2, step 1 is repeated as is step 2 until convergence is achieved.

It was found after performing the above steps that convergence did not always occur and that the values of both E_c and ν in the two directions varied considerably before averaging. Some of the difficulty appeared to be in accurately measuring the strain in tension. If a micro-crack occurred in the region of either of the 4 inch strain gages the strain readings were effected. Values of Poisson's ratio were extremely sensitive to very small changes in strain. The procedure was repeated using the results of strains obtained over 15 in. from mechanical strain gages, however, the accuracy of these strains over the range before generalized cracking was not sufficient to obtain reliable results.

Although the above readings were taken for all subsequent segments, for later segments the value of the modulus of elasticity for the concrete was obtained from the compression tests on the concrete cylinders. Strains were measured using a mechanical extensometer having a 5 inch length. Values of E_c obtained in this way are given in Table 3.1.

It was observed that if the value for the modulus of elasticity as recommended in the ACI Code (4) (i.e. $E_c = 57000 \sqrt{f'_c}$) were used in the equations from Hooke's Law, the computed value of Poisson's ratio for all segments did not differ too widely from a value of 0.2. Since this value is also the value reported by Kupfer et al. (7), a value of Poisson's ratio equal to 0.2 is used in all analytical predictions.

Also tabulated in Table 3.1 are values of E_c obtained from the segment tests. These values were obtained using the assumed value of $\nu = 0.2$ and performing only the first step of the general solution of Hooke's Law described above.

For those segments in which the values of E_c were obtained from both procedures a comparison of the values using a t-test indicated no significant difference at the 5 percent level of significance between the values.

The mean value of E_c obtained from segment tests was 3.65×10^3 ksi with a coefficient of variation of 7.7 percent. Expressing E_c as a function of the compressive strength the mean value is $54200 \sqrt{f'_c}$ with a coefficient of variation 13.5 percent. Although there was some variation in compressive strength between segments the differences are not large and the correlation between compressive strength and modulus of elasticity was not marked over this range. For this reason a constant value of 3.65×10^3 ksi was used as representative of all segments.

3.2 Grout for Prestressing Tendons

The tendon ducts were grouted using Masterflow 814 Cable Grout. The standard mix consisted of 55 lbs. of grout material and 20 lbs. of water. This grout, manufactured by Master Builders Ltd., is specially made for grouting prestressing tendons and is slightly expansive.

A standard 6 x 12 in. cylinder was made by pouring grout into a standard mould. This cylinder had a 28 day compressive strength of 4320 psi. It is possible that the strength of the group injected into the tendon under a pressure of 30 to 40 psi may be greater than that of the test cylinder.

3.3 Reinforcing Steel

The reinforcement used in the segment tests consisted of hot rolled deformed bars conforming to CSA G30.12-72. No. 3, 4 and 6 bars were used, all bars of the same size coming from the same heat at time of rolling. Four specimens of each size were tested in tension in a 200,000 lb. Baldwin universal testing machine. Strains were obtained using a Baldwin 2 in. electric extensometer. The strain and load readings were plotted directly on an x - y plotter to just beyond the yield stress at which time the extensometer was removed. Values of the modulus of elasticity and yield strength were obtained from the plots.

All specimens showed the typical ductile behavior having a well defined yield point and cup-cone fracture.

The following results are the averages of the four tests:

Bar Size	#3	#4	#6
Yield Strength, ksi	58.2	54.5	52.9
Ultimate Tensile Strength, ksi	87.5	82.8	80.5
Modulus of Elasticity, 10^3 ksi	28.9	29.5	28.4

3.4 Prestressing Tendons

The prestressing tendons were specially manufactured in pre-assembled units for this project by Canadian BBR Limited. A complete tendon unit is shown in Figure 2.3.

The prestressing tendon consists of six or seven individual straight smooth wires. Each wire had a diameter of 0.276 inches. The stress-strain properties of the wire, based on mill test results provided by the wire manufacturer, Shinko Wire Company, Ltd., and one tension test of a tendon was proportional limit of 205 ksi, yield strength (stress at 1.0% strain) of 236 ksi, ultimate strength of 264 ksi and modulus of elasticity of 29,200 ksi. In all cases the elongations at failure exceeded 4 percent.

4. TESTING APPARATUS AND PROCEDURE

4.1 Loading Apparatus

During testing of the segments the vertical loads were applied using a larger capacity universal testing machine and the horizontal loads using a specially designed load frame equipped with hydraulic rams. In the prototype structure the large tensile stresses occur in the circumferential or horizontal direction. To permit use of the greater capacity of the testing machine to apply the larger forces the segment for testing was rotated 90° compared to the corresponding orientation in the prototype. This is clearly shown by comparing orientation in Fig. 1.1(b) with that in Fig. 1.1(a).

The universal testing machine was a free-standing 1,400,000 lb. capacity machine manufactured by MTS Systems. A servo-controlled hydraulic ram is mounted on the moveable hydraulic upper head. The lower head is fixed and consists of a 24 inch thick steel plate prestressed to a concrete box girder 42 feet long and 12 feet wide such that plate and girder act as a unit. The top of the lower head is flush with the laboratory floor.

Built around the MTS machine and independent of it was a lateral loading frame designed specifically for the segment tests. Essentially the loading frame consists of four columns, one in each corner, which support transverse beams to which the outer ends of the four hydraulic rams acting in tension are mounted, four wide flange sections which resist the reaction from the rams and diagonal bracing to

maintain alignment and resist possible racking of the frame. Sections taken through the loading frame between the columns are given in Fig. 4.1 and 4.2.

Load was transmitted between the rams and the specimen using clevises and "whiffletree" type fittings as shown in Fig. 4.1 and 4.2. A closeup view of the horizontal load wiffletree and attachment to the segment is given in Fig. 4.3. Load was transferred to the tendons by threaded couplers screwed onto the threaded end fittings of the tendon assembly and onto rods attached to the whiffletree. These rods were instrumented to measure load transmitted to each tendon so that uniform loading could be achieved as described in the next section. The reinforcing bars extending from each edge of the segment were welded to two angles which in turn were bolted to the whiffletree mechanism with nuts that could be adjusted to provide uniformity of force.

Provision was made so that the whiffletree could be shifted laterally by up to 2.75 inches relative to the specimen. This permitted the application of an eccentric load to Segments 12 and 13.

The method of applying eccentric load to Segment 13 is shown in Fig. 4.4. In the vertical direction load was applied to both layers of reinforcement but only to the tendons closest to Face B. In the horizontal direction load was applied to the tendons and only to the layer of reinforcement closest to Face B. Segment 12 was similar but eccentricity was applied in the horizontal direction only.

4.2 Testing Procedure

A typical test for one wall segment took approximately six days to set up in the loading apparatus, one day to perform actual test and one day to dismantle. Set up included aligning the segment in the loading frame, attaching instrumentation and connecting and adjusting tendons and reinforcing bars to loading devices.

Connecting the steel in the segment so as to achieve a uniform force in the tendons and in the reinforcement was a time consuming operation. Each tendon coupler rod was instrumented so that the load in each tendon could be measured. In addition the main pull road which connected the hydraulic ram connected to the whiffletree assembly was instrumented as a check on the sum of the individual reinforcing readings. In general this instrumentation consisted of two SR-4 strain gages mounted diametrically apart to average out any incidental moment. In addition a single strain gage was placed on three protruding reinforcing bars on each face of each edge to obtain some idea of the distribution of forces in the reinforcement.

The protruding ends of the reinforcement bars were welded to steel angles which later could be bolted to the loading assembly. The actual linkage of the segment to the loading devices began by threading the couplers to the horizontal tendons and adjusting the couplers until a small uniform load was obtained in each tendon. The steel angles welded to the horizontal reinforcement was then bolted to the whiffletree assembly with the nuts being placed to finger tightness. The segment was then loaded in the horizontal direction to roughly one-third

of the cracking load and the force in each bar and tendon observed. The specimen was then unloaded and adjustments made to the couplers or bolts as required and then reloaded. This process was repeated until a satisfactory degree of uniformity of force was achieved. The entire procedure was then repeated in the vertical direction.

A test began by obtaining initial readings of all load, strain and deformation gages. Load was then applied in increments and complete sets of readings taken at each increment. A complete test generally took from eight to ten hours with each load level requiring from 30 to 40 minutes. The majority of this time was spent marking cracks and measuring their widths in addition to reading dial gages and taking the Demec strain readings.

Horizontal loads were controlled manually, care being taken to apply the load at an even rate to prevent horizontal displacement of the specimens due to uneven rates of loading at the two edges. A LVDT was mounted on the edge of the specimen to measure any lateral movement and adjustments made to the applied horizontal loading to keep specimen in alignment. The vertical loads were either controlled manually to the correct multiple of the horizontal load or by presetting the rate of loading adjustment on the MTS testing machine.

The magnitude of the load was held constant during measurement intervals except during the last one or two increments prior to the end of the test. At very high loads the deformations continued to increase during the measurement interval by an amount sufficient to affect the readings significantly. When this occurred the elongation of the speci-

men was held constant while measurements were being taken but the loads tended to drop off by up to 5 percent.

Testing of a segment was terminated when the maximum tendon forces reached approximately 95 percent of the breaking strength of the tendon. This was done to avoid damage to the instrumentation on the tendon pull rods.

5. INSTRUMENTATION AND DATA PROCESSING

5.1 Introduction

For each segment approximately 150 measurements were recorded at each load level. These measurements were of such quantities as loads, strains, elongations and crack widths. Wherever possible these measurements were taken electronically and processed directly using the data acquisition system in the laboratory. Other readings such as dial gages, mechanical strain gages and crack widths were read and recorded manually, but immediately following a test these readings were input to computer files for reduction and processing.

This chapter contains descriptions of the measuring devices and their locations along with a brief discussion of preliminary reduction of the data. The location and type of instrumentation for Segment 8, which is typical of all segments prestressed in two directions, is given in Fig. 5.1. This figure will be referenced in subsequent sections to facilitate description and discussion of segment instrumentation.

5.2 Data Acquisition System

The various pieces of data logging equipment in the laboratory provide excitation to the electric resistance strain gages and LVDT's (Linear Variable Differential Transformers), and convert the outputs to voltage readings in digital format. These data logging devices were monitored by and the voltage readings recorded by means of a Nova 210/E digital computer. This unit has a central processor core size of 32K words and a dual disk drive system with each disk having a capacity of

1.2 million words and can receive and process the input of up to 254 channels at one time.

In general, upon command, the system will take and average three readings of voltage during a period of 0.025 seconds for each channel, convert this to a digital signal and record the result. The signal is also processed by having initial zero readings subtracted and the result multiplied by appropriate gage factors, stiffness and material properties to convert the signal to engineering quantities such as force, strain, etc. These quantities are also stored for future use. During the course of the test up to 12 selected channels of processed data may be displayed on a video screen to permit monitoring the progress of the test.

Data contained in the files of the Nova computer may be transferred directly to data files of the Amdahl 470/V6, which is the digital computer residing in the Computing Centre, The University of Alberta. This is a very large computing facility complete with a full range of plotting and other ancillary units. Final data reduction and plotting was dne using this facility.

5.3 Measurement of Applied Loads

The vertical load applied to the segment by the MTS machine was measured by differential pressure transducers contained in the machine. These are accurate to ± 0.3 kips which is approximately ± 0.1% of the average cracking load in the vertical direction.

The horizontal loads were measured by electric resistance strain mounted on the axially loaded rods in the clevises between the

hydraulic rams and the whiffletree end fittings. These gages were 1/4 inch long foil type EA-06-250BG-120, gages manufactured by Micro-measurements Ltd. and were mounted diametrically in pairs as part of a 4 arm bridge. The rods were calibrated on three occasions during the course of the series of tests and were found to be accurate each time to ± 0.2 kips which is also approximately ± 0.1% of the average cracking load in the horizontal direction.

Similar gages were used to measure the forces in each tendon pull rod (locations 37 to 50 in Fig. 5.1) and also on six reinforcing bars on each face (locations 13 to 36 in Fig. 4.1).

Following each test the forces applied to the segment as measured by the MTS machine and the horizontal load cells were compared to those obtained by summing the forces in the tendons with the average measured force in the reinforcing bars times the number of bars. In every case the two measurements agreed to within 2 per cent at the cracking load. In reporting the test data the loads as obtained from the MTS machine and/or from the horizontal load cells have been used.

Due to misalignment of the end fittings, uneven tightening of couplers or other connections, unintentional moments were applied to the edges of the segments. These moments were calculated by summing the moments of the measured forces about the weak axis of each edge surface. In computing these moments, the force in all bars adjacent to a face was taken as the average force, measured by the three strain gages on the bars adjacent to that face. Moments about the strong axis were ignored because the resulting stresses in the concrete were very small.

5.4 Measurement of Strains

Values of strain were obtained using both electric resistance strain gages and hand held mechanical gages. The precise location of each gage for each segment is given in figures presented in Chapter 6 where the behavior of each segment under load is discussed in detail. This section contains a description of the actual measuring devices which were common to all segments and again refers to Fig. 5.1 for typical measurement locations. All electronic strain readings were read and stored using the Nova computer and data acquisition system. Readings from the mechanical gages are the change in length between two targets mounted on the segment surface. These were recorded manually but immediately following the test were typed into computer files and processed using computer subroutines in a manner similar to the electronic strain readings.

Strains in the steel reinforcement were measured using 1/4 inch long foil gages, Type EA-06-250BG-120, as manufactured by Micro-measurements Ltd. These gages were mounted on the reinforcement and suitably water-proofed prior to casting the concrete. Readings of electric resistance gages could be reproduced to nearest 10 μ in/in strain. These readings correspond to channels 1 to 12 in Fig. 5.1.

As discussed in section 3.1.3, 4 in. long electric strain gages were applied to both concrete surfaces in each direction. These gages were SR-4 type FAE-400N-12-SOL as supplied by BLH Electronics Ltd. and are points 51 to 52 in Fig. 5.1.

Concrete strains were also obtained using a mechanical dial gage. Stainless steel locating discs specially machined for the purpose were glued to the concrete surface at 5 inch spacing. The mechanical

gage manufactured by Baldwin Testing Equipment was a Whittemore, Model SN1435 having a dial sensitive to 0.0001 in. The results were reproduceable to within 5 dial divisions, hence the readings of strain were reliable to the nearest 0.0001 in/in (100 μ in/in strain). For the remainder of this report, values of strain obtained with the mechanical Whittemore extensometer are referred to as Demec readings.

Demec readings were also taken to determine strains in the steel reinforcement. Prior to casting, 3/16 in. diameter plugs were silver soldered to the reinforcing bars. These plugs were just long enough to reach the surface of the forms and were enclosed in a rubber tube with 3/8 in. outside diameter. After the concrete had hardened this tube was removed leaving a 3/32 in. gap around the plug so that if the reinforcement moved relative to the concrete during testing the plug would not bear on the concrete. Stainless steel Demec locating discs were mounted on the ends of the plugs.

Since the distance between Demec points was initially 5.0 in., the strain for a particular reading was obtained by dividing the change in length as measured by the dial gage, ΔL, by this length. For each gage interval a load vs. strain plot was obtained. Typical of these are the load vs. vertical strain plots in Fig. 5.2 as obtained from Demec readings on face B of Segment 8. The locations of these strain intervals are given in Fig. 6.8.1. The wide diversity in the measured values of adjacent intervals can be seen, for example, by comparing reading B1 which had two cracks crossing the gage length to B2 which had no cracks.

To obtain a representative strain in the concrete from the Demec readings for load levels greater than that to cause cracking, it is necessary to define some average value. The average concrete strain on a given face was obtained from either

$$\varepsilon_{conc} = \frac{\Delta L_{T2} + 0.5L_{T1} + 0.5\Delta L_{B1} + \Delta L_{B2}}{15} \qquad (5.1)$$

or

$$\varepsilon_{conc} = \frac{\Delta L_{T2} + \Delta L_{T1} + \Delta L_{B1} + \Delta L_{B2}}{20} \qquad (5.2)$$

where ΔL_{T2} is the change in length measured over gage interval T2, etc.

Equation (5.1) was used for those segments in which gage intervals T1 and B1 overlapped, (for example, Segment 1, Fig. 6.1.1) and Equation (5.2) was used when the intervals did not overlap (for example, Segment 8, Fig. 6.8.1). Hence the average strains plotted for Segment 8 in Fig. 5.3 were computed from Equation (5.2).

It should be noted that when computing the average concrete strain, the readings over the outer gage intervals T3 and B3 were not included since, in some segments, excessive cracking and/or spalling of the concrete near the edges were the force in the reinforcing bars is first transferred to the concrete was observed and this was considered unrepresentative of the strains distributed through the segment.

Steel strains were obtained using mechanical Demec readings only for Face A. To obtain an average gross strain for the segments for use in predicting cracking Equation (5.3) was used.

$$\varepsilon_{ave} = \frac{0.5\varepsilon_{conc}\ (\text{Face A}) + 0.5\varepsilon_{steel}\ (\text{Face A}) + \varepsilon_{conc}\ (\text{Face B})}{2} \qquad (5.3)$$

Of the strain measurements taken, the Demec readings proved the most useful since they provided an average strain over a length that included a crack. This was important since the analytical predictions give average strain values including the effects of cracks. The electric resistance gages on the reinforcement, being only 1/4 in. long, gave different readings depending on their proximity to cracks crossing the bar. The 4 in. long gages on the concrete surface ceased to operate meaningfully once they were crossed by a crack.

5.5 Crack Measurements

Two vertical and two horizontal lines were marked on each face of each segment, generally within the middle third of the segment but, for segments with spliced bars, outside the region of lapped splices. One line in each direction was located directly over a reinforcing bar and the other midway between two adjacent bars. The width of all cracks crossing these lines were measured using a 40 power microscope with a graduated optical scale. The microscope used for specimens 1, 2 and 3 was graduated to 0.1 mm, the microscope used in the balance of the tests was graduated to 0.001 in. These readings are given in Appendix A, or Volume II of this report. A discussion of crack widths and spacing is outside the scope of this report and is given in reference (2).

5.6 Slip of Prestressing Tendons

Dial gages graduated to 0.0001 in. were mounted on the couplers used to load the tendons and were used to measure the movements of the couplers relative to the edge of the concrete. The purpose of these gages was to give an indication of loss of bond in the tendons.

A typical plot from such dial gages versus the force in the corresponding tendon is given in Fig. 5.4. The deformation or end movement measured include the elongation of the coupler and wires outside of the wall segment and slip of the tendons inside the segment.

The dashed line O-A in Fig. 5.4 represents the calculated elongation of the coupler and end fittings up to a tendon force equal to the effective prestress force. From point A two dashed lines are shown. The flatter line A-B represents the calculated load-slip curve which woudl be measured if there were a complete loss of bond as soon as the initial prestress force was exceeded. The second line A-C corresponds to loss of bond within the anchorhead of the tendon itself but perfect bond within the segment. The non-linearity of line A-C results from inelastic strains in the tendon within the anchorhead.

Although the initial part of the curves are non-linear as slack in the system is removed, the slopes roughly correspond to line O-A. Beyond A, the slopes of the observed curves are roughly equal to the slope of line A-C up to a tendon force of 84 kips after which the slope decreases rapidly indicating loss of bond. The bond appears to be completely lost by the time the load is approximately 90 kips. These tendon forces correspond to stresses of 200 ksi and 215 ksi, respectively. The proportional limit of the wire in the tendons is about 200 ksi.

Fig. 5.4 is typical of the load-slip curves obtained for all segments indicating that bond of the tendon was lost shortly after the proportional limit of the wire was reached.

5.7 Initial Cracking Load and Tensile Strength of Concrete at First Cracking

In all cases initial cracking occurred during the application of a load increment. The presence of cracks following a given load increment was determined by examining the surface using an illuminated 5 power magnifying glass.

Determination of the cracking load involved preparing load-strain plots for the segment using the average Demec strain readings for each face of the specimen (for example Fig. 6.1.3 etc.). The cracking load was determined by passing a line through the initial straight portion of the curve and a second line through the first complete increment after the curve had bent over. The intersection of these two lines was taken as the cracking load. This procedure will tend to err on the high side if the curve after cracking is concave downwards as would happen if a series of cracks formed at successively higher loads, and will tend to err on the low side if the curve after cracking is concave upwards as would happen if the stiffness dropped rapidly from the uncracked stiffness until it reached an effective partially or fully cracked stiffness. Since Demec readings were not taken at every load increment, the values obtained in this way were not taken less than the last load of which the specimen was observed to be uncracked. The calculation of the cracking load is discussed more fully in Reference (1).

The tensile strength of the concrete at first cracking was computed for each specimen assuming linear elastic behavior. The calculation procedure is again presented and illustrated by an example in

Reference (1). In general, the tensile strength in the wall segments was about 60 percent of that in corresponding split cylinder tests.

6. TEST RESULTS

6.0 Organization of Presentation of Results

This chapter summarizes the observations and test results for each of the 12 segments considered in this report. A summary of the major variables for each segment is given in Table 2.1 Detailed readings of load and strain are given in Appendix A which is printed as Vol. II of this report.

Each segment is discussed in a separate section of this chapter. The second digit in the section number corresponds to the number of the segment being considered, i.e. Section 6.2 deals with Segment 2. This system is extended to the numbering of the figures by adding a third digit which indicates the nature of the information contained in the figure. The meanings assigned to this third digit are as follows: 1. indicates a figure showing the location of gages for measuring strain; 2. indicates a photograph of the segment faces at various levels of loading; 3. indicates a load vs strain plot for strains obtained using mechanical gages; 4. indicates a load vs strain plot for strains obtained from embedded electric resistance gages; and 5. indicates a crack histogram showing the distribution of crack widths measured at given load levels. When more than one sheet is required to present the material for a given figure an alphabetic character is added in parentheses. Thus Fig. 6.1.2(c) is the third photograph for Segment 1.

In all figures and discussion references to vertical and horizontal positions are to the orientation of the segment during testing. Face "A", which was the top face when the segment was cast, was the south face during testing. Face "B" is the other face.

A summary of the load at which cracking was first observed in each direction and on each face is given in Table 6.1. Since these cracks were generally observed between increments of applied loading the tabulated values were obtained as outlined in Section 5.7. The tensile stresses corresponding to first cracking are also given in Table 6.1 The calculation of these is described in Section 5.7 and Ref. 1.

The BOSOR5 analyses presented in Ref. 1 and used subsequently to analyze containment structures give response as a function of the average strain at the mid-surface of the wall or as a function of average strains at various points through the wall. For this reason the data plotted and tabulated in this report has been presented in terms of average strain.

All strains reported are average strains based on readings taken in the middle portion of the segments. The reasons for this and the methods of averaging are presented in Section 5.4. To permit a correlation between average strains and degree of cracking, only those cracks located in the corresponding region are included in the crack width histograms. In general, the strains measured during unloading cycles are, for clarity, omitted from the plots, however, such readings are included in Appendix A. Except for Segments 12 and 13 which were loaded eccentrically to produce a known bending moment, the cracks measured on both faces are included in the histograms.

During testing an initial preload of 5 to 10 kips was applied to facilitate alignment of the system and then further loading was applied. The loads reported in this chapter and in the various figures

and tables include this preload. The strains are all taken relative to the state at the initial preload. As a result the real strains are an infinitesimal amount larger than those reported.

6.1 Segment 1

Initially the ratio of loads applied to Segment 1 was 2:1 with the larger load applied vertically. As this was the only ratio of loading anticipated at the beginning of the test of this segment it was thought that it would be sufficient when taking photographs to indicate the level of loading by labelling only the larger or vertical load. Hence in Figs. 6.1.2(a) to (f) only one load is shown which is the vertical load or twice the horizontal load. This loading ratio was used until a vertical load of 550 kips was reached which was considered to be the maximum load that could be applied without danger of rupturing a tendon in that direction. However, at that load there was still reserve strength in the horizontal direction and the degree of vertical cracking was not as advanced as in the horizontal direction. It was then decided to increase the horizontal loading in three increments at values of 300, 325 and 350 kips keeping the vertical load constant at 550 kips in order to observe the development of further vertical cracking.

After measurements had been taken at a vertical load of 450 kips, well above the cracking load, the loads were reduced in proportion until the vertical load was 150 kips or below the load at which first horizontal cracking was observed, and then reloaded in proportion to a vertical load of 500 kips. The total elapsed time for the test was 5 hour.

Prior to loading a number of shrinkage cracks were observed on the concrete surfaces, particularly on Face A which was the exposed face during curing. These initial cracks are shown in Fig. 6.1.2(a) and (b) and are seen to occur along the reinforcement.

The first new cracking observed during loading was a horizontal crack near the top of the specimen on Face A and was the development of an existing shrinkage crack. With increasing load a number of additional horizontal cracks were formed on both faces before the first vertical crack was observed on Face B. The extent of these horizontal cracks is shown in Figs. 6.1.2(c) and (d) which are photographs taken following the load increment in which the first vertical crack was noted. For vertical loads above 450 kips there were horizontal cracks on both faces at approximately every reinforcing bar (Figs. 6.1.2(e) and (f)) but vertical cracking was limited to the upper portion of the specimen. Observations of the edges of the specimens suggested that approximately every second crack penetrated through the wall, the rest ending just inside the reinforcement. During the final load increments in which only the horizontal load was increased the vertical cracking developed again at locations essentially adjacent to the reinforcement but not necessarily at each bar. Final crack patterns are shown in Figs. 6.1.2(g) and (h).

The load-average concrete strain curves are given in Fig. 6.1.3. The concrete strains in these plots were obtained from Demec (mechanical strain gage) readings taken at locations given in Fig. 6.1.1 and which were averaged using Eqn. 5-1. The level at which first cracking occurred

was obtained from these plots. The unloading and reloading cycle which took place in the post cracking region between vertical loads of 450 kips and 500 kips was omitted from the plots.

The vertical surface strains on both Faces A and B follow the same pattern characteristic of reinforced concrete sections although the strains on Face A for loads below cracking are about twice those on Face B. This agrees with the earlier observed horizontal cracking on Face A as described above and is attributed to a small eccentricity of the applied vertical load. Following cracking the strains on Face A are still greater but the differences are not as great percentagewise.

In the horizontal direction, Fig. 6.1.3(b), the recorded strains on both faces agree closely at all levels of loading. No explanation is given for the second last point for Face A other than a mistake in either reading or recording this gage reading.

Corresponding plots of the strain obtained from embedded electric resistance gages on the reinforcement are presented in Fig. 6.1.4. The agreement between the horizontal strains measured with mechanical gages (Fig. 6.1.3(b) and Fig. 6.1.4(b)) is very close at all load levels. Vertical strains obtained from electric resistance gages agree at loads below the cracking load; the random nature of the strain readings for loads above the cracking load is not unexpected. Since the length of each strain gage is only 1/4 in., the strain measured in the post-cracking region is very much dependent on the proximity of the gage to a crack. This randomness was not observed in the horizontal strains since very little cracking was observed in that direction nor in the strains from Demec readings which averaged the strains across cracks.

In Fig. 6.1.4(a), although the vertical load for the last three increments was maintained at 550 kips, the strain was observed to increase. This increase in steel strain with constant total load indicates that as the horizontal load was increased there was some increase in cracking and creep in the concrete in the vertical direction resulting in a transfer of some of the vertical load from the concrete to the steel. This transfer was accompanied by an opening of some of the cracks and hence the observed increase in strain.

This rapid increase in crack widths at high loads is clearly demonstrated in Fig. 6.1.5. While neither the segment face nor the order in which the cracks formed is designated in this figure, a more detailed analysis shows that in many instances a crack which formed at a higher load level may end up with a greater width than a crack that was formed at a lower load level. While all cracks tended to follow the reinforcement at the surface, those cracks closest to prestressing tendons seemed to open the widest.

The two lines in the histograms represent the 50th and 75th percentiles of the crack widths. A more complete interpretation of crack formation and crack widths is given in Reference (2).

6.2 Segment 2

Segment 2 was intended to be a replica of Segment 1 to ascertain how closely the results from two essentially identical segments could be duplicated. The tensile and compressive strengths of Segment 2 were both about 90 percent of those in Segment 1. Again the ratio of vertical

to horizontal loading was 2:1 until the vertical load of 550 kips was reached. When the vertical load reached 350 kips the loads were reduced in proportion until the vertical load was 200 kips and then the loads were increased to the 350-175 kips level. This was repeated at 400 kips. Also, similar to Segment 1, with the vertical load held at 550 kips, the horizontal load was increased from 275 kips to 388 kips. The total elapsed time for the test was 7 hours.

Prior to loading Segment 2 showed very little shrinkage cracking in contrast to Segment 1 which had extensive shrinkage cracking on Face A. However, the development of cracks due to load was similar to Segment 1. The first cracks were horizontal cracks but occurred at a slightly lower load than for Segment 1. Vertical cracks appeared first on Face A and several such cracks were well developed before any occurred on Face B. This is clearly seen by comparing Fig. 6.2.2(e) and (f) for a horizontal load of 200 kips. At the time loading was terminated, cracking along the reinforcement in both directions was noted with the widest cracks adjacent to the tendons. At some of the wider cracks wedge shaped pieces of concrete were seen to form between two closely spaced cracks but no pieces were observed to spall off. At the end of the test, gaps were visible above and below the center tendon anchorage plate on the vertical edges. The cracks in this vicinity appeared to converge on the tendons. At a load of 500 kips slip of the vertical tendon anchorages relative to the concrete was noted.

The average surface strains obtained from Demec readings on the concrete vs load are shown in Fig. 6.2.3. The vertical strains

measured on both faces agree very closely up to the cracking load after which the strains on Face A are slightly greater. However in the horizontal direction the strains on Face A are much greater at all load levels which agrees with the greater degree of vertical cracking on this face. Unlike Segment 1 the difference in strains between faces increases for higher load levels. The reason for the greater strains on Face "A" compared to Face "B" is attributed to a small eccentricity in the applied tensile loading on the vertical direction.

Strains obtained from embedded strain gages correspond closely with concrete strains at load levels below cracking. After cracking they tend to be less than the average concrete strains since some of the gages were located between cracks where the strains would be less than at cracks. The horizontal strains in Fig. 6.2.4(b) agree fairly well with the average concrete strains on Face B at all load levels.

A comparison of Fig. 6.1.3 and 6.2.3 shows that the cracking load of Segment 2 was lower than that of Segment 1 as expected because its tensile strength was lower. Once cracking had occurred, however, Segment 2 was stiffer than Segment 1. A comparison of Fig. 6.1.2 and 6.2.2 suggests that although Segment 1 had more shrinkage cracks, there are more load-induced cracks in Segment 2. In Segment 1, the cracks tended to converge on the tendons forming a few large cracks.

The distribution of crack widths is given in Fig. 6.2.5(a) and (b). At the highest horizontal load the width of one very wide vertical crack was seen to have a marked effect on the average concrete strain.

6.3 Segment 3

Segment 3 was fabricated and instrumented as closely as possible to duplicate Segments 1 and 2 but was loaded in a different sequence. Initially equal loads were applied in the vertical and horizontal directions until a nominal load of 300 kips was reached at which time the segment was unloaded to 100 kips. The segment was reloaded again with equal horizontal and vertical loads until a nominal load level of 350 kips. At this point the horizontal load was maintained but the vertical load was increased to 400 kips. The next load increment saw the horizontal load increased to 375 kips and the vertical load decreased to 375 kips so that equal loads were again applied in the two directions. This nominal load of 375 kips in the horizontal direction corresponds approximately to the final horizontal load levels in Segments 1 and 2. This level of horizontal load was maintained for all future load increments (except for the unloading to 100 kips following the increment when the vertical load was 450 kips), but the vertical load was increased in increments to 530 kips. Thus the final load intensities on Segment 3 were similar to those applied to Segments 1 and 2 except that the sequence of loading to arrive at these intensities was quite different.

Although the loading in the two directions was equal, the initiation of cracking was not due to the different levels of prestress. Vertical cracks were first observed on both faces at a load level just greater than 200 kips. At a loading of 250 kips there was essentially a vertical crack extending along each reinforcement bar but no horizontal cracks were observed. The same situation was observed at a loading of

300 kips at which time the loading was reduced to approximately half the load at which cracks were first observed and then reloaded.

In the increment between 300 kips and 350 kips horizontal cracks were seen to form at midheight on Face B in the vicinity of the tendon. At this stage the vertical load only was increased to 400 kips during which time horizontal cracking appeared on Face A again adjacent to the tendons. The crack patterns at this loading are shown in Figs. 6.3.2(a) and (b) where the vertical cracks at each reinforcement bar are well developed but the few horizontal cracks are not always visible across the segment.

During the final load increments, in which the horizontal load was held constant and the vertical load increased, more horizontal cracking was observed that again followed the reinforcement and with the larger cracks near the tendons.

The plots of load-average strain as measured on the concrete faces by mechanical gages are given in Fig. 6.3.3. The influence of crack development on the gross strain is shown clearly in this figure. As mentioned earlier, under equal loading the first cracking expected would be vertical cracks due to the lesser initial prestress in the horizontal direction. In the loading increment between 200 kips and 250 kips these vertical cracks were observed to form on both faces almost immediately after that loading commenced. After only a very small increase in load, additional cracks formed at essentially every reinforcing bar on both faces. This phenomena of the formation of a large number of cracks over a very small increase in load introduces a very

abrupt transfer of tensile load from the concrete to the steel which results in the sharp break in the load-strain curve of Fig. 6.3.3(b) and the almost linear relationship for loads above first cracking. This phenomena is also reflected in Fig. 6.3.5(b) in which a large number of vertical cracks are seen to form at a small strain and these cracks open up relatively uniformly as the load increases.

On the other hand, when cracks develop slowly over a large loading increment as was observed with the horizontal cracks in this segment the transfer of load between concrete and steel is much more gradual (Fig. 6.3.5(a)). This results in a gradual transition in the stiffness from that based on uncracked concrete to that where the tensile stiffness is provided almost solely by the reinforcement as seen in Fig. 6.3.3(a).

The differences in behavior in the two directions from the differences in crack development is also reflected in the differences in the plots of load-average strain obtained from embedded steel gages shown in Fig. 6.3.4.

6.4 Segment 4

This segment was reinforced with mild steel reinforcement only consisting of #4 bars at 4 inch spacing in each direction near each face.

Load was applied equally in both directions to 100 kips at which time a well developed crack pattern was observed. The segment was then unloaded and then reloaded until general yielding of the reinforce-

ment occurred. The loading was terminated at 160 kips because of the large deformations.

Prior to loading some shrinkage cracking was observed in Face A as indicated in Fig. 6.4.2(a). As usual this cracking tended to follow the location of the reinforcement. The first observed cracking occurred at a load level of approximately 60 kips near the mid-height of each face. The extent of this cracking at the end of the load increment at 80 kips is shown in Fig. 6.4.2(c) and (d). When the load was increased to 100 kips a crack was observed on both faces at approximately every second reinforcing bar. Although on Face A some of these cracks did not extend the full width of the segment after unloading and reloading, increasing the load to 120 kips resulted in a crack at essentially every reinforcing bar. Little additional cracking was observed as the load was increased to 160 kips at which time general yielding of the reinforcement occurred and several cracks began to open rapidly. The crack pattern at the termination of the test is shown in Fig. 6.4.2(e) and (f).

The locations at which strains were measured are given in Fig. 6.4.1. In addition to the mechanical Demec readings on the surface of the concrete, Demec readings were also taken on one vertical and one horizontal bar in Face A, which was located closest to the midpoint of the segment.

The load vs average strain plots for strains obtained from Demec readings on the surfaces of the concrete are given in Fig. 6.4.3. The concrete Demec readings for Face A are the results obtained using

the averaging assumptions of Section 5.4. However a comparison of Figs. 6.4.2(e) and (f) indicates that, whereas the cracks on Face B are reasonably uniformly spaced and of similar widths, the cracking pattern on Face A tends to be more random with a very noticeable variation in widths of cracks. For example the horizontal strain on Face A is measured by intervals C4, C5 and C6, but due to edge influences the reading C6 is not included when evaluating the representative average strain. From Fig. 6.4.2(e) it can be seen that there are no vertical cracks through the intervals C4 and C5 but that there are two very wide vertical cracks adjacent to but just outside of this interval. Thus an average strain based on a weighting of intervals C4 and C5 will be very much smaller than the true strain. At the load of 160 kips the strain over interval C4 is only 0.00018 in/in and over interval C5 was recorded as a negative strain of 0.00012 in/in. This is contrasted with the corresponding strain for interval C6, which contains a noticeable crack, of 0.00686 in/in a value much larger than the representative strain. Obviously a better value would be the arithmetic mean of the three intervals which is 0.00231 although with the proximity of a very wide crack just to the left of interval C4, even this value may be smaller than the true average strain. For the sake of consistency in presenting data the values for Face A are plotted in Fig. 6.4.3 using the usual averaging expression but no significance can be given to these values.

On the other hand, due to the more uniform distribution of cracking on Face B the average concrete strain computed from Eqn. (5.1) is probably reasonably representative of the true strain. The average

strains computed from the Demec readings on the reinforcing steel located near Face A are also plotted in Fig. 6.4.3. It is seen that the average strain obtained from the steel Demec readings on Face A, which are located in a region of more uniform cracking than the concrete Demec readings on the same face, agree very closely with the average strains obtained from concrete Demec readings on Face B.

One further comment is required in interpretting Figs. 6.4.3 and 6.4.4. The final strains plotted are for a load at which yielding of the reinforcement has occurred. Thus the value of strain is dependent on the amount of travel permitted for the jacks but is independent of the load applied by them. This is clearly seen in Fig. 6.4.4 where strains from embedded electric resistance gages are plotted against load. Steel Demec strains are also plotted to facilitate comparisons. With the computer plots a straight line of appropriate designation is plotted between points as a guide to the eye. No interpolation between points based on this straight line is meaningful. Hence in Fig. 6.4.4, even though embedded steel gage strain readings are plotted at closer strain intervals than the Demec readings, the slopes of the lines joining strains between load intervals of nominal 140 kips and 160 kips are not meaningful but should have a sharp cusp located by extending the load-strain plot until it intersects the horizontal line located at the yield load.

The distribution of crack widths measured for Segment 4 are shown in Fig. 6.4.5. Again, while a full discussion of crack widths is given in Reference (2), the actual crack widths for the last increment

of strain for this segment due to the general yielding of the reinforcement in both directions is dependent primarily on the amount of travel permitted by the loading jacks before the termination of the test.

6.5 Segment 5

Segment 5 was fabricated with only horizontal prestress tendons and was loaded only in this direction. Normal reinforcement bars, however, were provided in both directions near each face in a manner similar to the previous segments. While this condition of initial prestress and loading is not representative of any specific location in a prestressed containment it should give some insight to the uniaxial response of the section.

Horizontal load was applied in increments to 330 kips at which time it was unloaded and then reloaded to 410 kips. The locations of the strain measurements are given in Fig. 6.5.1. Although it is seen that measurements of strain were taken in both directions and are presented in Appendix A, the strains in the vertical direction (direction of zero applied load) were an order of magnitude smaller than the horizontal displacements and are not plotted in this report.

Prior to loading there did not appear to be any shrinkage cracks visible. Loads were applied in increments of 50 kips to 250 kips without any cracks being observed. However, very early in the next increment of loading, the first cracks appeared on both faces and the load increments were reduced to 25 kips. The degree of cracking after the first load increment in which cracking was observed is shown in

Fig. 6.5.2(c) and (d) and again the cracks were seen to follow the location of the reinforcing bars.

Vertical cracking increased as the load increased so that at the end of the test, Fig. 6.5.2(e) and (f), there was a vertical crack extending across the segment at each bar location on both faces. These cracks were observed to penetrate through the segment.

The effects on axial stiffness are clearly shown in Fig. 6.5.3. The agreement between the concrete Demec readings on both faces and the steel Demec readings on Face A agree closely over the entire range of loading. The break at approximately 275 kips represents first general cracking of the concrete and the reduced stiffness. The creep in the segment, transfer of load from concrete to steel, at a load of 330 kips is a consequence of the loading and unloading sequences, the results of which are not plotted in Fig. 6.5.3. The large strains at a load of 400 kips are due to yielding of the reinforcement. During this period no new cracking was observed but rather only the widening of existing cracks.

A similar plot is given in Fig. 6.5.4 where the strains obtained both from Demec readings on the reinforcement and embedded gages on the reinforcement are plotted. This curve from embedded steel gages shows more clearly the sharp break at 400 kips due to the yielding of the reinforcement as these gages could be read at frequent intervals while the load was being applied, whereas the mechanical Demec readings could be taken only at the end of a load interval.

The creep in the segment at a load of 330 kips, which is well below the proportional limit for the reinforcement, is also clearly seen in Fig. 6.5.4. This occurred during the unloading and reloading cycle and represents a transfer of load from the concrete in tension to the steel.

The number and width of vertical cracks are shown in Fig. 6.5.5. Again it is seen that most of the final cracks occurred almost simultaneously at low strains and with further loading increased in width. The very large widths correspond, of course, with the yielding of the reinforcement and since these widths depend on the amount of elongation of the jacks permitted before the test was terminated, the relative widths rather than the absolute widths are all that should be considered at this strain level.

6.6 Segment 6

Segment 6 was fabricated and loaded in a manner similar to Segment 5. The major difference in fabrication is that the area of normal reinforcement in Segment 6 is about 1.5 times that of Segment 5, see Table 2.1. The essential difference in loading is that once loading began for Segment 6 it was increased without an unloading cycle to just below the level to cause yielding of the reinforcement at which time it was unloaded in three increments. This contrasts with Segment 5 which was unloaded midway between first cracking and yielding of the reinforcement and then loaded well into the yielding range.

Prior to loading some horizontal hairline cracking was observed along a couple of reinforcement bars near Face A, see Fig. 6.6.2(a). Since no vertical load was applied these cracks did not appear to propagate as the test progressed.

The first cracking observed due to load were the vertical cracks shown in Fig. 6.6.2(c) and (d). With further load these cracks progressed along the reinforcement bars and at the end of the test there was such a crack at almost each bar, Fig. 6.6.2(g) and (h).

The location of strain measurements for Segment 6 are given in Fig. 6.6.1. The plots of load vs average strain obtained from mechanical Demec readings are given in Fig. 6.6.3. The agreement between the readings on the concrete of Face A and on the steel adjacent to Face A is excellent. While the agreement between the concrete readings on Face B (Fig. 6.6.3) and for the strains from embedded resistance gages on the steel adjacent to Face B (Fig. 6.6.4) is also excellent there is some difference in stiffness between the readings of the two faces. This is likely due to some eccentricity in the applied load and the true stiffness is somewhere between the two plotted lines.

As mentioned previously the loading was terminated prior to yielding of the reinforcement and there were no unloading cycles prior to reaching maximum load. Thus the slope of the load-strain plots is remarkably linear in the post-cracking region. The number of cracks and crack widths are given in Fig. 6.6.5. Comparing this figure with Fig. 6.5.5 for Segment 5 it is seen that the majority of the cracks form at low strain, i.e. essentially one along each vertical reinforcement bar

on each face and these open up reasonably uniformly with increasing load.

6.7 Segment 7

This segment contained only nonprestressing reinforcement consisting of two orthogonal layers of 6-#6 bars at 6 inch spacing near each face. The thickness, concrete cover and bar diameter were all set at 1.5 times those in Segment 4. The overall size of the segment was thus 31.5 in by 31.5 in by 15.75 in. The compressive and tensile concrete strengths in Segment 7 were 3500 and 339 psi, respectively, compared to 5590 and 536 psi in Segment 4. Details of the segment are given in Table 2.1. Equal loads were applied in both directions until general yielding of the reinforcement was observed.

The degree of shrinkage cracking observed for this segment was greater than for all other segments as can be seen from Fig. 6.7.2(a) and (b). Since much of the shrinkage of the prestressed segments takes place prior to the post-tensioning operation it is possible that the prestressed segments also had this degree of shrinkage cracking, but the cracks had been closed by the prestressing. This theory is contradicted, however, by the fact that the cracking in Segment 7 was much more extensive than in the companion specimen, Segment 4, which was not prestressed and which had the same steel percentage as Segment 7. The shrinkage cracking tended to follow the location of the reinforcing bars and was more pronounced on Face A which was exposed during casting than on Face B as shown in Fig. 6.7.2(a) and (b).

The locations of measurements of strain are given in Fig. 6.7.1. The plots of load vs average strain obtained from Demec readings are given in Fig. 6.7.3. First cracking was observed at horizontal and vertical loads of 100 kips. Based on extrapolations of the load strain data used to plot Fig. 6.7.3 horizontal cracks were found to have started on Faces A and B at vertical loads of 75.1 and 100 kips. Vertical cracking started on both faces at a horizontal load of 82.1 kips. As shown in Fig. 6.7.2(c) and (d), these cracks followed the reinforcement.

Loading was terminated when yielding occurred in the horizontal bars. Because the vertical load was slightly lower, the vertical bars did not yield during the test.

The load-average strain curves in Fig. 6.7.3(a) and (b) are similar in the two directions up to a strain of 0.0017, the three plots of vertical strain measurements falling between the highest and lowest values for the horizontal strains. A pronounced decrease in horizontal stiffness was observed at cracking. In the vertical direction, Fig. 6.7.3(a), the difference berween initial and final stiffness is less pronounced suggesting that the shrinkage cracks along the horizontal bars had extended farther into the specimen than the corresponding cracks along the vertical bars. This is reasonable since the horizontal bars were inside the vertical bars. The embedded strain gaes mounted on the horizontal reinforcement gave strains similar to, but lower than, those measured on the surface as shown in Fig. 6.7.4(b). This is to be expected since two of the three embedded gages were located between vertical cracks. The vertical strains measured by the embedded gages

are erratic as shown in Fig. 6.7.4(a) due to poor readings in two of the six gages (gages 1 and 8). When these two gages are excluded from the average, the average of the remaining four is close to that for the steel Demec gages.

As was observed from the crack photographs only a few large cracks occur. This is also indicated from the plots of crack widths in Fig. 6.2.5.

During the period that the reinforcing bars remained elastic the widths of the vertical cracks were roughly 0 to 20 percent greater than those of the horizontal cracks and the distributions of crack widths were also quite similar as shown by Fig. 6.7.5(a) and (b). Since the loading was terminated just after yielding in the horizontal direction (vertical cracks) but just before yielding in the opposite direction, very large strains and cracks were observed in one direction only.

As stated earlier, Segments 4 and 7 were nominally similar with Segment 7 having bar size, thickness and cover equal to 150 percent of those in Segment 4. A comparison of the crack width histograms for Segments 4 and 7 suggests that the mean crack widths in Segment 7 were roughly 130 to 150 percent of those in Segment 4. This will be discussed more fully in Ref. 2.

6.8 Segment 8

Segment 8 was similar to Segments 1 and 2 except that the minimum cover was 1.25 in. rather than 0.5 in.

During the test the ratio of horizontal to vertical load was kept nominally at 1:2 up to a horizontal load of 291 kips and a vertical load of 571 kips. At this load yielding had occurred in the vertical direction but not in the horizontal direction as shown by the load strain curves in Fig. 5.3, 6.8.3 and 6.8.4. The vertical load was then held relatively constant while the horizontal load was increased to 392 kips by which time yielding had occurred in that direction.

Horizontal cracking occurred at a vertical load of 350 kips and vertical cracking occurred at a horizontal load of 175 kips. The first vertical cracks coincided with the locations of the vertical tendons. As shown in Fig. 6.8.2 cracks occurred parallel to most of the reinforcing bars in the two directions. At failure, however, those cracks nearest to the tendons tended to open up more than the cracks along bars between the tendons. This is particularly evident in Fig. 6.8.2(a).

Close agreement was observed between the average vertical strains for Faces A and B as shown in Fig. 5.3. On the other hand, the horizontal strains on Face A were found to be much larger than those on Face B as in Fig. 7.8.3. This can be explained by the locations of the strain measuring zone relative to the major cracks. On each face, two major vertical cracks developed essentially along the two vertical tendons adjacent to that face. On Face A these cracks fell inside the strain measuring zone while on Face B they fell just outside this zone.

A comparison of the strains in Segments 1, 2 and 8 (Fig. 6.1.3, 6.2.3 and 6.8.3) shows that after cracking the stiffness of

Segment 8 was close to that of Segment 2 and greater than that of Segment 1.

6.9 Segment 9

Segment 9 was similar to Segments 1 and 2 in construction and loading sequence except that all the horizontal bars in both faces were lap spliced for a length of 15 inches. The center of each splice was placed at the vertical center-line of the specimen and the lapped portion extended 7.5 inches on each side of this center-line. This length of lap corresponds to a Class C splice for a Grade 60, #3 bar as required in such a case by the ACI and CSA Codes. The horizontal bars were inside the vertical bars in each face so that the cover to the surface of the spliced bars was 0.875 in. The concrete strengths of Segment 9 were closer to those of Segment 2 than Segment 1.

The locations of the strain measuring stations are indicated in Fig. 6.9.1. The location of the targets for the horizontal steel Demec gages will be discussed when the strain data is presented.

The ratio of the applied loads was 2:1 with the larger load being applied vertically. At a vertical load of 300 kips, horizontal cracks developed on Face B, followed by horizontal cracks on Face A at about 350 kips vertical load. Graphical extrapolation of the strain data indicated that vertical cracking developed on both faces at a horizontal load of 182 kips.

The ratio of loads was maintained at 2:1 until the vertical and horizontal loads reached 561 kips and 285 kips, respectively.

Subsequently, the vertical load was held at 561 kips while the lateral load was increased to 380 kips.

Figure 6.9.2 shows the specimen after the test was completed. Several things should be noted. There are more horizontal cracks in the spliced region than adjacent to the edges of the specimen. In a number of cases, two cracks formed along one splice. These extend inward to the bars, isolating wedges of concrete which could drop out at high strains. Very large vertical cracks were observed adjacent to the ends of the splices, particularly on Face A where one such crack reached 1/4 inch in width.

Load average strain plots are given in Fig. 6.9.3 and 6.9.4. A comparison of Fig. 6.1.3(a), 6.2.3(a) and 6.9.3(a) indicates that Segment 9 had roughly the same stiffness in the vertical direction after cracking as Segment 2. This was higher than the vertical stiffness of Segment 1. In the horizontal direction Segment 9 again was stiffer than Segment 1 but all the curves in Fig. 6.9.3(b) fall between the two curves plotted in Fig. 6.2.3(b), indicating that its horizontal stiffness was similar to that of Segment 2. At very high loads, the horizontal strains increased rapidly in Segment 9 due to bond slippage in the lap splice.

In the vertical direction the strains measured using the steel Demec gages agreed closely with those from the concrete Demec gages and the embedded steel gages as shown in Fig. 6.9.3(a) and 6.9.4(a). In the horizontal direction the steel Demec gages gave higher readings than the other two types of gages, however. This is due to the arrangement of

the targets for the steel Demec gages on the spliced bars. The targets for both ends of gage lengths S6, S7 and S8 were mounted on one bar while the points for both ends of gage length S10 were mounted on the other bar. The targets at the two ends of length S9 gage, however, were mounted on different bars and hence the readings from this includes strain plus any relative slip of the bars. At the final load stage plotted in Fig. 6.9.3(b) the average strain in the gages S7, S8 and S10 was 0.0026 while that in S9 was 0.0091.

Figure 6.9.5 shows distributions of crack widths in Segment 9. The mean vertical cracks tended to be larger than the horizontal cracks at all strains plotted in this figure. This is primarily due to the large cracks near the ends of the splices.

6.10 Segment 10

Segment 10 was similar to Segments 1 and 2 in properties and loading. It was loaded biaxially and air was forced through the cracks while under load. The behavior of this segment is described in Ref. 3.

6.11 Segment 11

Segment 11 was similar to Segment 9 except that every second horizontal bar was lap spliced.

The locations of the strain measuring stations are indicated in Fig. 6.11.1. Embedded steel gages were located as shown in Fig. 6.9.1. The horizontal line of steel Demec gages was mounted on a bar that was lap spliced. On the other hand, the horizontal line of embedded steel gages was mounted on a bar that was was not spliced.

The development of cracking is illustrated in Fig. 6.11.2. First horizontal cracking occurred on Face A at a vertical load of 284 kips. Face B cracked at 300 kips. Vertical cracking was first observed at a horizontal load of 175 kips. Load vs average strain curves are shown in Fig. 6.11.3 and 6.11.4. A comparison of Fig. 6.11.3(a) and 6.2.3(a) and 6.9.3(a) shows that the vertical stiffnesses of Specimens 2, 9 and 11 were similar. From Fig. 6.2.3(b), 6.9.3(b) and 6.11.3(b) it can be seen that the horizontal stiffnesses of Segments 2 and 11 were similar. Segment 9 had a similar lateral stiffness up to a lateral load of about 300 kips after which time its lateral stiffness decreased rapidly. Thus, it appears that bond distress in the lapped splices was significant in Segment 9 where all bars were lap spliced and much less significant in Segment 11 where only half the bars were lap spliced.

Figures 6.11.5(a) and (b) illustrate the development of cracking. The mean horizontal crack widths were essentially the same in Segments 9 and 11 for a given vertical strain. On the other hand, the mean vertical crack widths were smaller in Segment 11 for a given horizontal strain. Thus, the alternate continuous bars in this segment restrained the opening of large cracks.

6.12 Segment 12

Segment 12 was designed to study the effects of biaxial tension and uniaxial bending on the response of a wall segment. Such a situation may occur near axially-symmetric discontinuities in a containment structure

such as the wall to base joint or wall to ring-beam joint. The properties and axial loadings were chosen to resemble Segments 1 and 2. The compressive and tensile concrete strengths were higher than for those two specimens, however.

During testing, the axial forces were increased in the ratio 2:1 with the vertical load being the larger of the two. When the vertical load reached 535 kips it was then held constant while the horizontal load was increased from 375 kips to 320 kips. The moment was applied by pulling on the three horizontal tendons located at mid-thickness of the wall and on the horizontal reinforcing bars adjacent to Face A. The rebars adjacent to Face B were left free. This method of applying the moment implied that the moment increased linearly with the total applied horizontal force until the rebars yielded. Beyond that, the moment would remain essentially constant with further horizontal load until the bars reached the strain hardening region.

The locations of instrumentation are shown in Fig. 6.12.1. The embedded strain gages were located as shown on Fig. 6.9.1.

The development of cracking is traced in Fig. 6.12.2. The first cracks to appear were horizontal cracks which started on Face A at when the vertical load was 300 kips. These cracks extended through the specimen when the vertical load was about 340 kips. Vertical cracking started on Face A at a horizontal load of 170 kips. A few isolated vertical cracks occurred on Face B in the very late stages of the test. These occurred in regions in which the vertical loads were introduced into the specimen by bond in the No. 3 bars. The effect of the moments on the crack pattern is clearly visible in Fig. 6.12.2(g) and (h).

Plots of load vs average strains are given in Fig. 6.12.3 and 6.12.4. In the vertical direction the load-strain diagrams for Segments 1 and 12 shown in Fig. 6.1.3(a) and 6.12.3(a) are very similar. The horizontal strains on the face in tension (Face A) are also similar to the horizontal strains in Segment 1 as shown in Fig. 6.1.3(a) and Fig. 6.12.3(a). The strains on Face B were essentially equal to zero throughout the test. The steel strains in the embedded gages on bars adjacent to Face B show tensile strains after cracking had occurred on Face A. These gages were located on the inside surface of these bars and hence were 1.25 inches from Face B. This represents 12 percent of the total thickness of the wall. At a horizontal load of 300 kips the strain in these gages was roughly 18 percent of that in the concrete Demecs on Face A.

Crack width distributions are presented in Fig. 6.12.5. A comparison of Fig. 6.12.5(a) and (b) with 6.1.5(a) and 6.2.5(a) shows that the average width of the horizontal cracks in the two faces of Segment 12 was approximately the same as the average width of those in Segments 1 and 2. This suggests that the moment in the opposite direction had little effect on the width of the horizontal cracks.

6.13 Segment 13

Segment 13 was loaded with vertical and horizontal loads which were applied eccentrically by pulling on the tendons and the reinforcing bars on one face in the manner shown in Fig. 4.5. The eccentric loads thus created moments about the two axes which increased linearly until

the bars or tendons yielded. The loading arrangement resulted in biaxial tension and biaxial bending with Face B sustaining high tensile stresses in both directions. The vertical and horizontal loads were increased in the ratio 2:1 until the vertical load reached 335 kips. The vertical load was then held constant while the horizontal load was increased from 167 kips to 340 kips.

The location of the instrumentation is shown in Fig. 6.13.1. The development of cracking is illustrated in Fig. 6.13.2. The first cracks to appear were horizontal cracks on Face B at a load of 175 kips. These cracks were uniformly distributed on the face, one over each horizontal reinforcing bar. A few vertical cracks were observed when the vertical and horizontal loads reached 300 and 150 kips and extensive vertical developed on Face B by the time the load ratio was 335:167. At this load the diagonal cracks shown in Fig. 6.13.2(g) began to appear.

Load-average strain diagrams are given in Fig. 6.13.3 and 6.13.4. Crack width data is plotted in Fig. 6.13.5.

6.14 Segment 14

Segment 14 was similar to Segment 5 in properties and loading. It was loaded uniaxially and air was forced through the cracks while under load. The behavior of this segment is described in Ref. 3.

7. DISCUSSION OF TEST RESULTS

This report is intended to present the test data. Extensive analyses of stress-strain behavior are presented in References (1) and (2) and the leakage behavior is analyzed in Reference (3). These discussions will not be repeated here. Two aspects of the test behavior have not been discussed in these references and will be presented briefly in this chapter.

7.1 Relationship between Steel Strains from Demec Gages and Embedded Gages

Throughout this project, all parameters have been related to the average strains at the surfaces of the walls or at center of the containment wall. In Ref. 1, the analytical predictions are compared to the average of the concrete strains measured in the center portion of each side using the Demec strain gages. As shown in Fig. 6.1.3, 6.2.3,... 6.x.3 in this report, there is generally very good agreement between the Demec strains measured in the concrete and on the reinforcement in the same face. The agreement between the average strains measured on the reinforcement by the Demec gages and the strains measured by individual electrical resistance gages mounted on the bars is not as good, however. In the interpretation of the leakage specimens data only electrical resistance strain data is available, and hence some relationship between the average Demec strains and the average of the electrical resistance strains is desirable.

Figure 7.1 compares the Demec strains and electric resistance strain measurements for specimens 4 to 9. The data plotted is limited to the period between cracking as detected by both types of gages and strains of two times the yield strain of the mild steel reinforcement. Outside of these ranges the agreement of the strains is strongly influenced by the proximity of the embedded gages to the cracks. The best fit line to the data can be closely approximated by

$$\varepsilon_{Demec} = 0.0004 + 0.9\ (\varepsilon_{ERS}) \qquad (7.1)$$

where ε_{Demec} is the average strain measured by Demec gages and ε_{ERS} is the strain measured by embedded electrical resistance strain gages. This equation is plotted with a solid line in Fig. 7.1. The shaded band is extends 0.0005 above and below Eq. 7.1 and includes most of the data. Equation 7.1 has a mean ratio of test to calculated of 1.07 and coefficient of variation of 24.1 percent which shows the great difficulty in correlating strain data from varying sources.

7.2 BOSOR5 Analyses of Wall Segment Response

Reference (1) compares the test data and the BOSOR5 load deformation predictions for Segments 1 and 3 to 8. This comparison will not be repeated here. Segments 2 and 10 were similar to 1 in loading and construction and were not studied. Similarly, Segment 14 was similar to Segment 5 and was not analyzed. Segments 9 and 11 had lap splices and hence fell outside the scope of the BOSOR5 analysis. The two remaining

specimens, Segments 12 and 13 were subjected to axial loads applied eccentrically with respect to one or both axes. The BOSOR5 analysis is applicable to axi-symmetric structures and hence can only be applied to Segment 12 which has moments about only one axis.

Figures 7.2 and 7.3 compare the measured and predicted load-strain response of Segment 12 for vertical loading and for horizontal loading. The loads were applied in the ratio 2:1 vertical to horizontal. The vertical loads were nominally axially applied while the horizontal loads were applied eccentrically so that Face A was in tension and Face B was nominally held at zero strain.

As shown in Fig. 7.2, the BOSOR5 analysis closely approximated the vertical load-strain response of Face B and somewhat over-estimated the response of Face A. On the other hand, the agreement between the measured and predicted horizontal load-strain response is excellent for both faces. This confirms that the BOSOR5 analysis will give entirely acceptable predictions of load-strain response in the regions near the hinge and ring beam of the containment vessel.

8. SUMMARY

This report describes the fabrication and testing of a series of 14 reinforced and prestressed concrete specimens representing segments from the walls of nuclear containment structures. The test data and descriptions of the behavior observed in the tests are presented graphically. An Appendix presents the individual strain data in engineering units.

The analysis of the data is carried out in References (1), (2) and (3). Results of a BOSOR5 analysis of Segment 12 are presented in Chapter 7.

REFERENCES

1. Chitnuyanondh, L.; Rizkalla, S.; Murray, D.W.; and MacGregor, J.G.; "An Effective Uniaxial Tensile Stress-Strain Relationship for Prestressed Concrete", Structural Engineering Report No. 74, Department of Civil Engineering, University of Alberta, Edmonton, Canada, February 1979.

2. MacGregor, J.G.; Rizkalla, S.H.; and Simmonds, S.H.; "Cracking of Reinforced and Prestressed Concrete Wall Segments", Structural Engineering Report No. 82, Department of Civil Engineering, University of Alberta, Edmonton, Canada, November 1979.

3. Rizkalla, S.H.; Simmonds, S.H.; and MacGregor, J.G.; "Leakage Tests of Wall Segments of Reactor Containments", Structural Engineering Report No. 80, Department of Civil Engineering, University of Alberta, Edmonton, Canada, October 1979.

4. ACI Committee 318, "Building Code Reuquirements for Reinforced Concrete, ACI-318-77", American Concrete Institute, Detroit, 1977.

5. Libby, J.R.; "Modern Prestressed Concrete", Van Nostrand-Reinhold, 1977.

6. Mirza, S.A.; Hatzinikolas, M.; and MacGregor, J.G.; "Statistical Descriptions of the Strength of Concrete", Journal of the Structural Divisions, Proceedings of American Society of Civil Engineers, Vol. 105, No. ST6, June 1979, 1021-1038.

7. Kupfer, H.; Hilsdorf, H.K.; and Rüsch, H.; "Behavior of Concrete Under Biaxial Stresses", Journal of American Concrete Institute, Vol. 66, No. 8, Aug. 1969, pp. 656-666.

Table 2.1 - Overview of Variables Considered in Wall Segment Tests

Specimen*	Prestressed	Non-Prestressed Reinforcement per Layer, 1**	Min. Concrete Cover in.	Loading Ratio H/V	Applied Moment	Thickness in.	Lap Splices
1	two	10 #3 @ 3 in.	0.5	1:2		10.5	
2	two	10 #3 @ 3 in.	0.5	1:2		10.5	
3	two	10 #3 @ 3 in.	0.5	1:1		10.5	
4	none	8 #4 @ 4 in.	0.5	1:1		10.5	
5	one***	10 #3 @ 3 in.	0.5	1:0		10.5	
6	one***	8 #4 @ 4 in.	0.5	1:0		10.5	
7	none	6 #6 @ 6 in.	0.75	1:1		15.75	
8	two	10 #3 @ 3 in.	1.25	1:2		10.5	
9	two	10 #3 @ 3 in.	0.5	1:2		10.5	yes
11	two	10 #3 @ 3 in.	0.5	1:2		10.5	yes
12	two	10 #3 @ 3 in.	0.5	1:2	yes	10.5	
13	two	10 #3 @ 3 in.	0.5	1:2	yes	10.5	

* Two additional tests involving air leakage (Specimens 10 and 14) are presented in Reference (3).

** Each face of the specimen had one such layer in each direction.

*** Three tendon direction only, other tendons omitted.

Table 2.2 Prestress in Tendons

Specimen	Vertical Tendons (4 Tendon Direction)			Vertical Tendons (3 Tendon Direction)		
	Initial	Effective after Losses		Initial	Effective after Losses	
	Stress, ksi	Stress, ksi	Force, ksi	Stress, ksi	Stress, ksi	Force, kips
1	153.5	135.1	226.3	134.0	123.3	132.7
2	151.6	133.4	223.5	134.9	124.1	133.6
3	153.3	134.9	226.0	135.2	124.3	133.9
4	-	-	-	-	-	-
5	-	-	-	132.0	121.4	130.8
6	-	-	-	138.0	126.9	136.7
7	-	-	-	-	-	-
8	154.0	135.6	227.1	139.9	128.7	138.6
9	150.6	132.6	222.1	134.3	123.6	133.1
10	152.4	134.1	225.3	134.0	123.3	132.8
11	151.5	133.3	223.3	135.0	124.2	133.8
12	152.8	134.5	225.2	135.8	124.9	134.6
13	152.4	134.1	225.3	134.0	123.3	133.1
14	-	-	-	134.0	123.3	133.1

Table 3.1 Strengths and Modulus of Elasticity of Concrete

Specimen No.	Age At Prestress Days	Age At Test Days	From Cylinder Tests					From Specimen	
			Compressive Strength psi	Split Tensile Strength psi	$f_t/\sqrt{f'_c}$	Modulus of Elasticity 10^3 ksi	$E_c/\sqrt{f'_c}$	Modulus of Elasticity 10^3 ksi	$E_c/\sqrt{f'_c}$
1	30	84	5093	490	6.87	-	-	3.76	52.7
2	30	92	4456	436	6.53	-	-	3.92	58
3	35	99	5690	426	5.65	-	-	3.22	42
4	-	109	5590	536	7.17	3.23	43.2	3.47	46.4
5	63	109	5690	444	5.89	4.22	55.9	3.51	46.5
6	57	127	4540	325	4.82	3.53	52.4	3.37	50.0
7	-	104	2390 (A)* 3720 (B)*	312 (A) 365 (B)	5.44 (A) 5.99 (B)	-	-	4.05	68.5
8	42	92	4920	424	6.04	3.82	54.5	5.56	50.8
9	76	159	3920	437	6.98	3.08	49.2	3.57	57.0
11	-	186	4920	411	5.86	3.10	44.2	4.11	70.1
12	131	372	5930	486	6.31	3.52	45.7	-	-
13	63	391	6130	566	7.23	-	-	-	-

* Specimen 7 was made from two batches, one on face A, and the other on face B.

Table 6.1 Load and Tensile Stress at First Cracking

Segment	Vertical Load at First Horizontal Cracking, kips		Horizontal Load at First Vertical Cracking kips		Tensile Stress at First Cracking, psi
	Face A	Face B	Face A	Face B	
1	300.0	325.0	194.0	179.3	307
2	287.5	300.0	183.5	200.0	174
3	350.0	300	206.8	206.8	229
4	80.3	60	60	60	259
5	--	--	280.2	255.5	389
6	--	--	185.0	196.0	223
7	75.1	100.0	82.1	82.1	168
8	350.0	350.0	175.0	175.0	321
9	350.0	300.0	181.8	181.8	221
10	350	350	187	187	321
11	284	300	175	175	170
12	300	340	170	--	292
13	--	175	--	150	300
14	--	--	225	225	289

The reported tensile stresses correspond to the underlined loads.

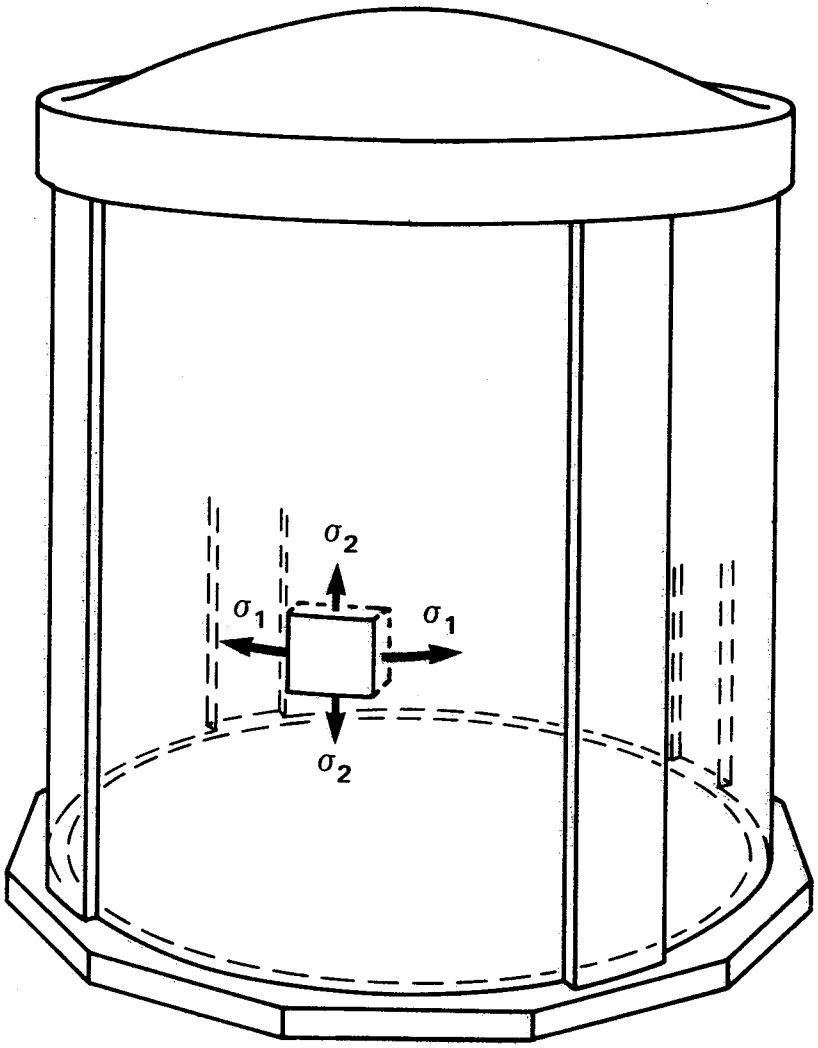

(a) Element in Prototype

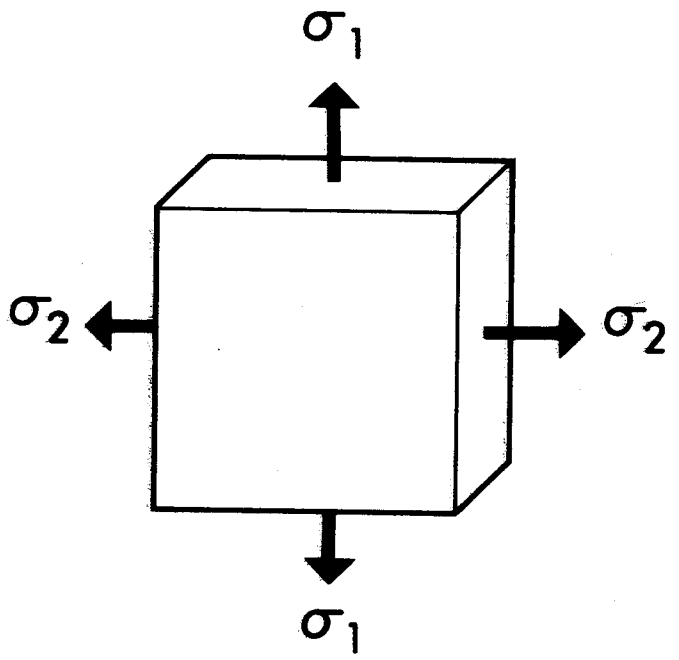

(b) Wall Segment Specimen

Fig. 1.1 Relationship between Specimen and Prototype

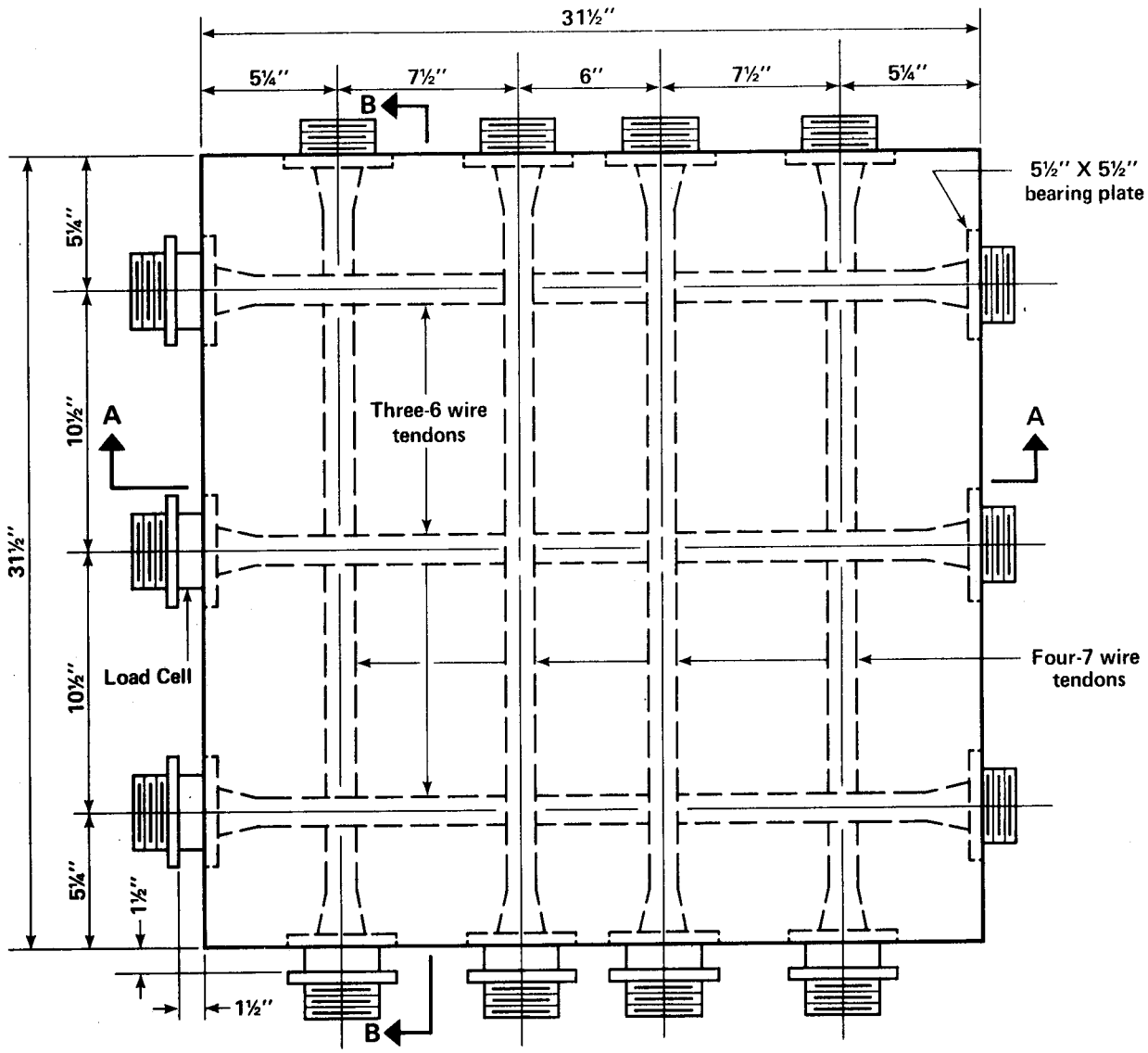

Figure 2.1 Side View of Wall Segment Specimen

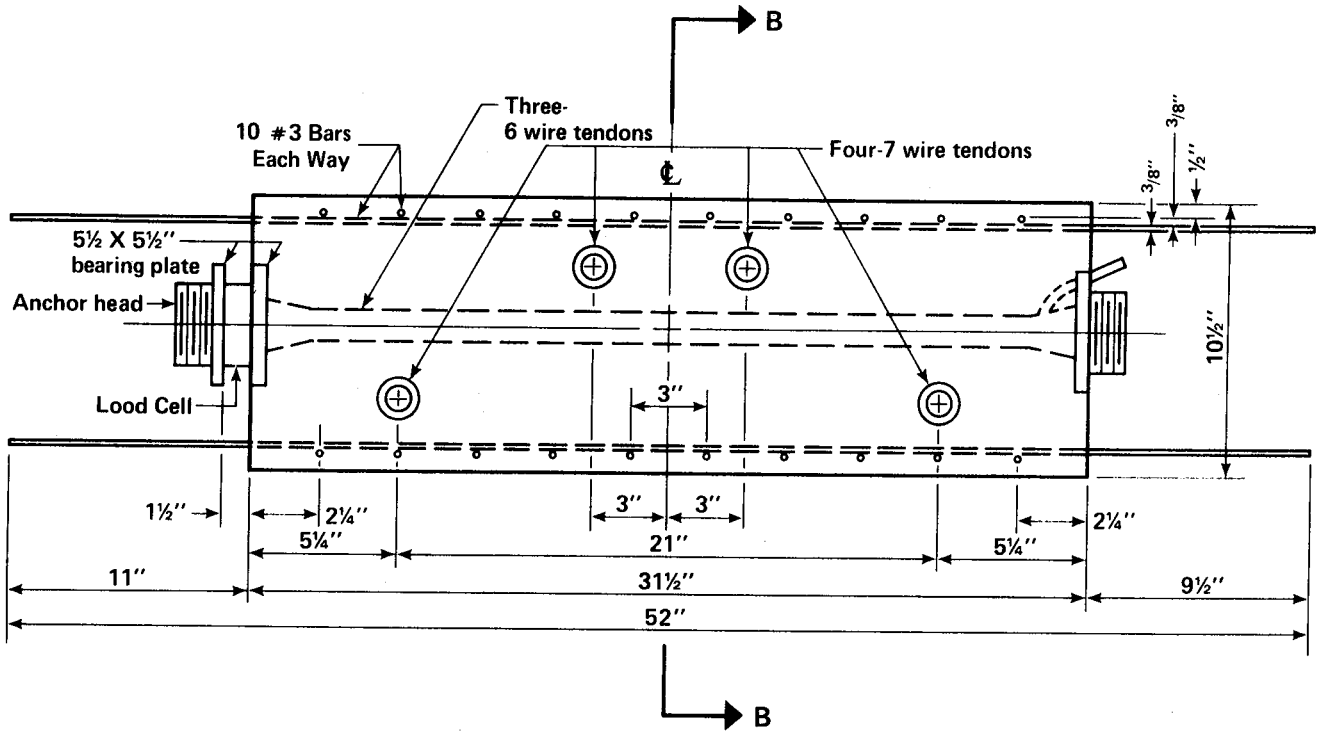

Section A-A

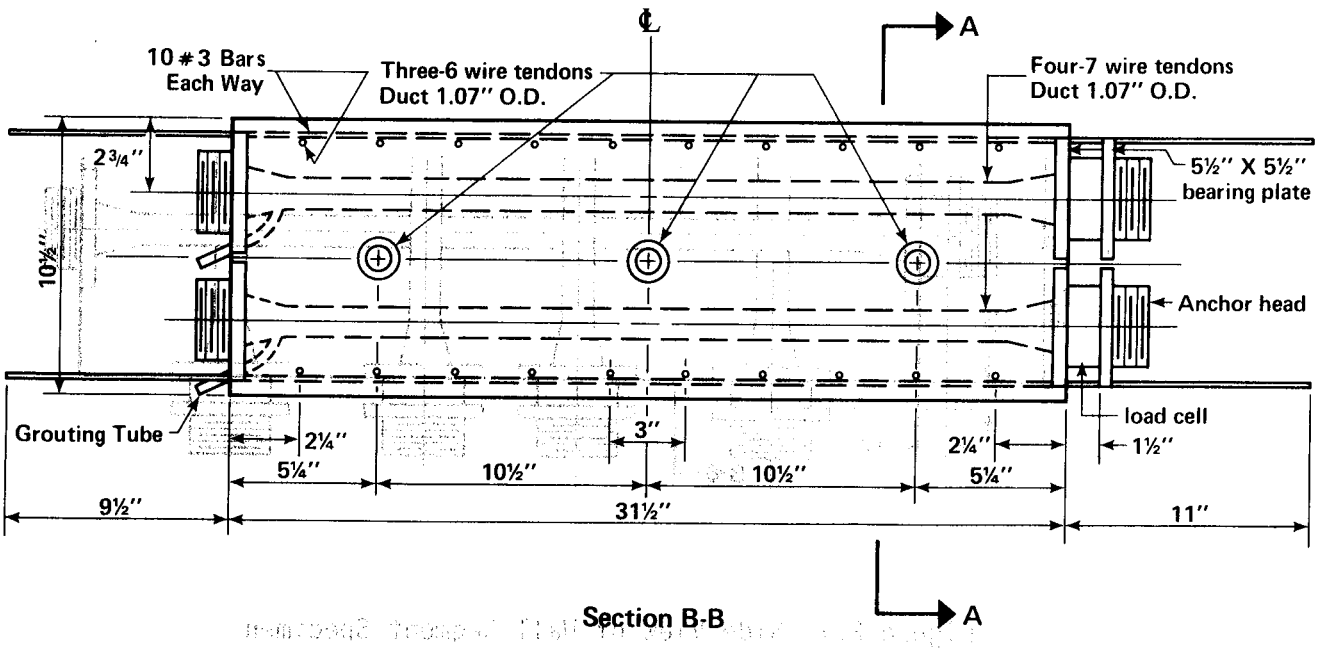

Section B-B

Figure 2.2 Sections Through Wall Segment Specimen

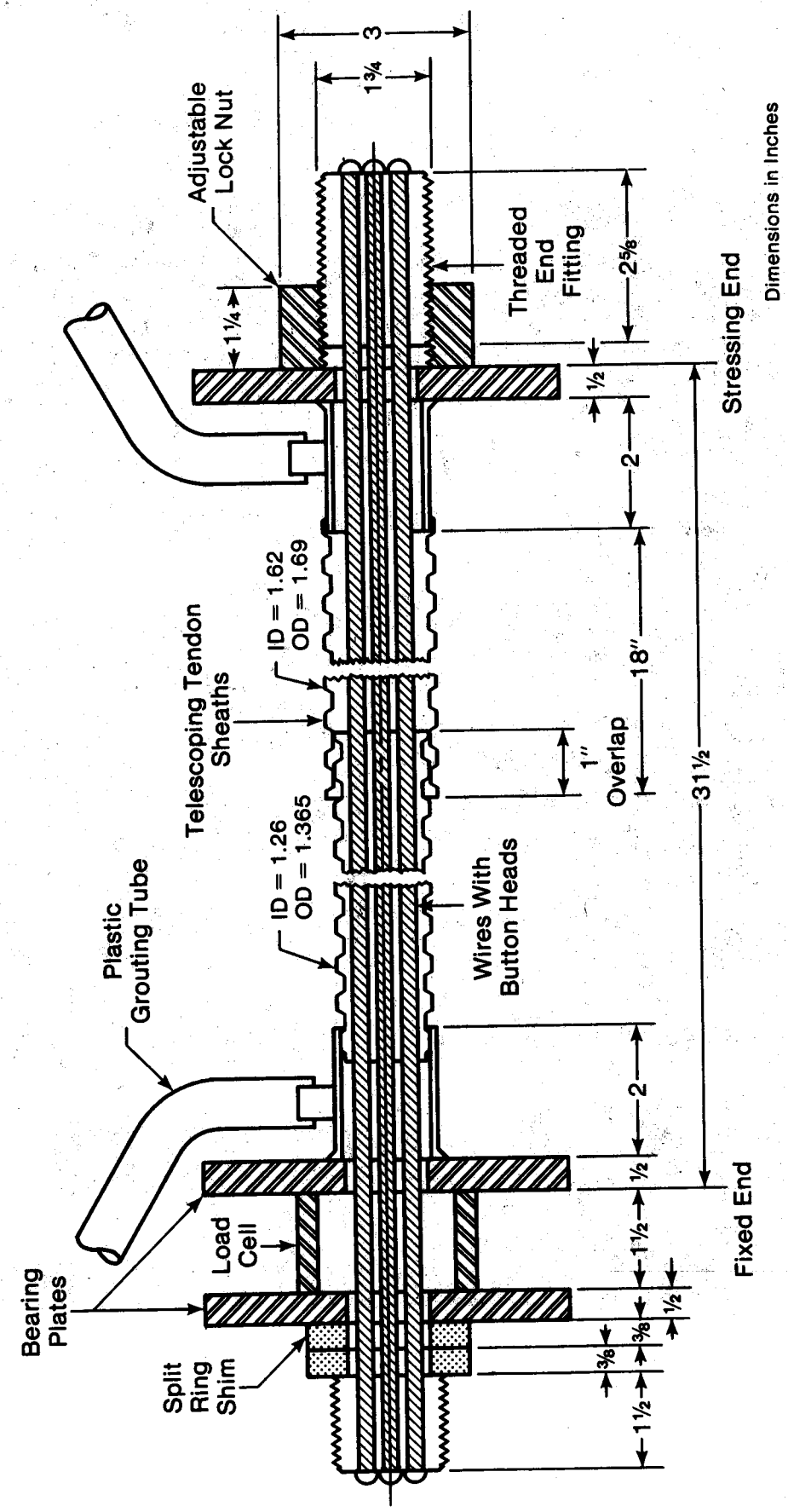

Figure 2.3 Prestressing Tendon Assembly

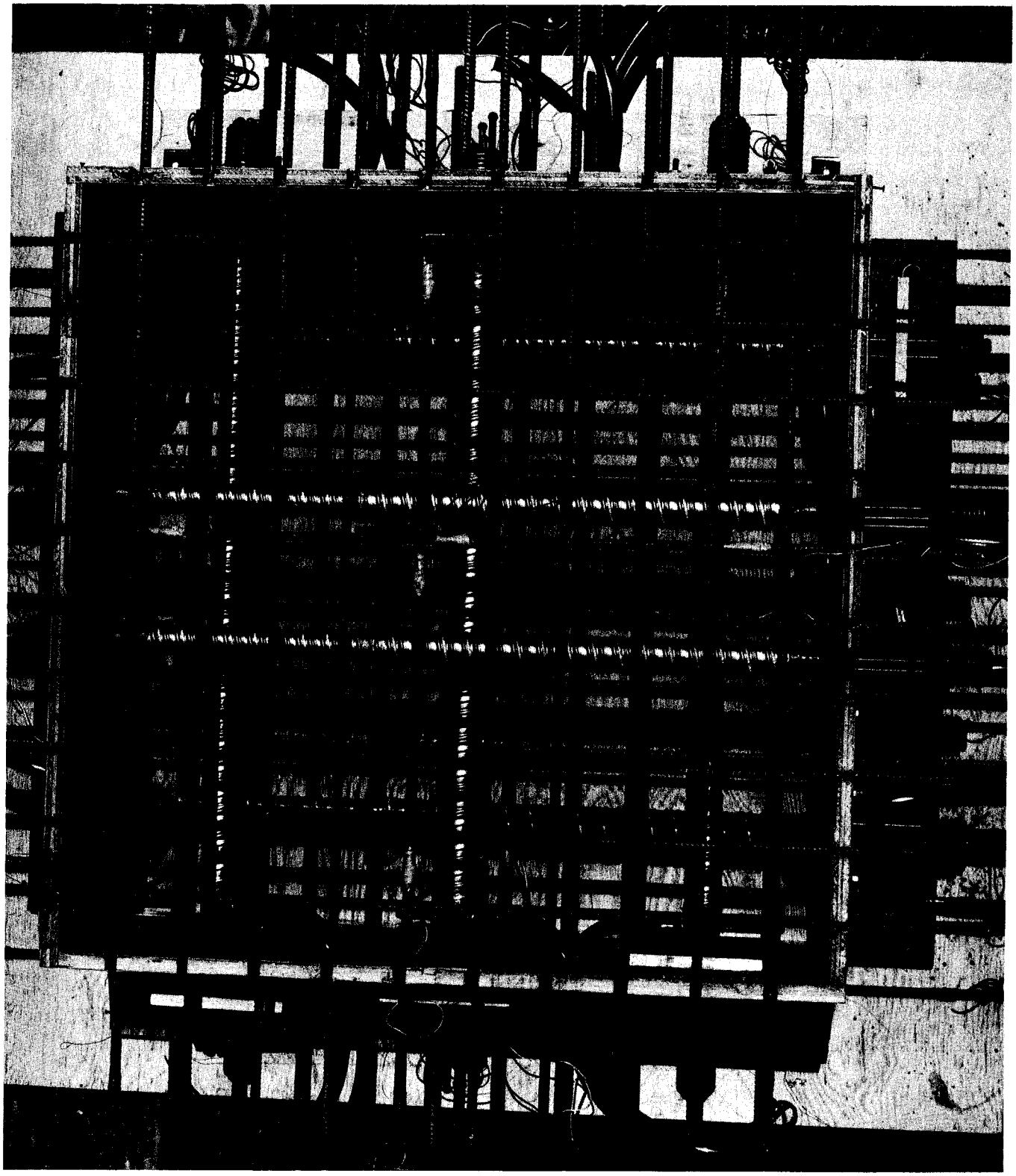

Figure 2.4 Specimen 2 Before Concreting

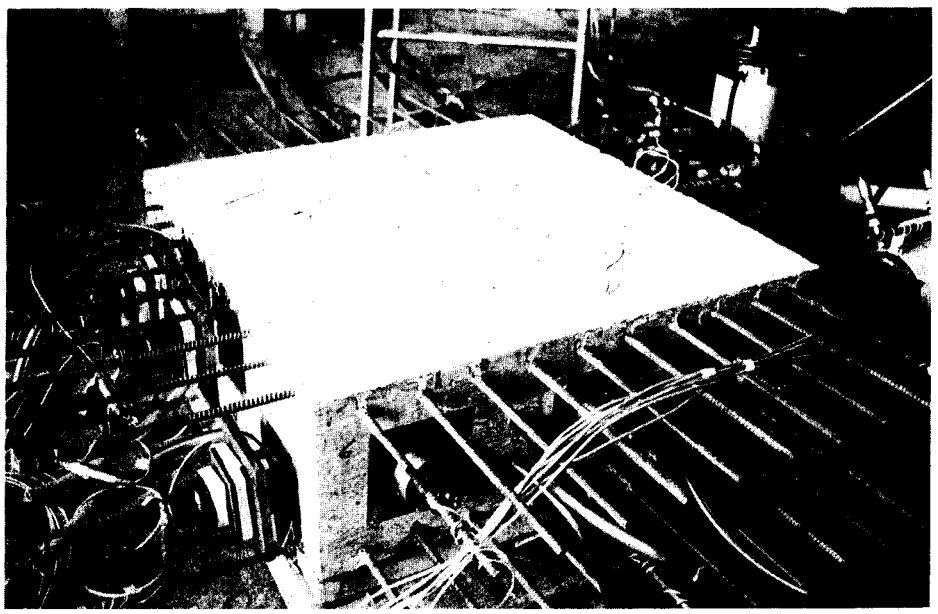

Figure 2.5 Specimen 2 After Prestressing

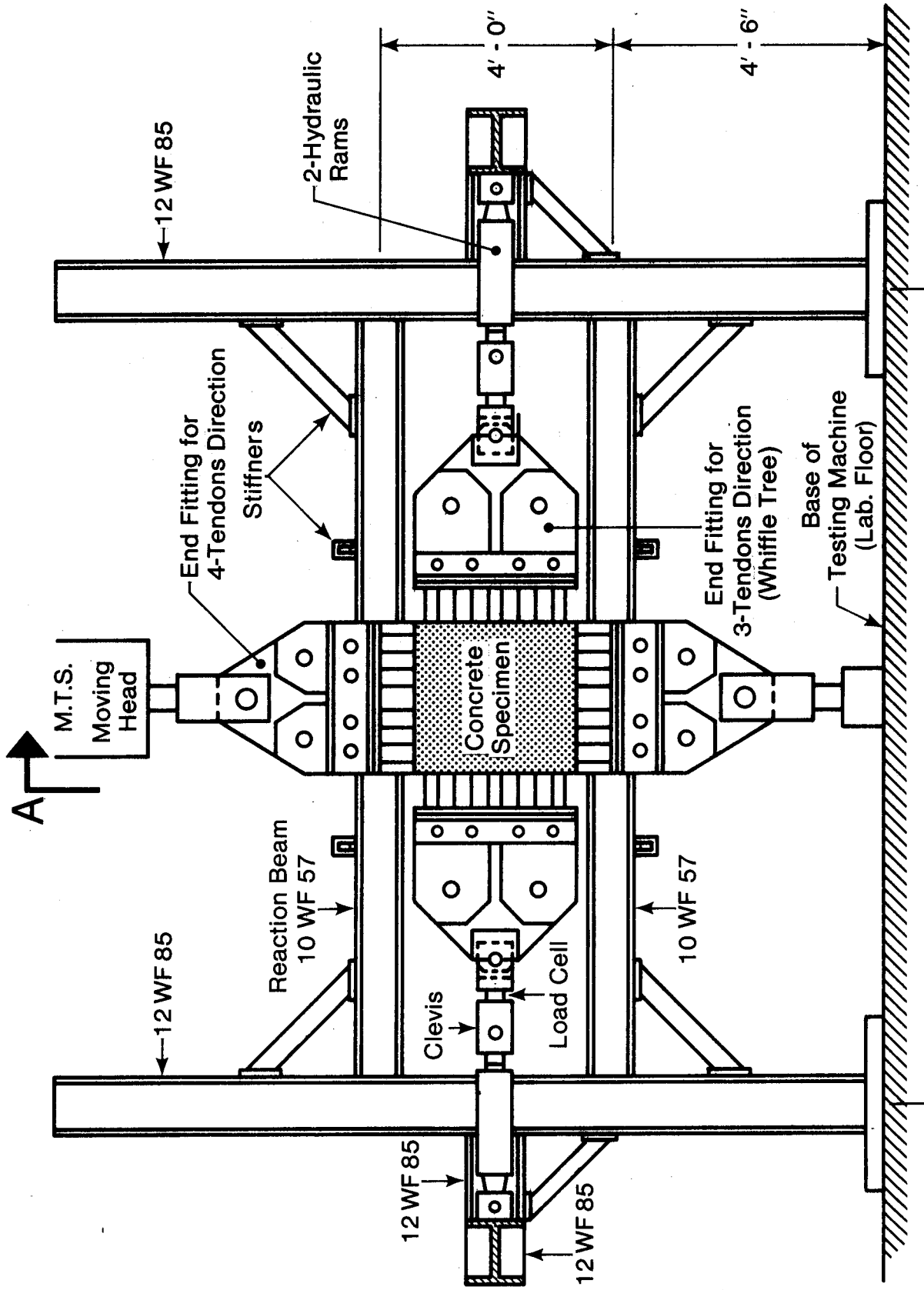

Figure 4.1 East-West Section Through Loading Frame

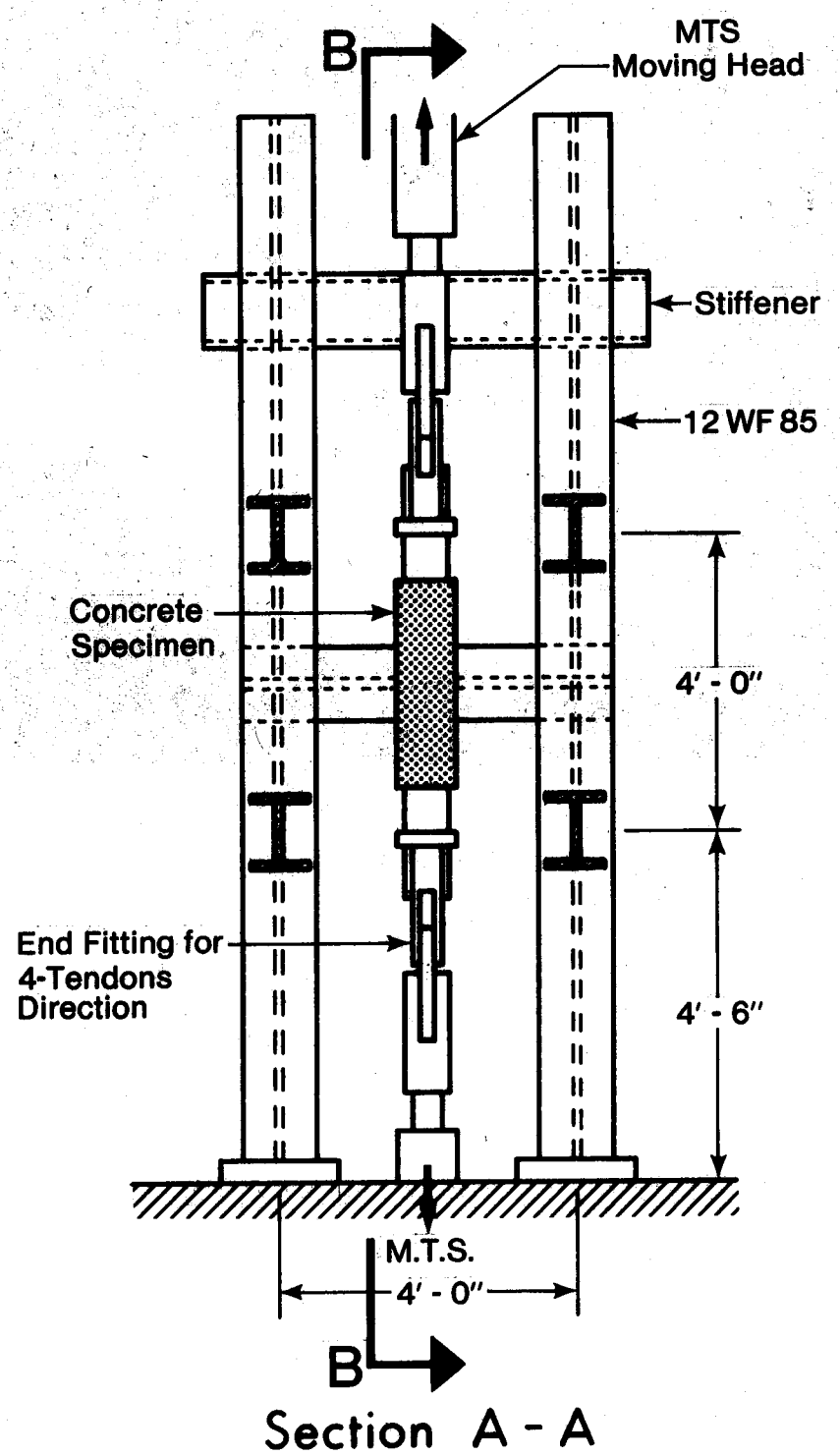

Figure 4.2 North-South Section Through Loading Frame

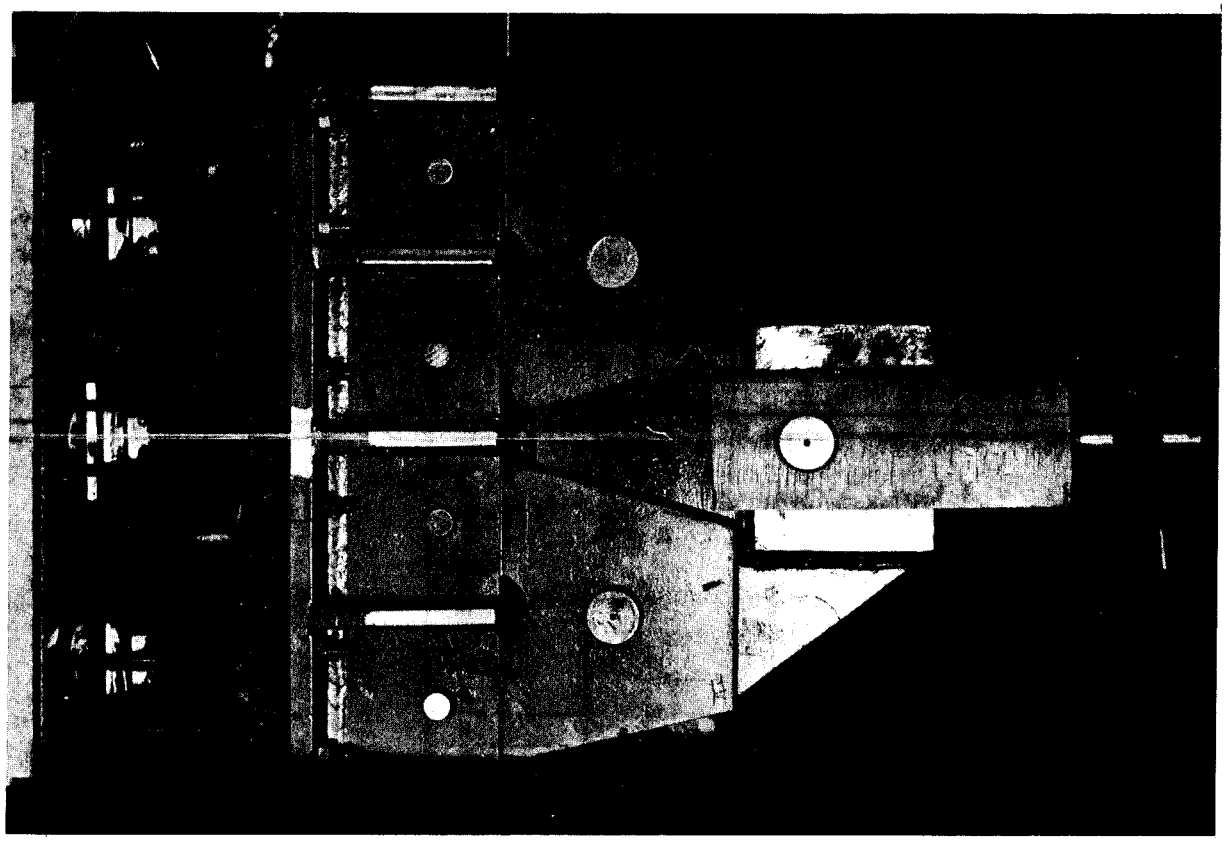

Figure 4.3 Horizontal Load Whiffletree

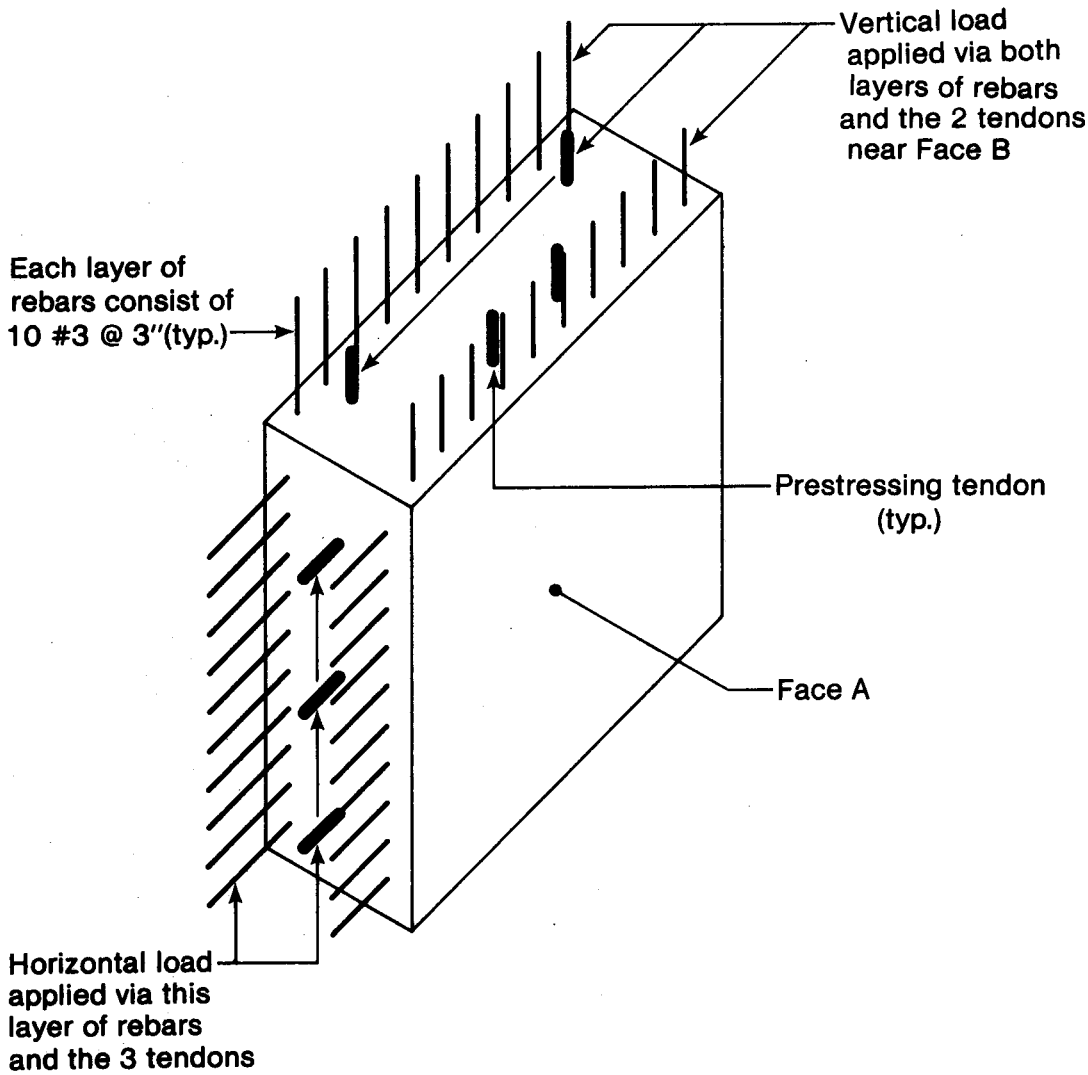

Figure 4.4 Eccentric Loading on Specimen 13

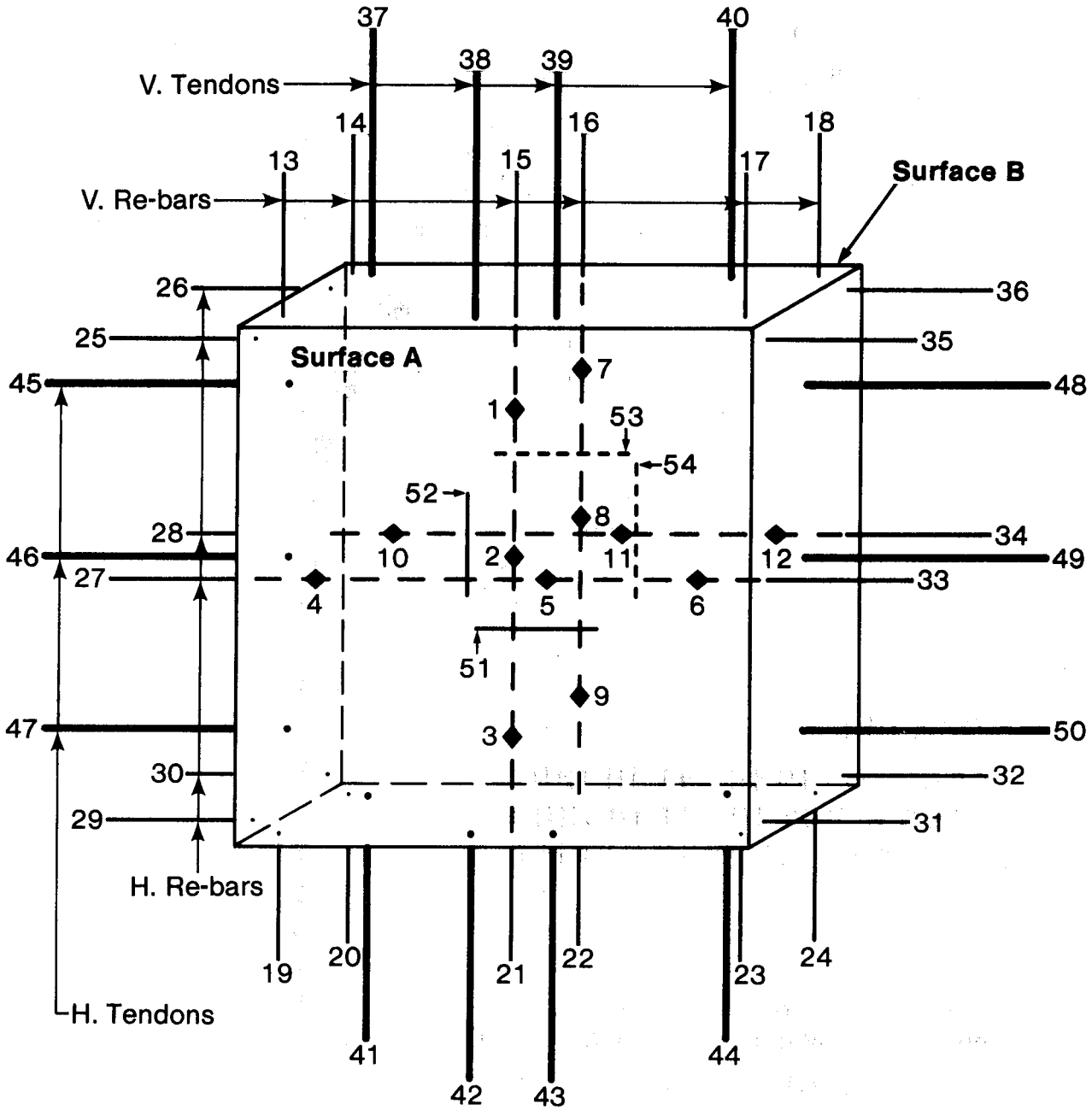

55 West L.C.
56 East L.C.
57 Top Trans.
58 Bot. Trans.
59 West Trans.
60 East Trans.
61 M.T.S. LD
62 M.T.S. ST

◆◆ Embeded Steel Electric Strain Gauges

Concrete Electric Strain Gauges

Figure 5.1 Location of Electrical Strain Gages and Transducers, Specimen 8

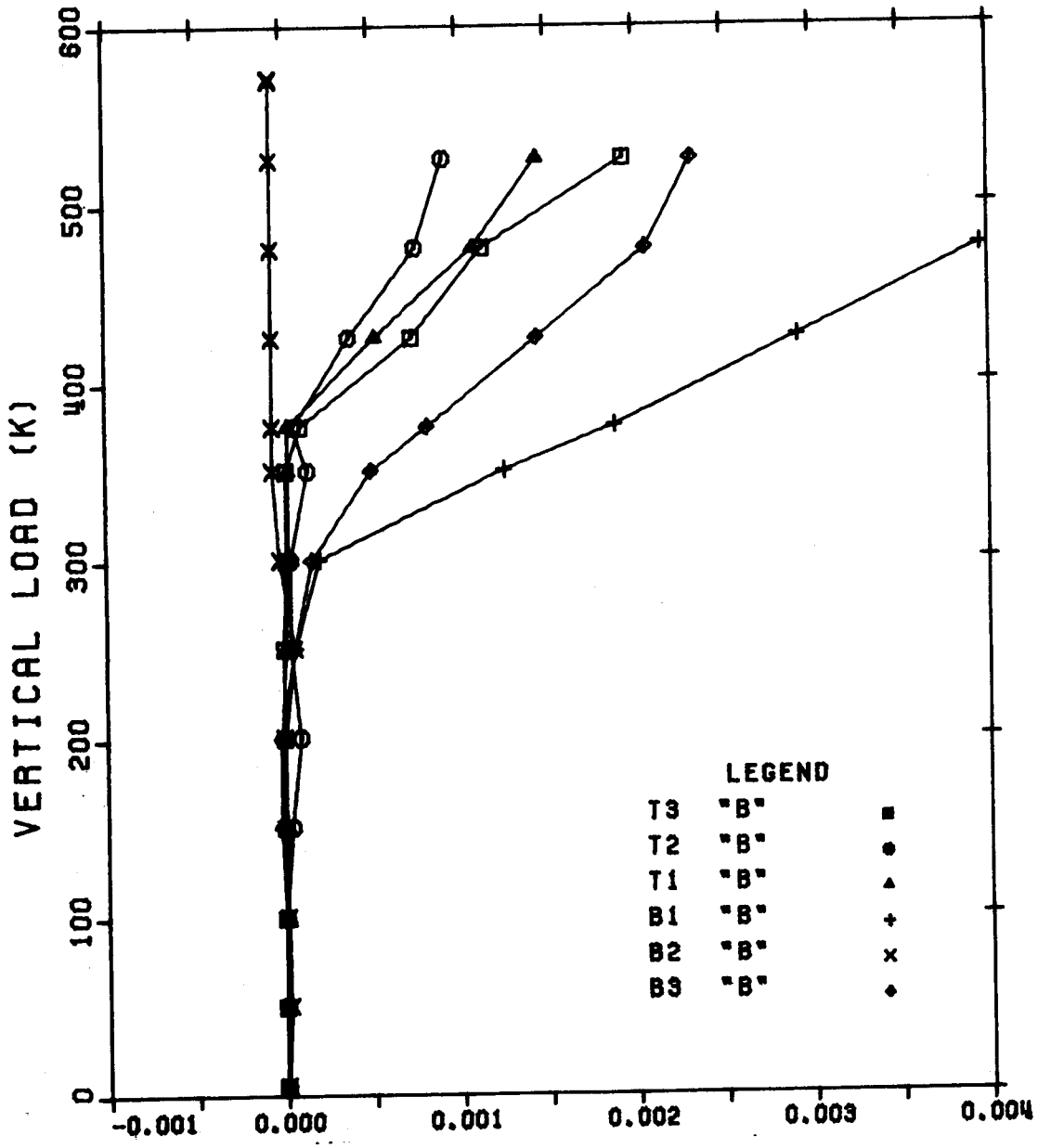

Figure 5.2 Load-Strain Curves for Face B, Specimen 8

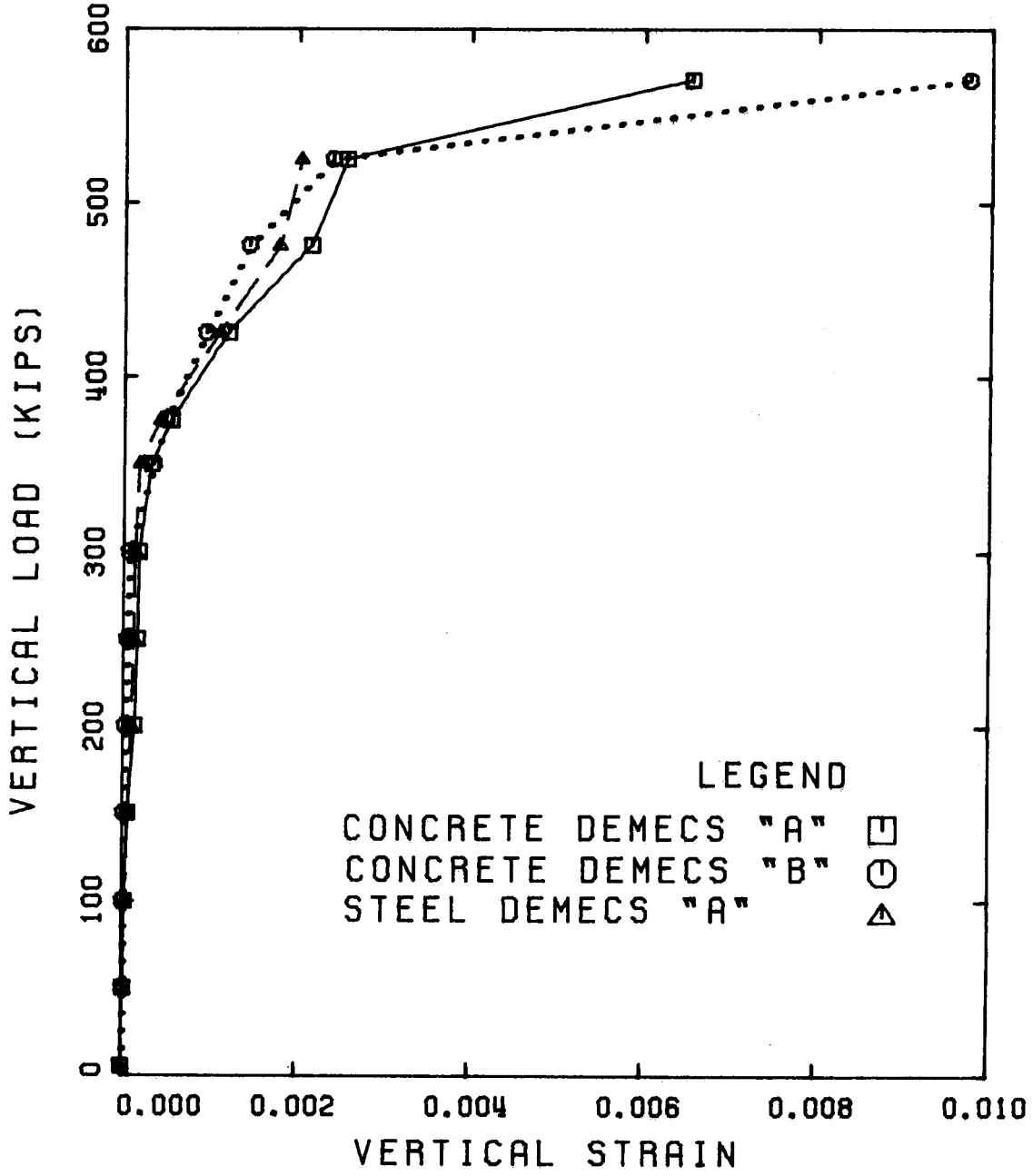

Figure 5.3 Load-Average Strain Curves, Specimen 8

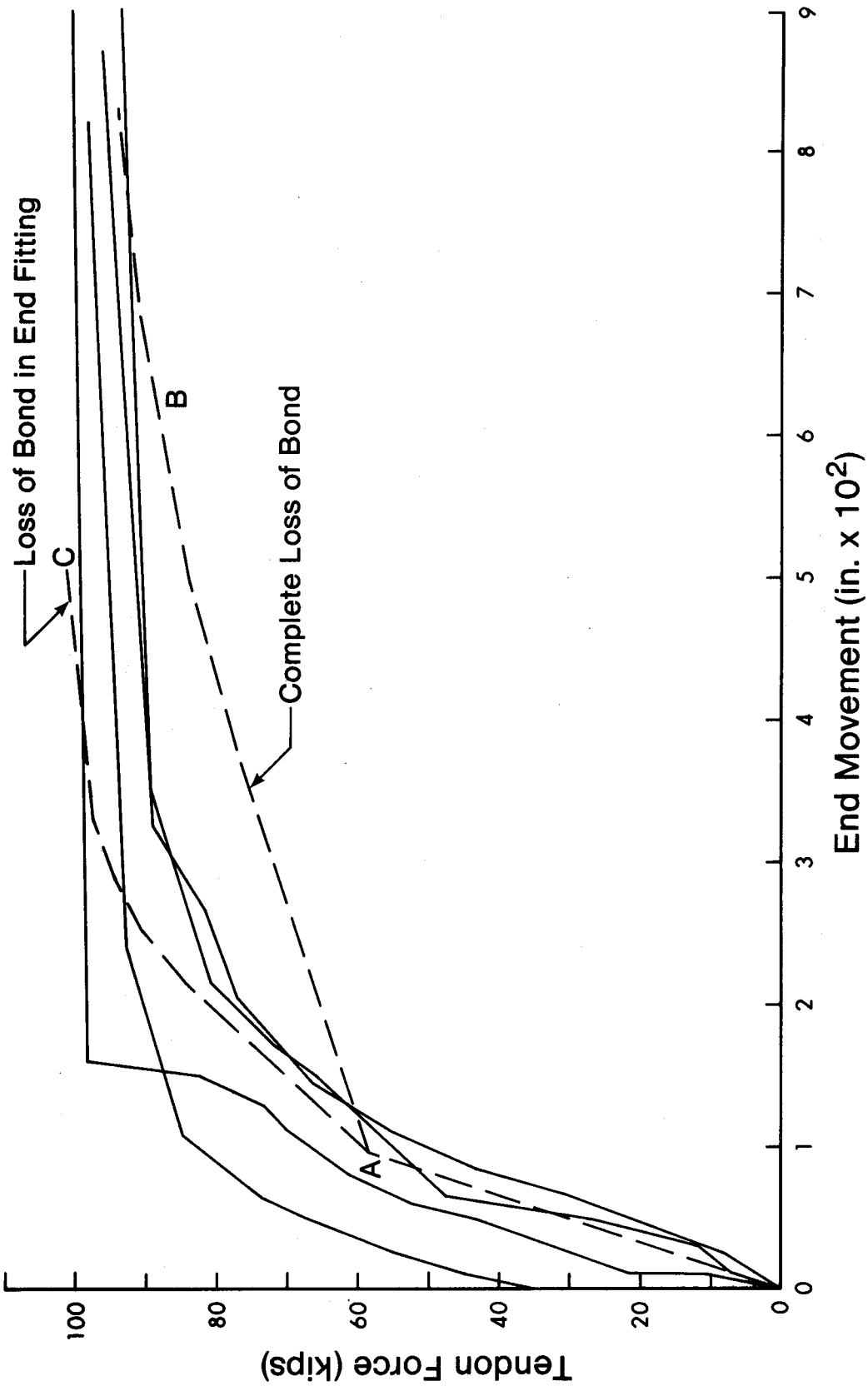

Figure 5.4 Tendon Force vs Movement of End of Tendon, Specimen 8, 4 Tendon Direction

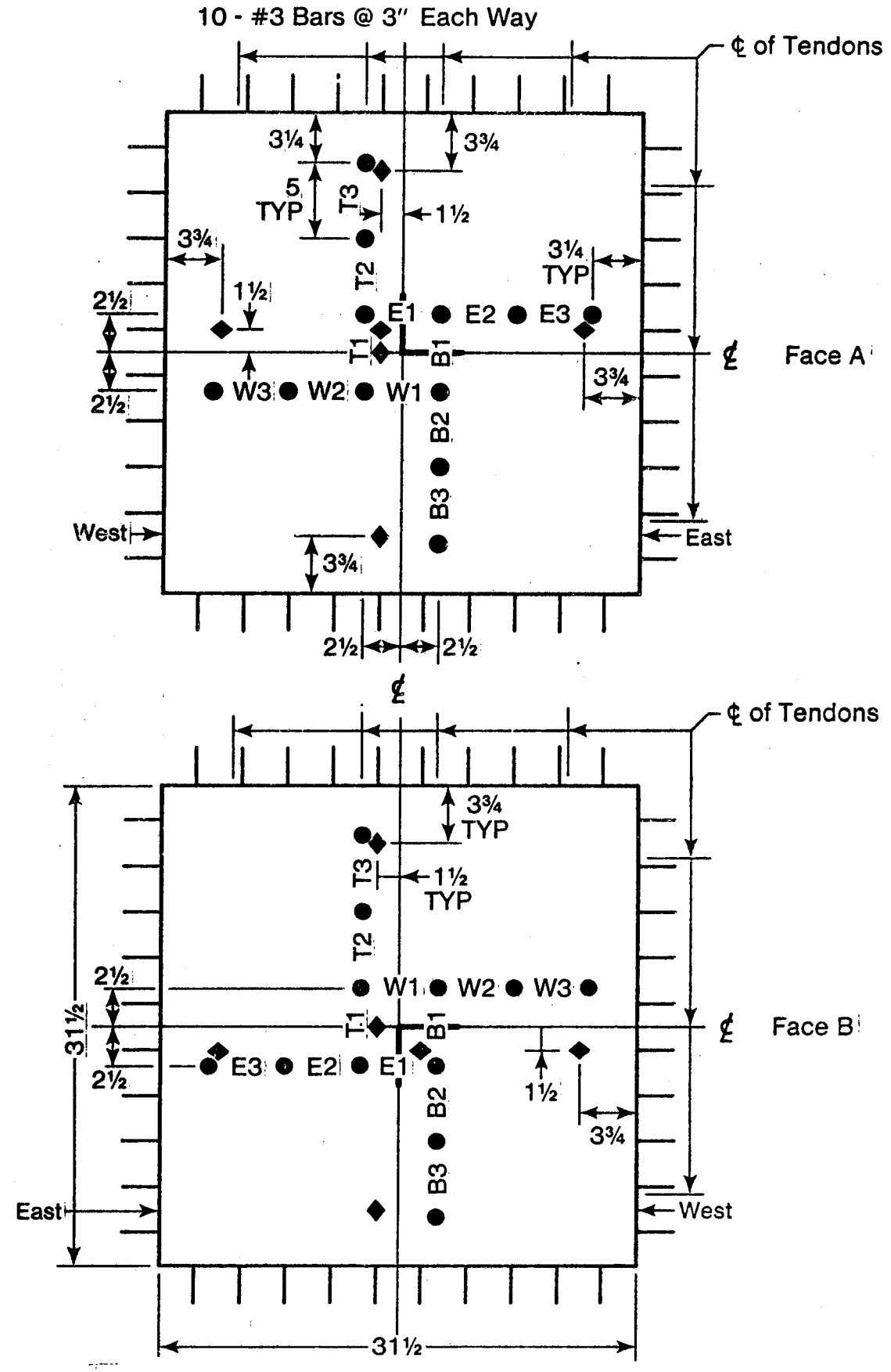

Fig. 6.1.1 Location of Strain Measurements, Segment 1

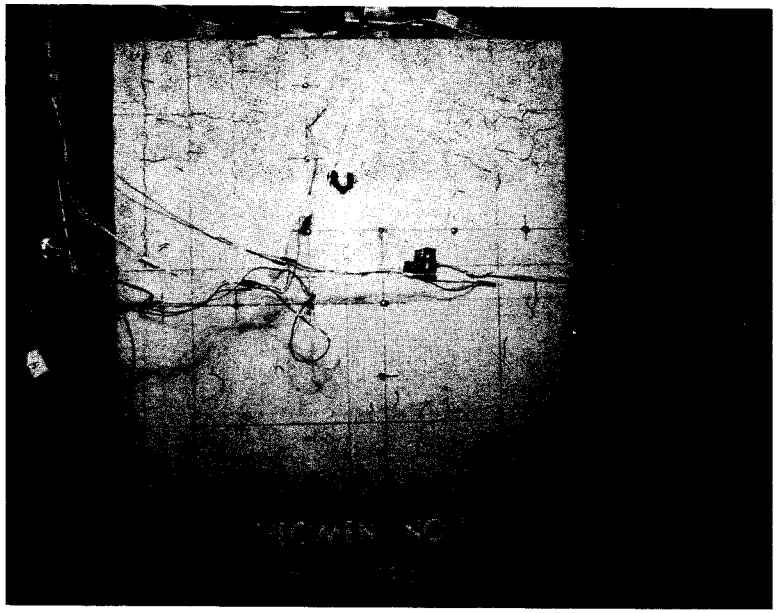

(a) Face A Before Loading

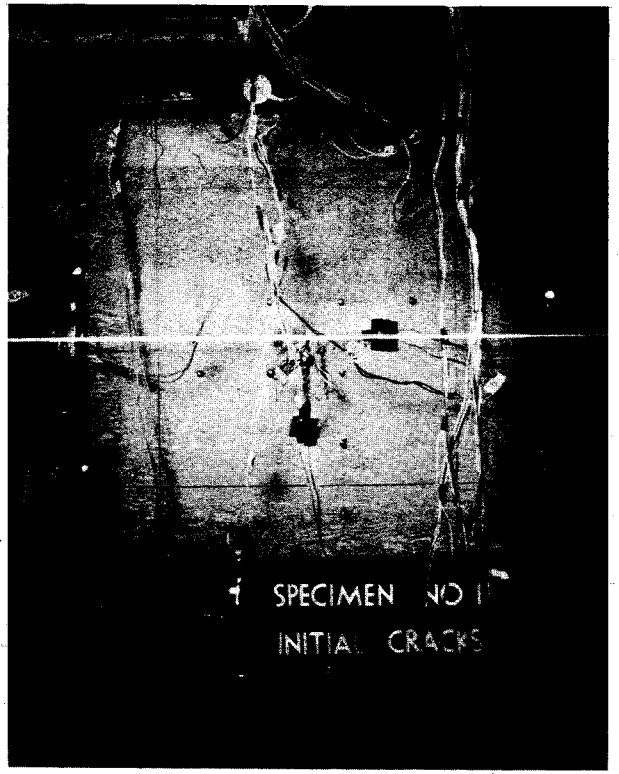

(b) Face B Before Loading

Figure 6.1.2 Development of Cracking in Segment 1

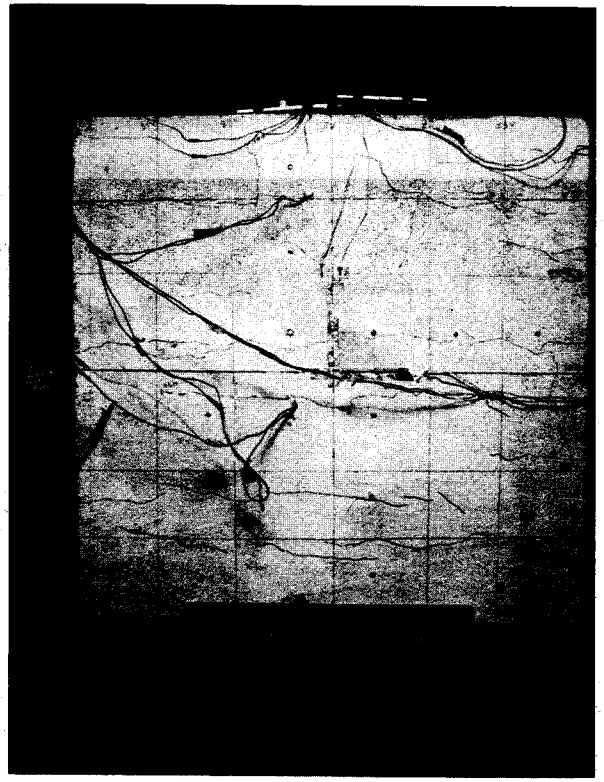

(c) Face A at Onset of Horizontal Cracking

(d) Face B at Onset of Horizontal Cracking

Figure 6.1.2 Development of Cracking in Segment 1

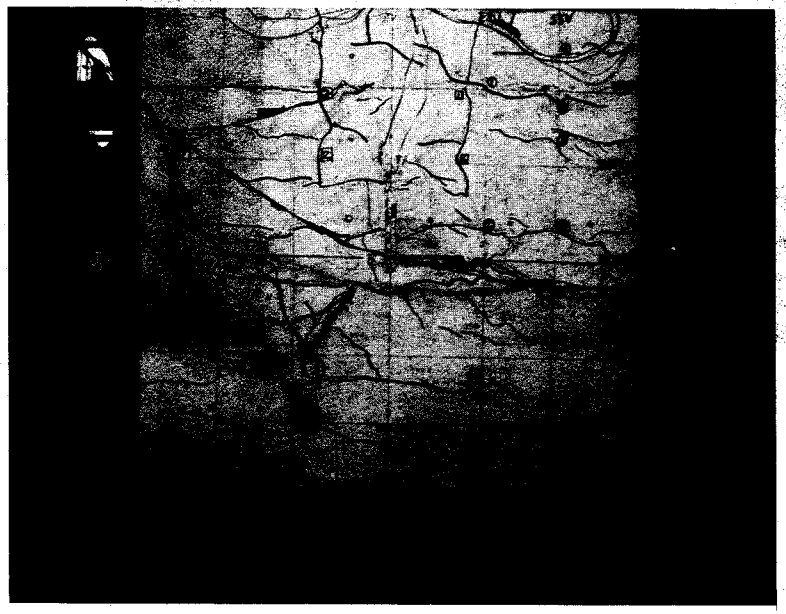

(e) Face A of Vertical Cracking

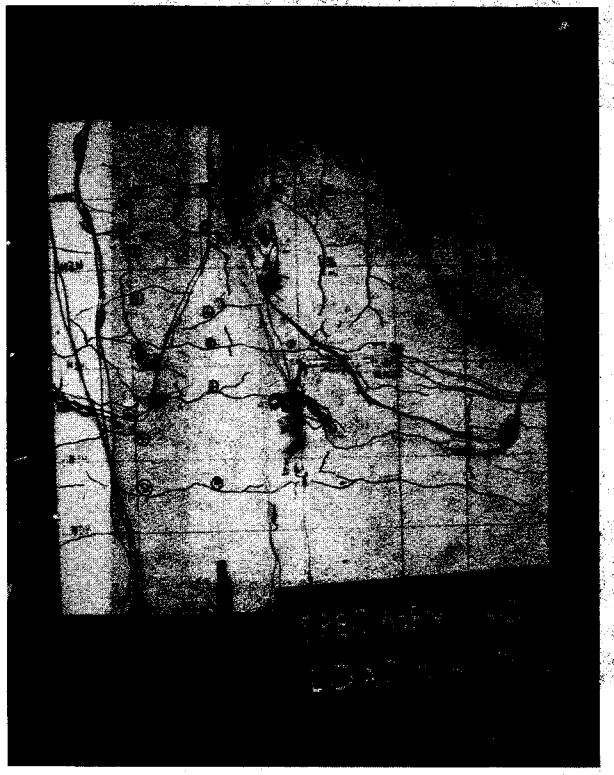

(f) Face B of Vertical Cracking

Figure 6.1.2 Development of Cracking in Segment 1

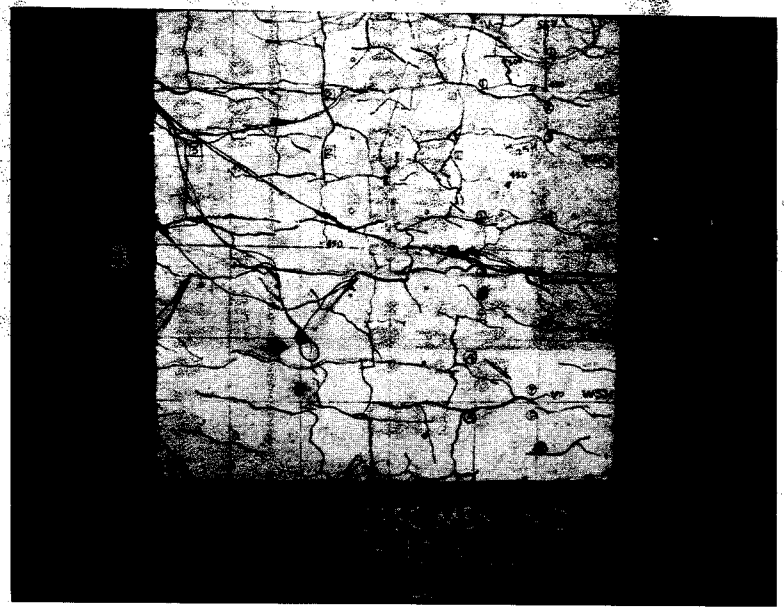

(g) Face A at End of Test

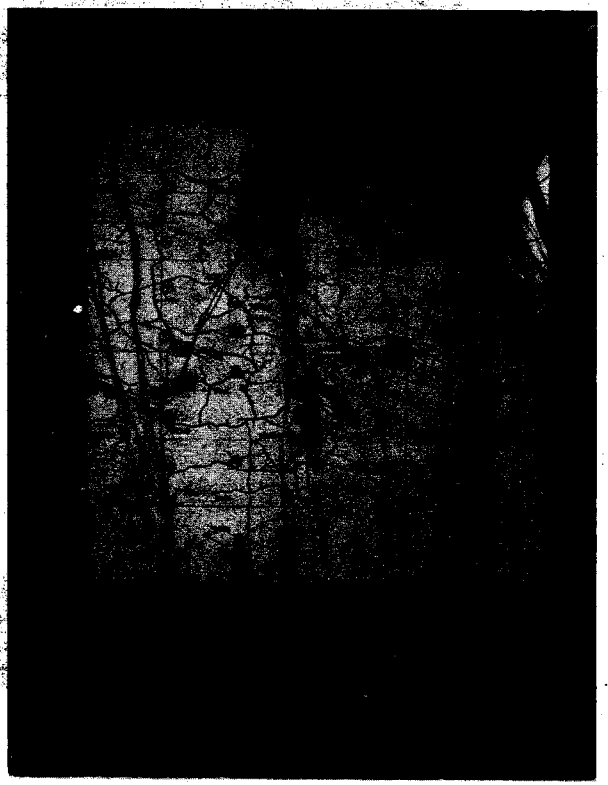

(h) Face B at End of Test

Figure 6.1.2 Development of Cracking in Segment 1

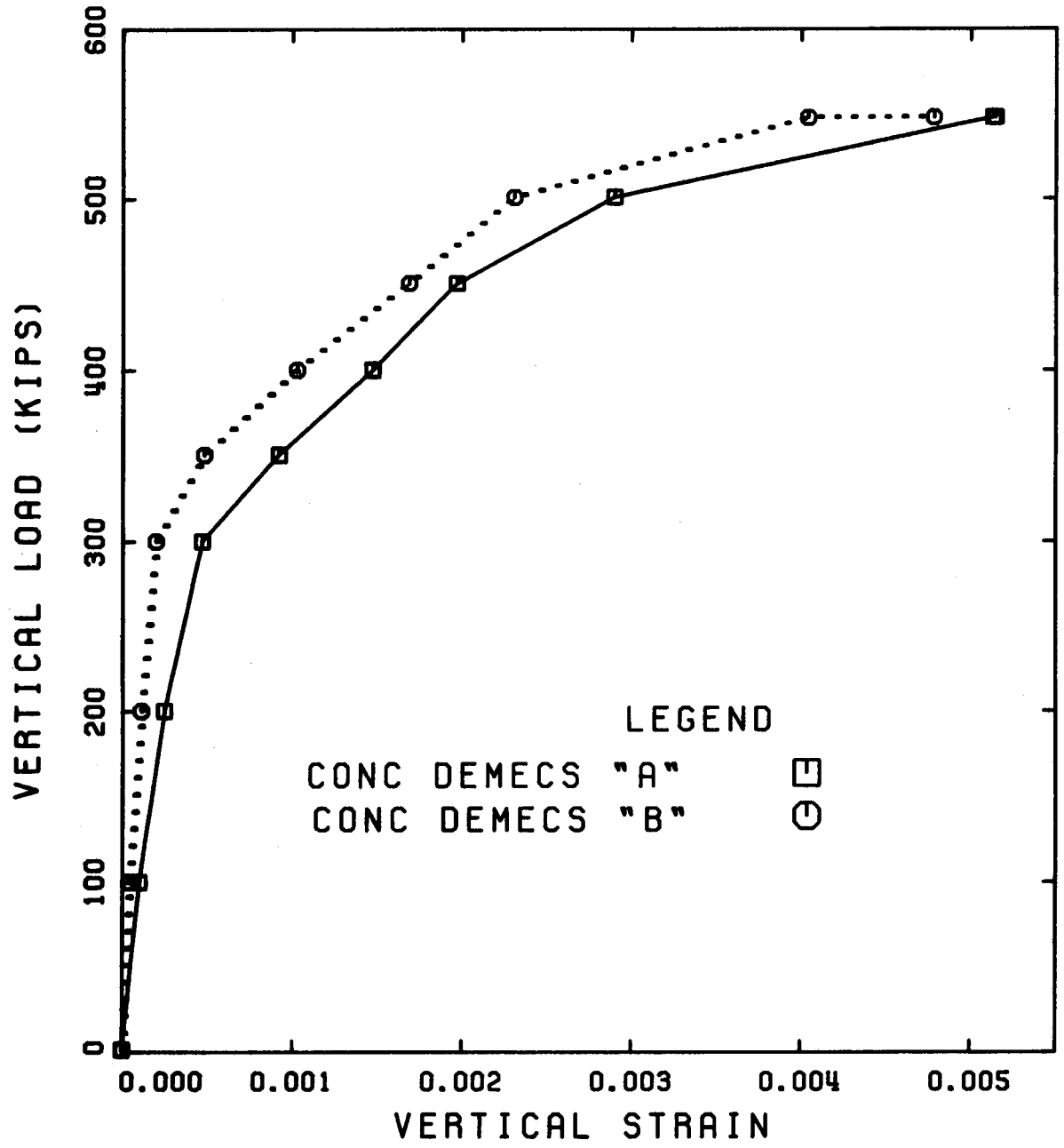

(a) Vertical Direction

Figure 6.1.3 Load-Average Strain Curves, Segment 1

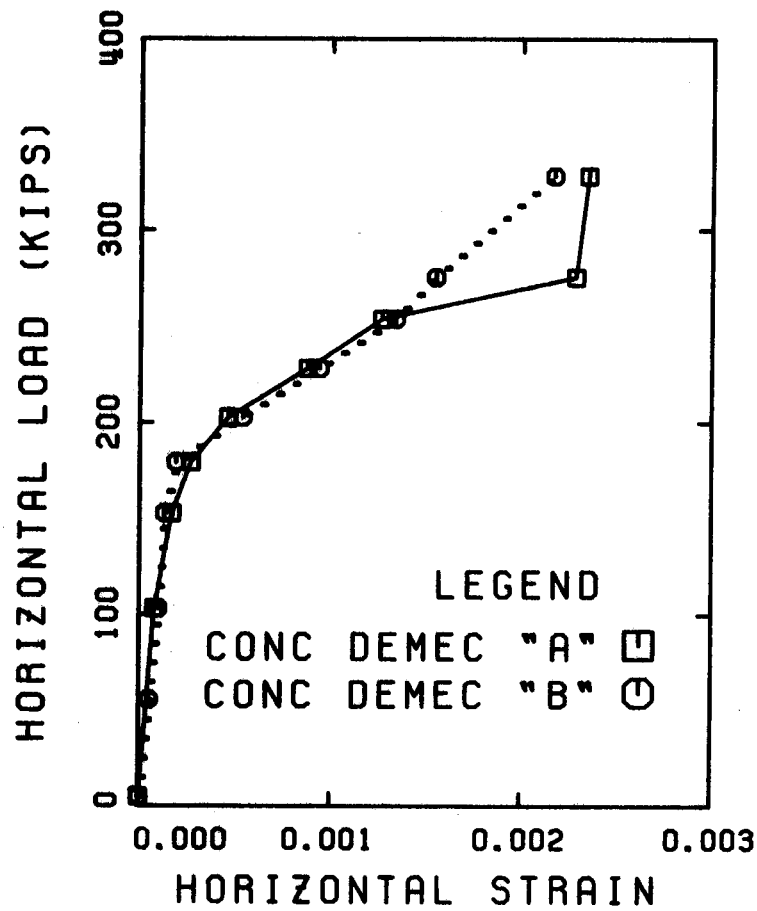

(b) Horizontal Direction

Figure 6.1.3 Load-Average Strain Curves, Segment 1

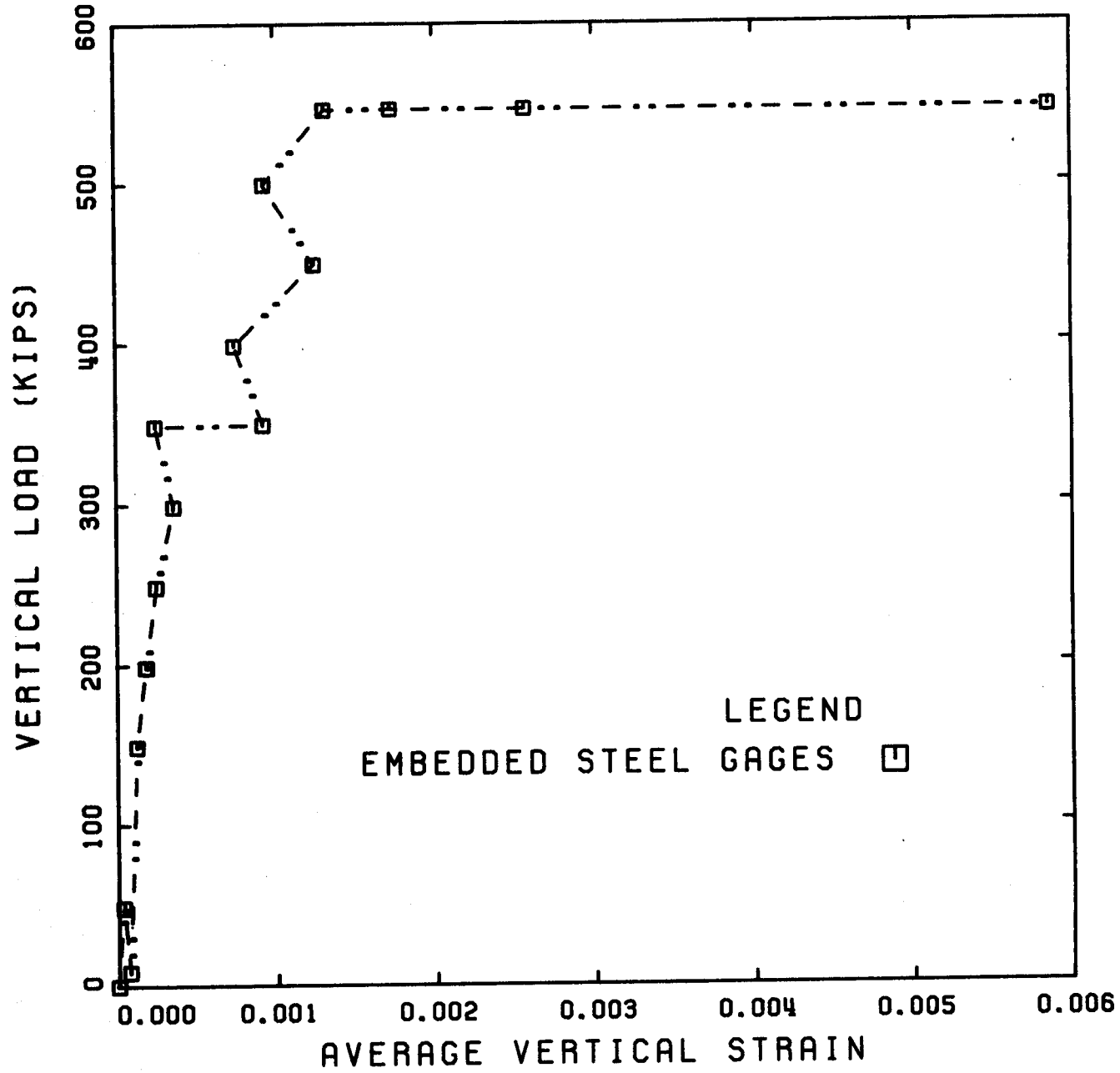

(a) Vertical Direction

Figure 6.1.4 - Load - Average Steel Strain Curves, Segment 1

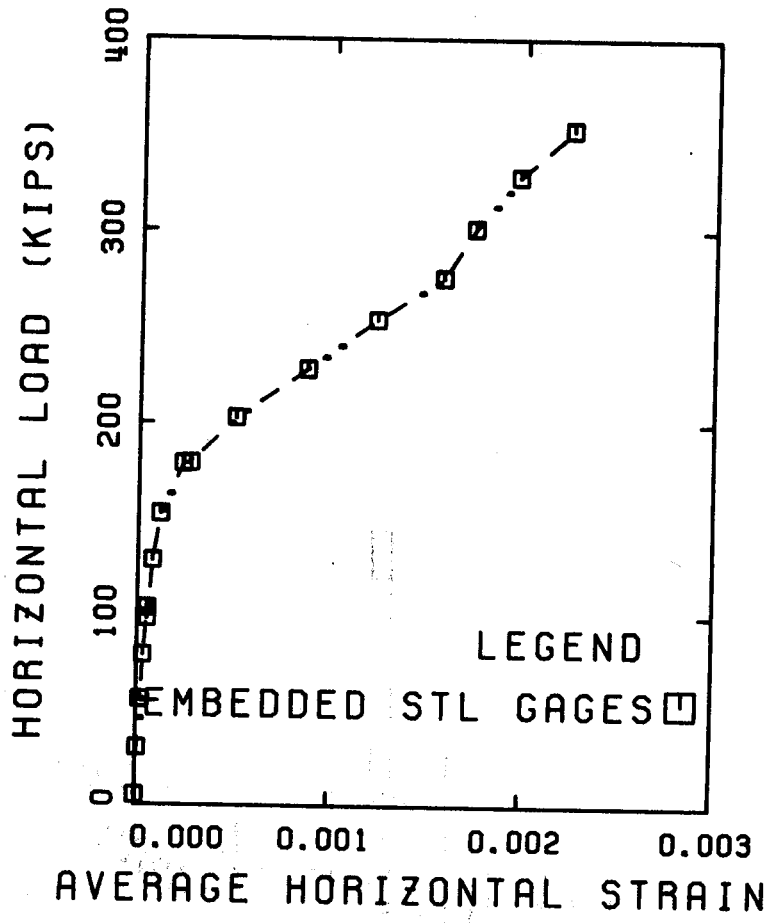

(b) Horizontal Direction

Figure 6.1.4 Load - Average Steel Strain Curves, Segment 1

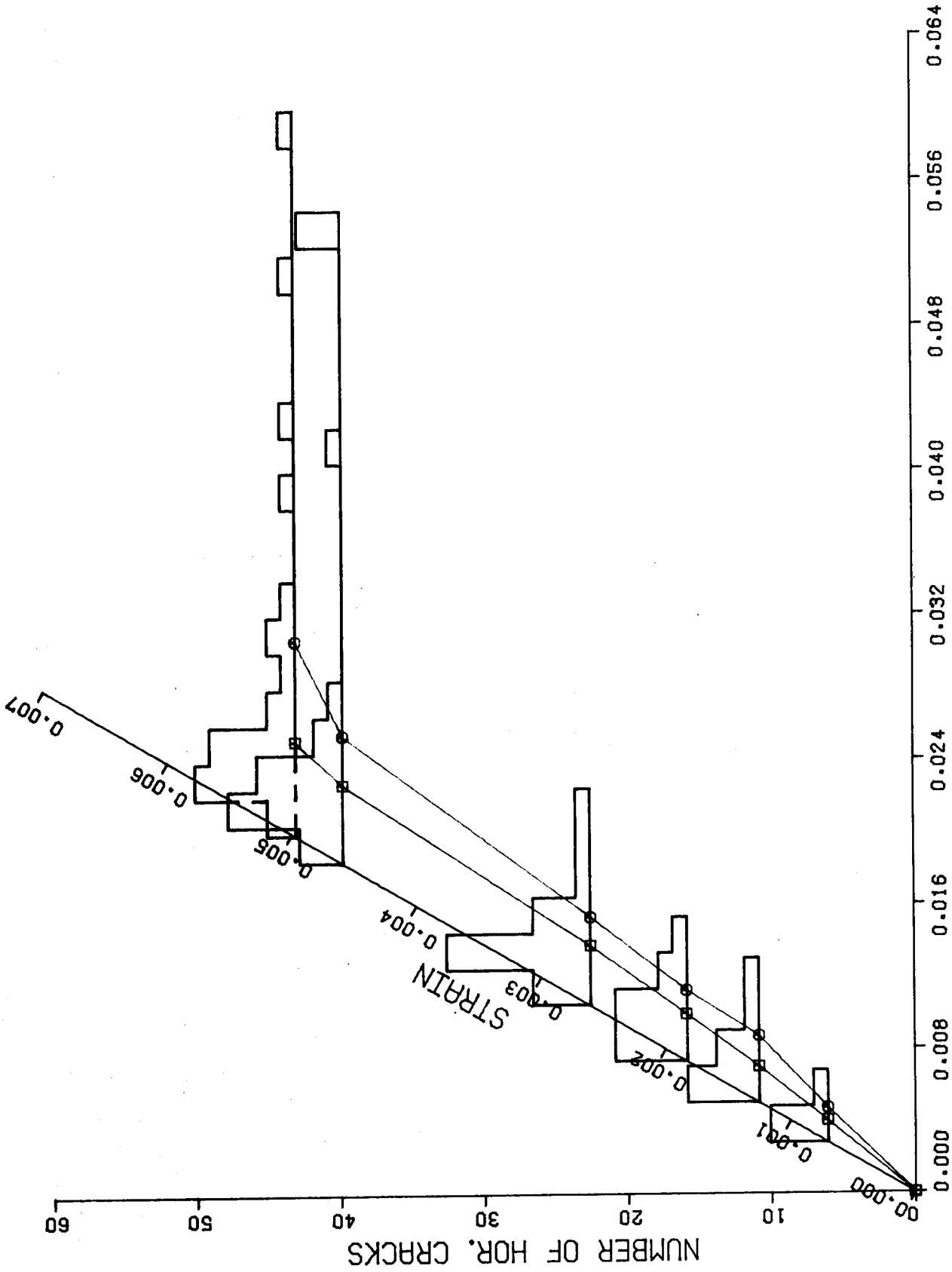

(a) Horizontal Cracks

Figure 6.1.5 Distribution of Crack Widths, Segment 1

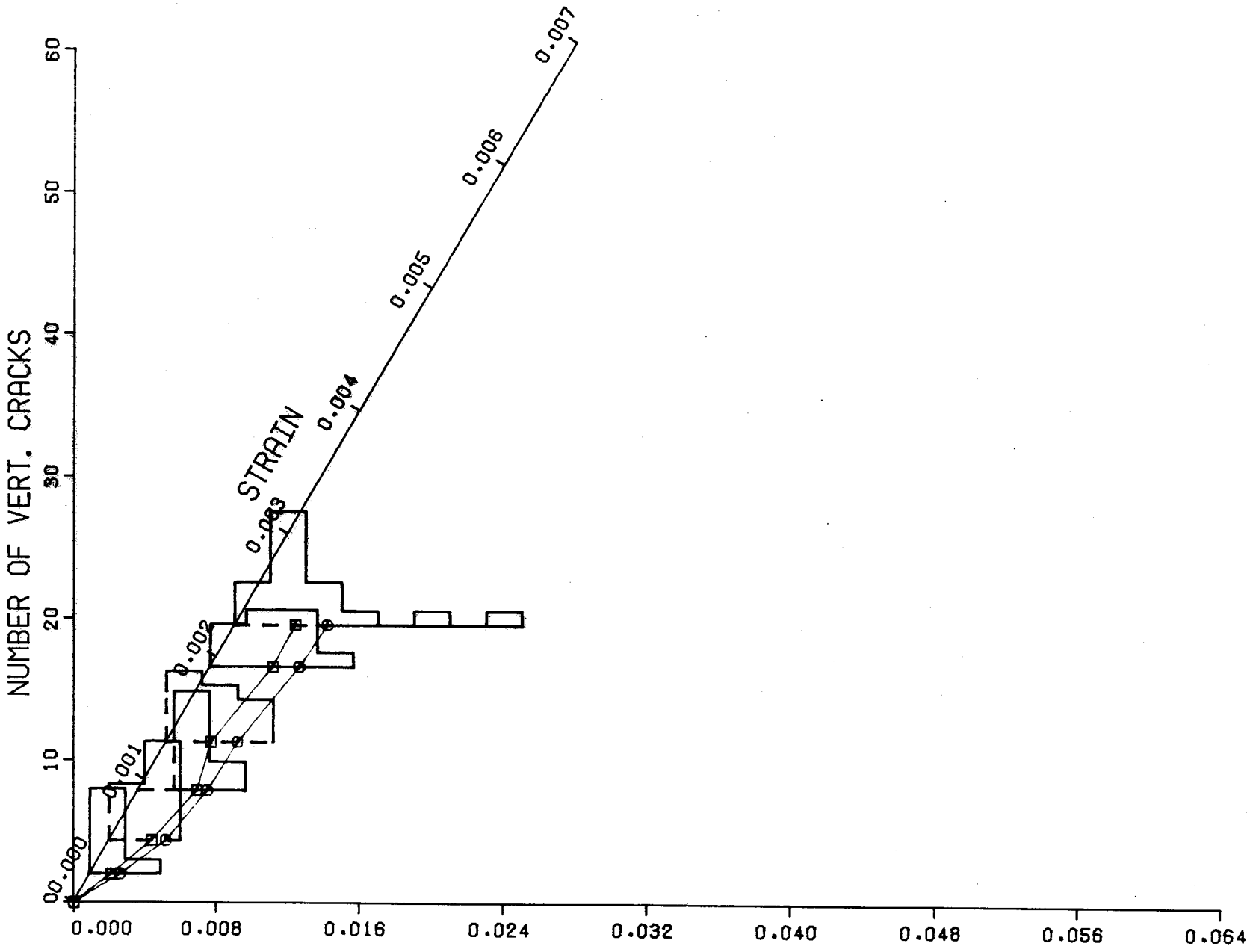

(b) Vertical Cracks

Figure 6.1.5 Distribution of Crack Widths, Segment 1

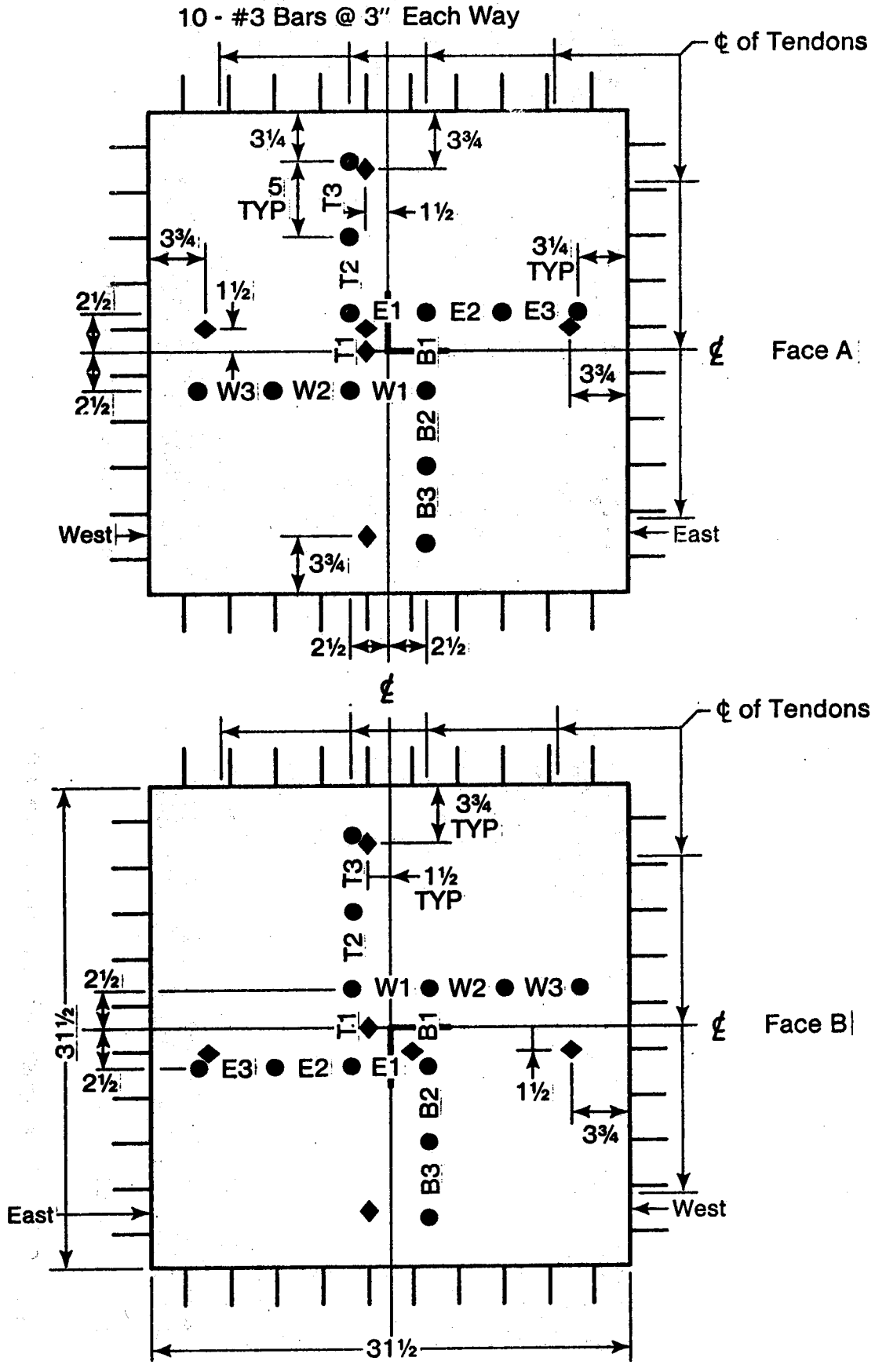

Fig. 6.2.1 Location of Strain Measurements, Segment 2

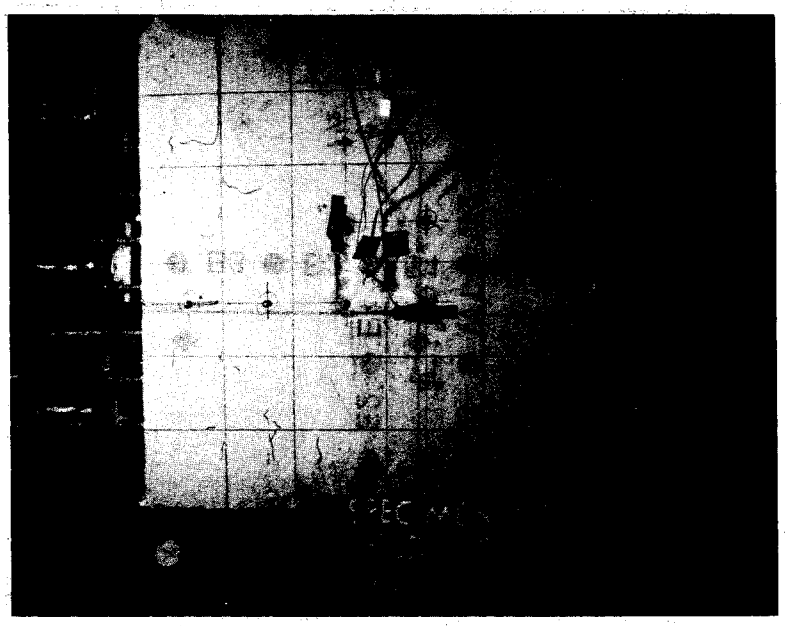

(a) Face A Before Loading

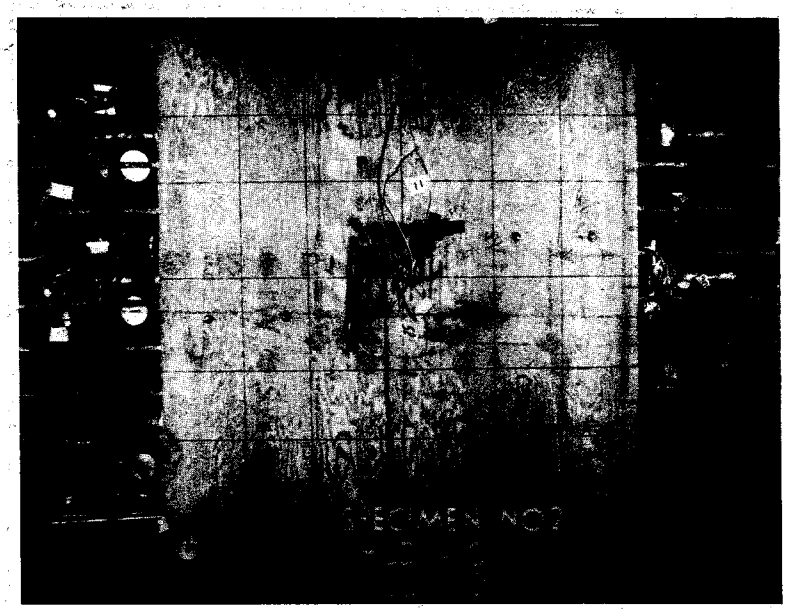

(b) Face B Before Loading

Figure 6.2.2 Development of Cracking in Segment 2

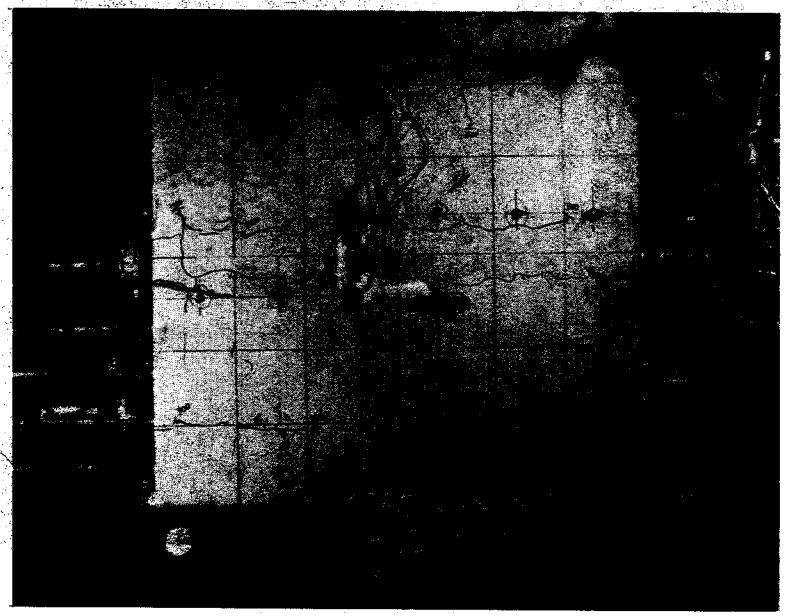

(c) Face A of Onset of Horizontal Cracking

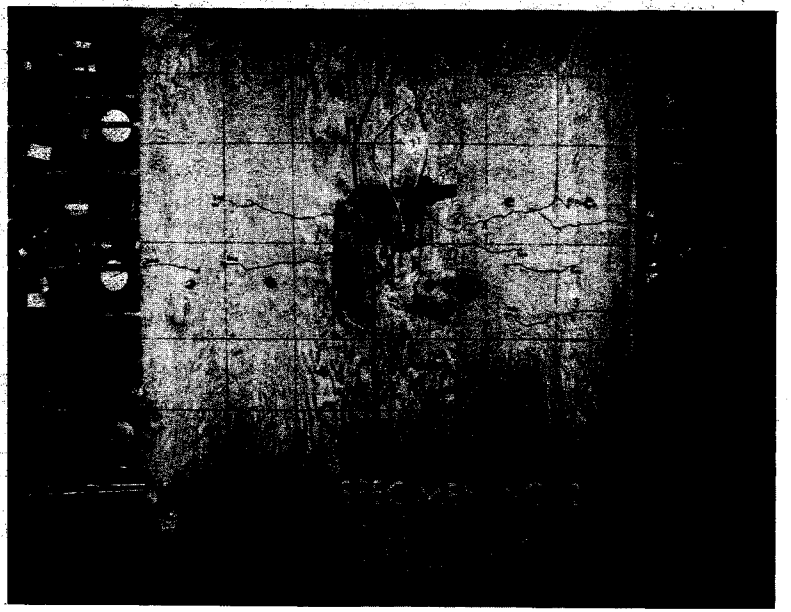

(d) Face B of Onset of Horizontal Cracking

Figure 6.2.2 Development of Cracking in Segment 2

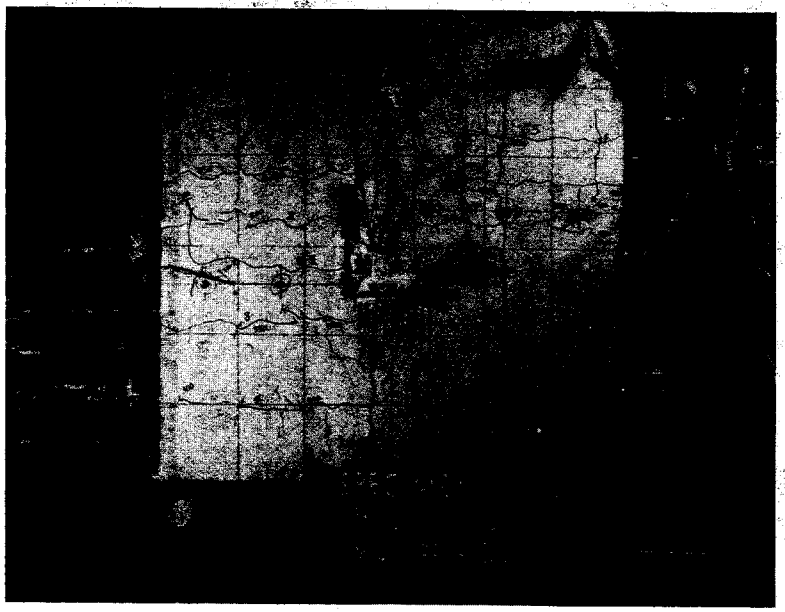

(e) Face A at Onset of Vertical Cracking

(f) Face B at Onset of Vertical Cracking

Figure 6.2.2 Development of Cracking in Segment 2

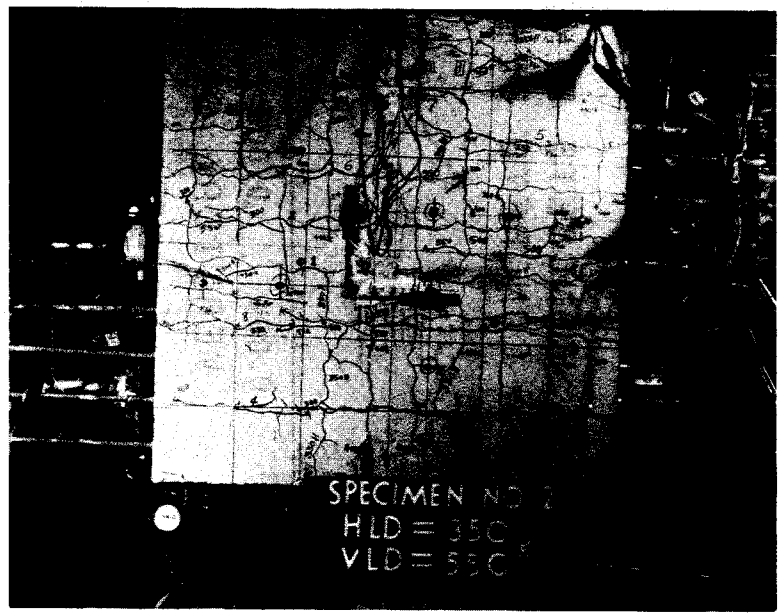

(g) Face A at End of Test

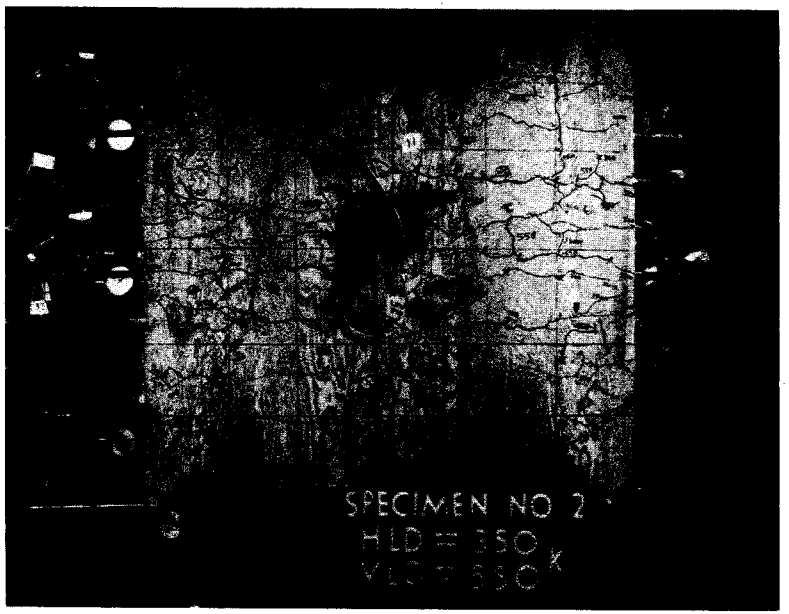

(h) Face B at End of Test

Figure 6.2.2 Development of Cracking in Segment 2

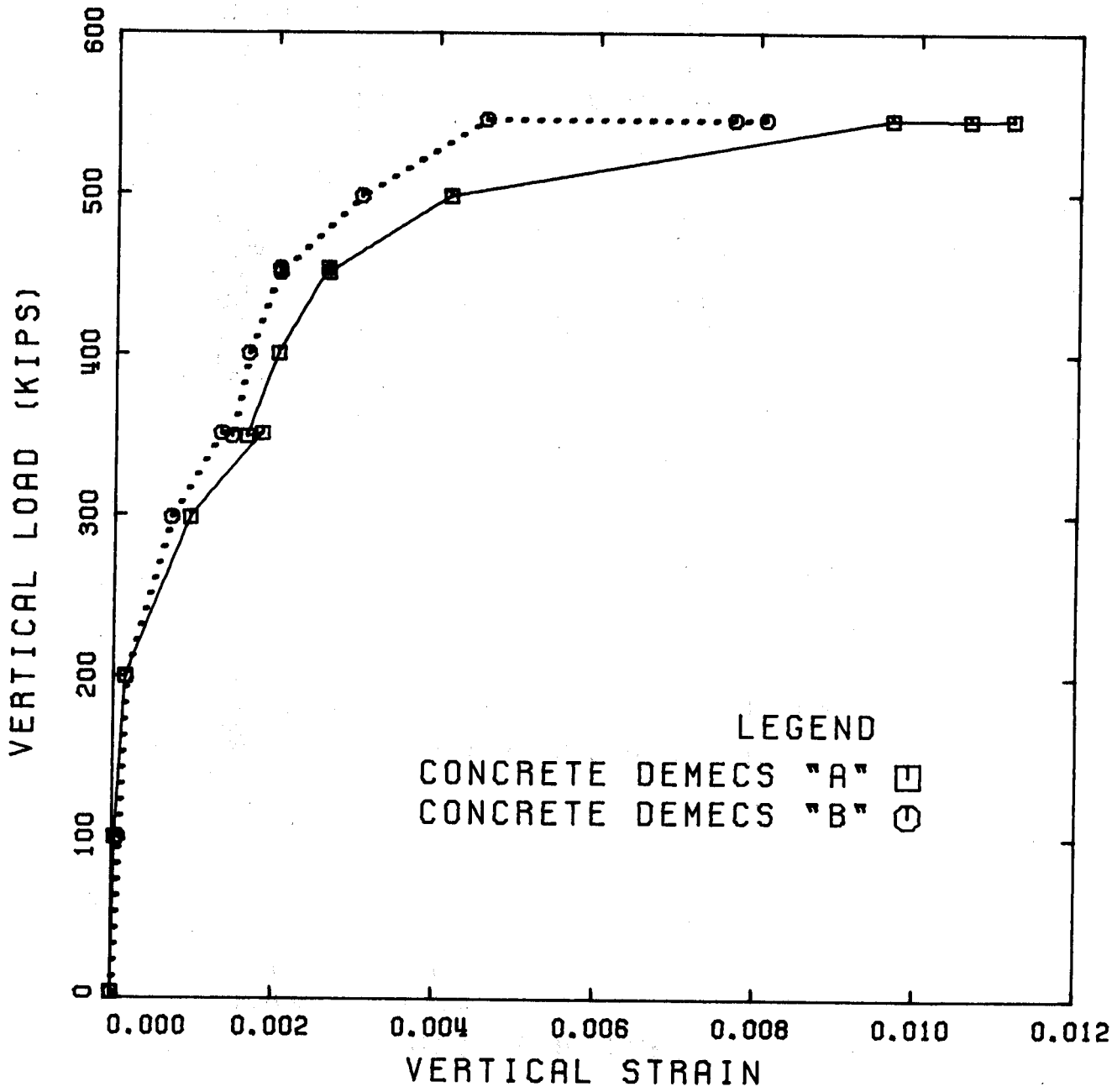

(a) Vertical Direction

Figure 6.2.3 Load-Average Strain Curves, Segment 2

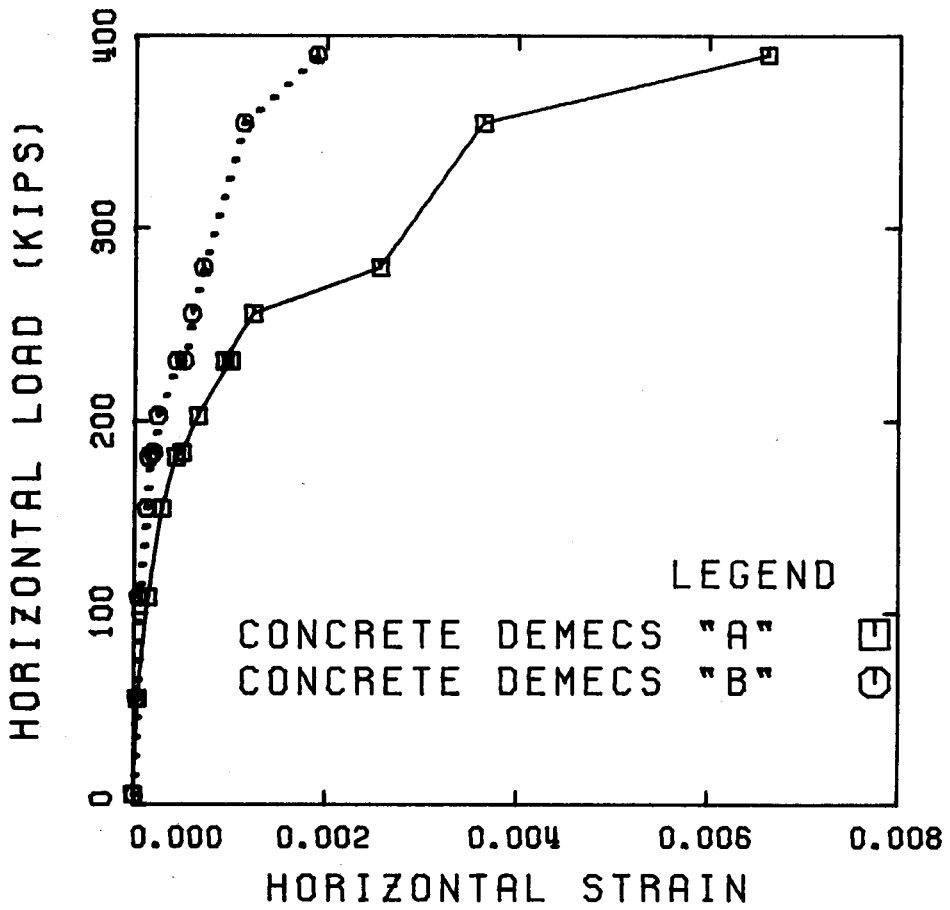

(b) Horizontal Direction

Figure 6.2.3 Load-Average Steel Strain Curves, Segment 2

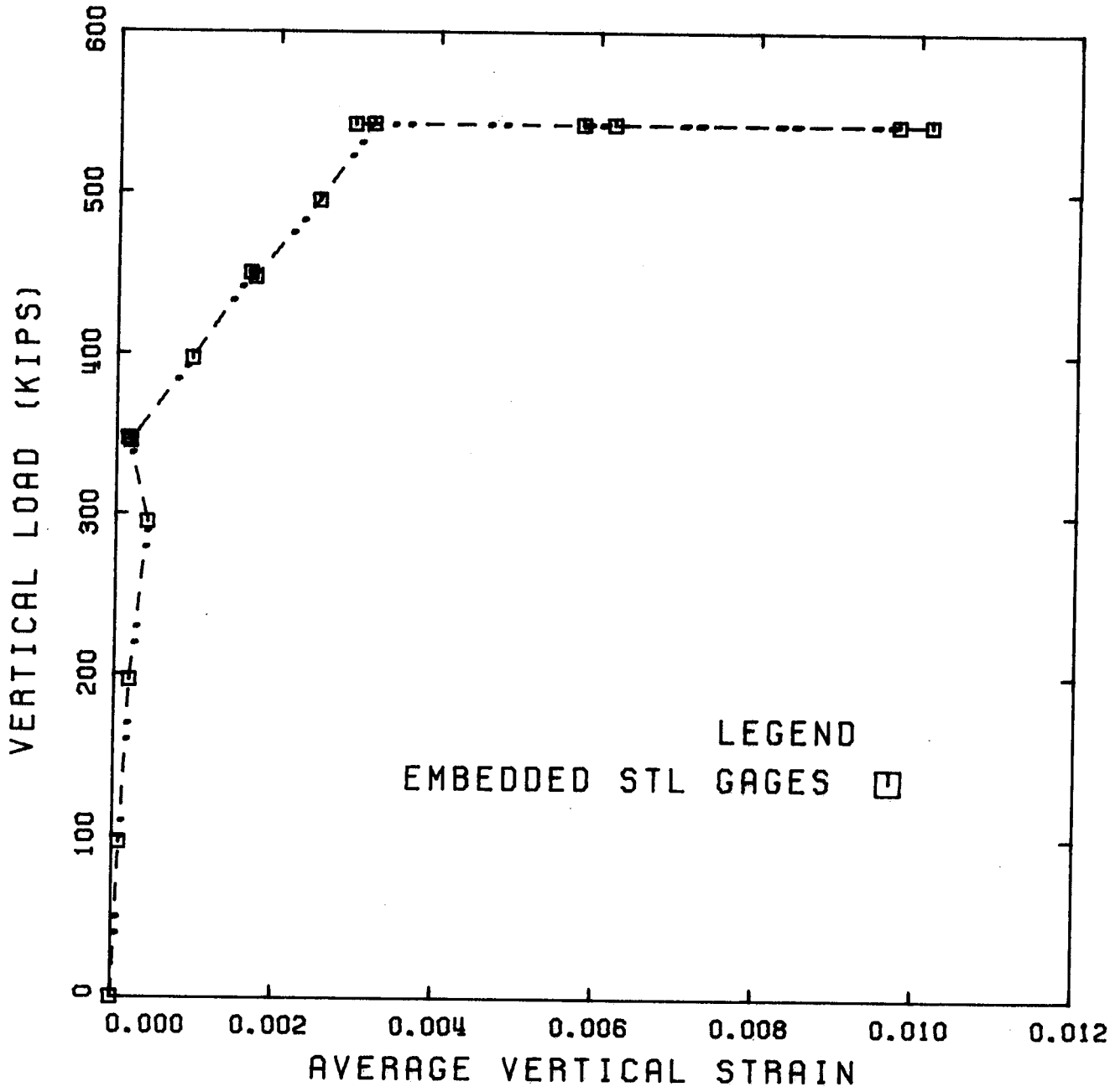

(a) Vertical Direction

Figure 6.2.4 Load-Average Steel Strain Curves, Segment 2

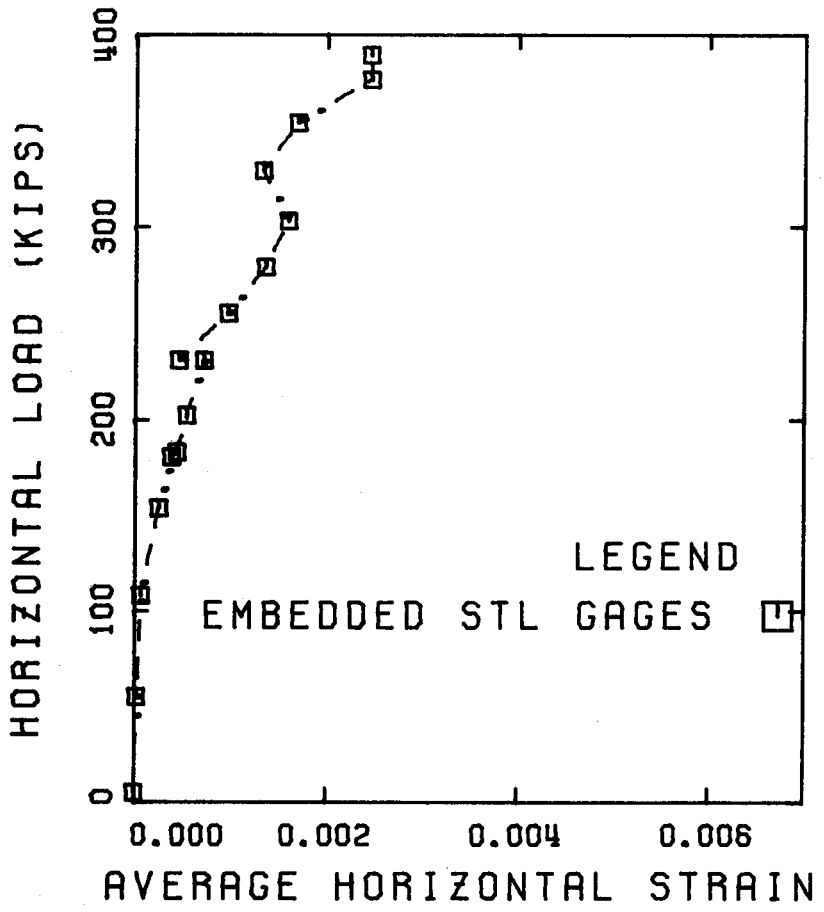

(b) Horizontal Direction

Figure 6.2.4 Load-Average Strain Curves, Segment 2

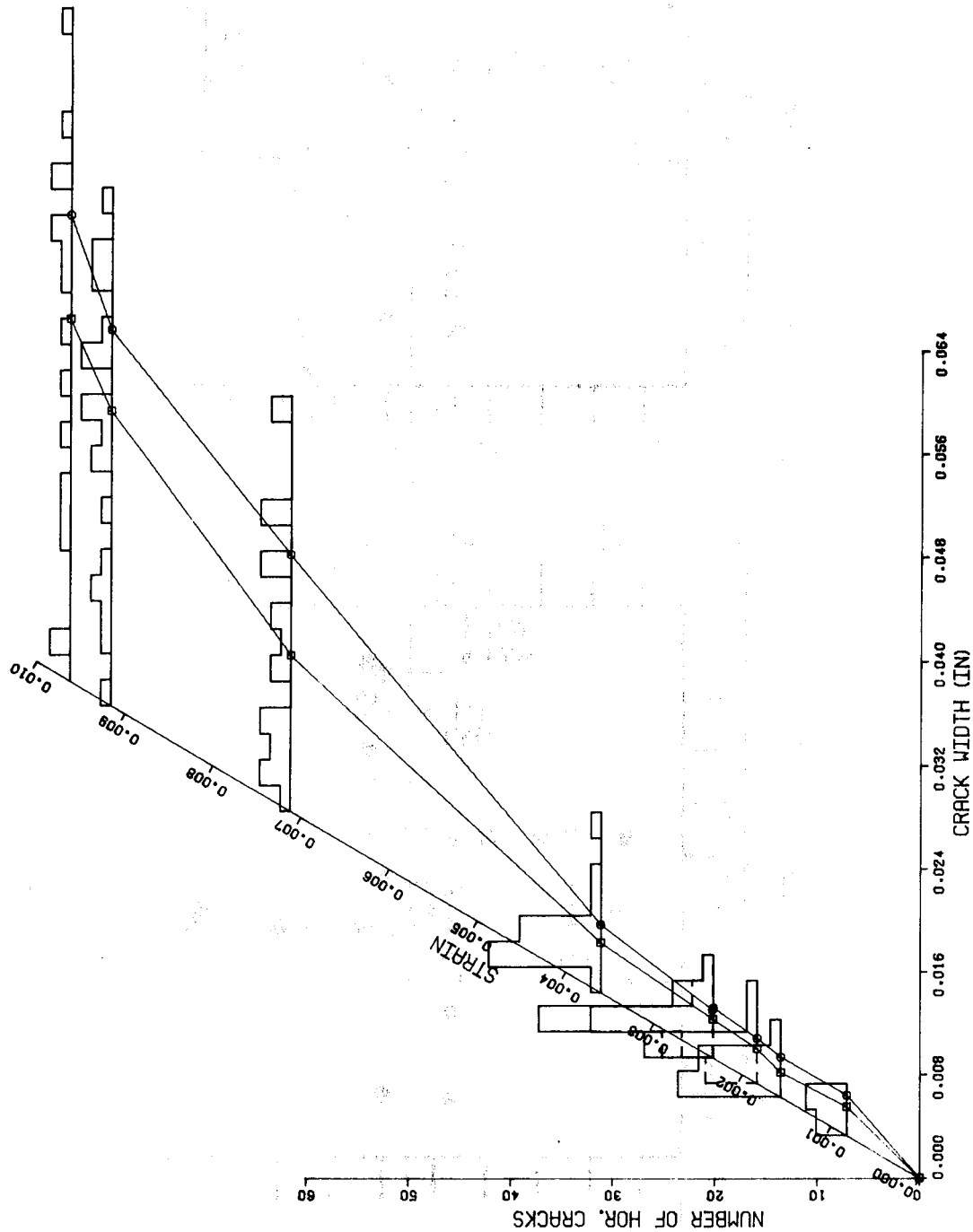

(a) Horizontal Cracks

Figure 6.2.5 Distribution of Crack Widths, Segment 2

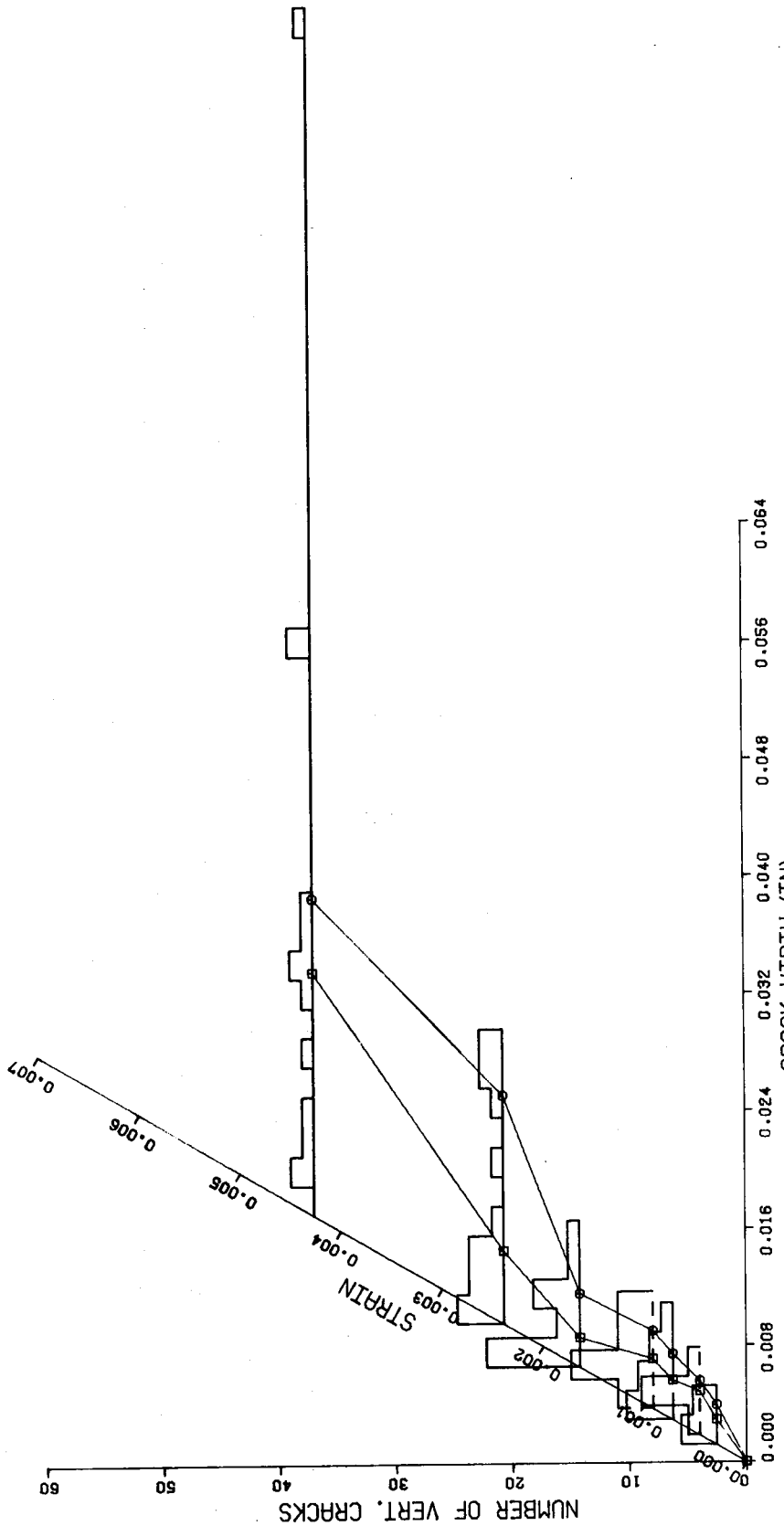

(b) Vertical Cracks

Figure 6.2.5 Distribution of Crack Widths, Segment 2

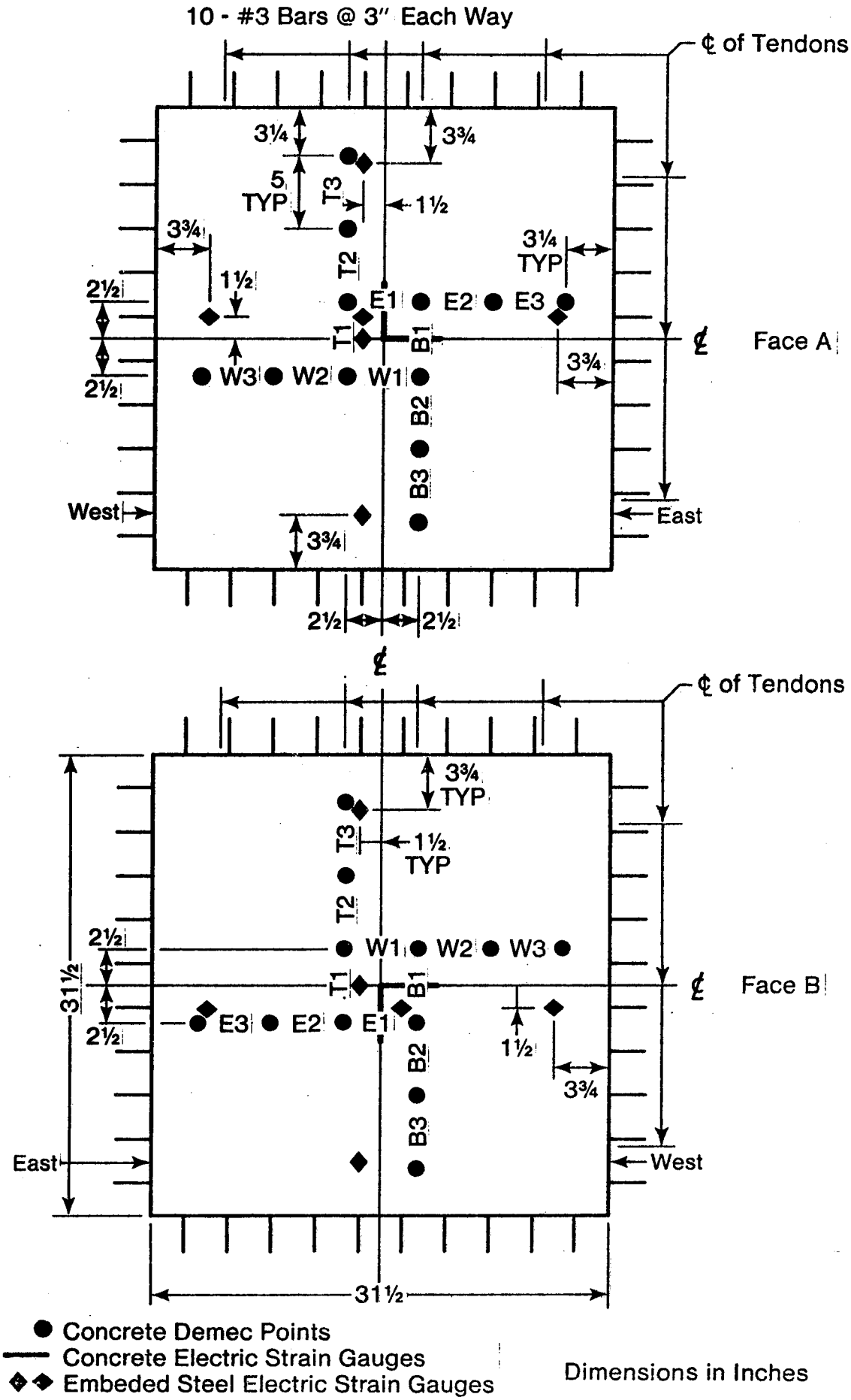

Fig. 6.3.1 Location of Strain Measurements, Segment 3

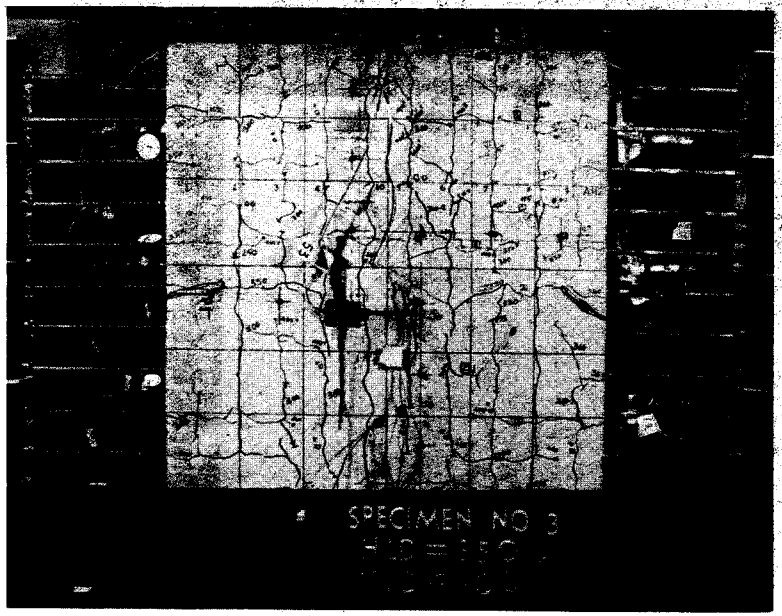

(a) Face A

(b) Face B

Figure 6.3.1 Development of Cracking in Segment 3

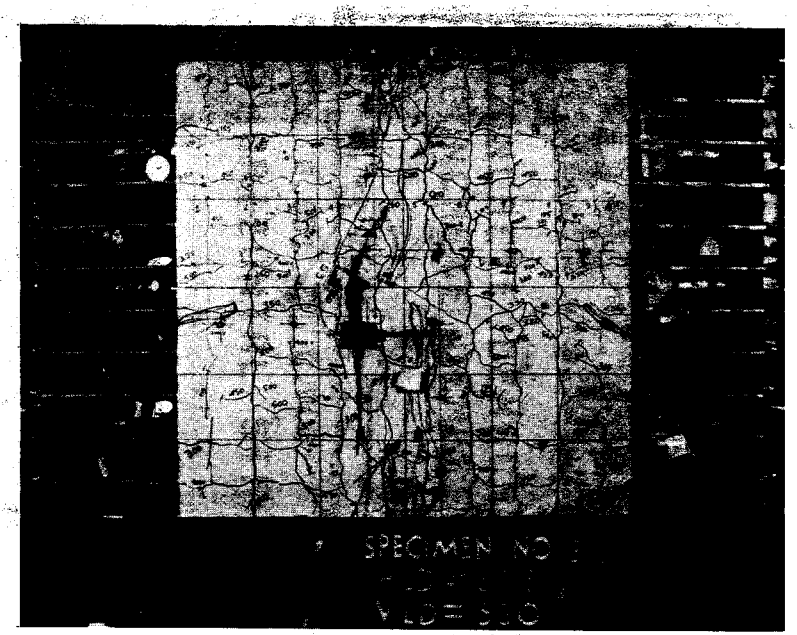

(c) Face A at End of Test

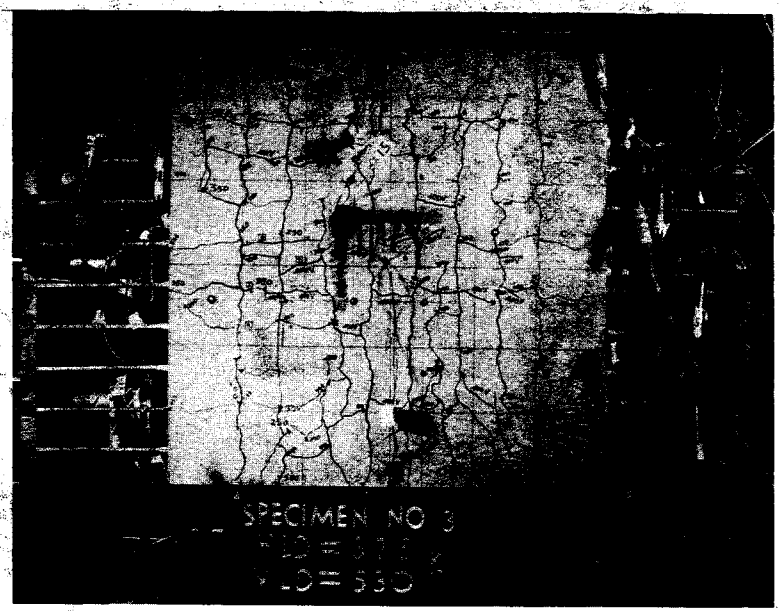

(d) Face B at End of Test

Figure 6.3.1 Development of Cracking in Segment 3

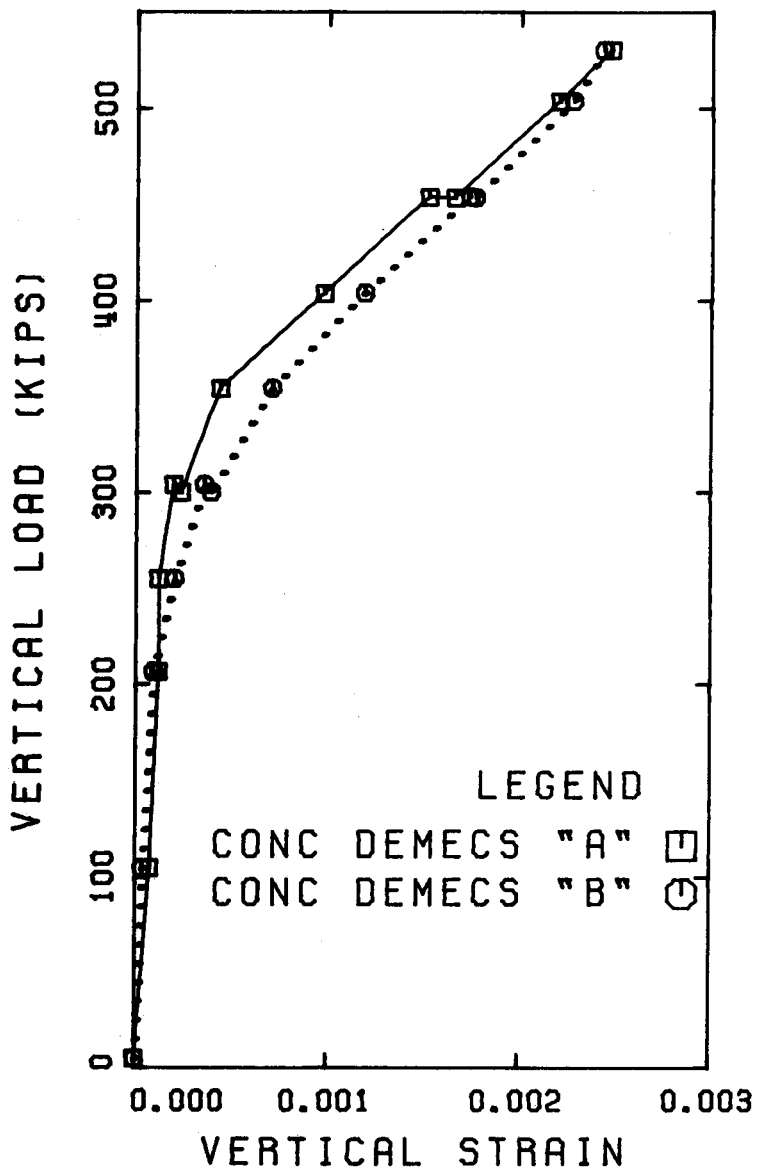

(a) Vertical Direction

Figure 6.3.3 Load-Average Strain Curves, Segment 3

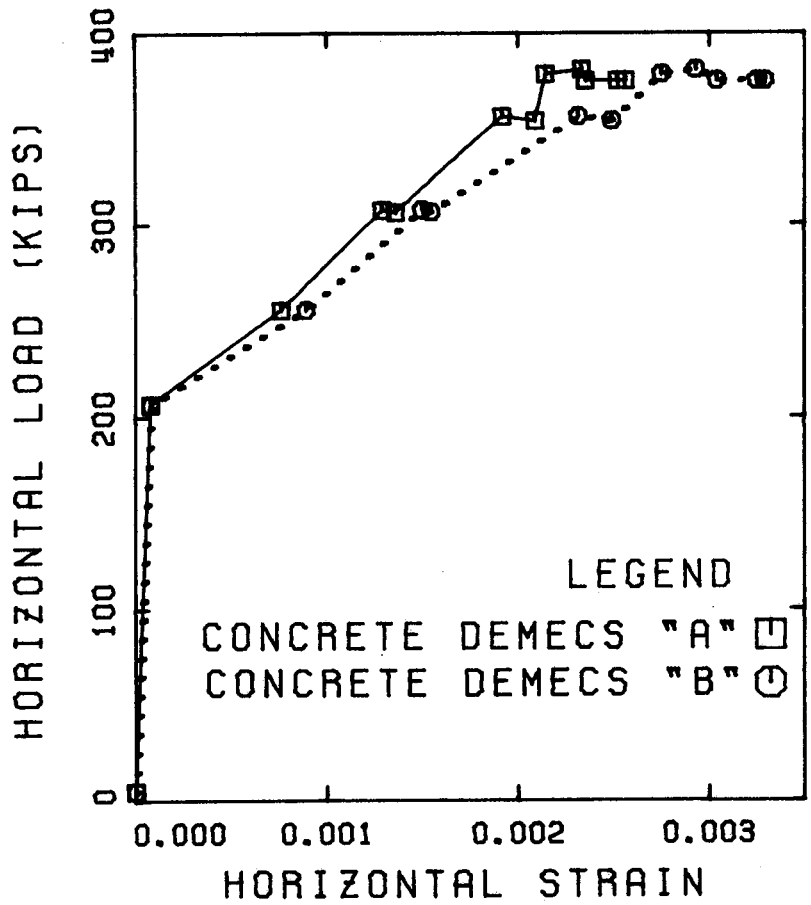

(b) Horizontal Direction

Figure 6.3.3 Load-Average Strain Curves, Segment 3

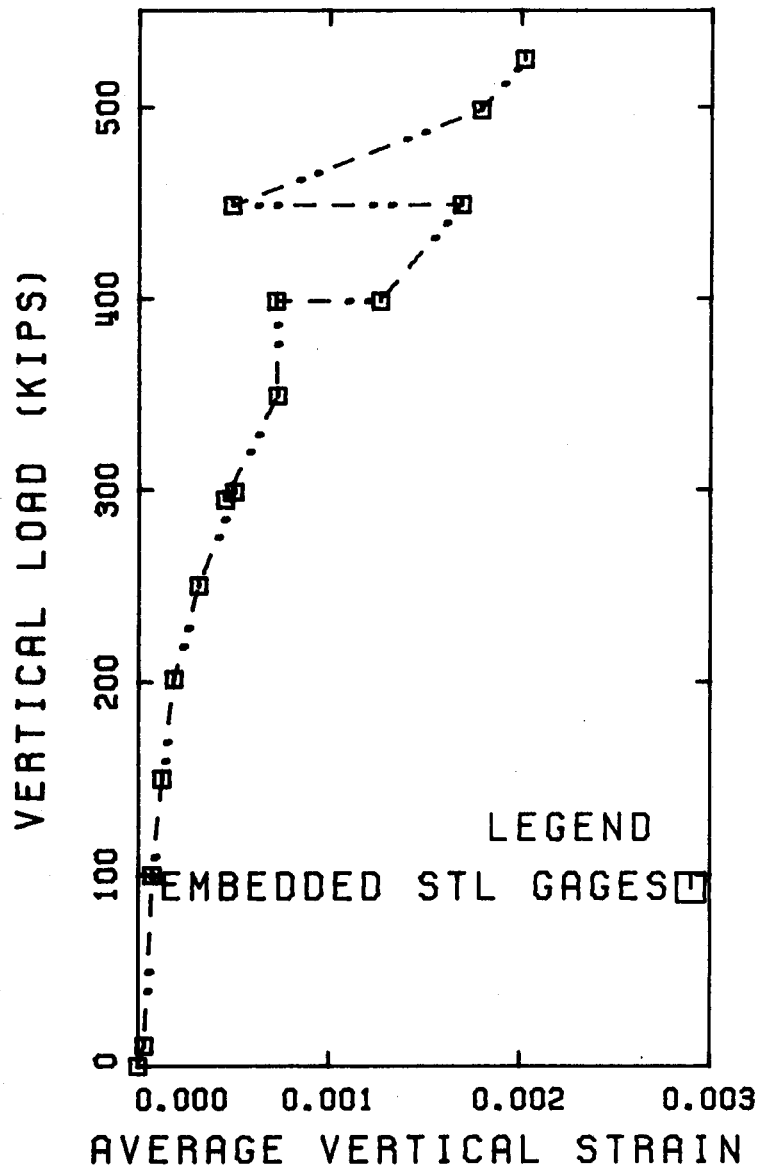

(a) Vertical Direction

Figure 6.3.4 Load-Average Steel Strain Curves, Segment 3

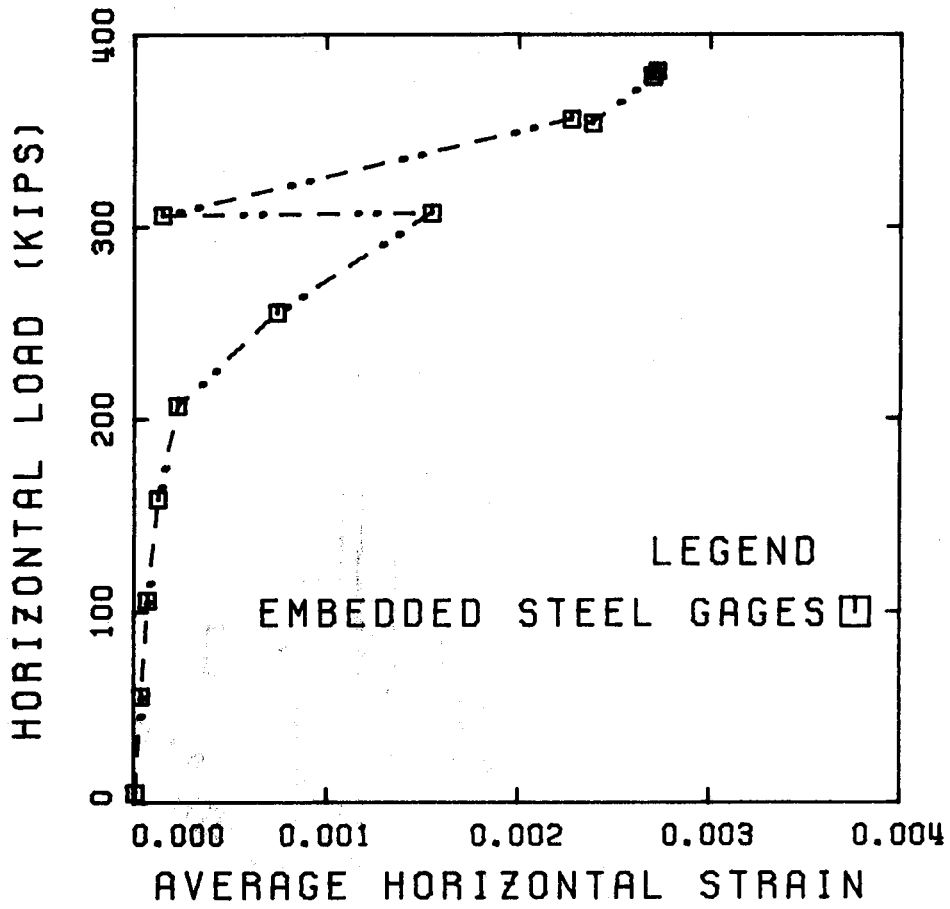

(b) Horizontal Direction

Figure 6.3.4 Load-Average Steel Strain Curves, Segment 3

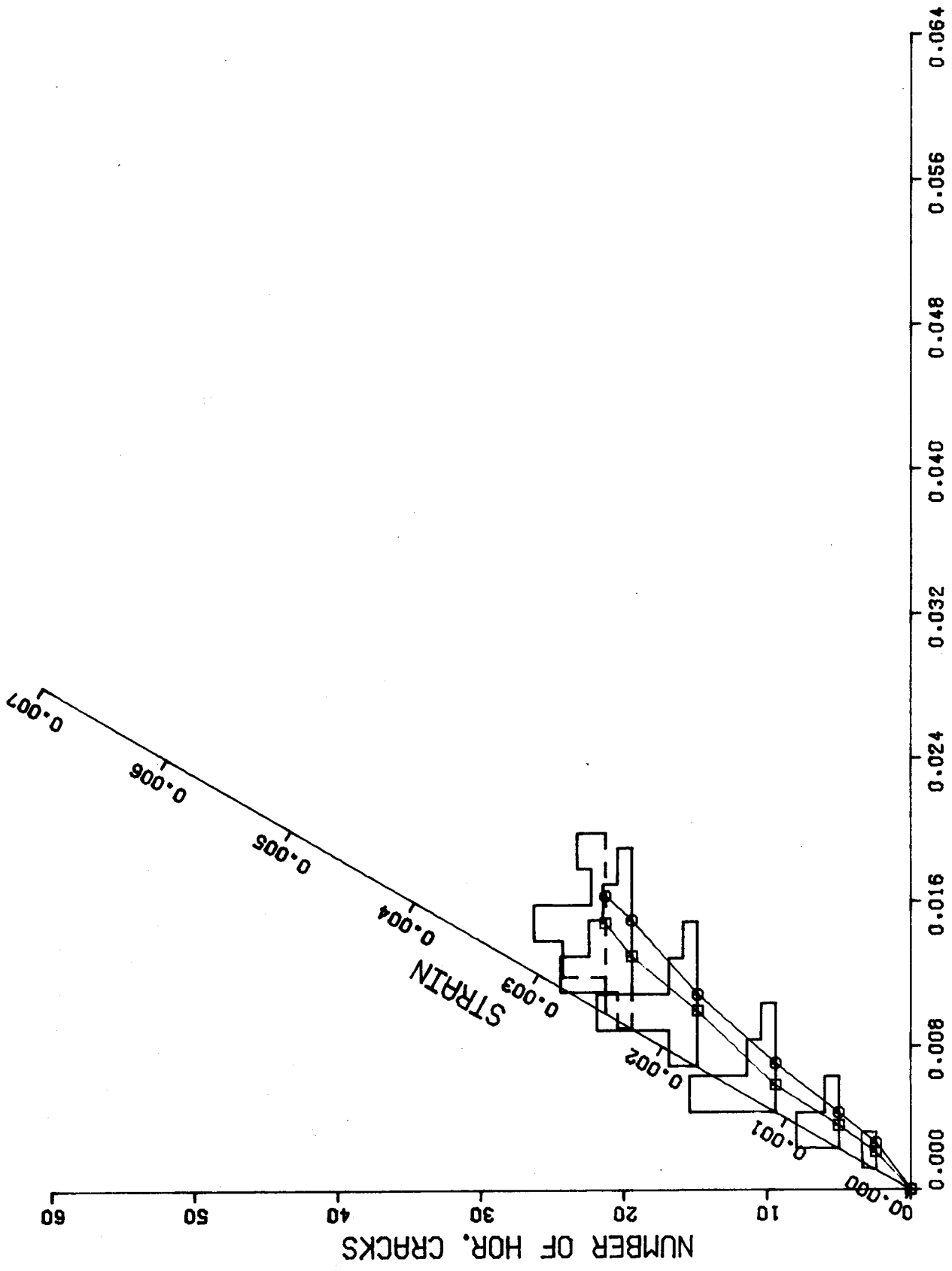

(a) Horizontal Cracks

Figure 6.3.5 Distribution of Crack Widths, Segment 3

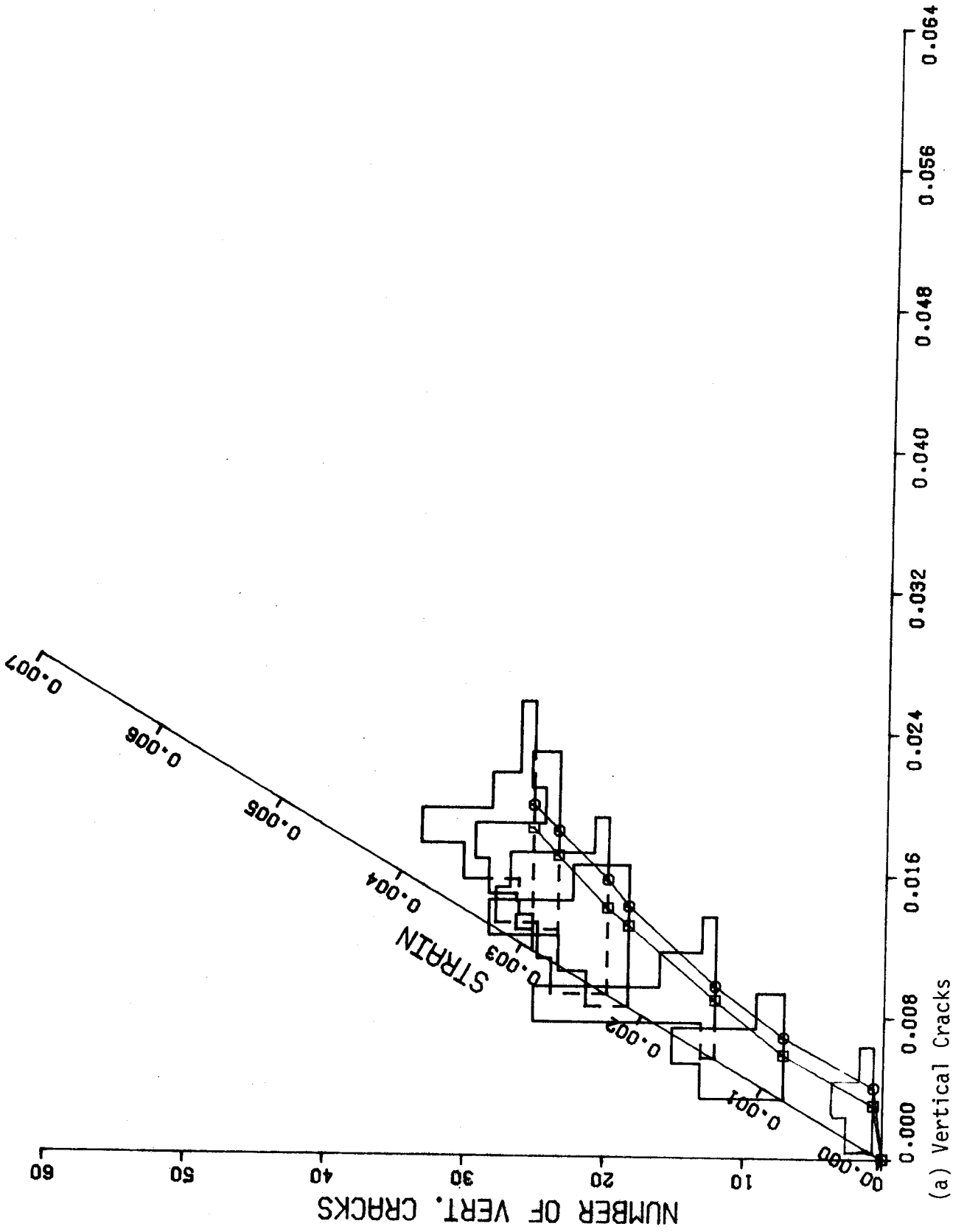

(a) Vertical Cracks

Figure 6.3.5 Distribution of Crack Widths, Segment 3

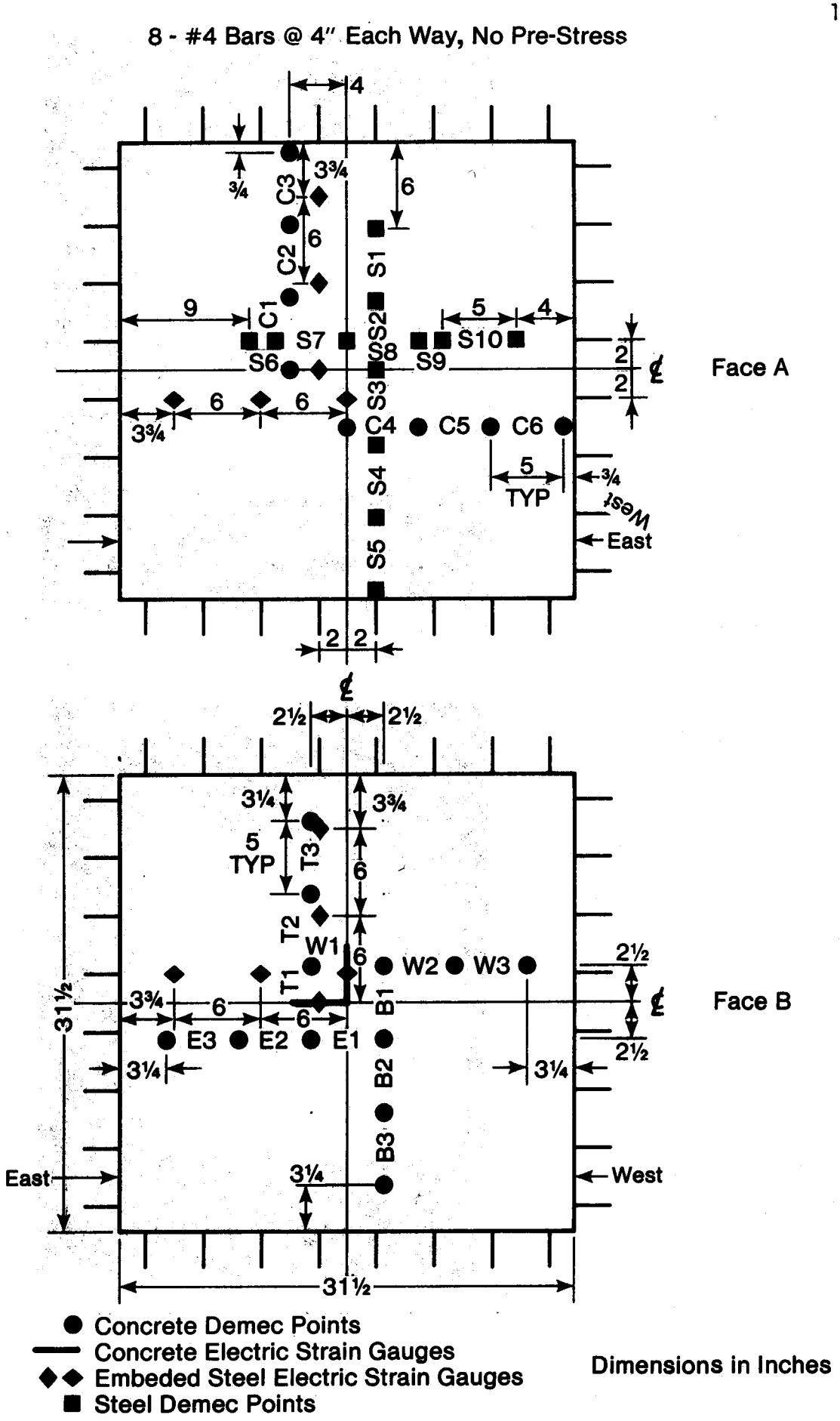

Figure 6.4.1 Location of Strain Measurements, Specimen 4

(a) Face A Before Loading

(b) Face B Before Loading

Figure 6.4.2 Development of Cracking in Segment 4

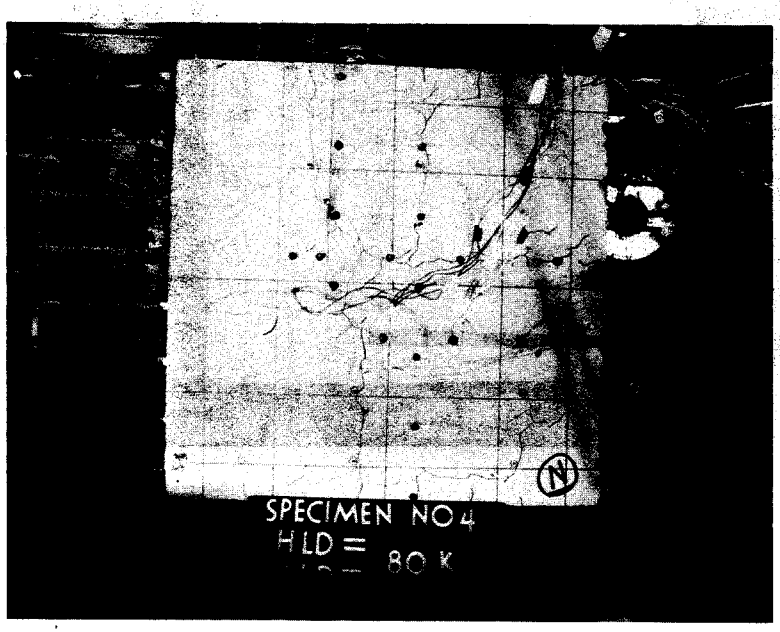

(c) Face A at Onset of Cracking

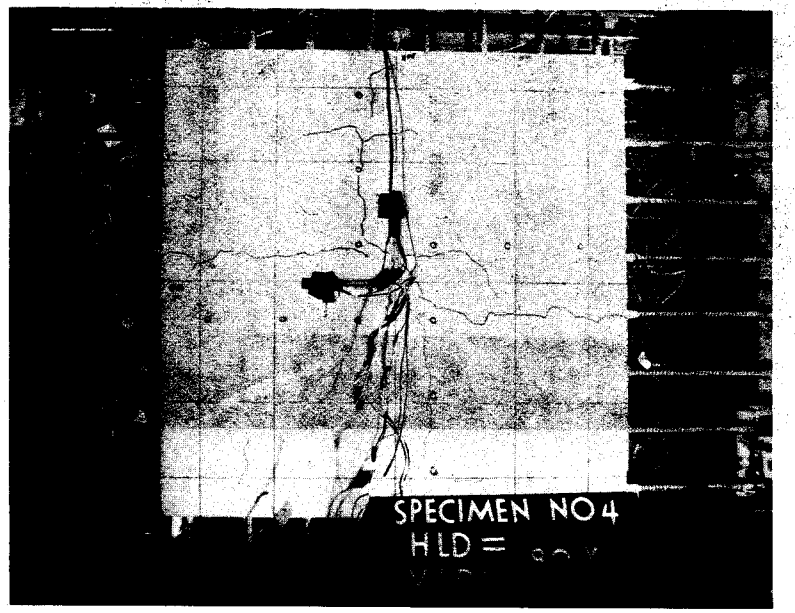

(d) Face B at Onset of Cracking

Figure 6.4.2 Development of Cracking in Segment 4

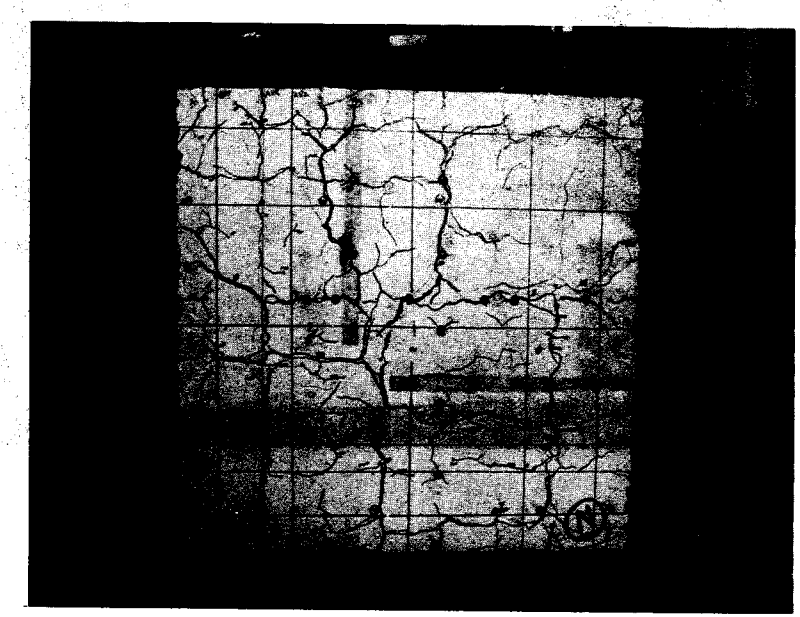

(e) Face A at End of Test

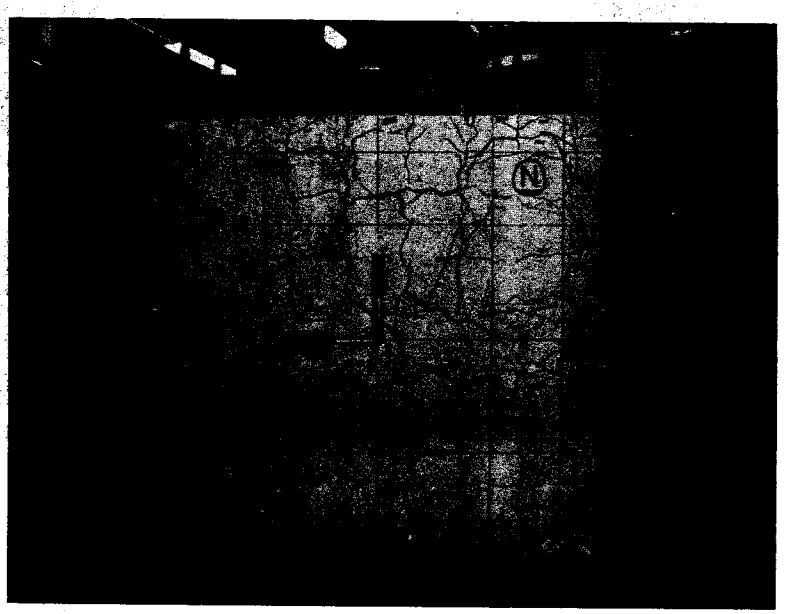

(f) Face B at End of Test

Figure 6.4.2 Development of Cracking in Segment 4

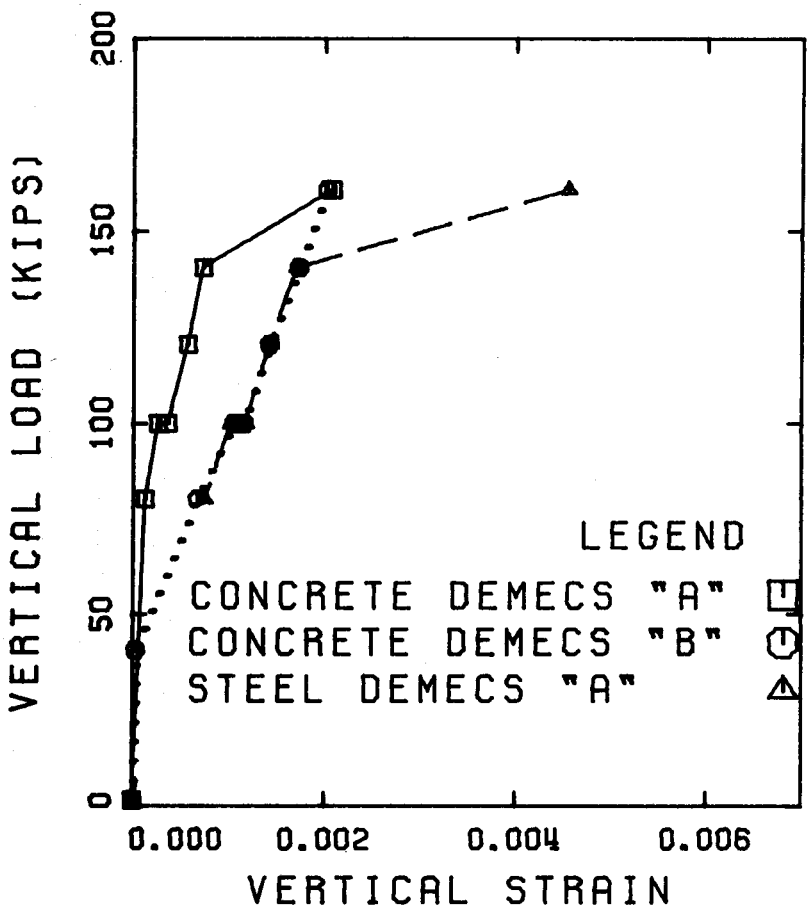

(a) Vertical Direction

Figure 6.4.3 Load-Average Strain Curves, Segment 4

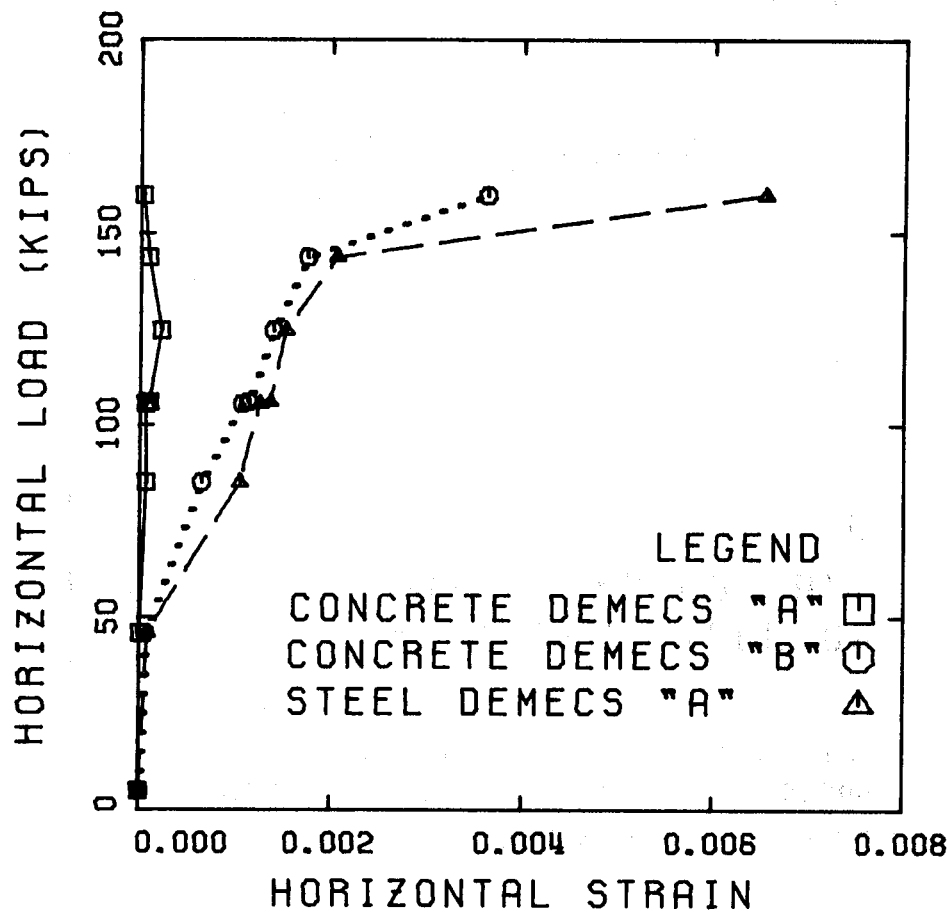

(b) Horizontal Direction

Figure 6.4.3 Load-Average Strain Curve, Segment 4

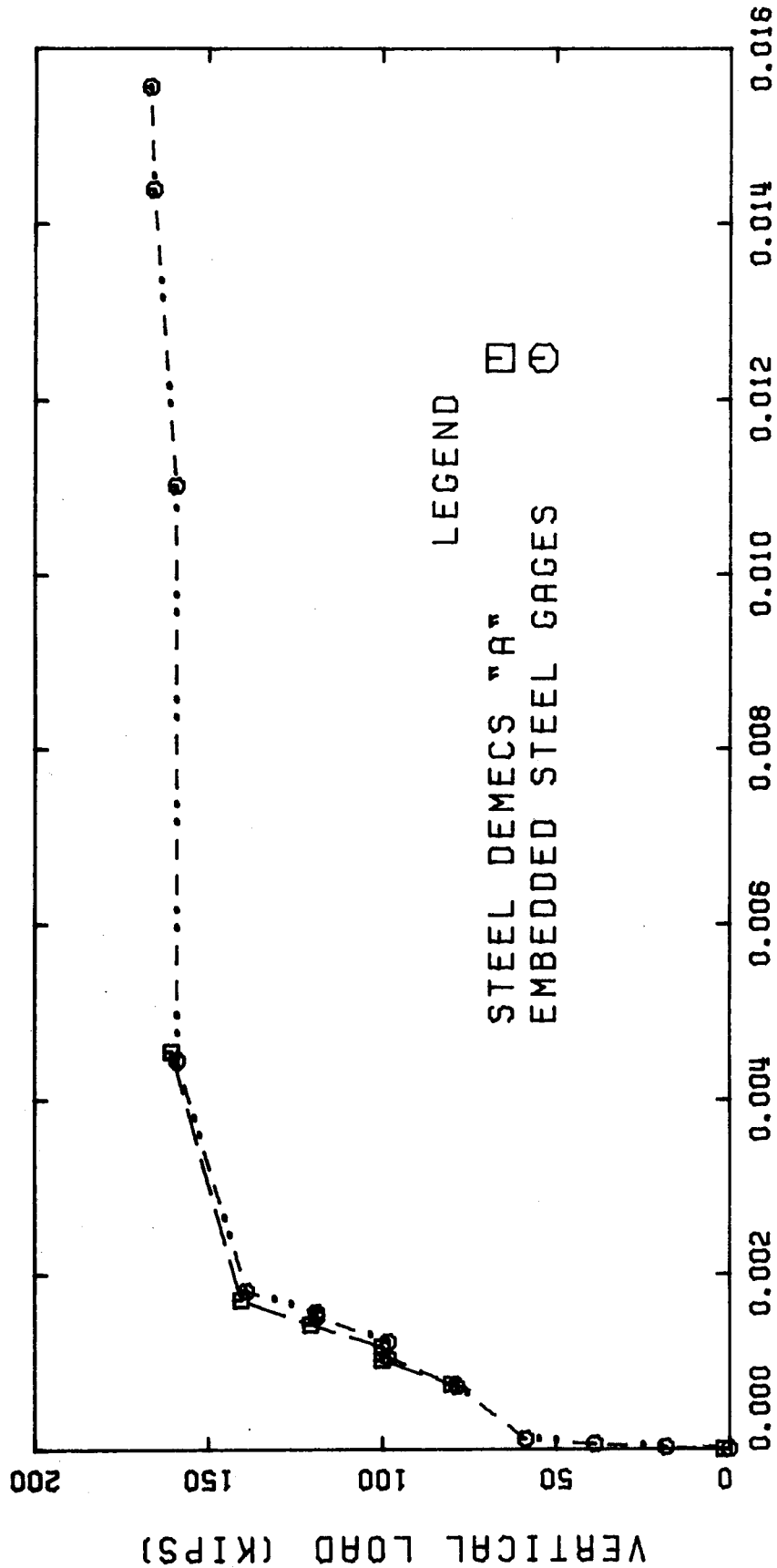

(a) Vertical Direction

Figure 6.4.4 Load-Average Steel Strain Curves, Segment 4

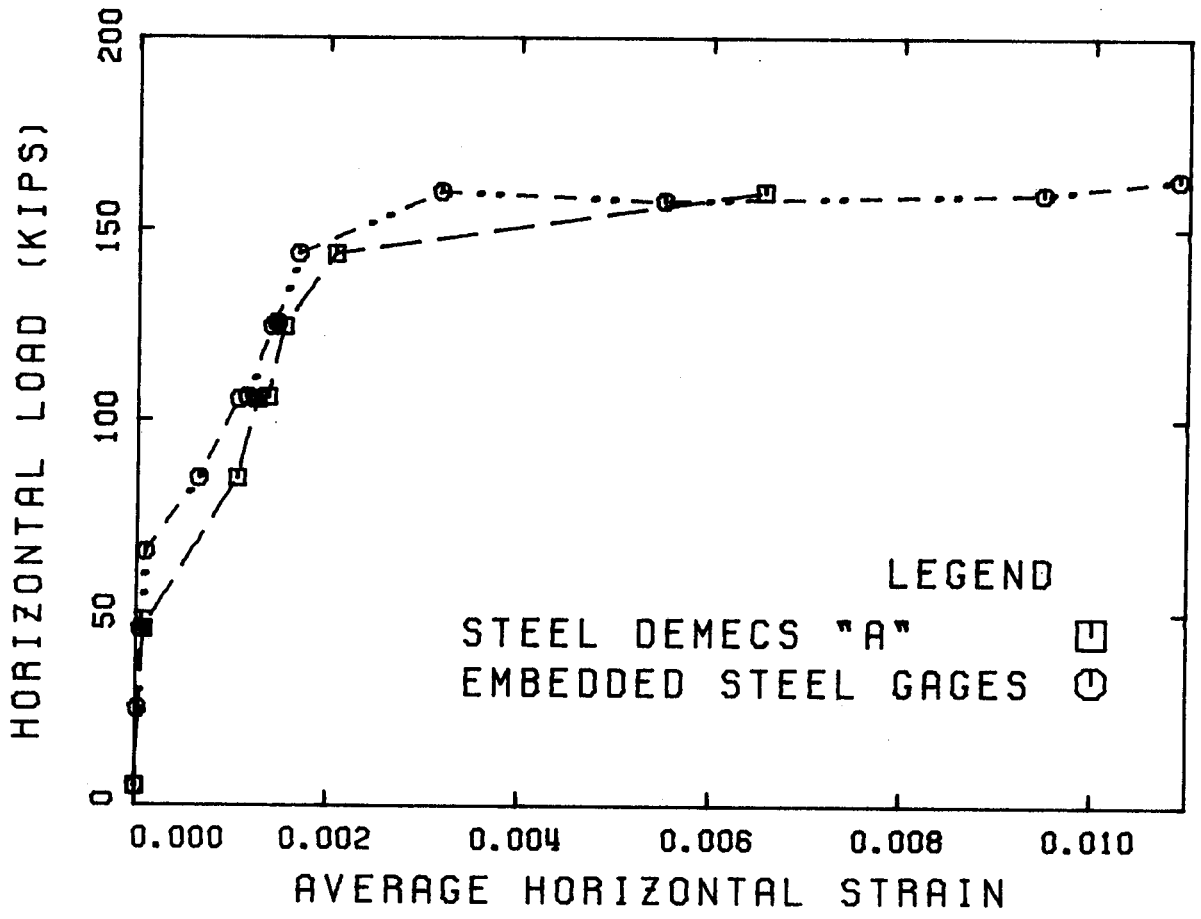

(b) Horizontal Direction

Figure 6.4.4 Load-Average Steel Strain Curves, Segment 4

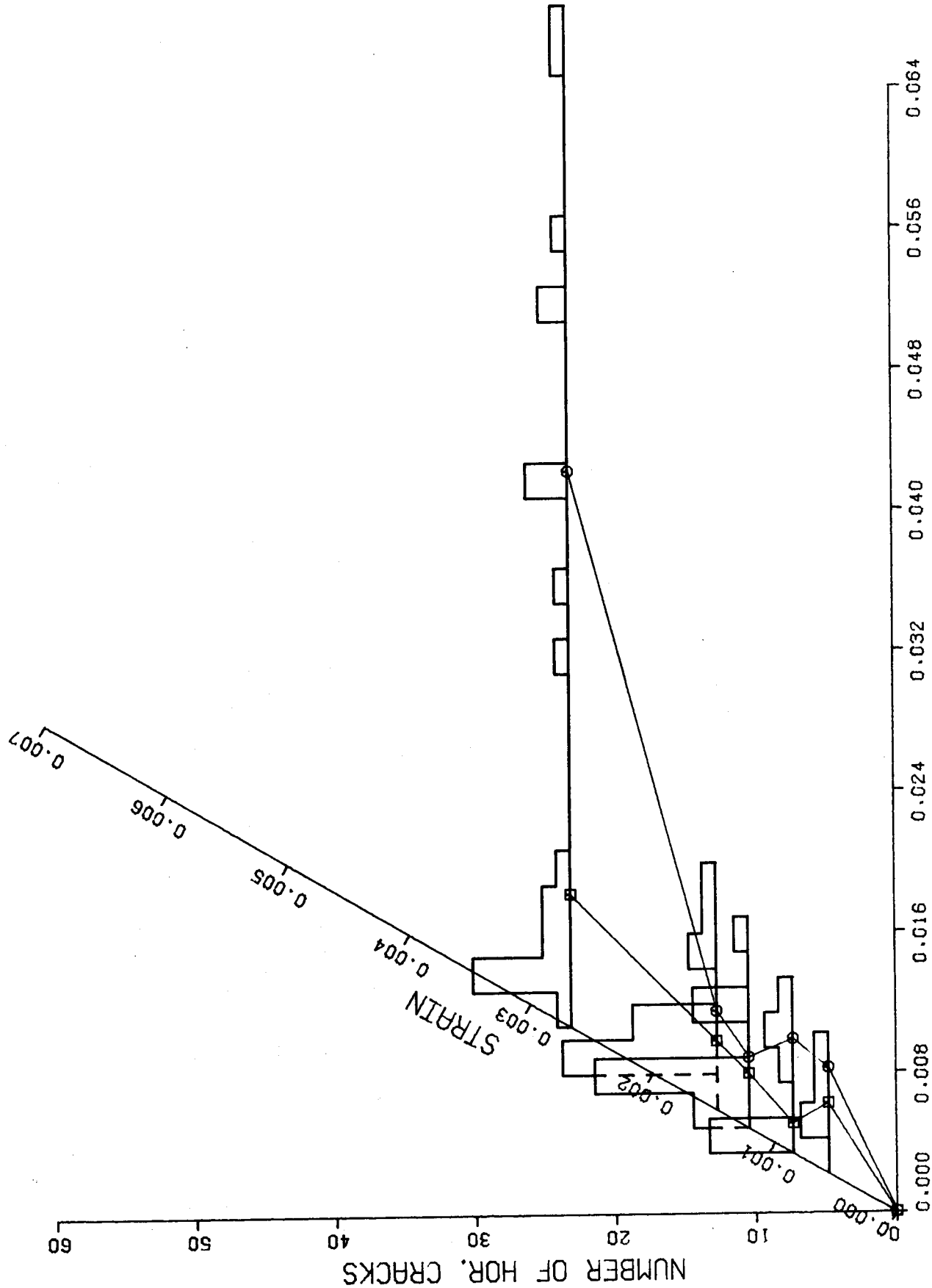

Figure 6.4.5 Distribution of Crack Widths, Segment 4

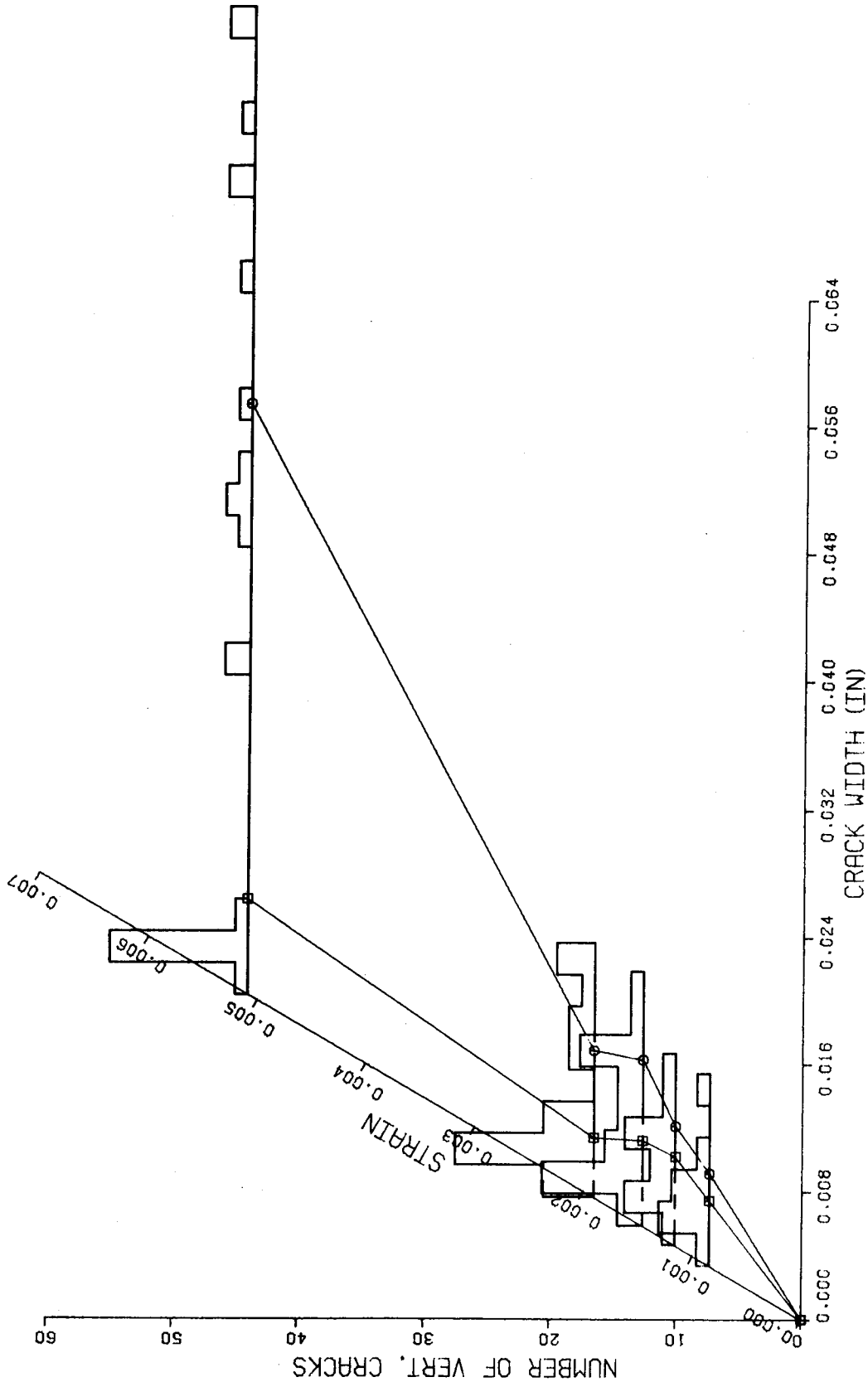

(b) Vertical Cracks

Figure 6.4.5 Distribution of Crack Widths, Segment 4

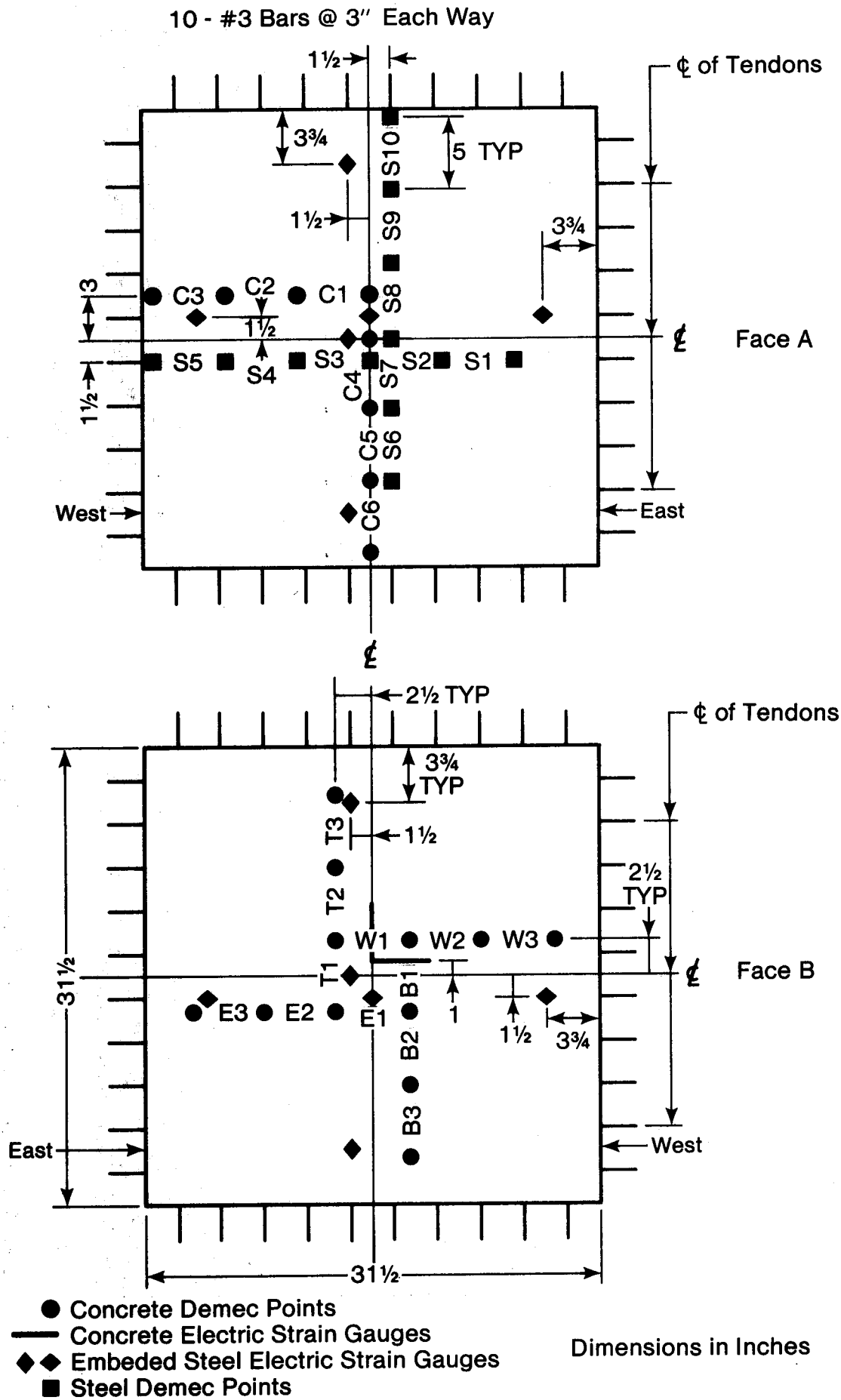

Figure 6.5.1 Location of Strain Measurements, Specimen 5

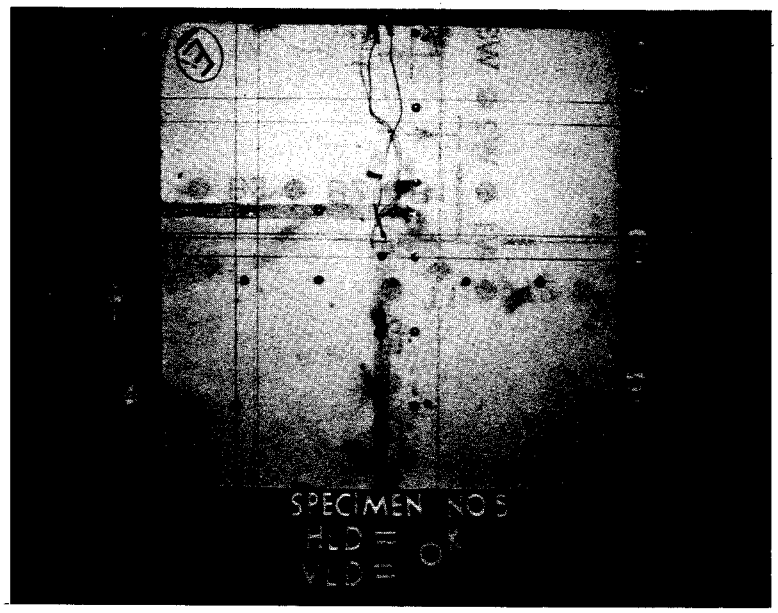

(a) Face A Before Loading

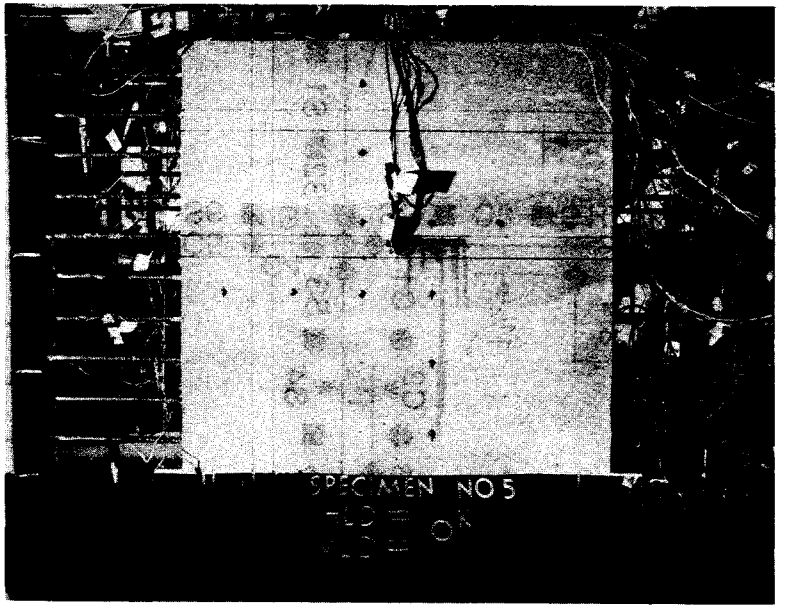

(b) Face B Before Loading

Figure 6.5.2 Development of Cracking in Segment 5

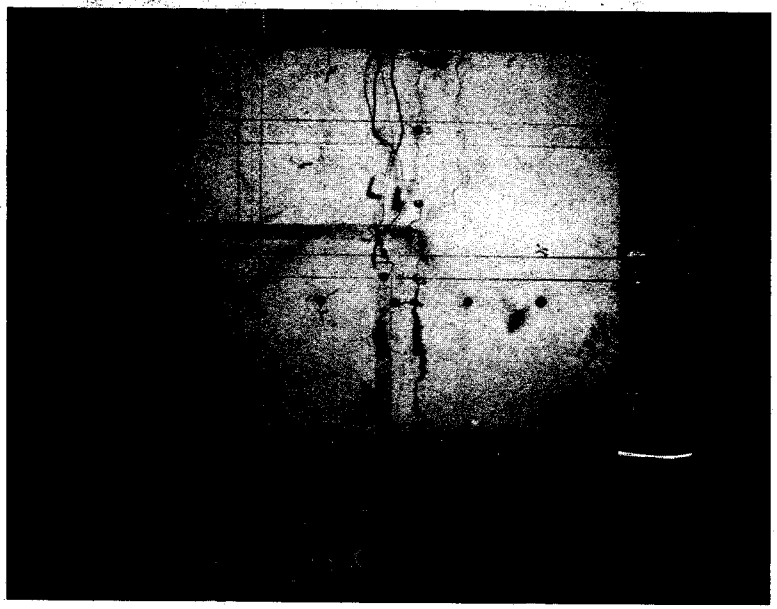

(c) Face A at Onset of Vertical Cracking

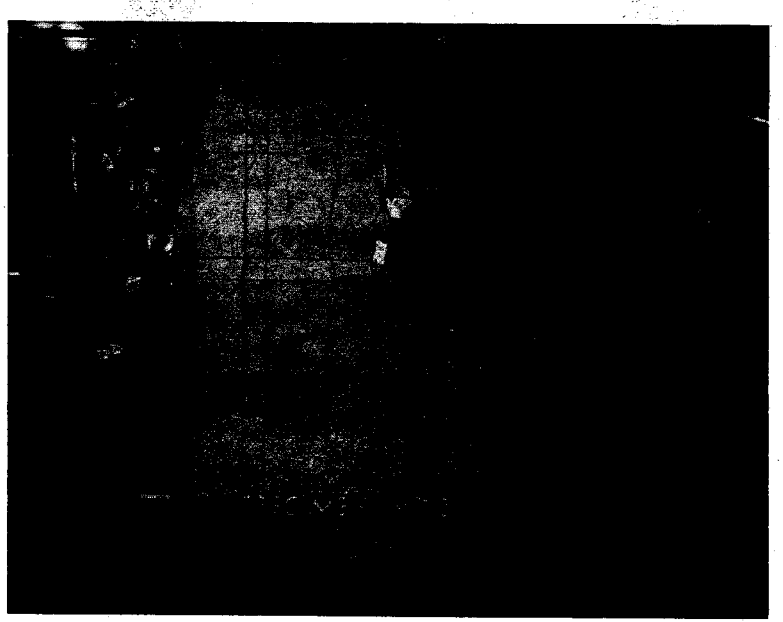

(d) Face B at Onset of Vertical Cracking

Figure 6.5.2 Development of Cracking in Segment 5

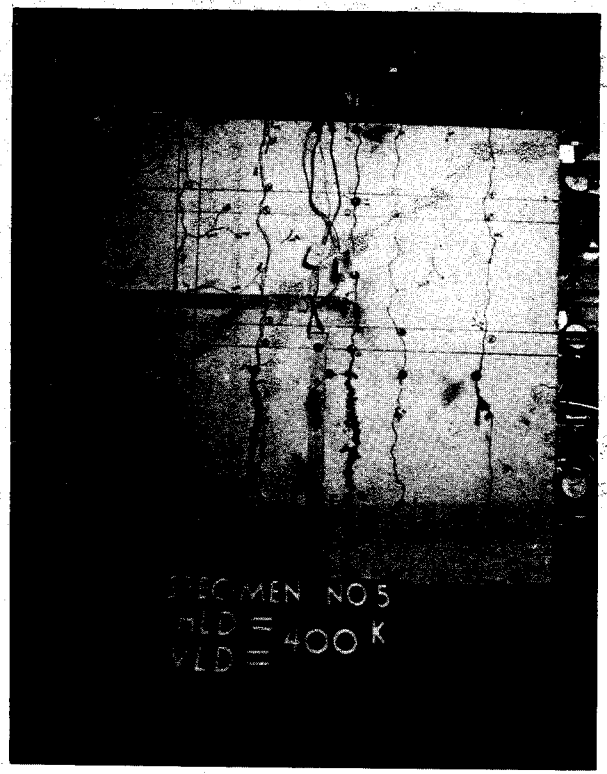

(e) Face A at End of Test

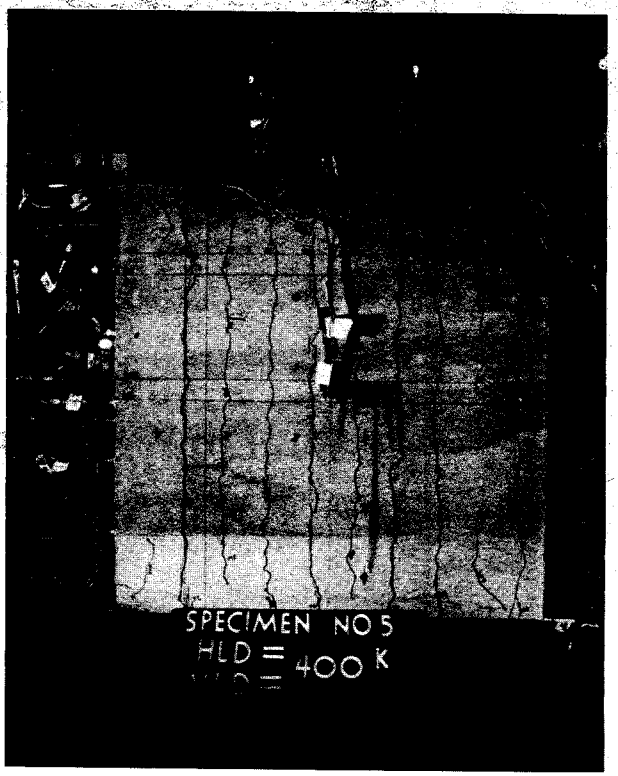

(f) Face B at End of Test

Figure 6.5.2 Development of Cracking in Segment 5

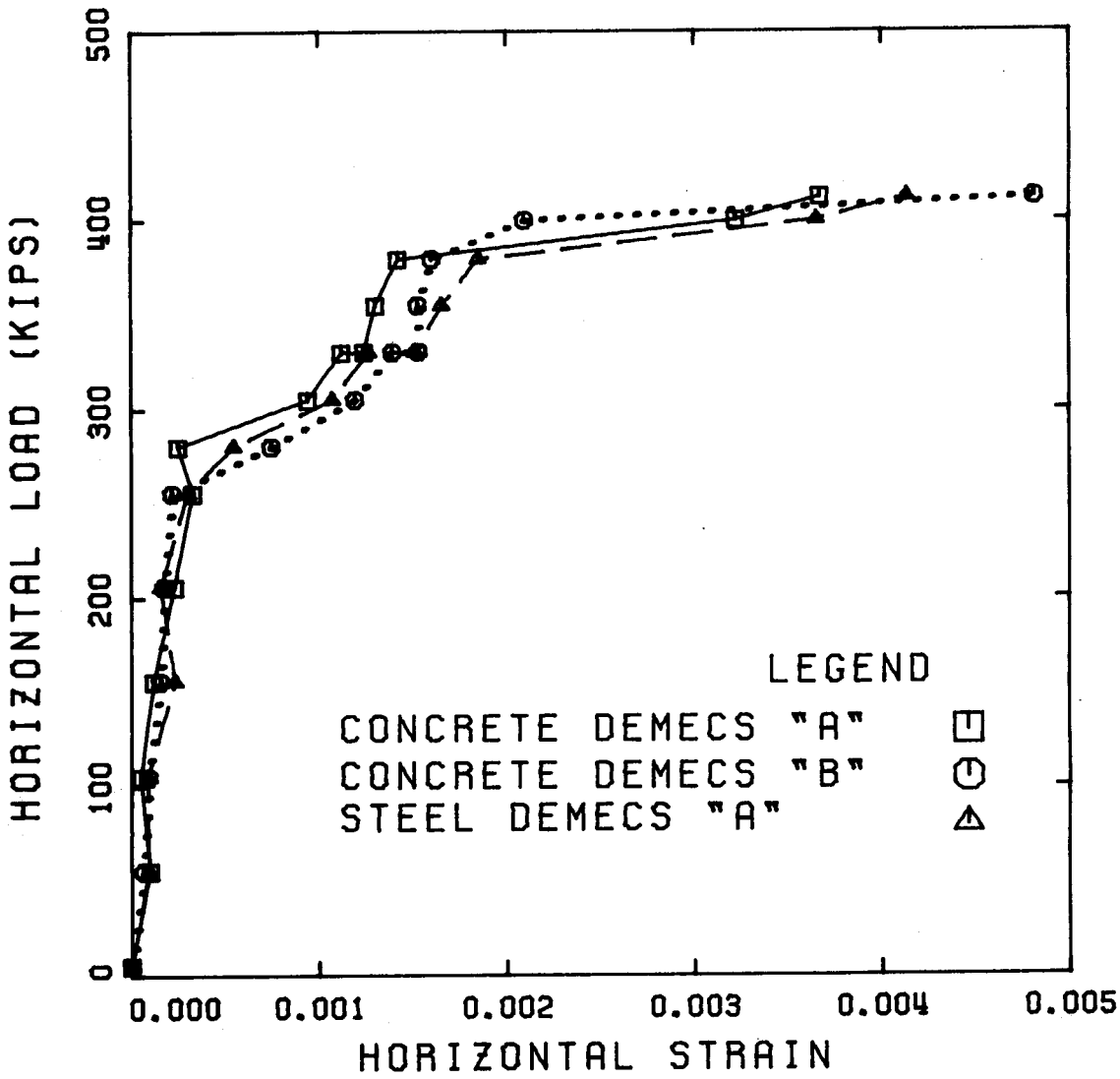

Horizontal Direction

Figure 6.5.3 Load-Average Strain Curves, Segment 5

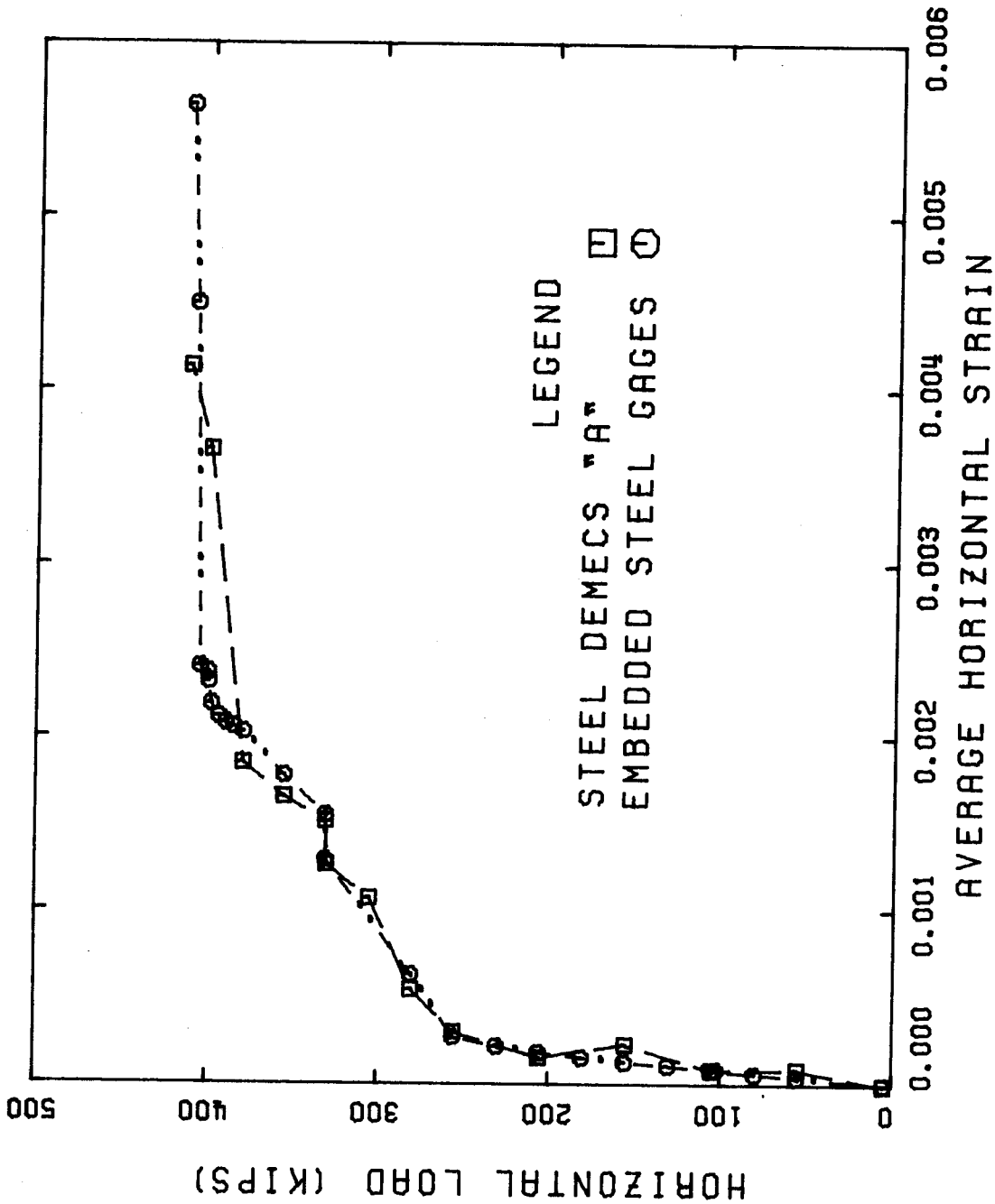

Horizontal Direction

Figure 6.5.4 Load-Average Steel Strain Curves, Segment 5

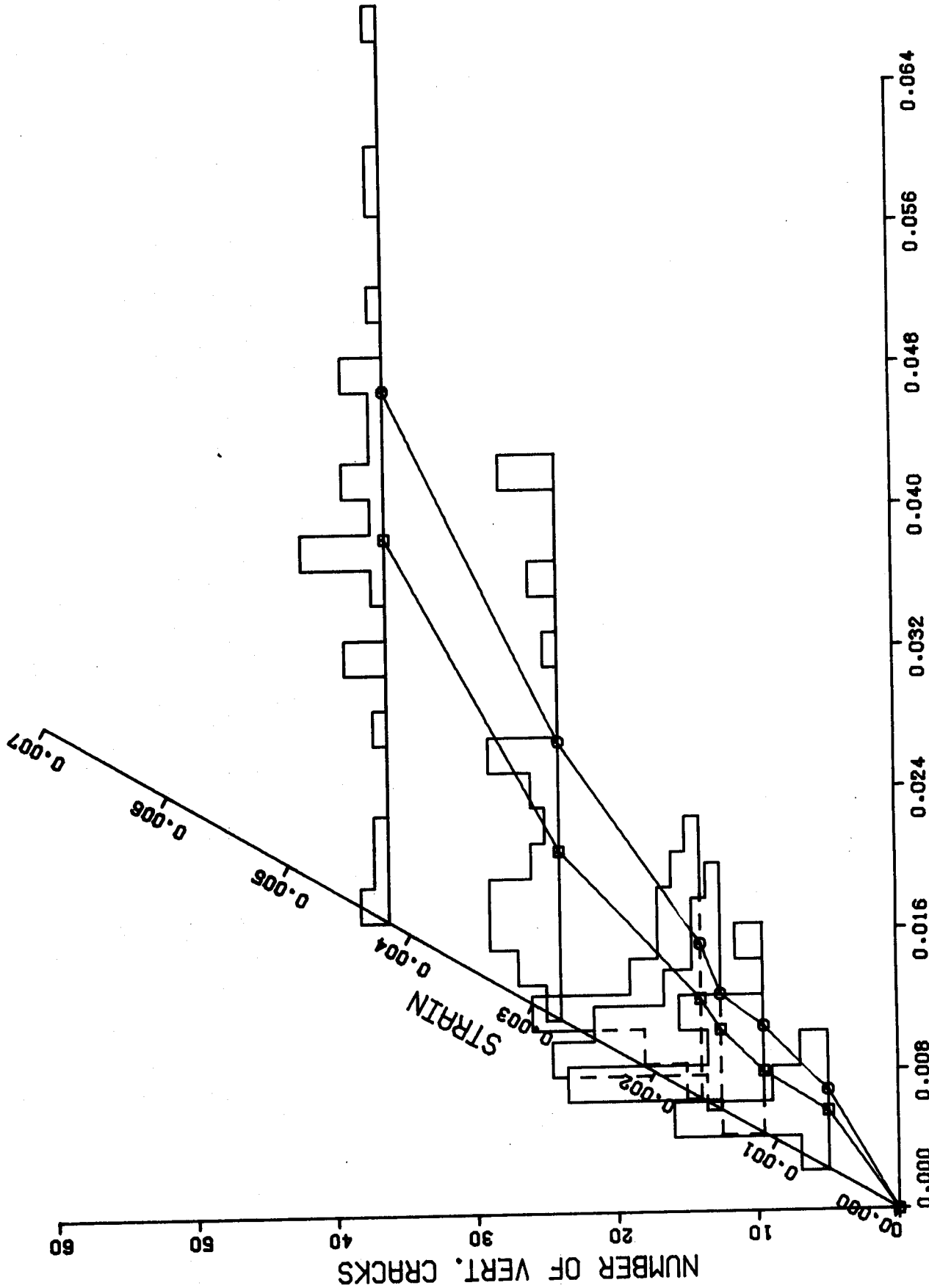

Vertical Cracks

Figure 6.5.5 Distribution of Crack Widths, Segment 5

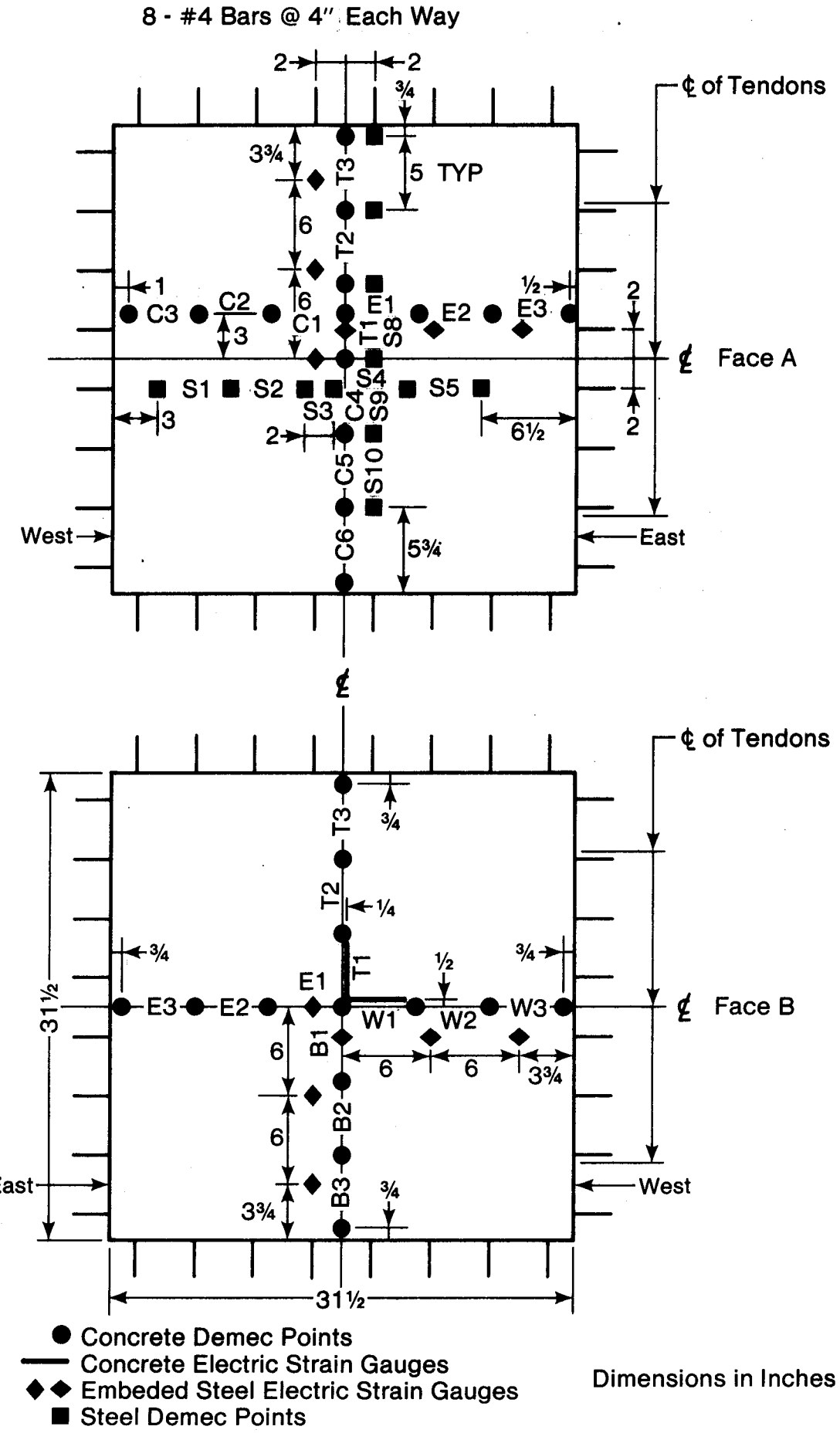

Figure 6.6.1 Location of Strain Measurements, Specimen 6

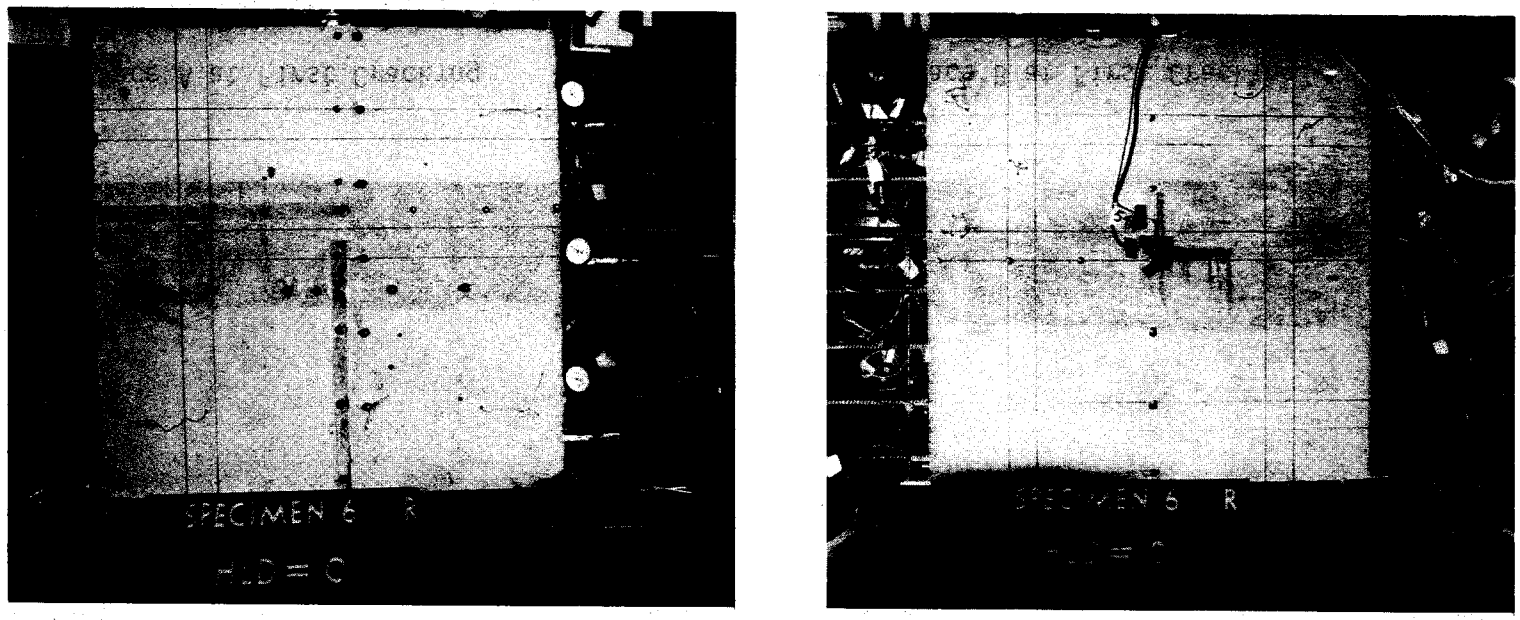

(a) Face A Before Loading

(b) Face B Before Loading

Figure 6.6.2 Development of Cracking in Segment 6

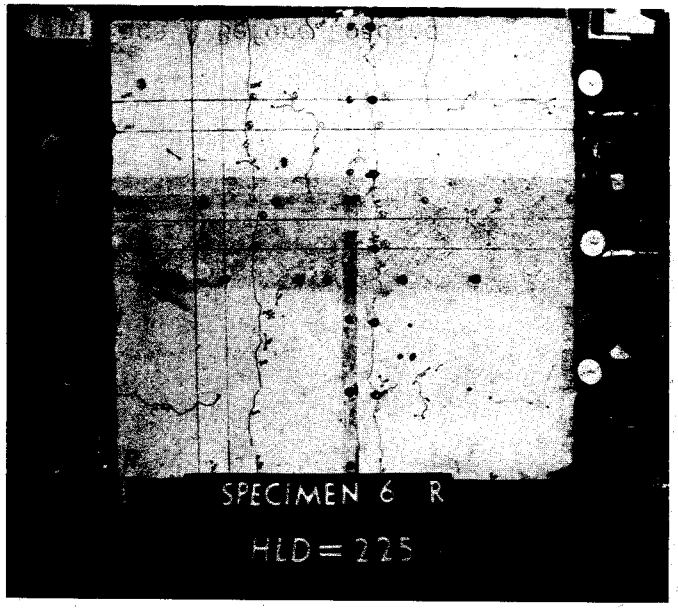

(c) Face A at First Cracking

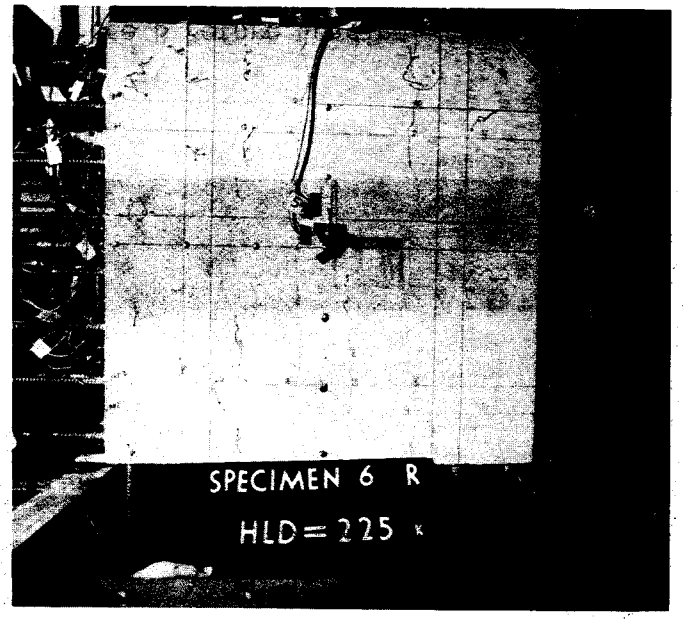

(d) Face B at First Cracking

Figure 6.6.2 Development of Cracking in Segment 6

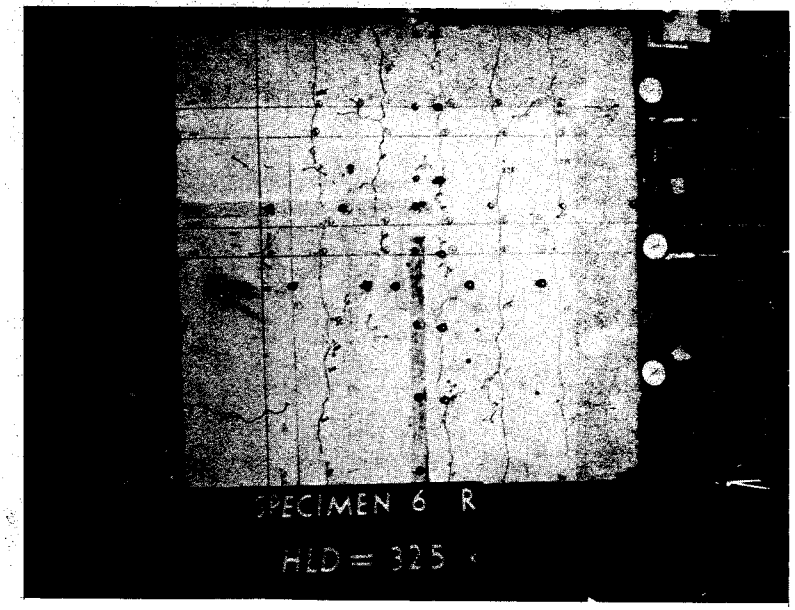

(e) Face A at Onset of Vertical Cracking

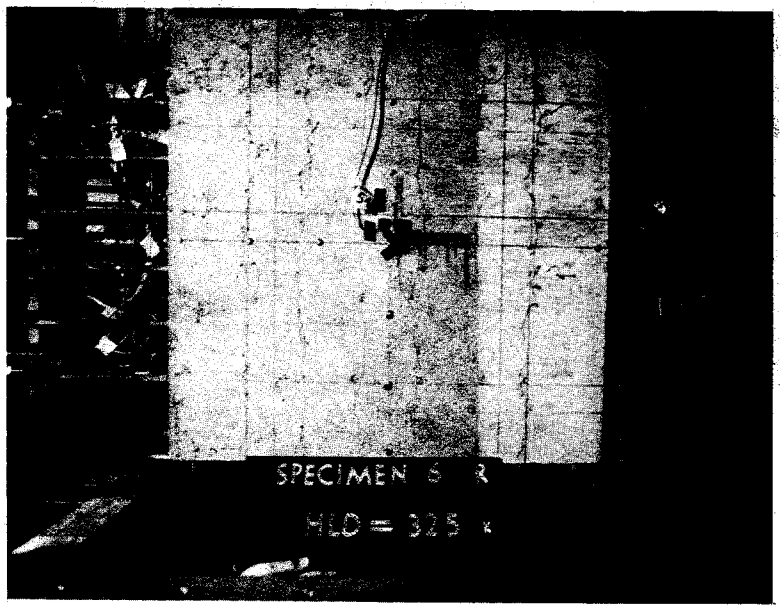

(f) Face B at Onset of Vertical Cracking

Figure 6.6.2 Development of Cracking in Segment 6

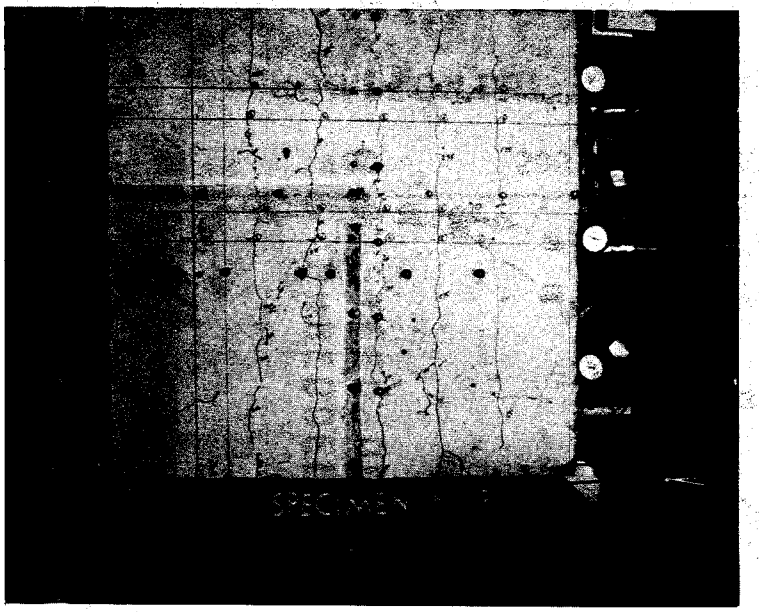

(g) Face A at End of Test

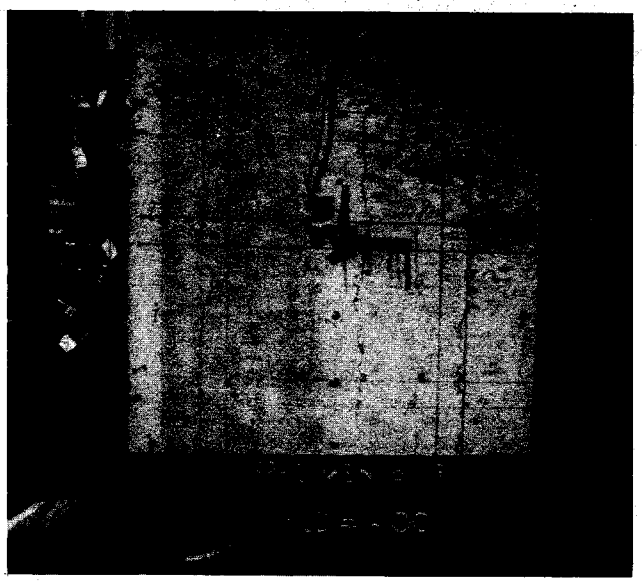

(h) Face B at End of Test

Figure 6.6.2 Development of Cracking in Segment 6

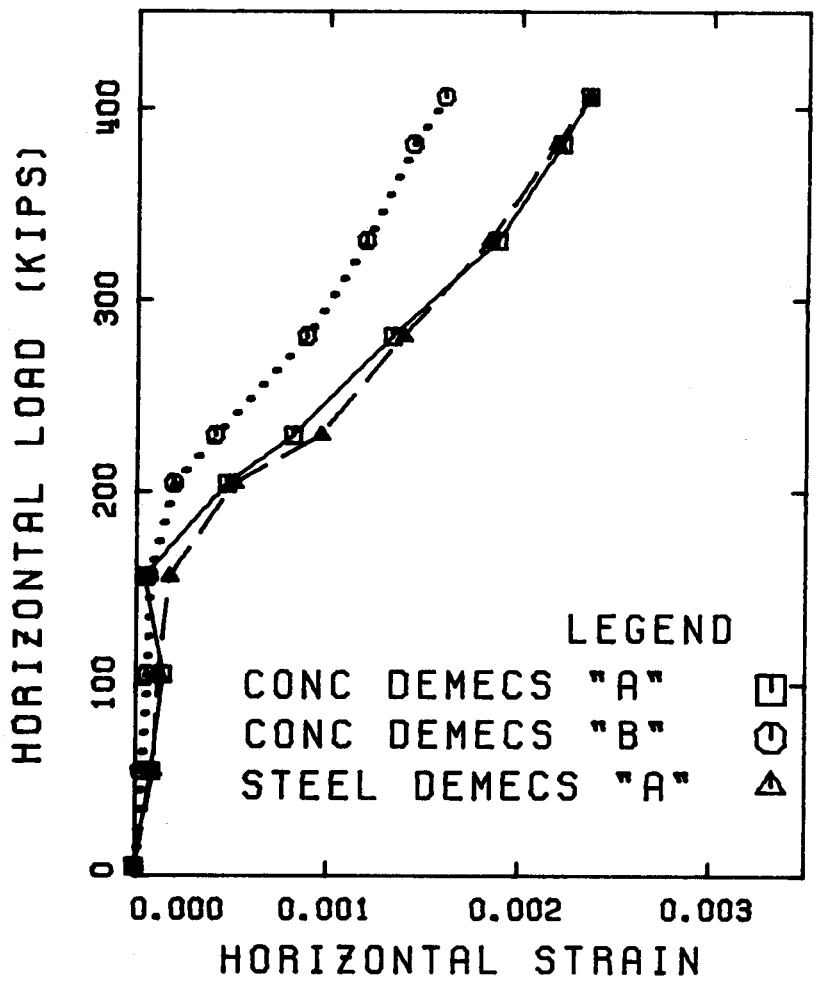

Horizontal Direction

Figure 6.6.3 Load-Average Strain Curves, Segment 6

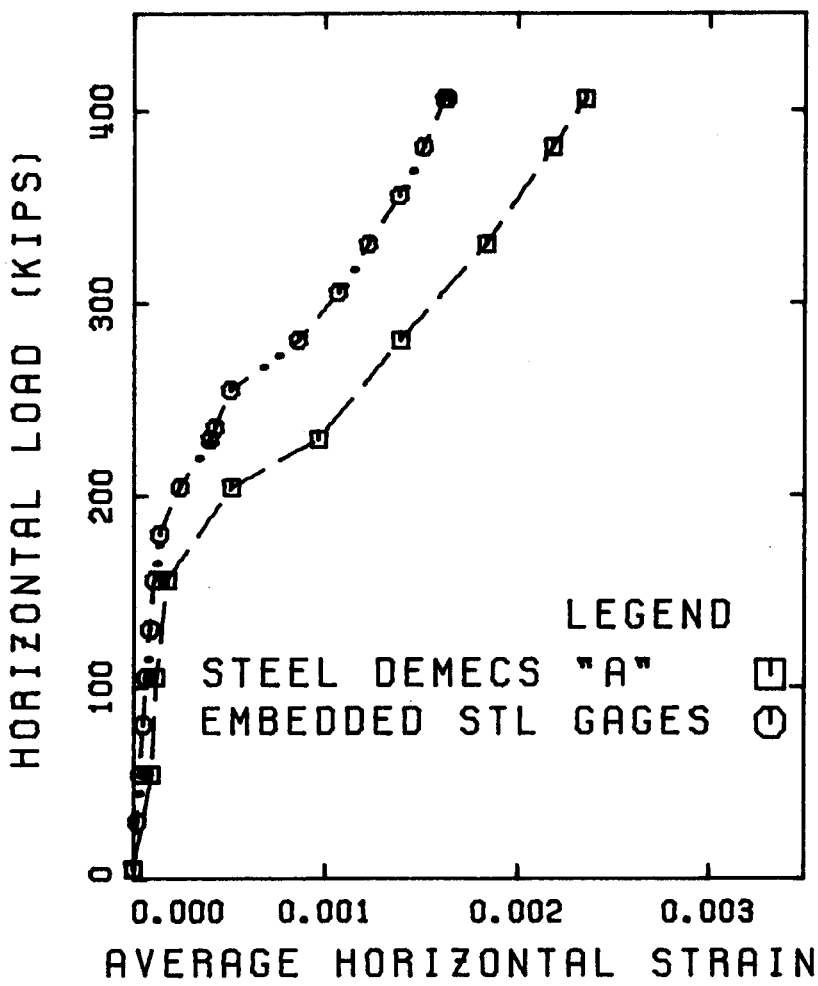

Horizontal Direction

Figure 6.6.4 Load-Average Steel Strain Curves, Segment 6

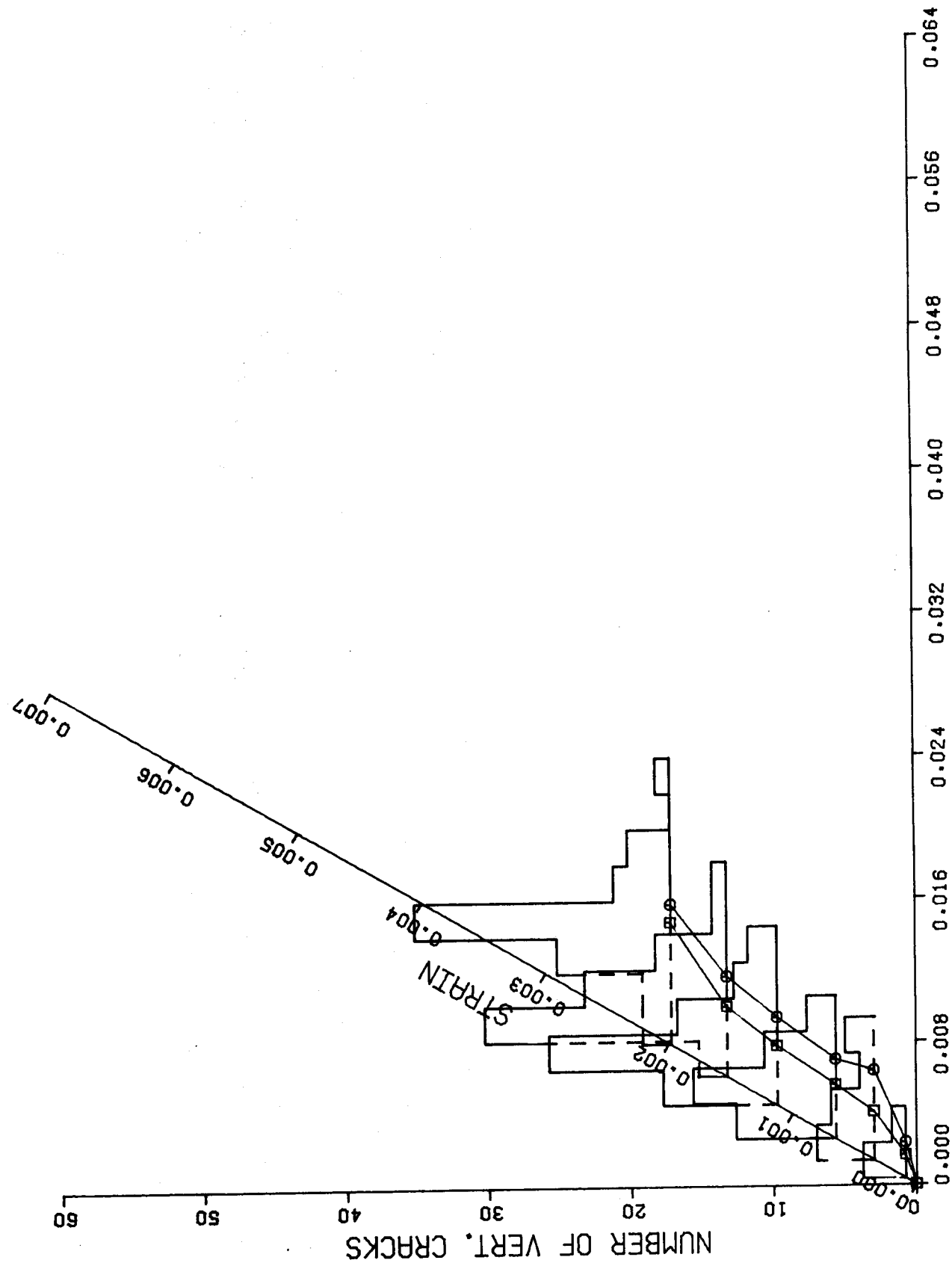

Vertical Cracks

Figure 6.6.5 Distribution of Crack Widths, Segment 6

6 - #6 Bars @ 6″ Each Way, No Pre-Stress

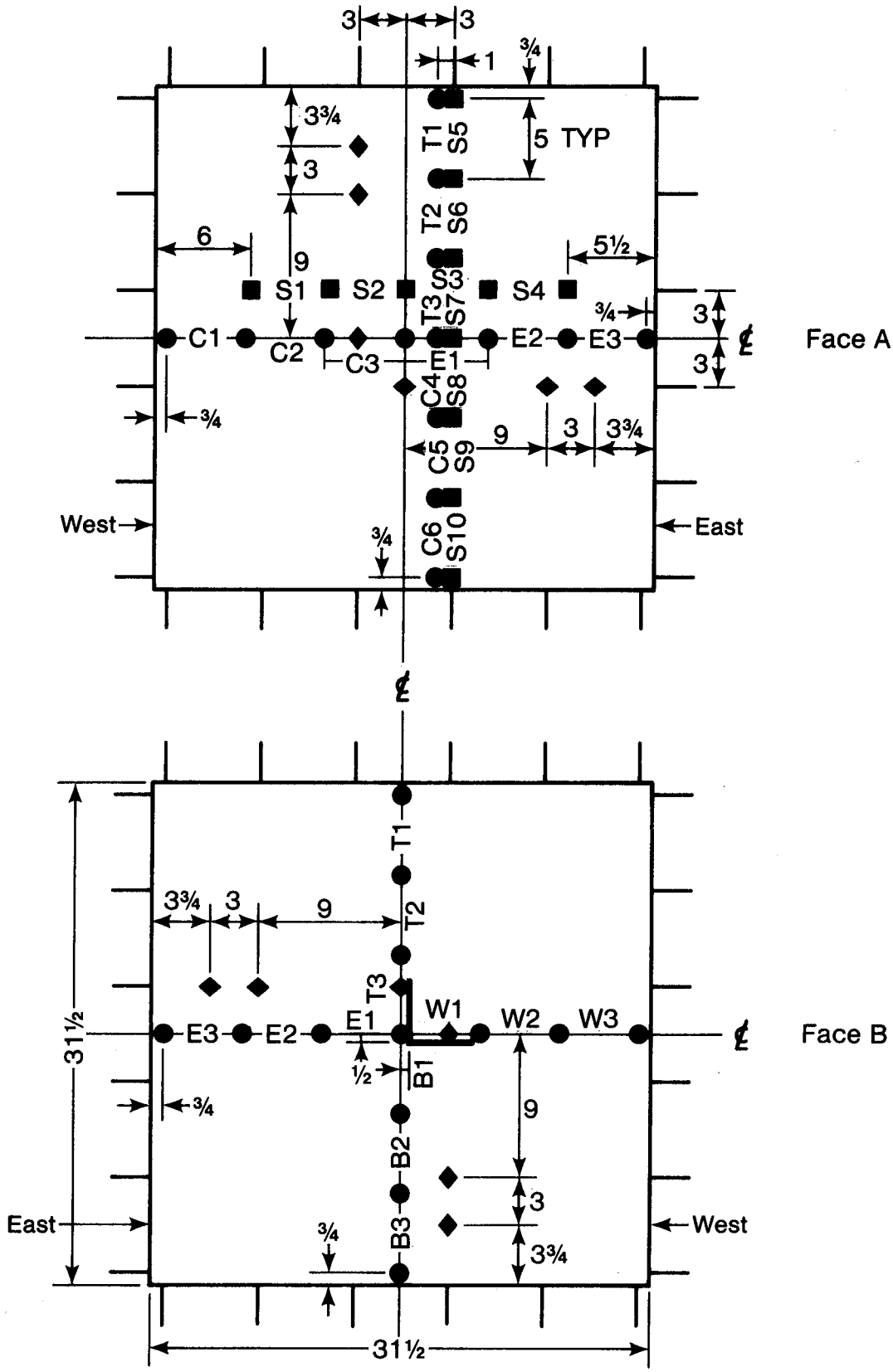

Figure 6.7.1 Location of Strain Measurements, Specimen 7

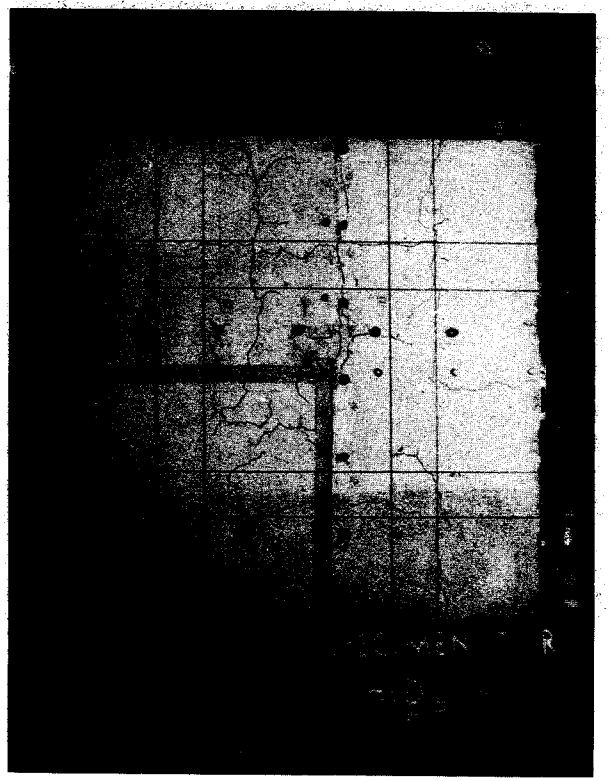

(a) Face A Before Loading

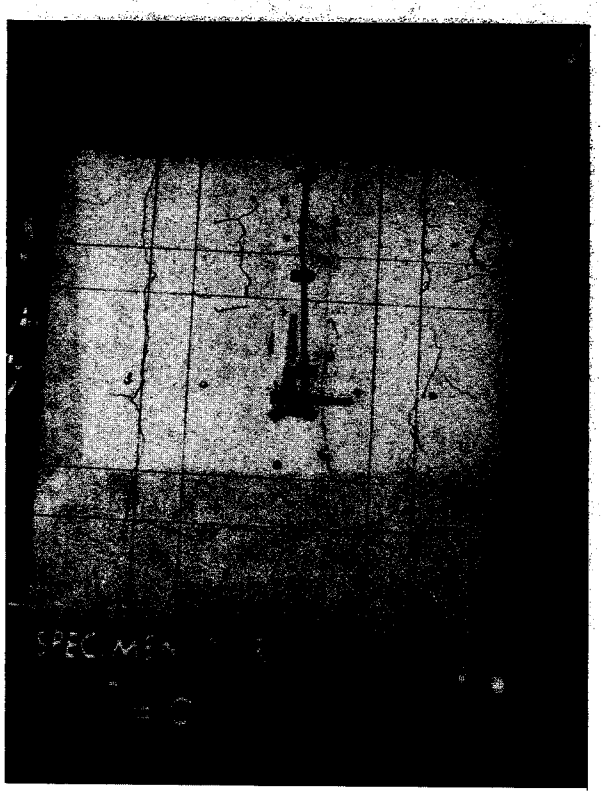

(b) Face B Before Loading

Figure 6.7.2 Development of Cracking in Segment 7

(c) Face A at Onset of Vertical Cracking

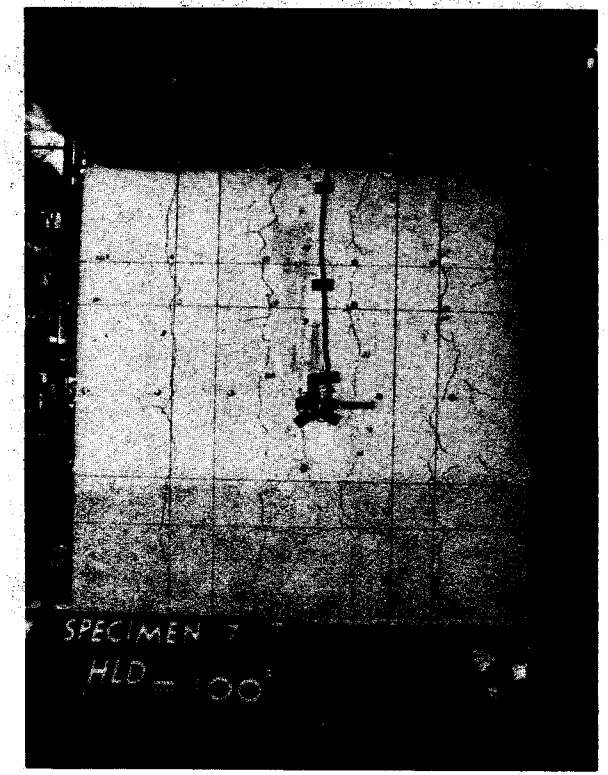

(d) Face B at Onset of Vertical Cracking

Figure 6.7.2 Development of Cracking in Segment 7

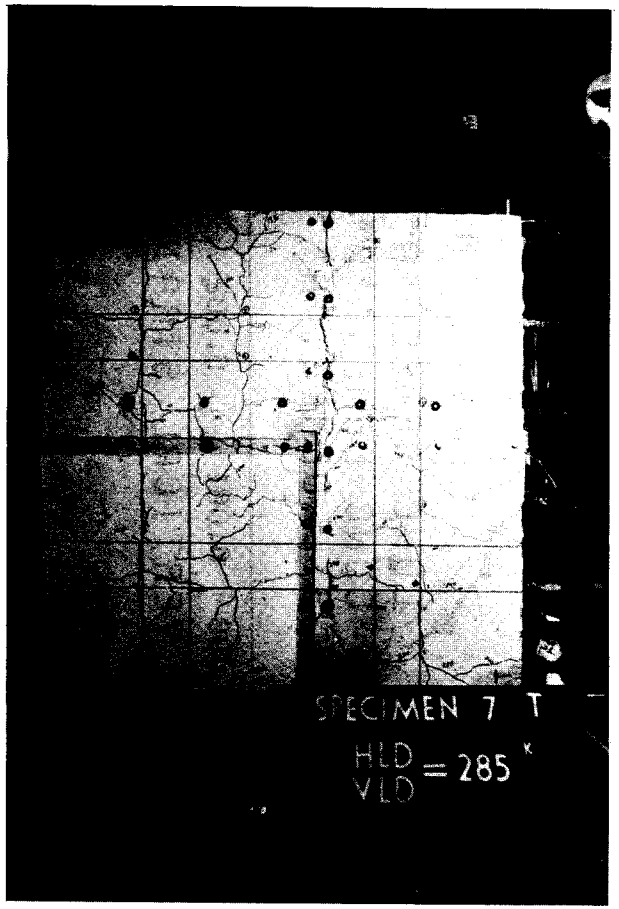

(e) Face A at End of Test

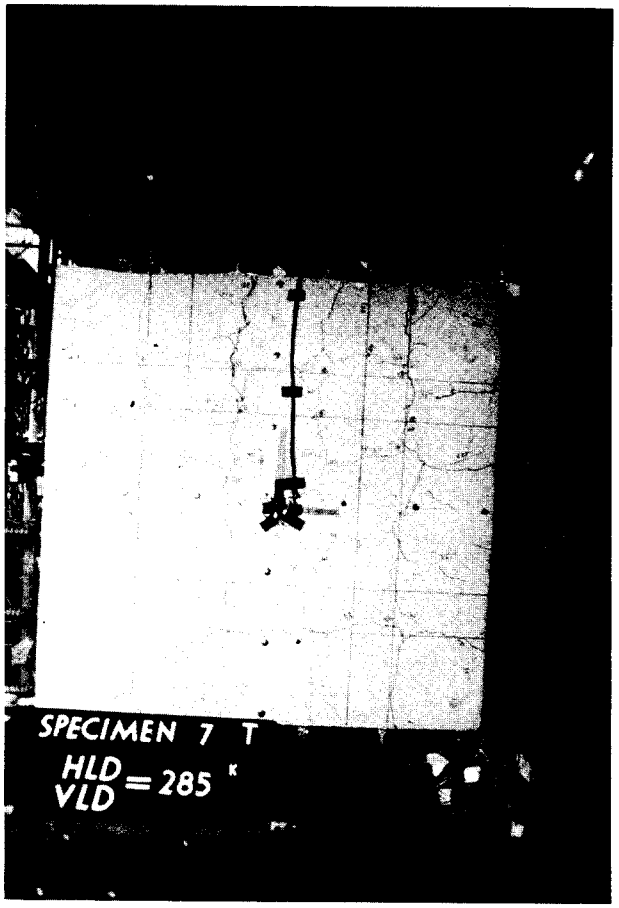

(f) Face B at End of Test

Figure 6.7.2 Development of Cracking in Segment 7

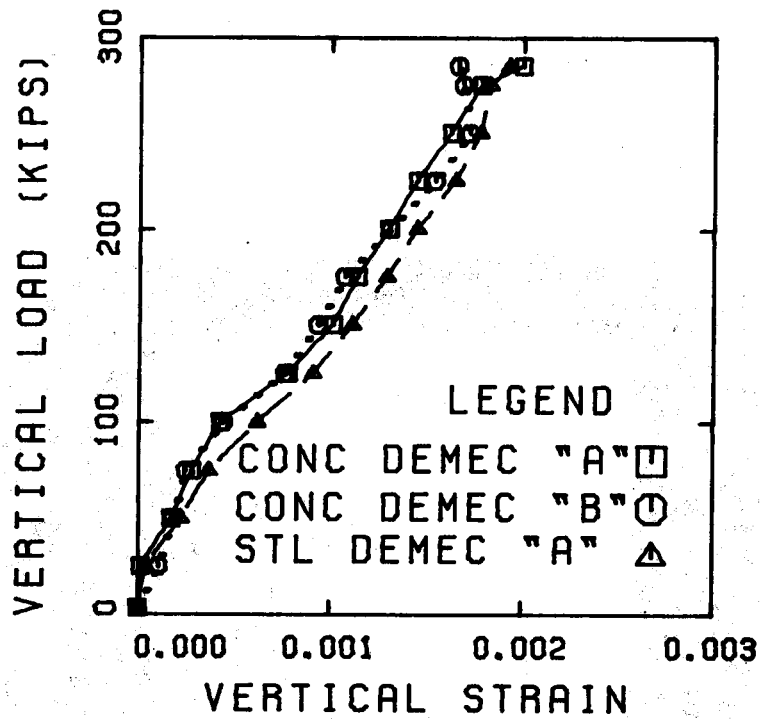

(a) Vertical Direction

Figure 6.7.3 Load-Average Strain Curves, Segment 7

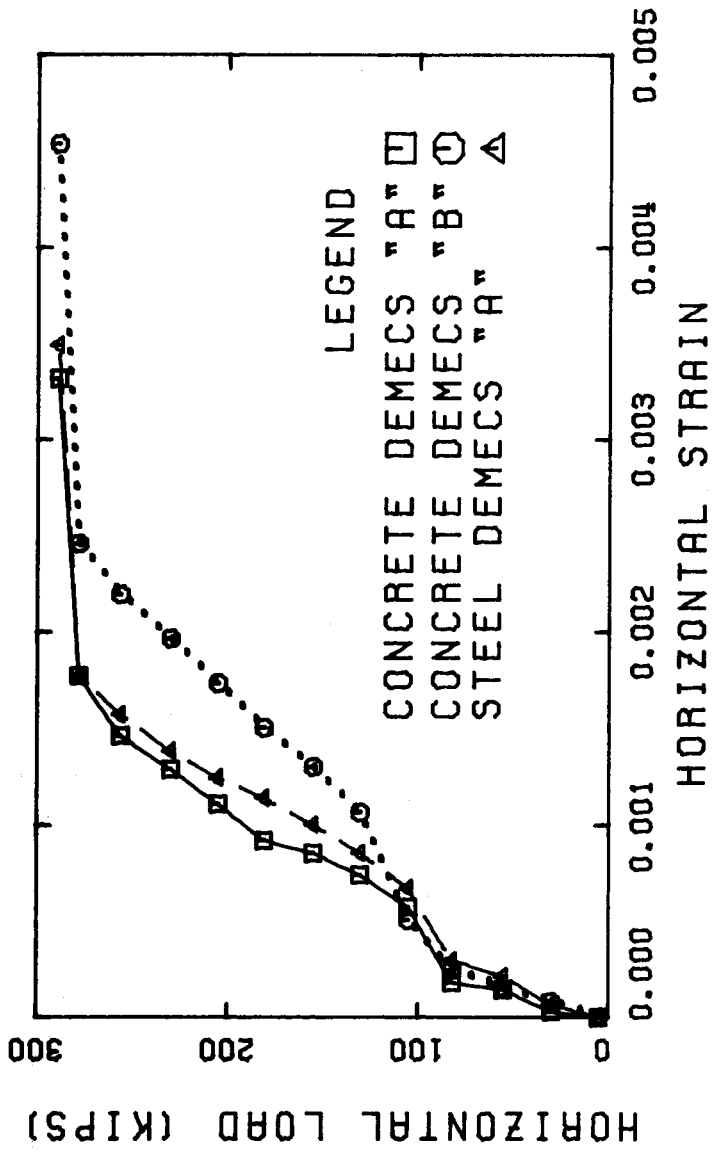

(b) Horizontal Direction

Figure 6.7.3 Load-Average Strain Curves, Segment 7

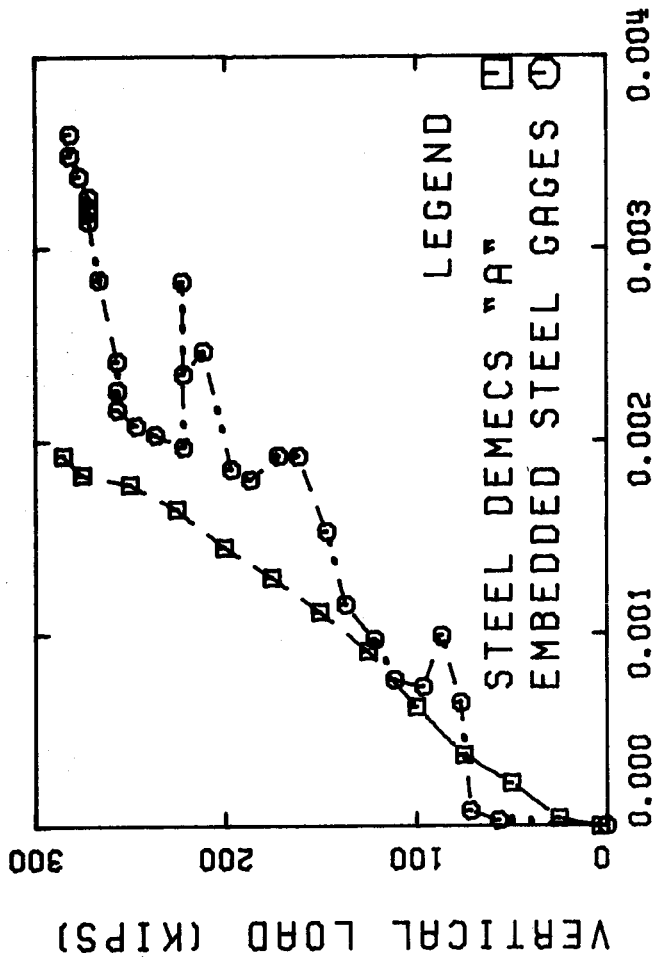

(a) Vertical Direction

Figure 6.7.4 Load-Average Steel Strain Curves, Segment 7

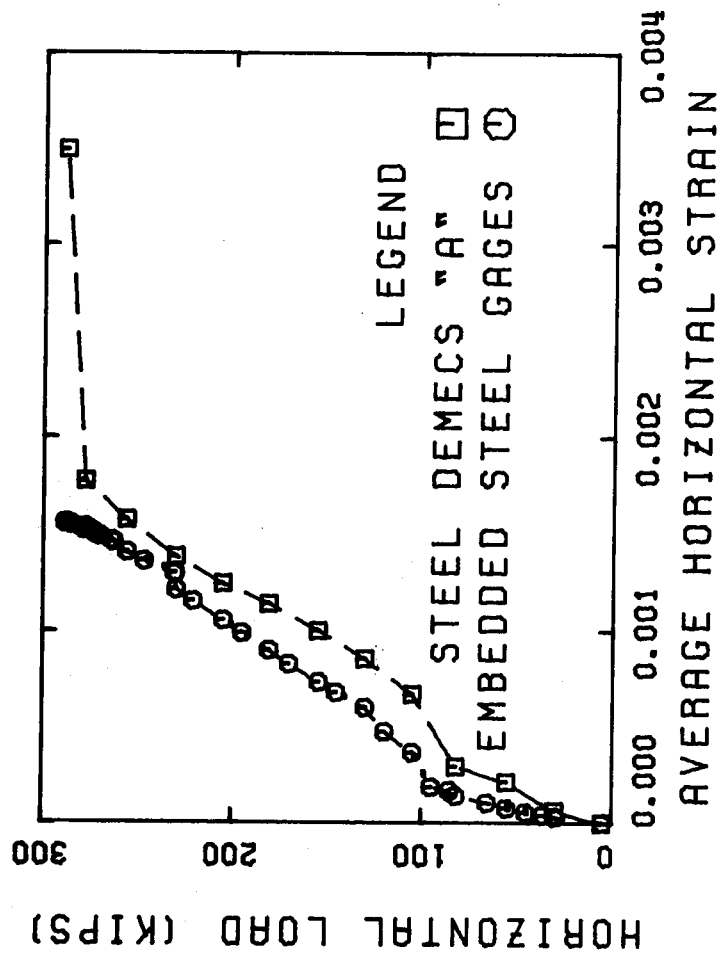

(b) Horizontal Direction

Figure 6.7.4 Load-Average Steel Strain Curves, Segment 7

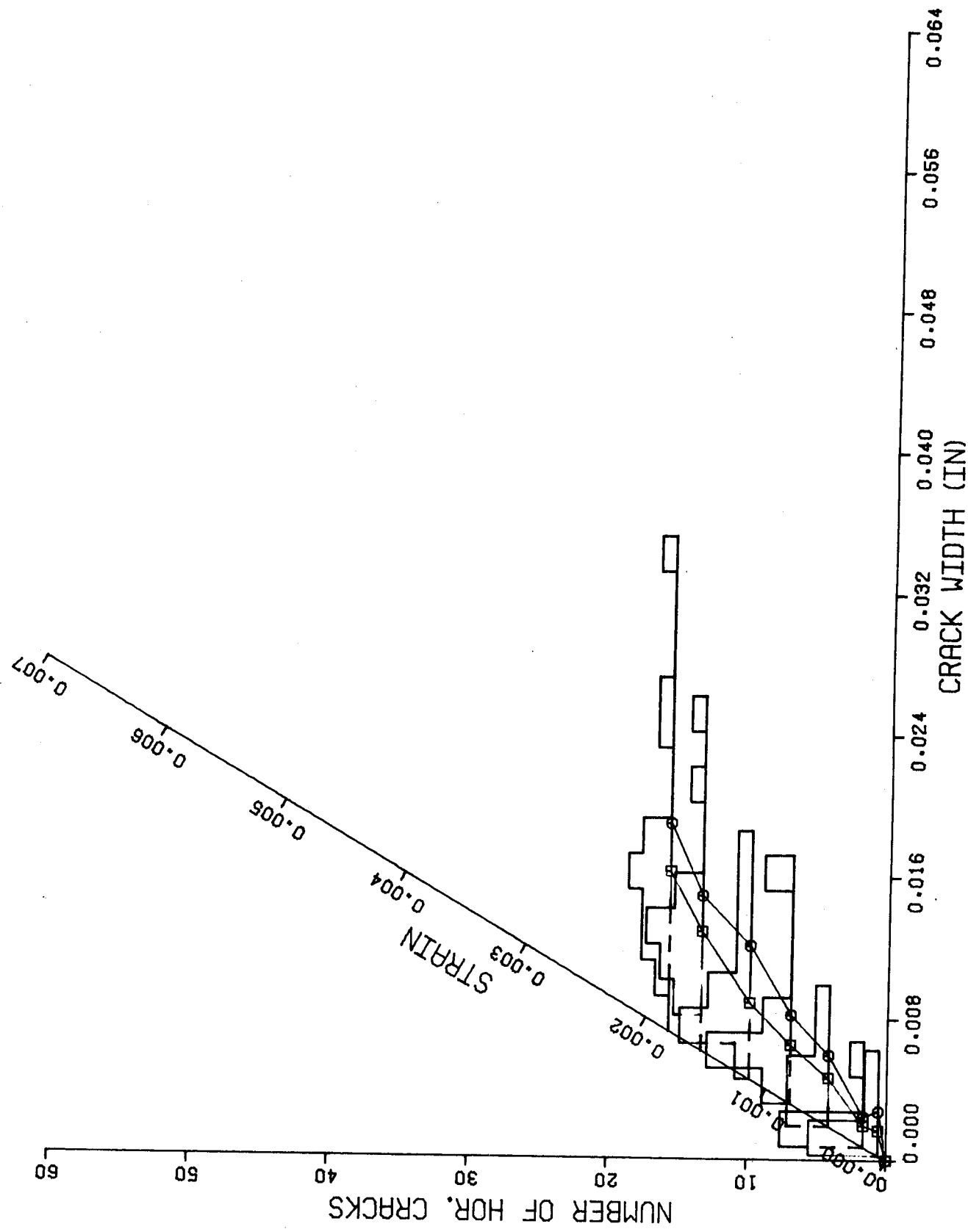

(a) Horizontal Cracks

Figure 6.7.5 Distribution of Crack Widths, Segment 7

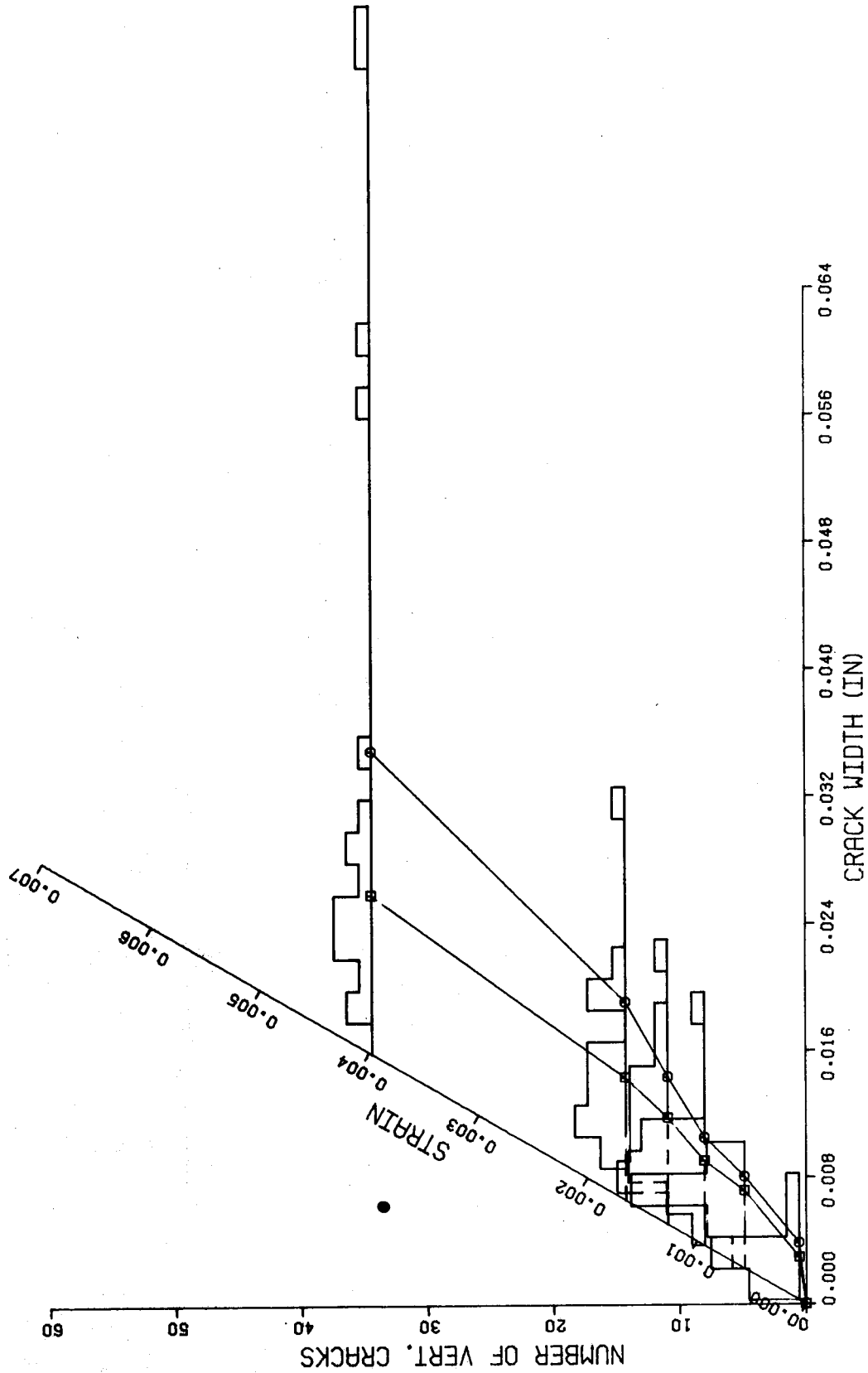

(b) Vertical Cracks

Figure 6.7.5 Distribution of Crack Widths, Segment 7

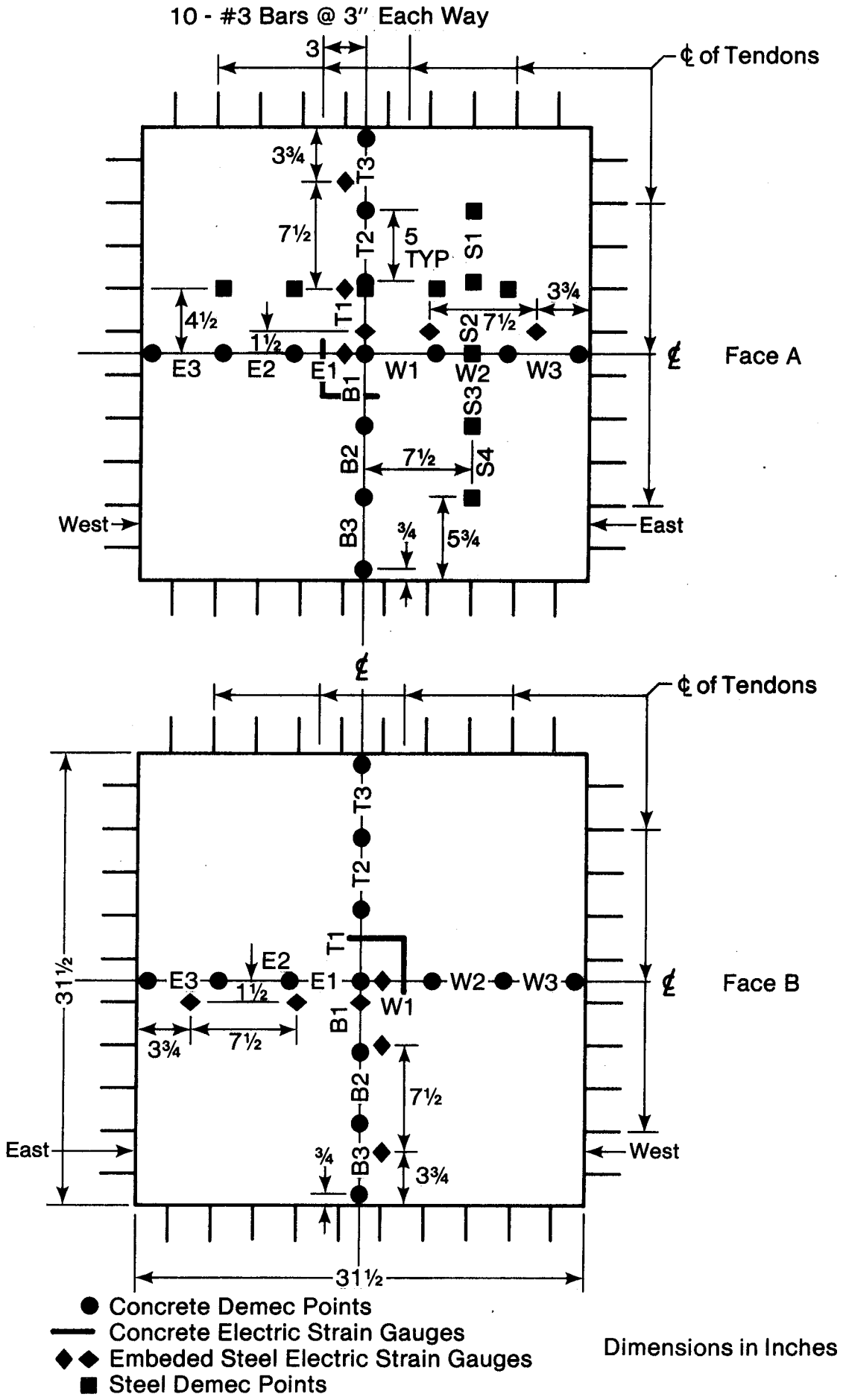

FIGURE 6.8.1 Location of Strain Measurements, Specimen 8

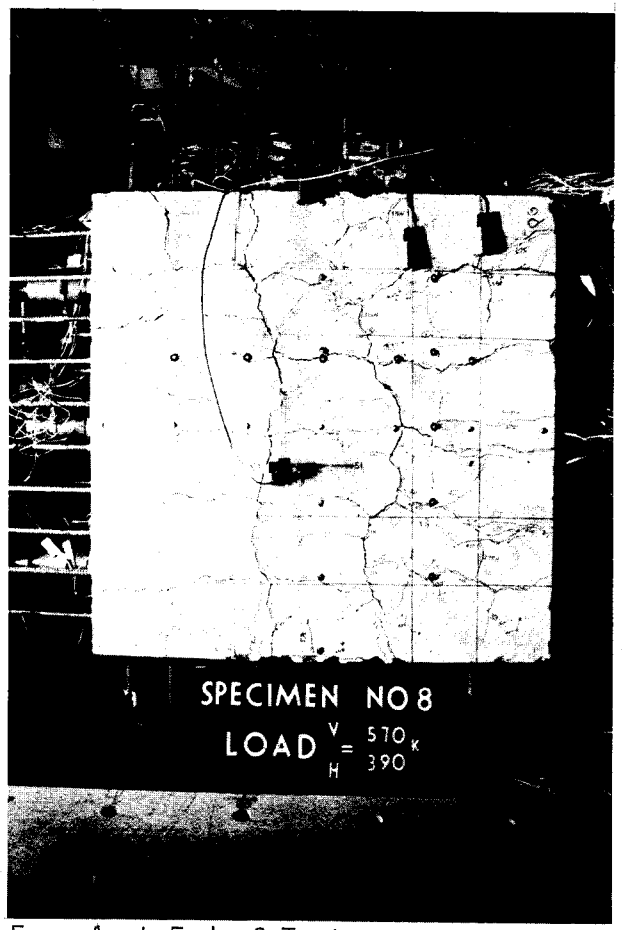

(a) Face A at End of Test

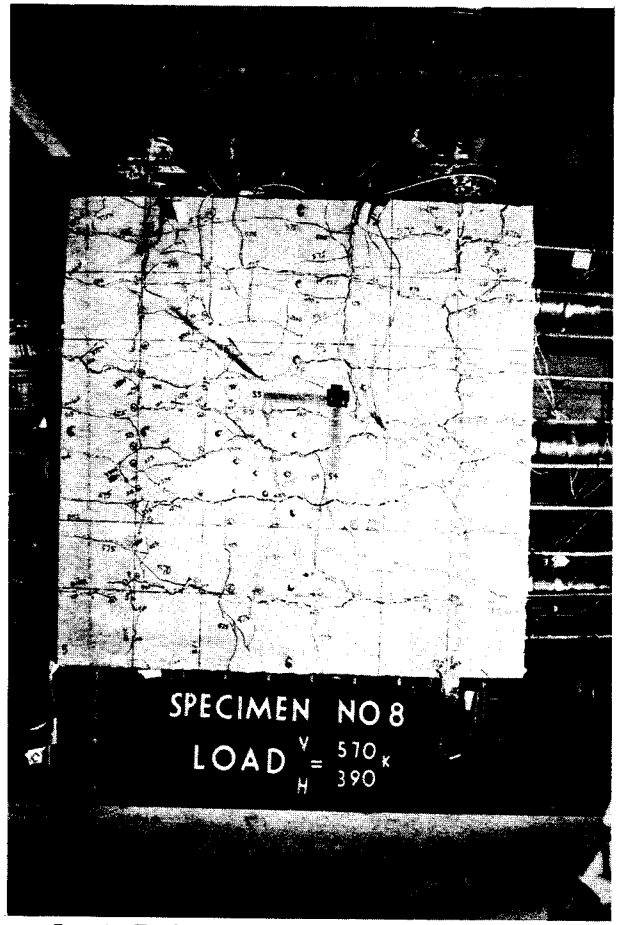

(b) Face B at End of Test

Figure 6.8.2 Development of Cracking in Segment 8

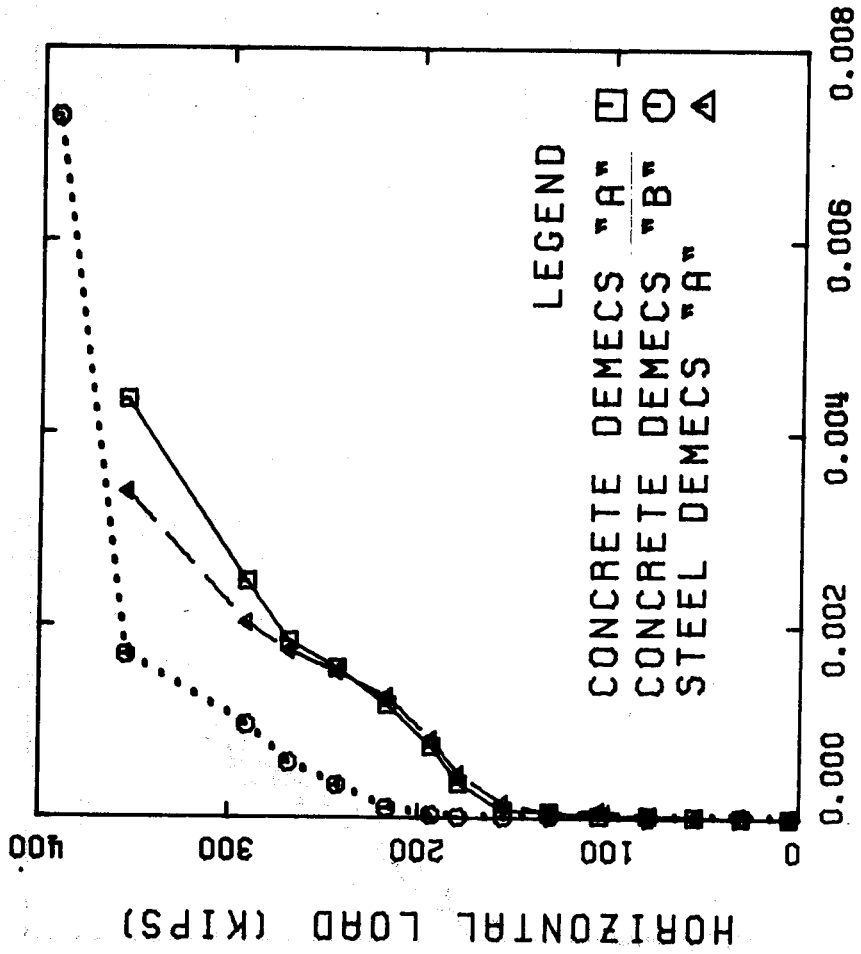

Horizontal Direction (For Vertical Direction See Figure 5.3)

Figure 6.8.3 Load-Average Strain Curves, Segment 8

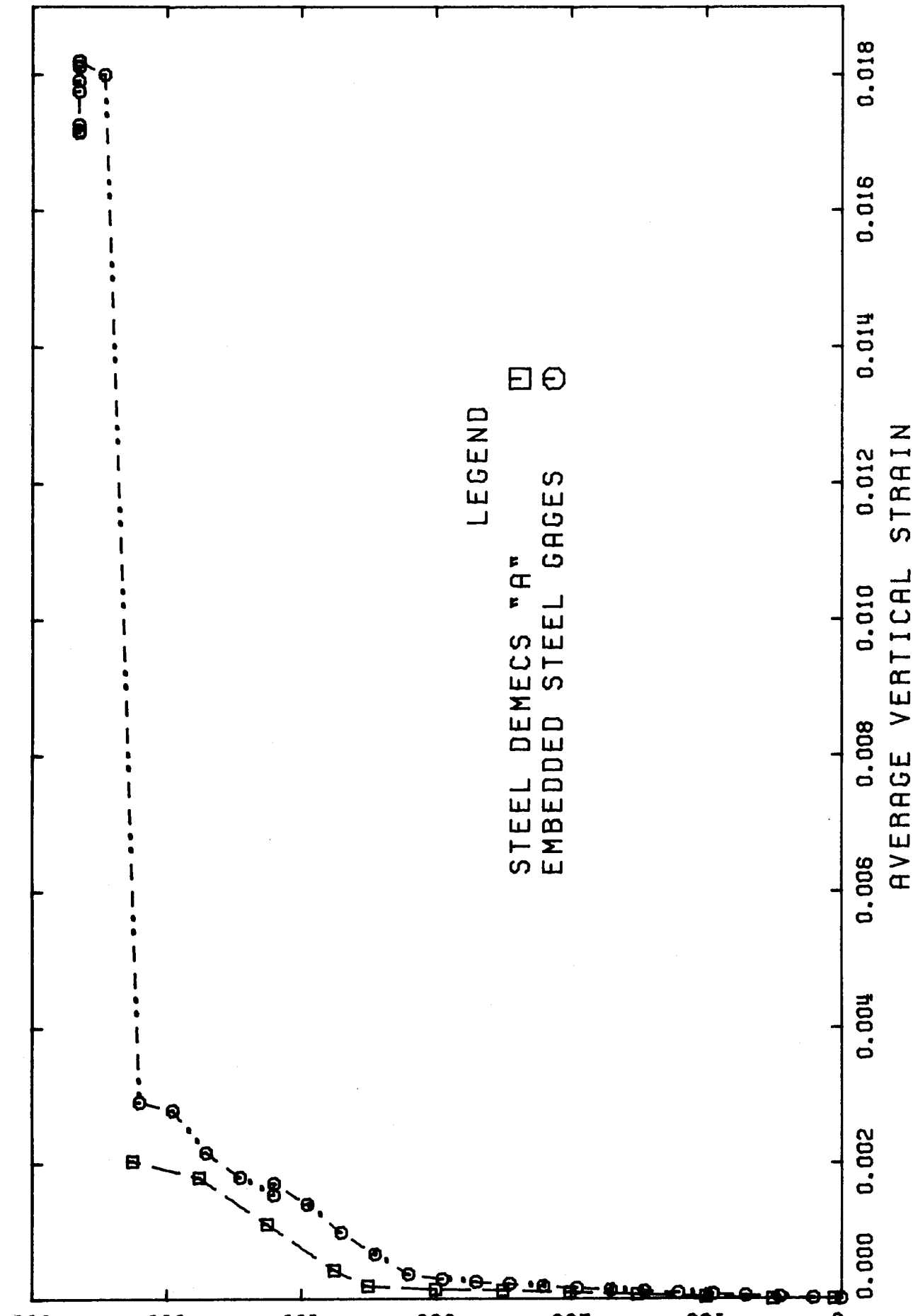

(a) Vertical Direction

Figure 6.8.4 Load-Average Steel Strain Curves, Segment 8

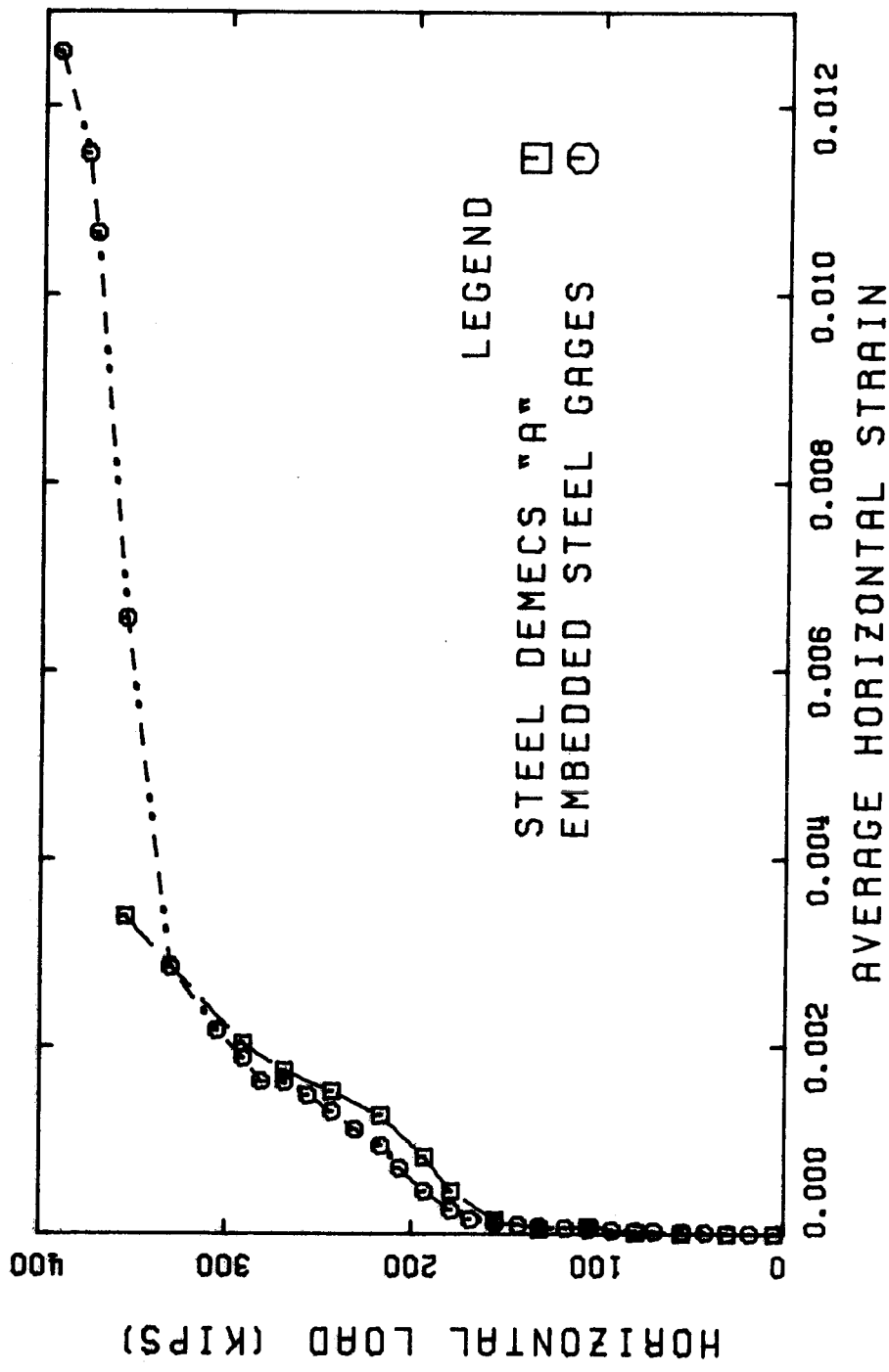

(b) Horizontal Direction

Figure 6.8.4 Load-Average Steel Strain Curves, Segment 8

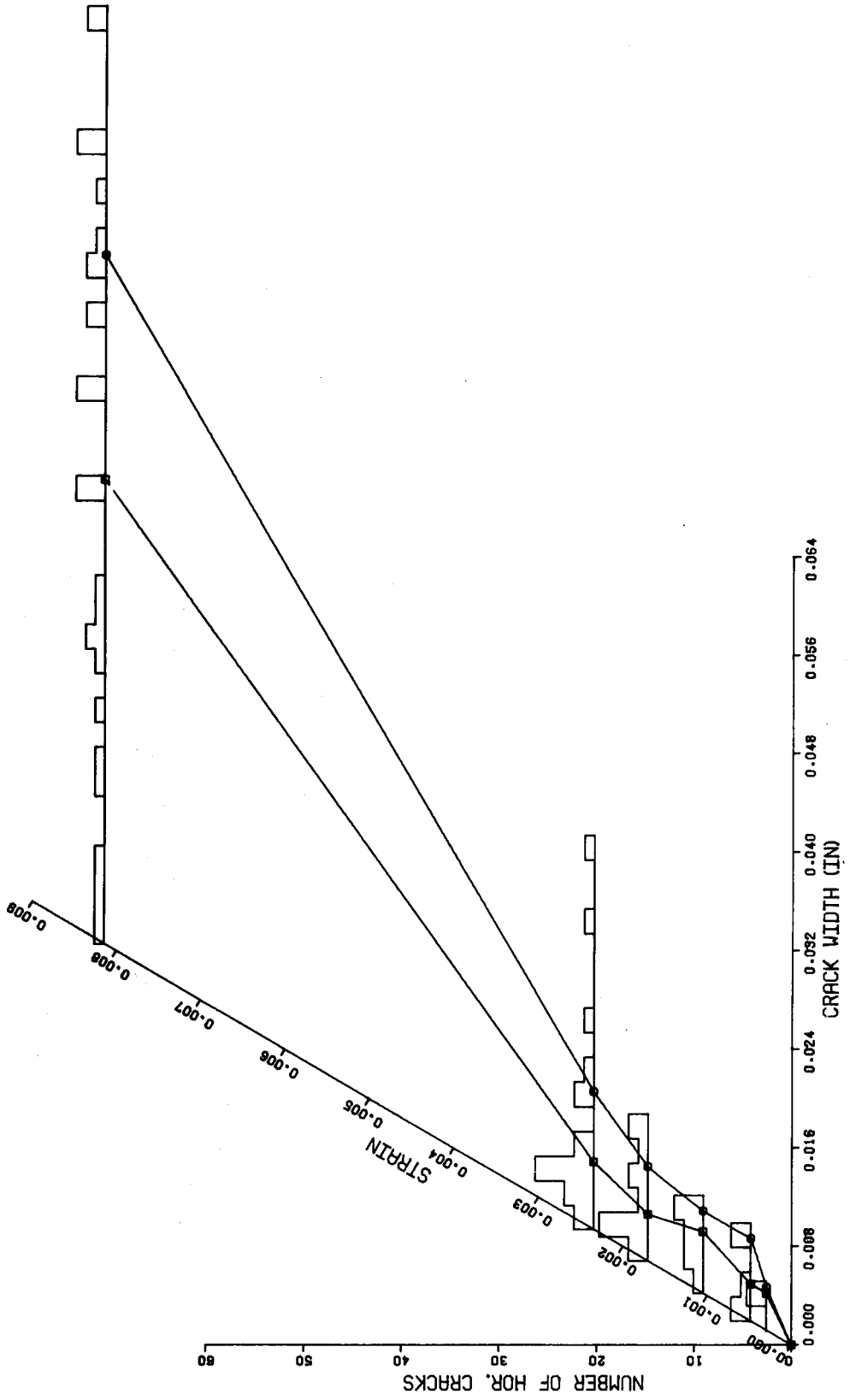

(a) Horizontal Cracks

Figure 6.8.5 Distribution of Crack Widths, Segment 8

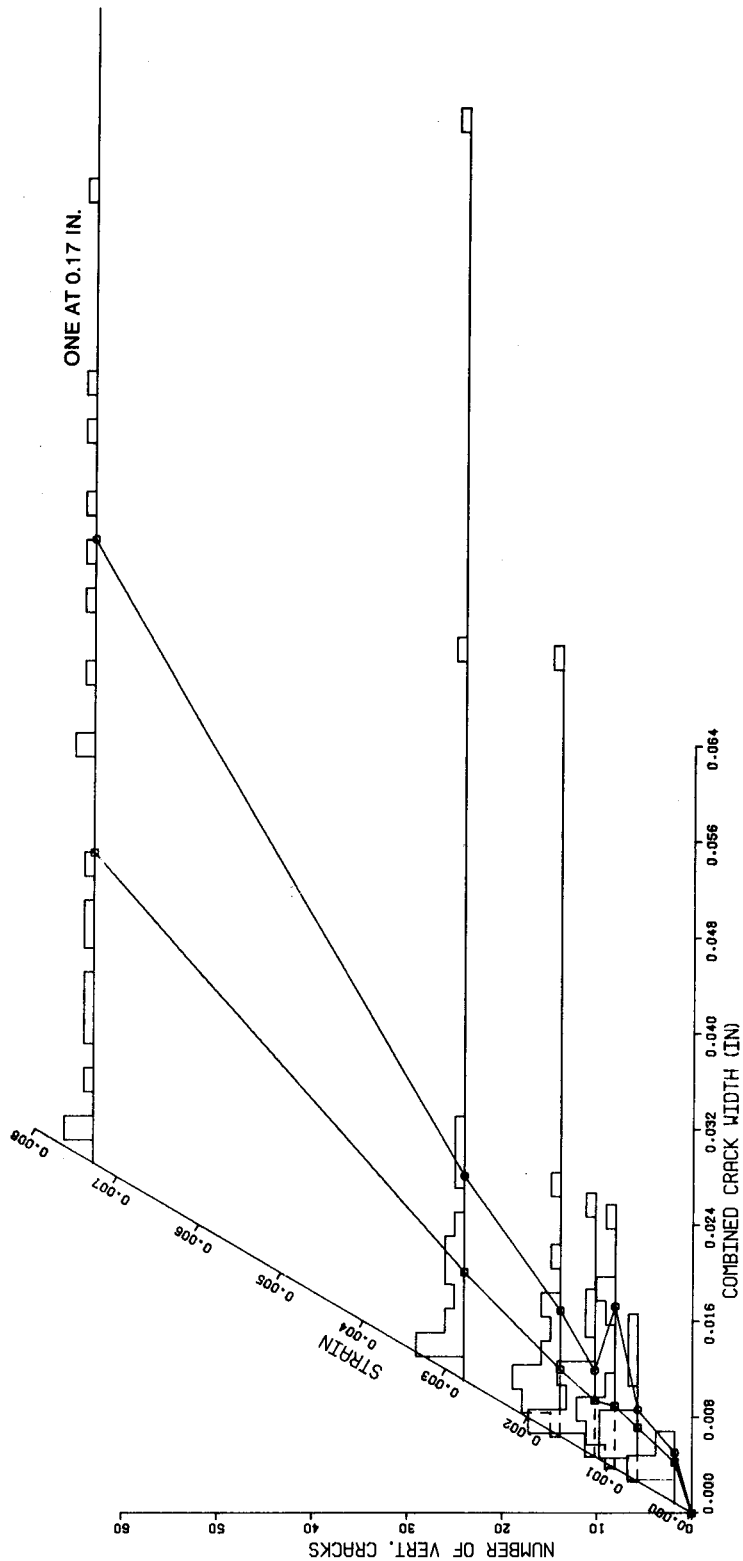

(b) Vertical Cracks

Figure 6.8.5 Distribution of Crack Widths, Segment 8

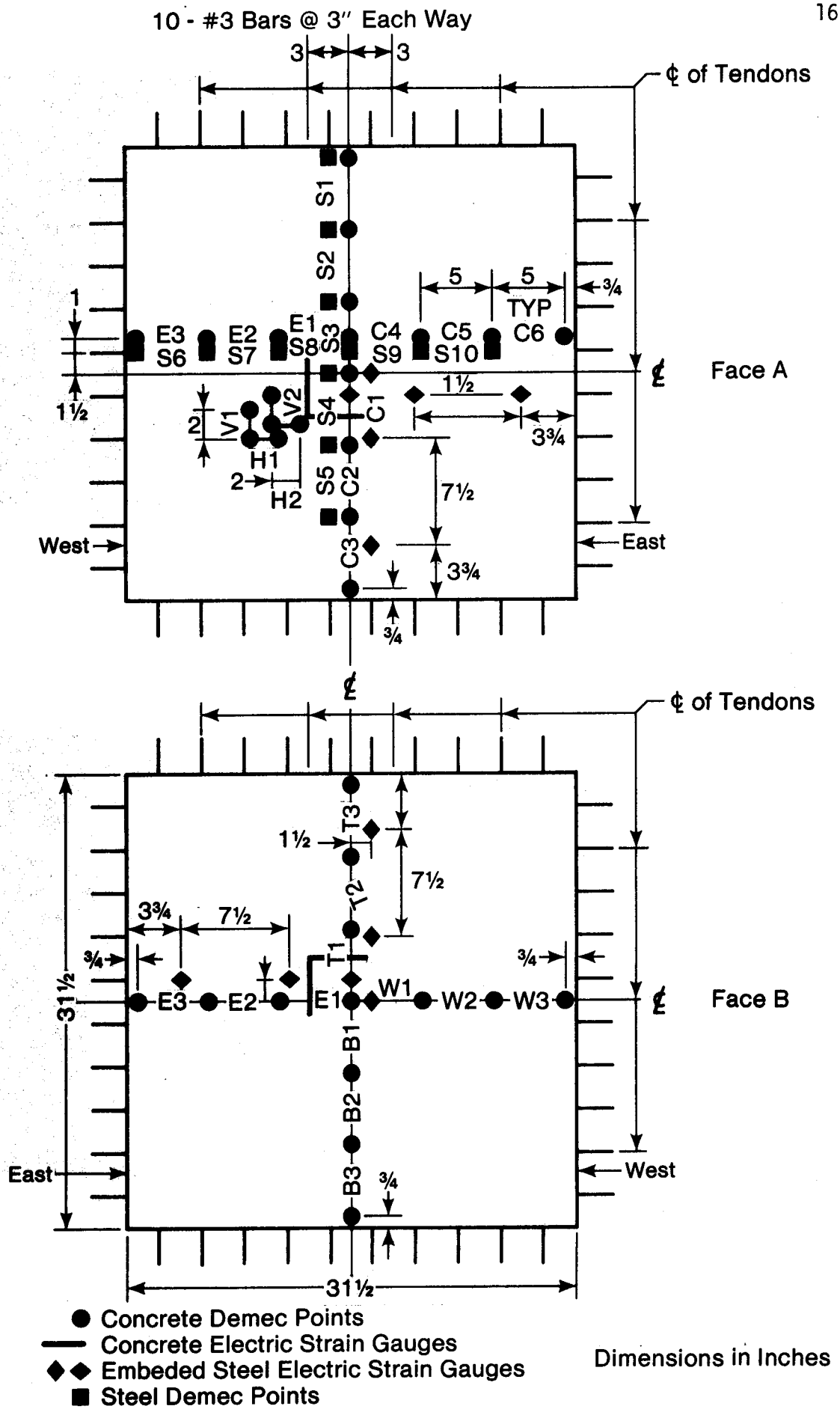

Figure 6.9.1 Location of Strain Measurements, Specimen 9

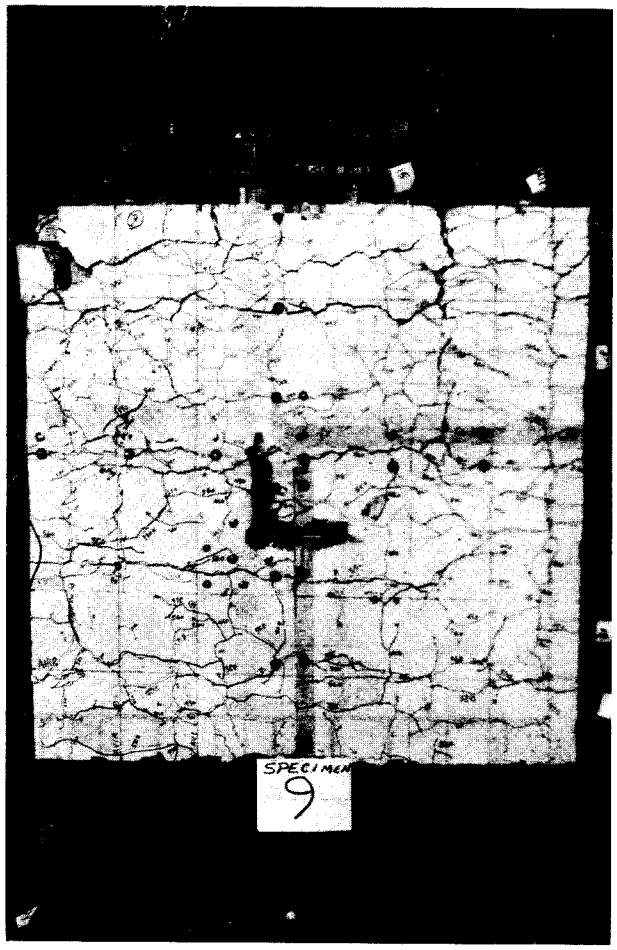

(a) Face A at End of Test

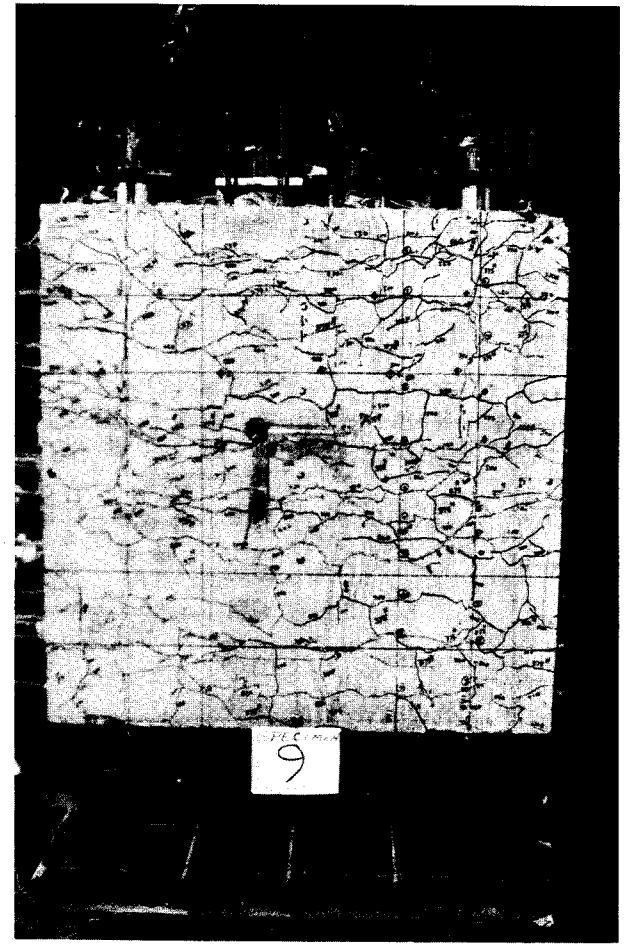

(b) Face B at End of Test

Figure 6.9.2 Development of Cracking in Segment 9

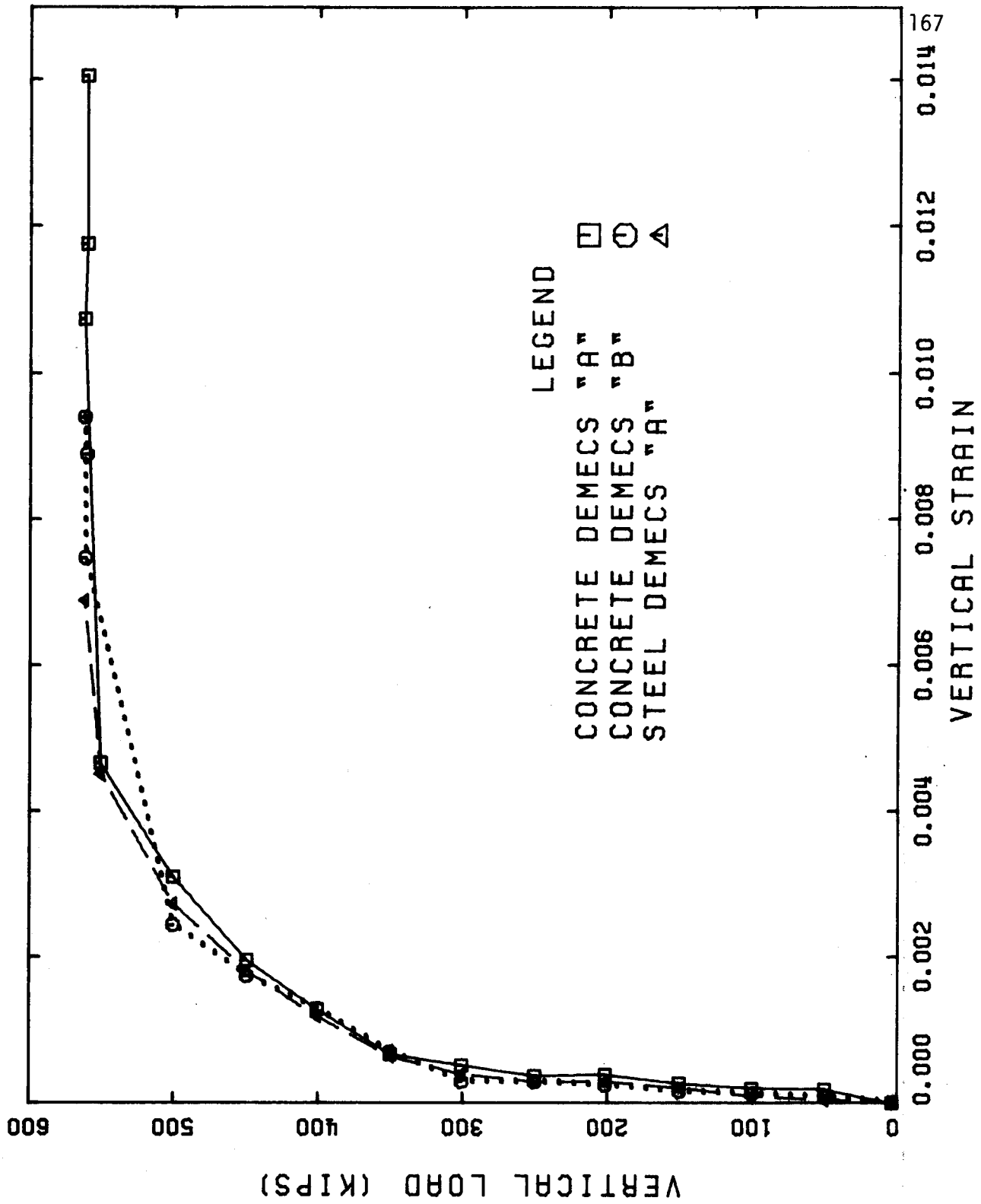

(a) Vertical Direction

Figure 6.9.3 Load-Average Strain Curves, Segment 9

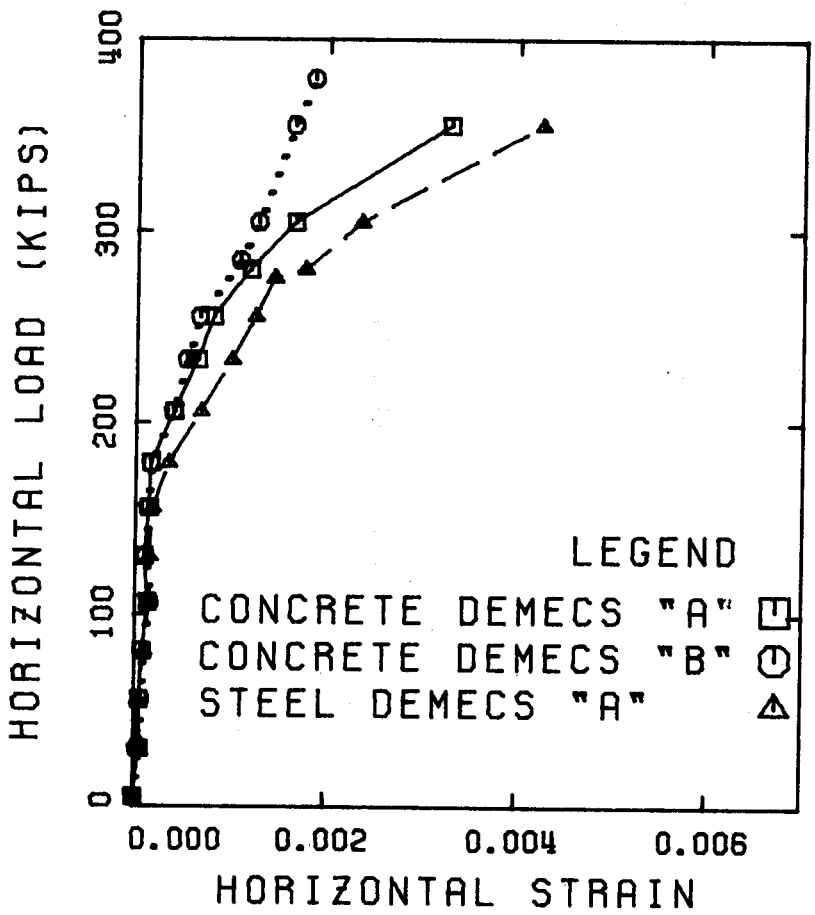

(b) Horizontal Direction

Figure 6.9.3 Load-Average Strain Curves, Segment 9

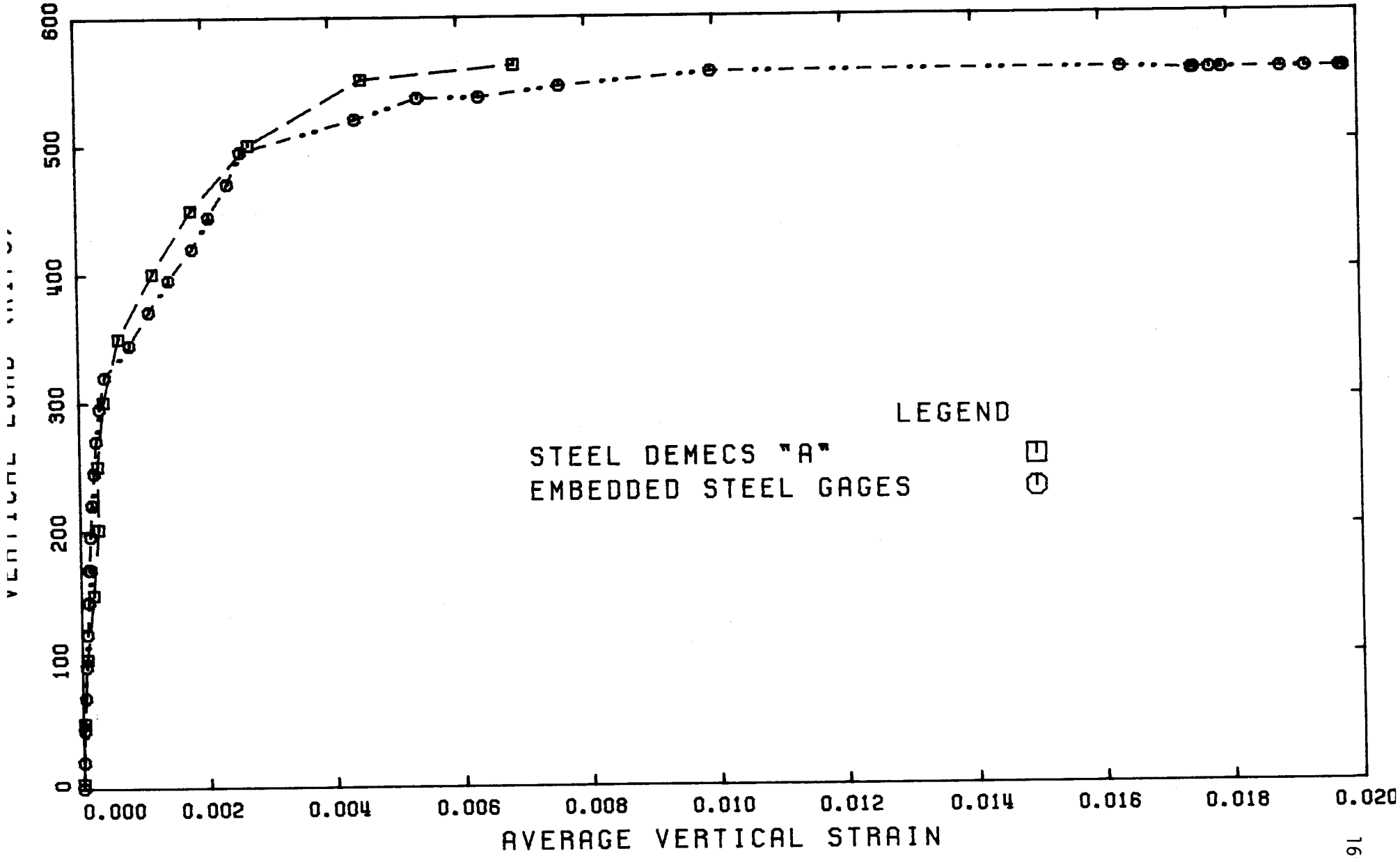

(a) Vertical Direction

Figure 6.9.4 Load-Average Steel Strain Curves, Segment 9

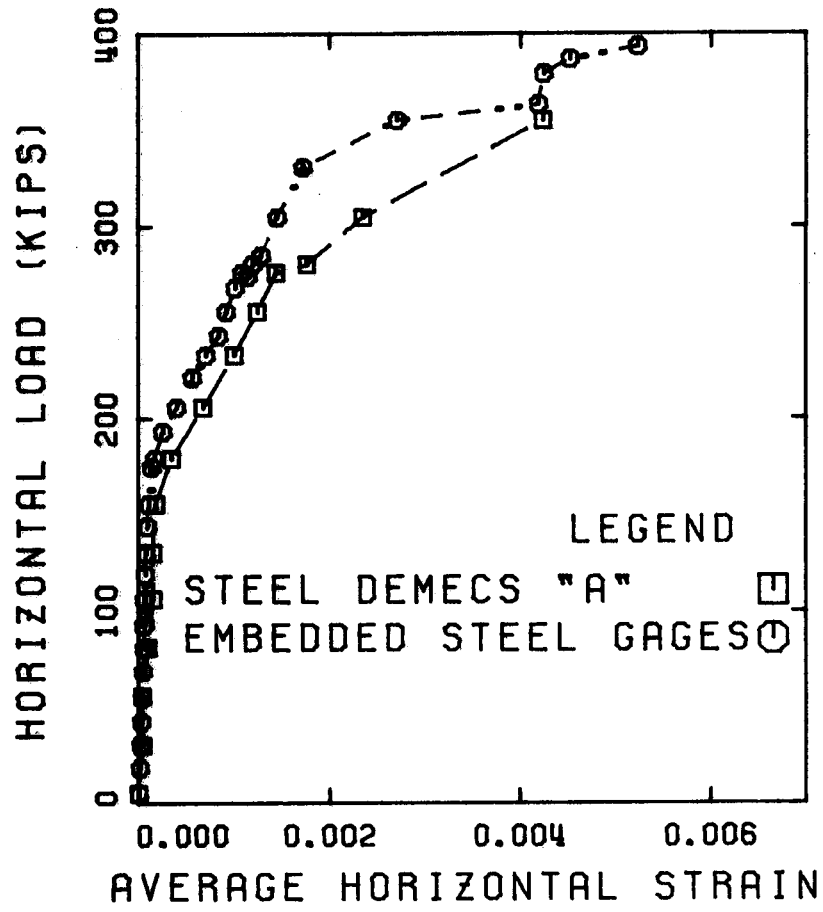

(b) Horizontal Direction

Figure 6.9.4 Load-Average Steel Strain Curves, Segment 9

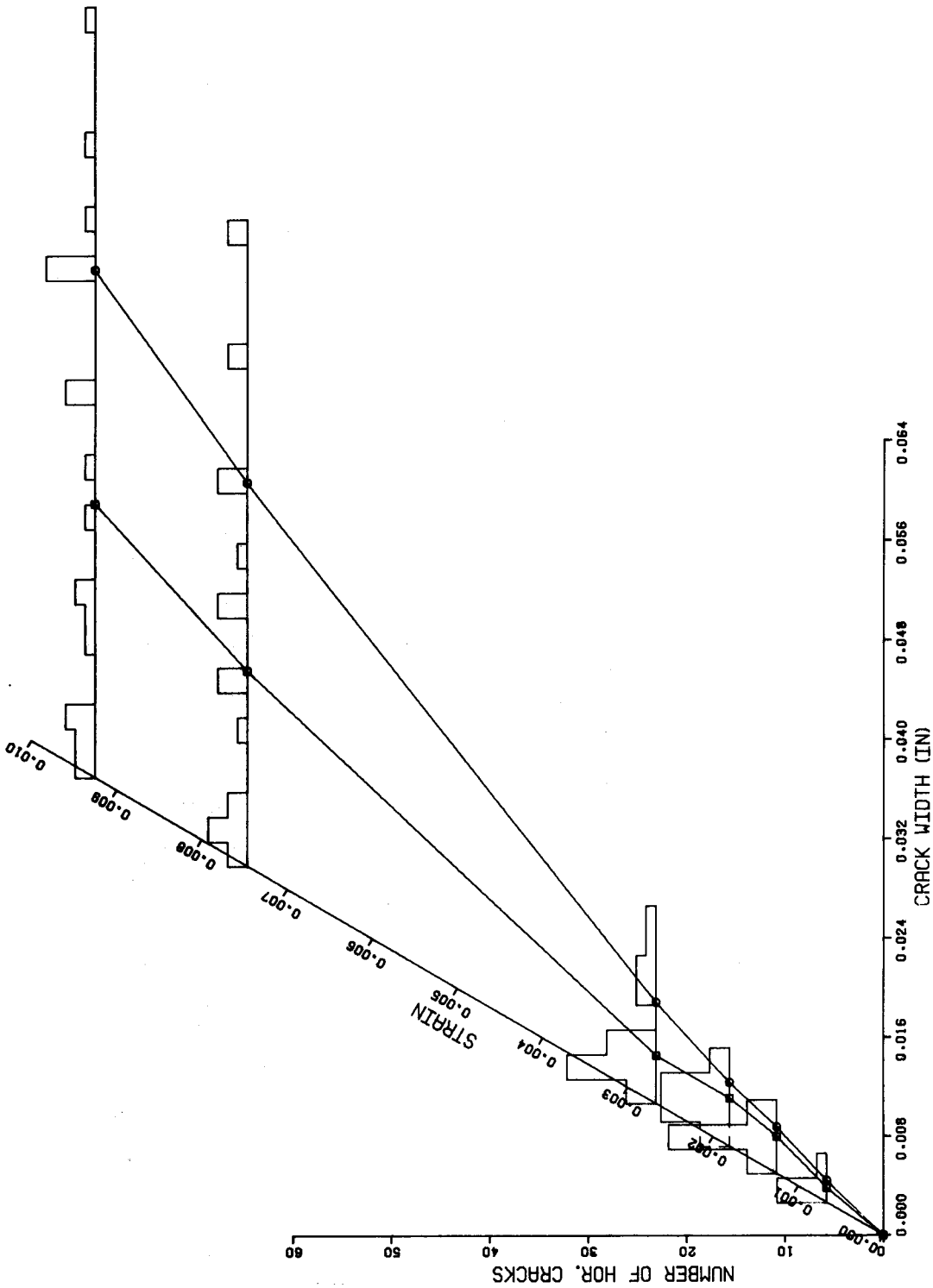

(a) Horizontal Cracks

Figure 6.9.5 Distribution of Crack Widths, Segment 9

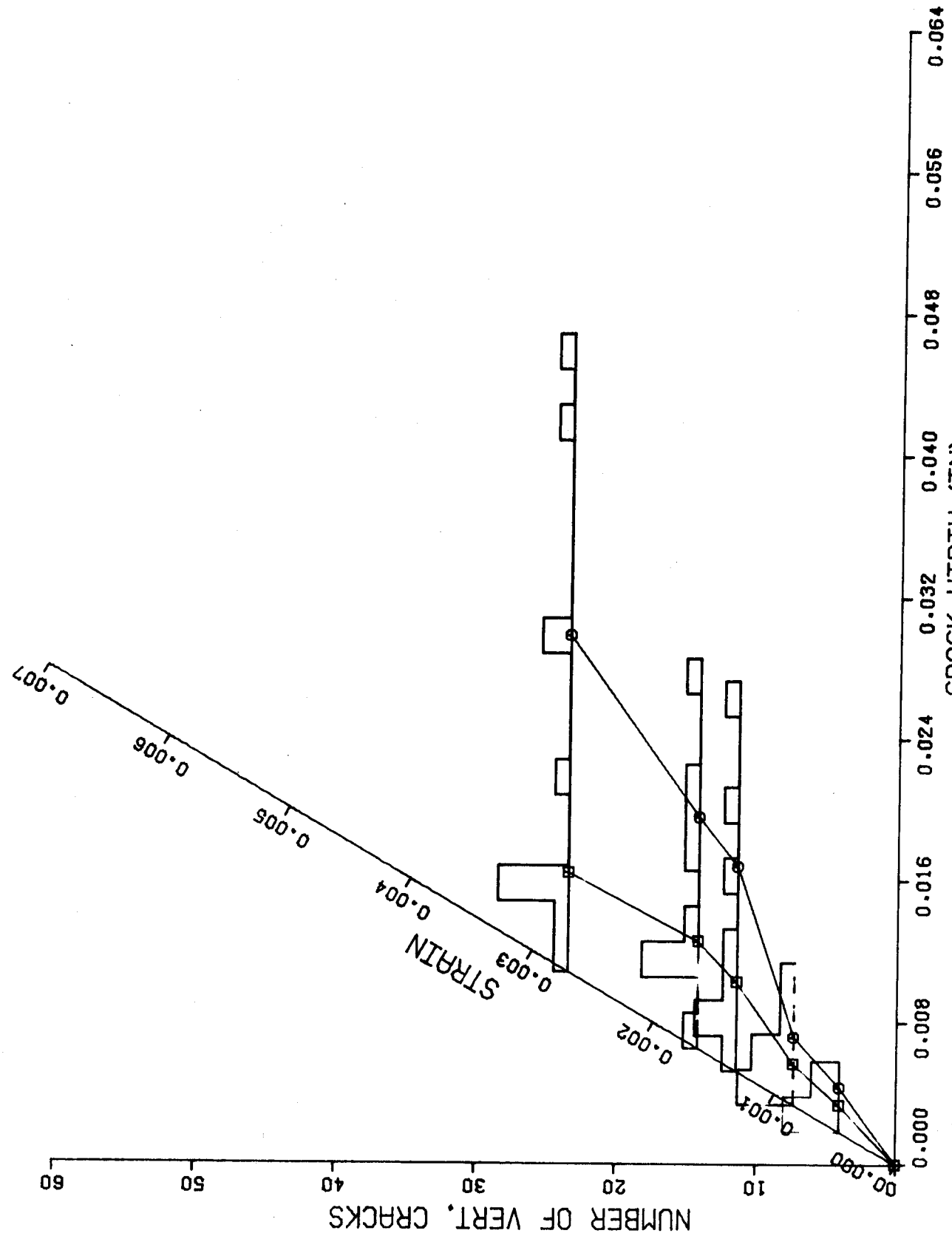

(b) Vertical Cracks

Figure 6.9.5 Distribution of Crack Widths, Segment 9

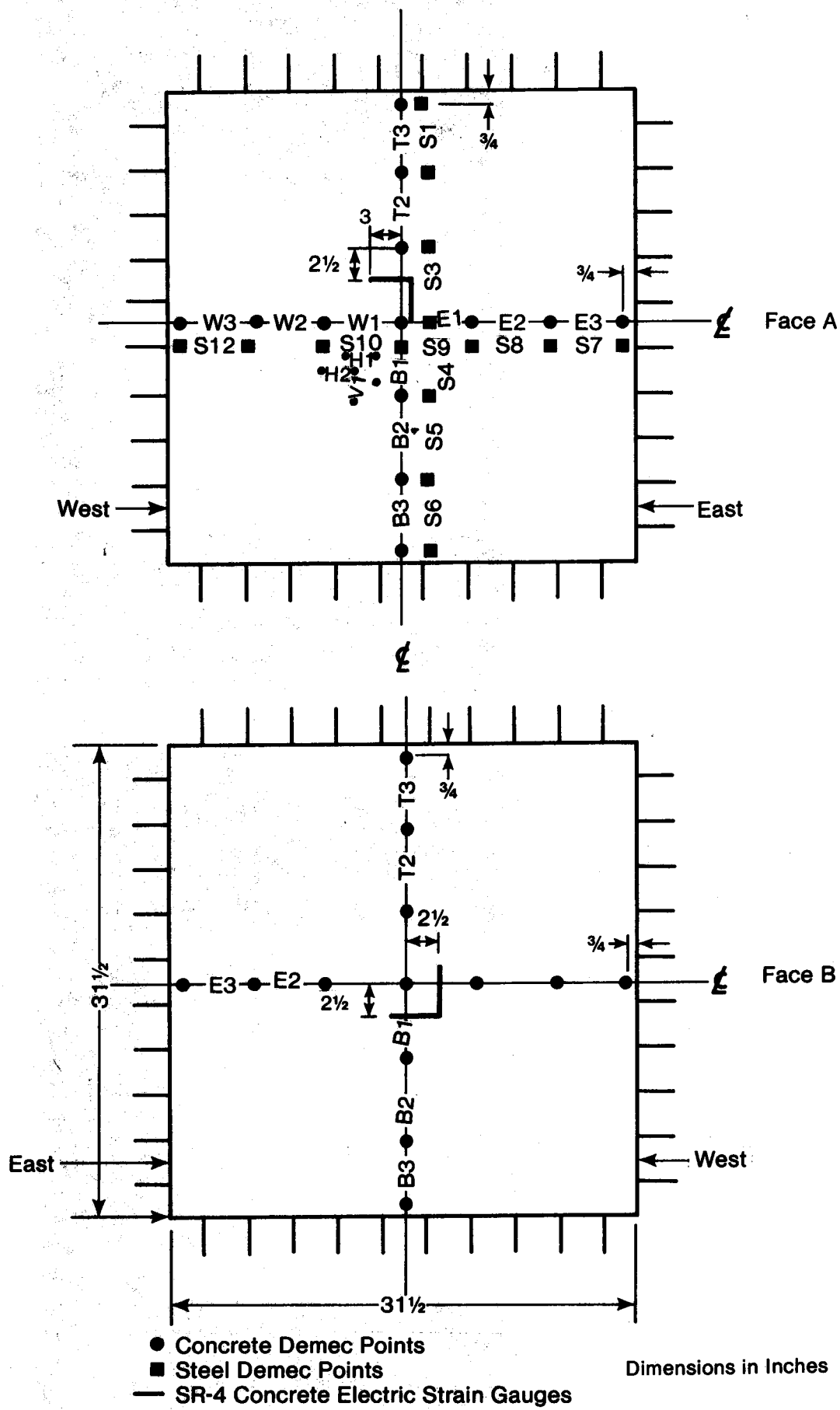

Location of Strain Measurements, Specimen 11

Figure 6.11.1 Location of Strain Measurements, Segment 11

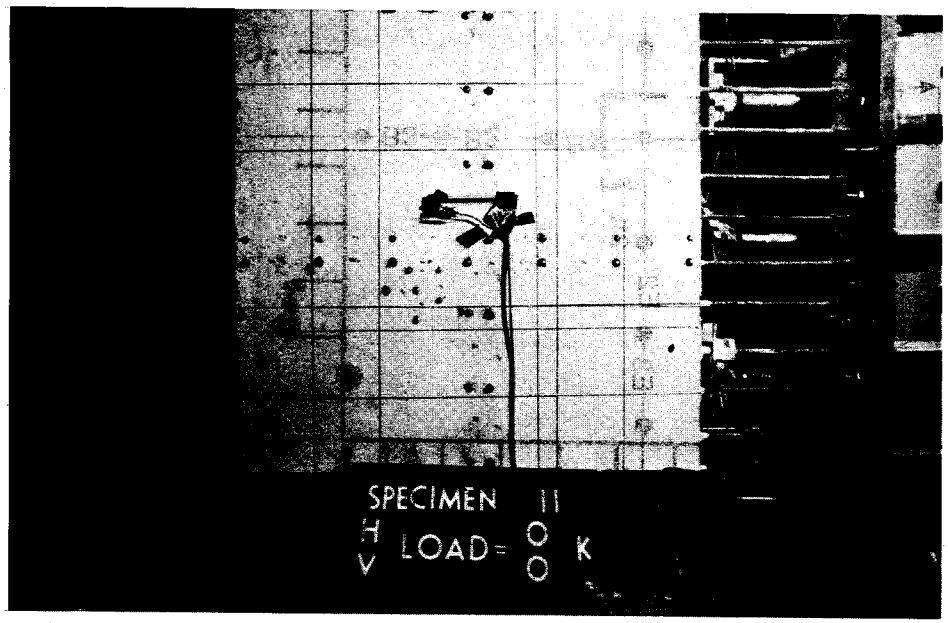

(a) Face A Before Loading

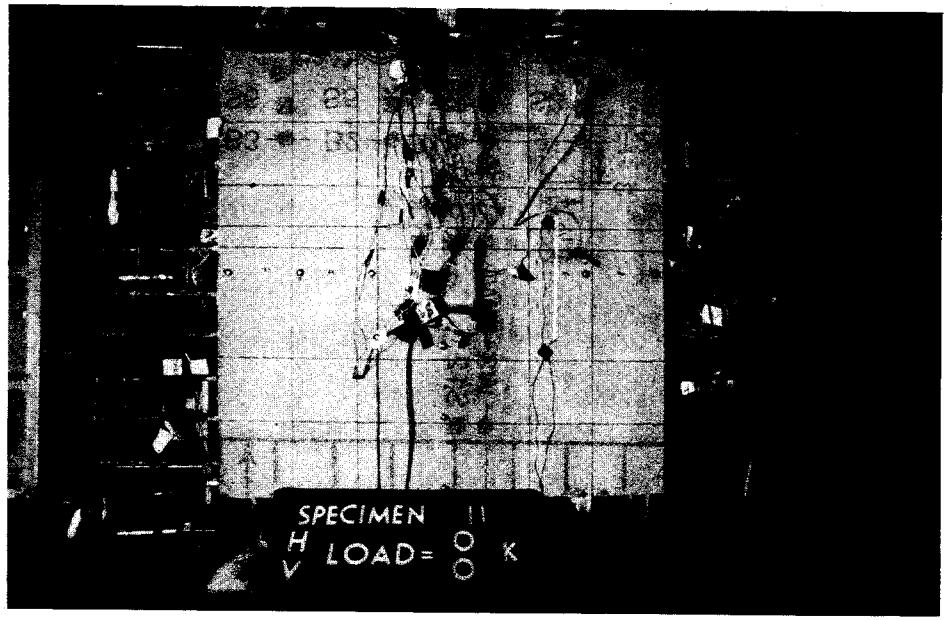

(b) Face B Before Loading

Figure 6.11.2 Development of Cracking in Segment 11

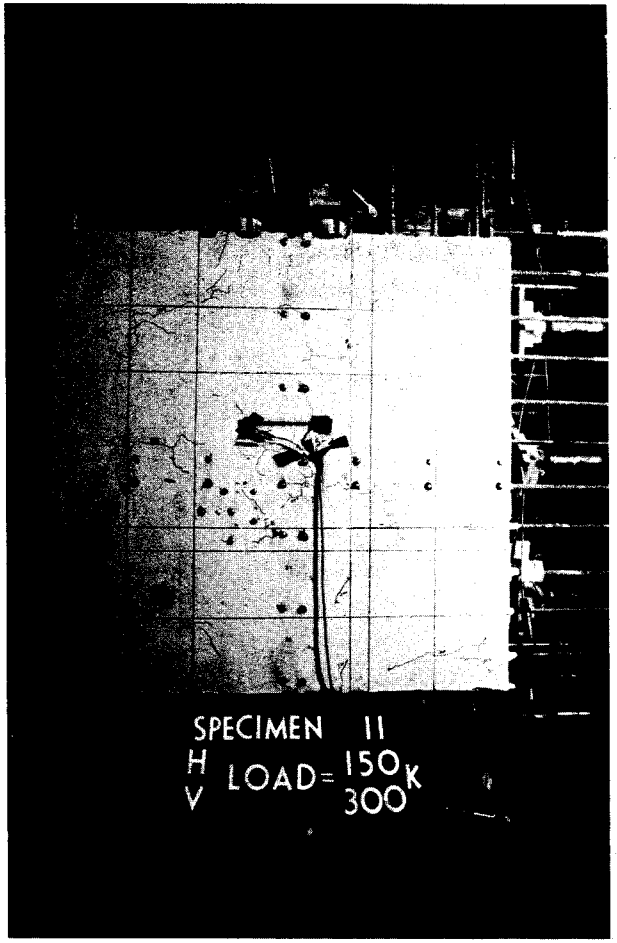

(c) Face A at Onset of Horizontal Cracking

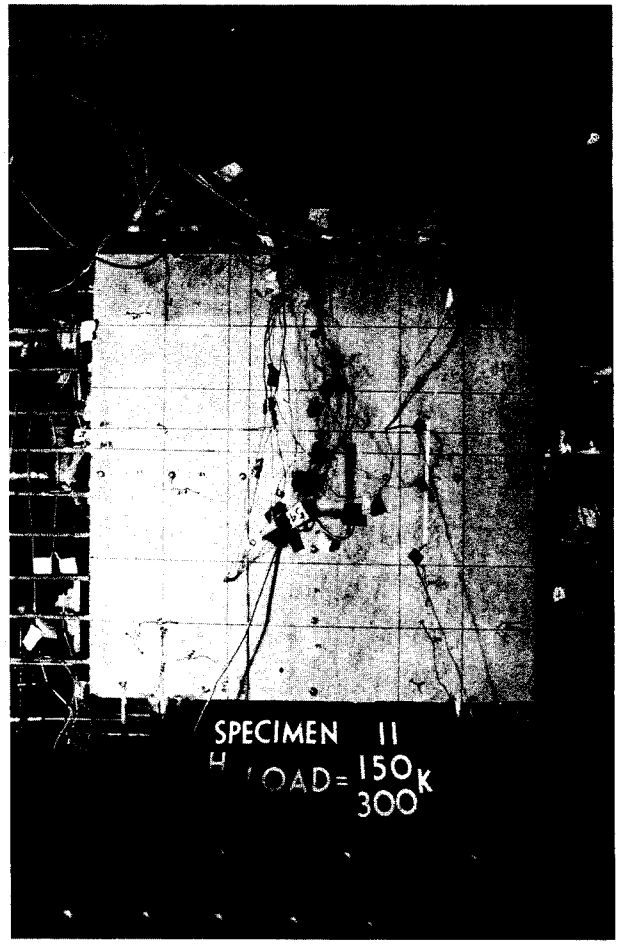

(d) Face B at Onset of Horizontal Cracking

Figure 6.11.2 Development of Cracking in Segment 11

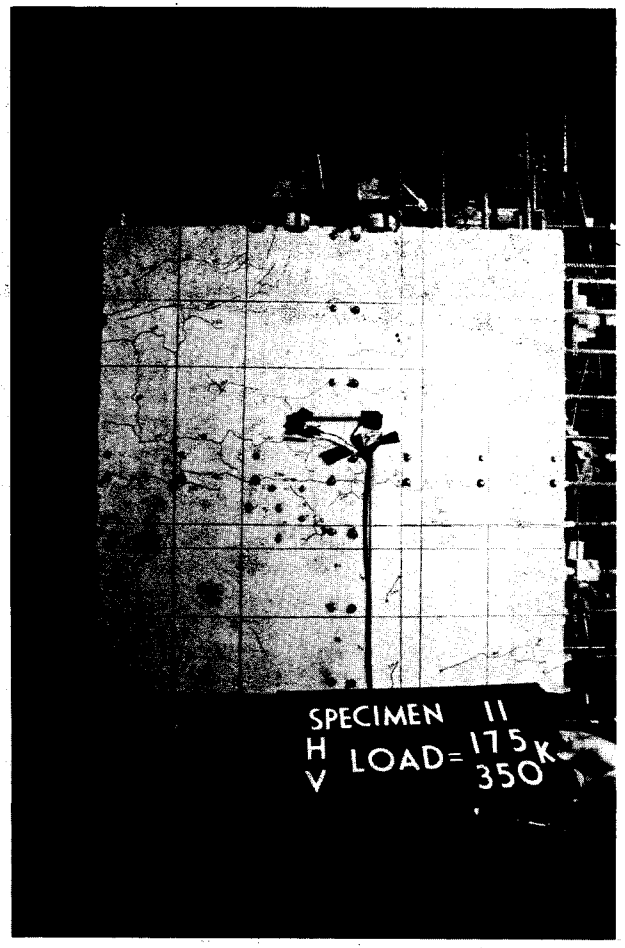

(e) Face A at Onset of Vertical Cracking

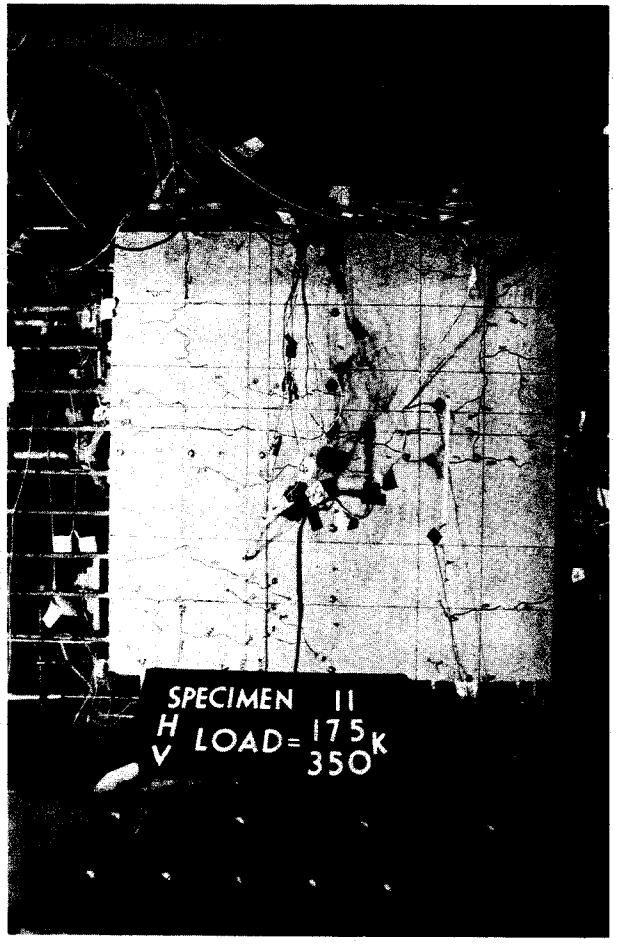

(f) Face B at Onset of Vertical Cracking

Figure 6.11.2 Development of Cracking in Segment 11

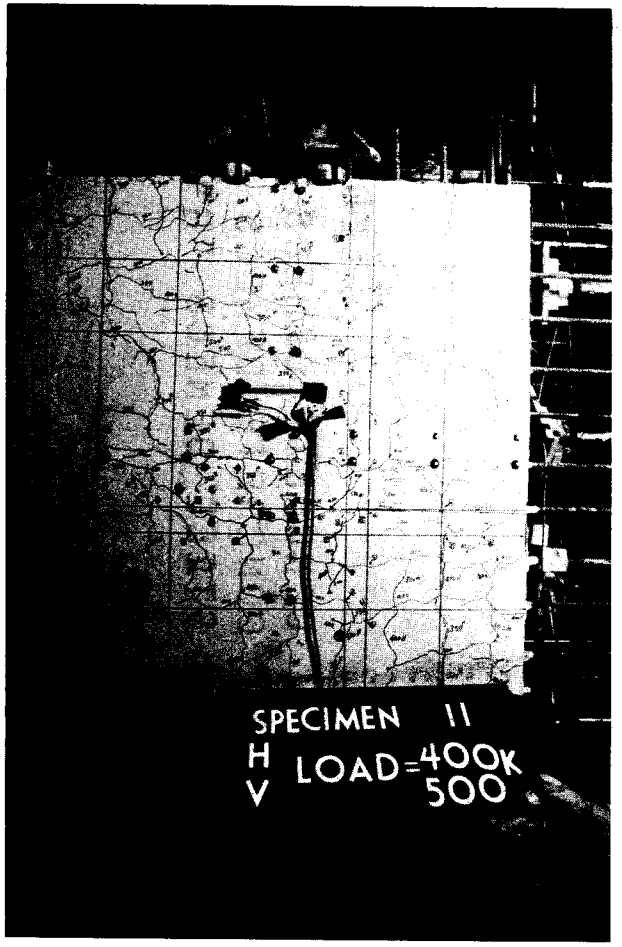

(g) Face A at End of Test

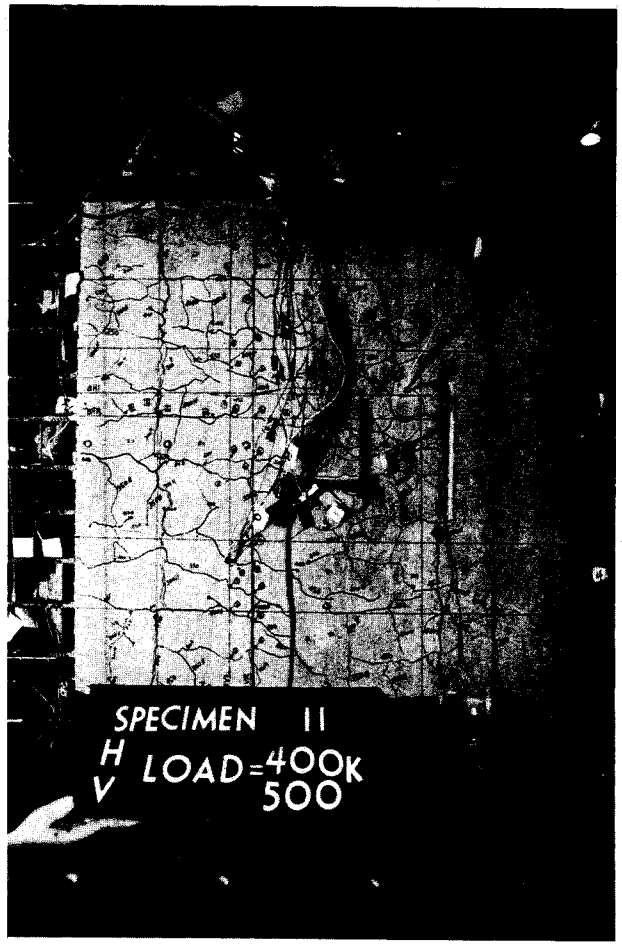

(h) Face B at End of Test

Figure 6.11.2 Development of Cracking in Segment 11

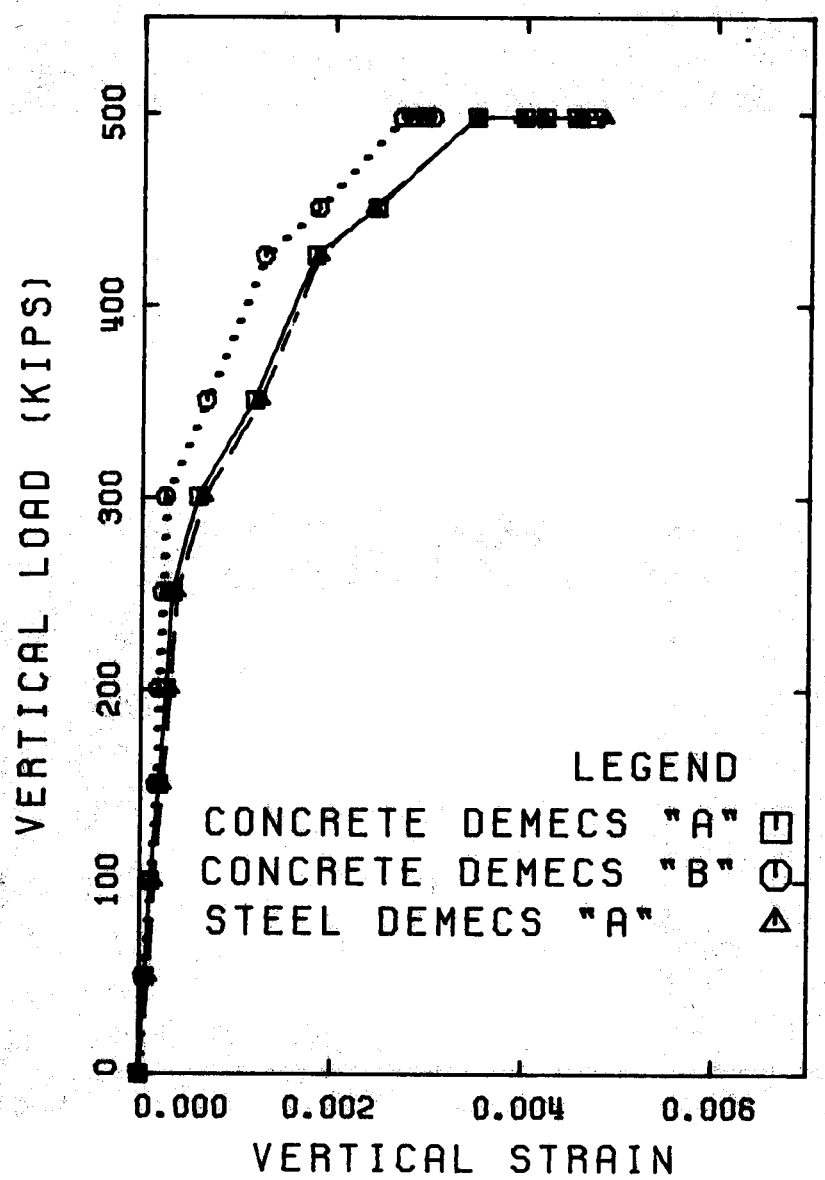

(a) Vertical Direction

Figure 6.11.3 Load-Average Strain Curves, Segment 11

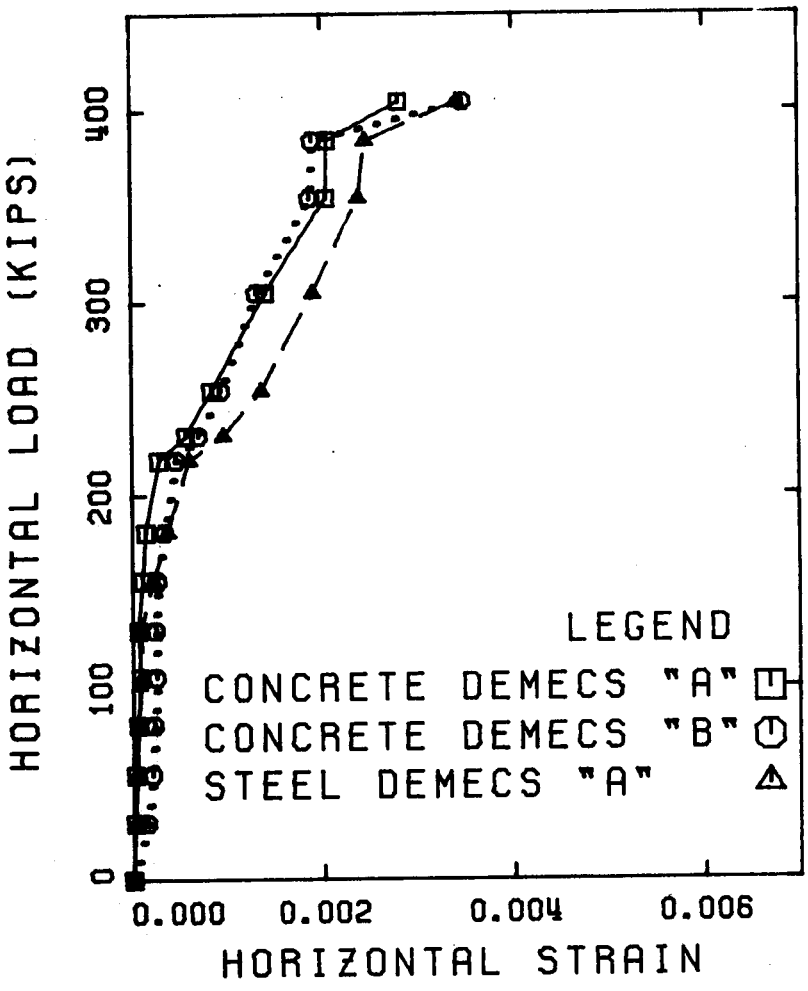

(b) Horizontal Direction

Figure 6.11.3 Load-Average Strain Curves, Segment 11

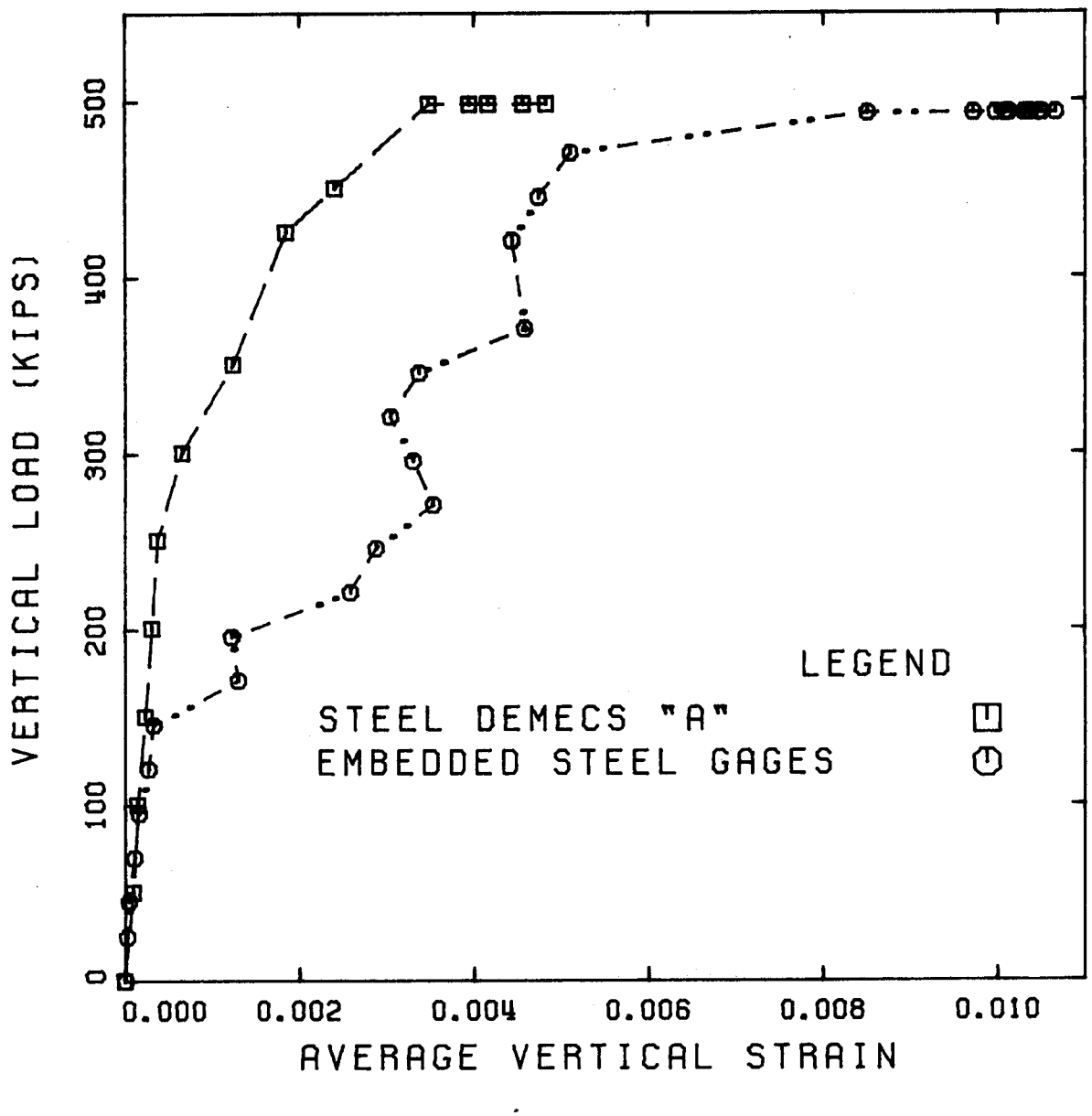

(a) Vertical Direction

Figure 6.11.4 Load-Average Steel Strain Curves, Segment 11

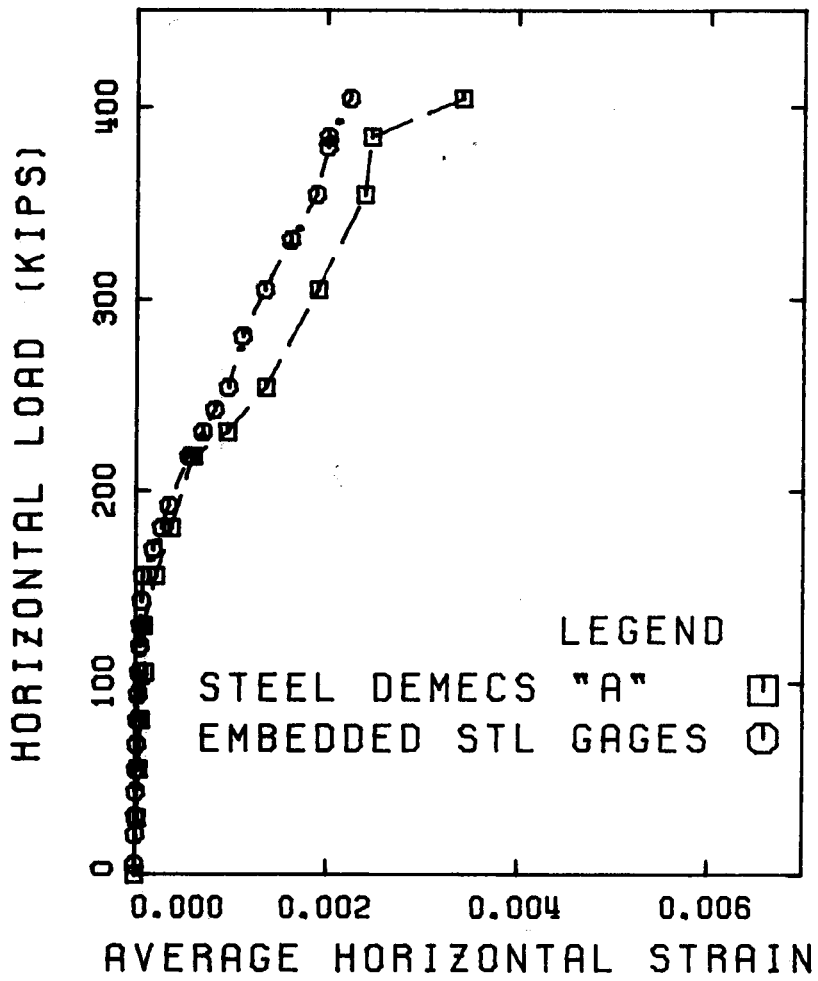

(b) Horizontal Direction

Figure 6.11.4 Load-Average Steel Strain Curves, Segment 11

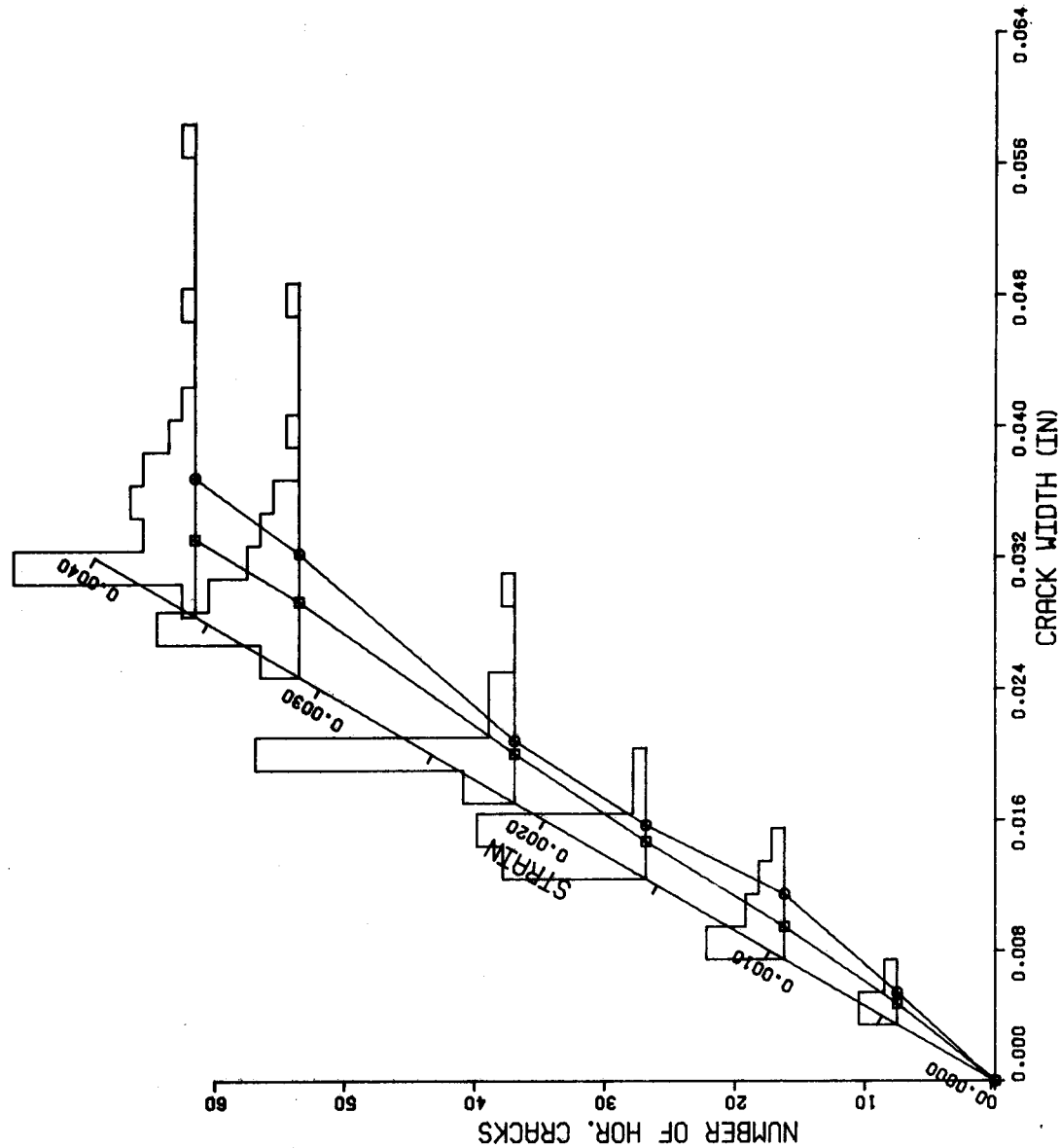

(a) Horizontal Cracks

Figure 6.11.5 Distribution of Crack Widths, Segment 11

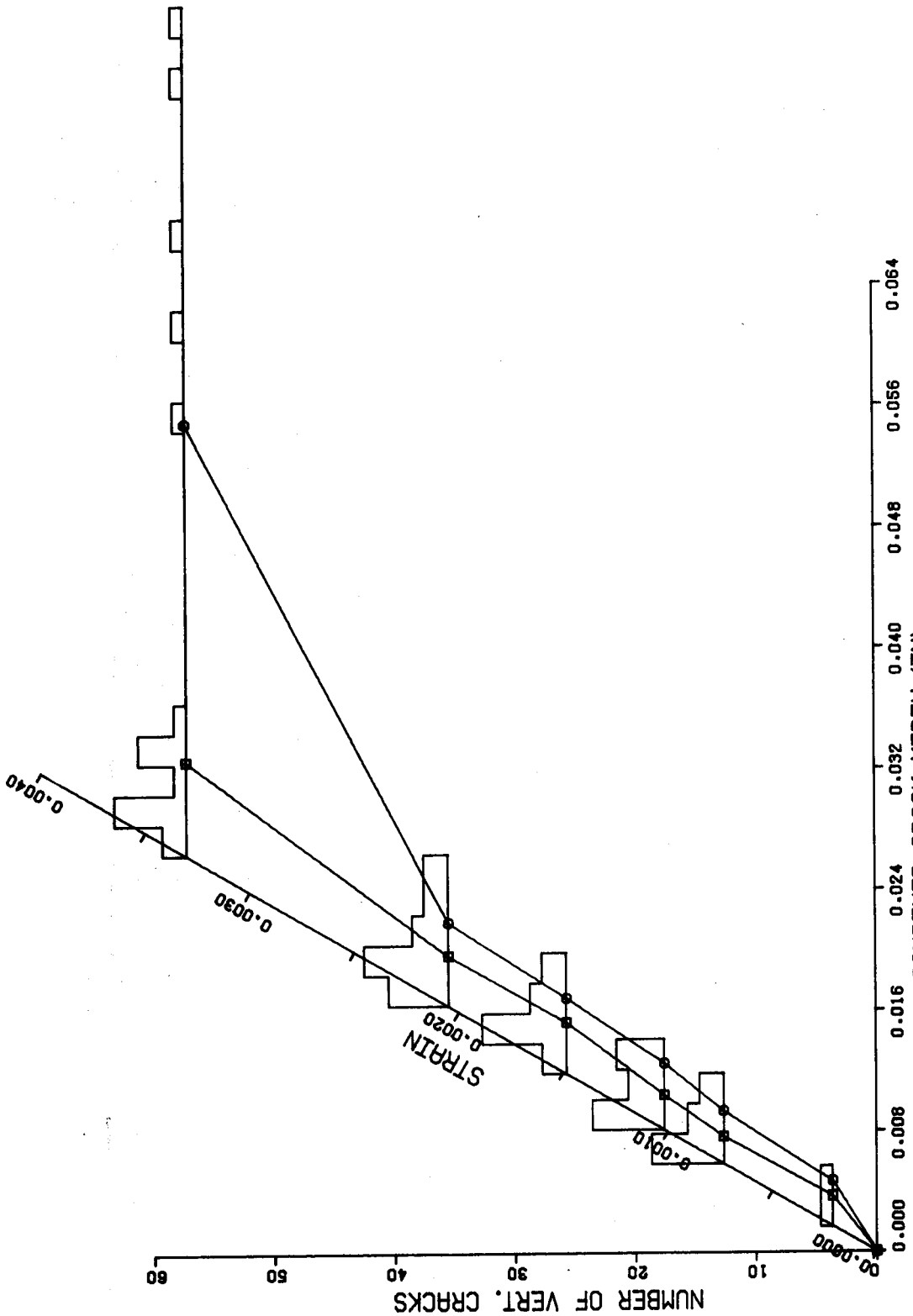

(b) Vertical Cracks

Figure 6.11.5 Distribution of Crack Widths, Segment 11

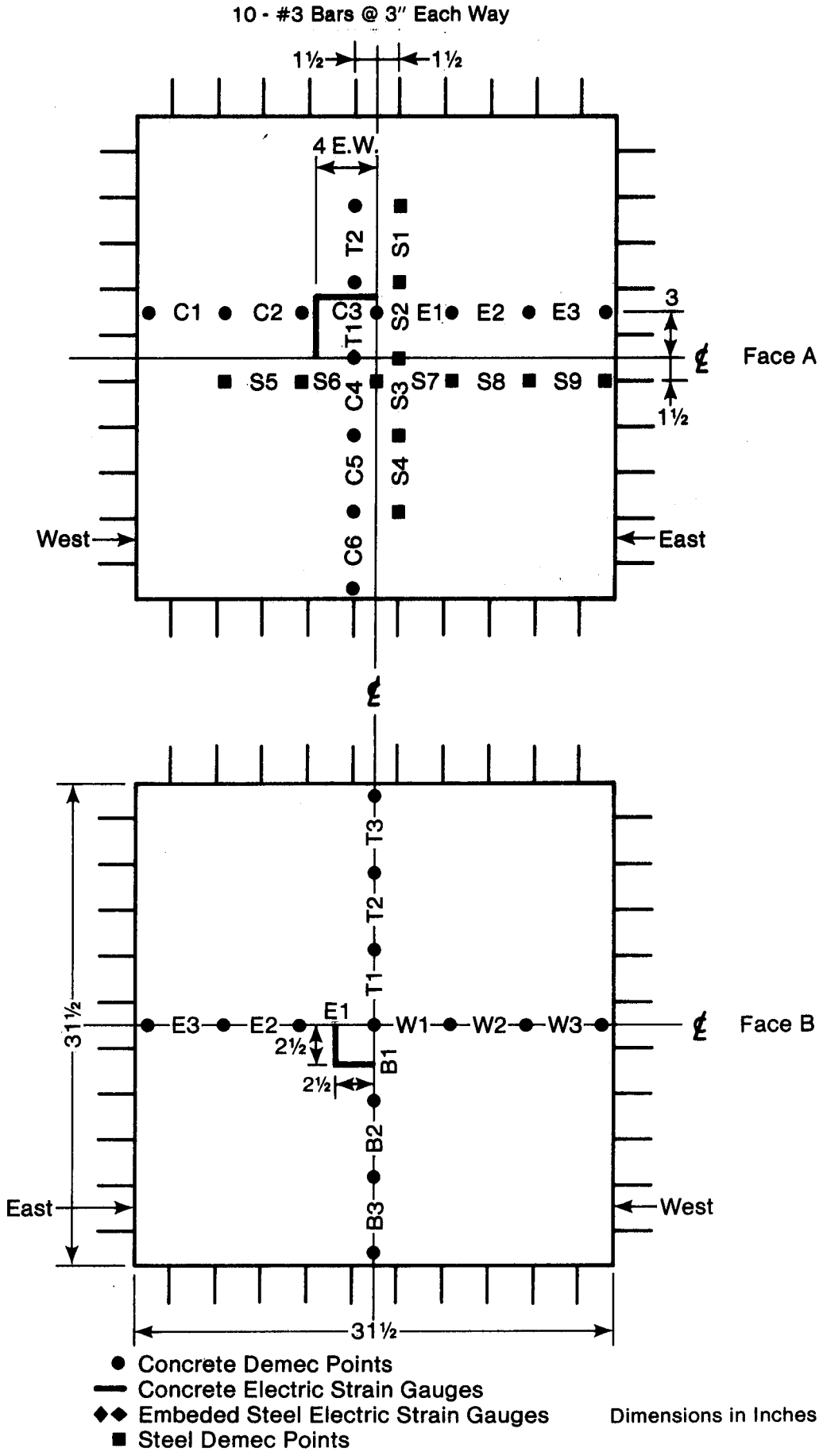

Figure 6.12.1 Location of Strain Measurements, Specimen 12

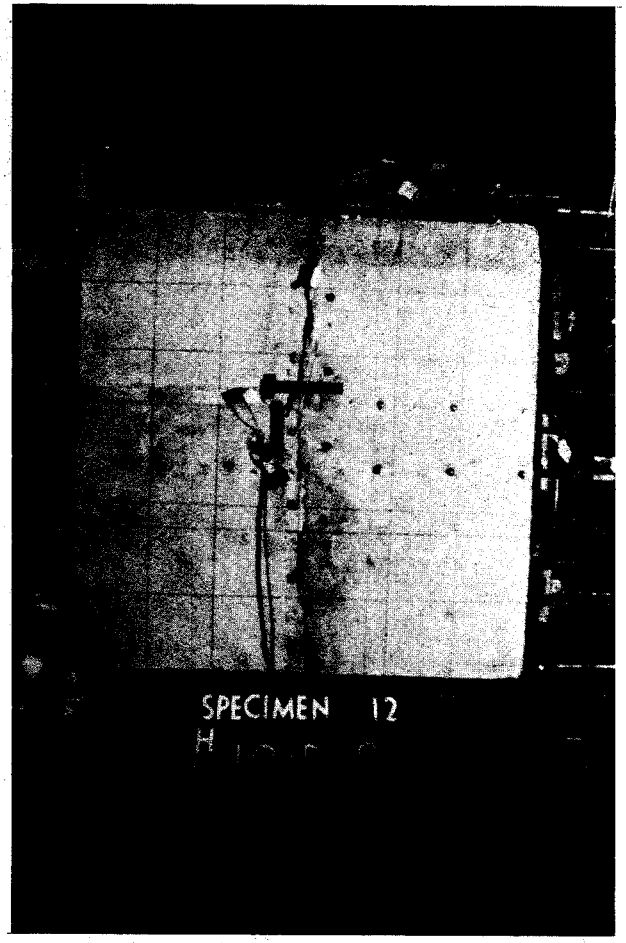

(a) Face A Before Loading

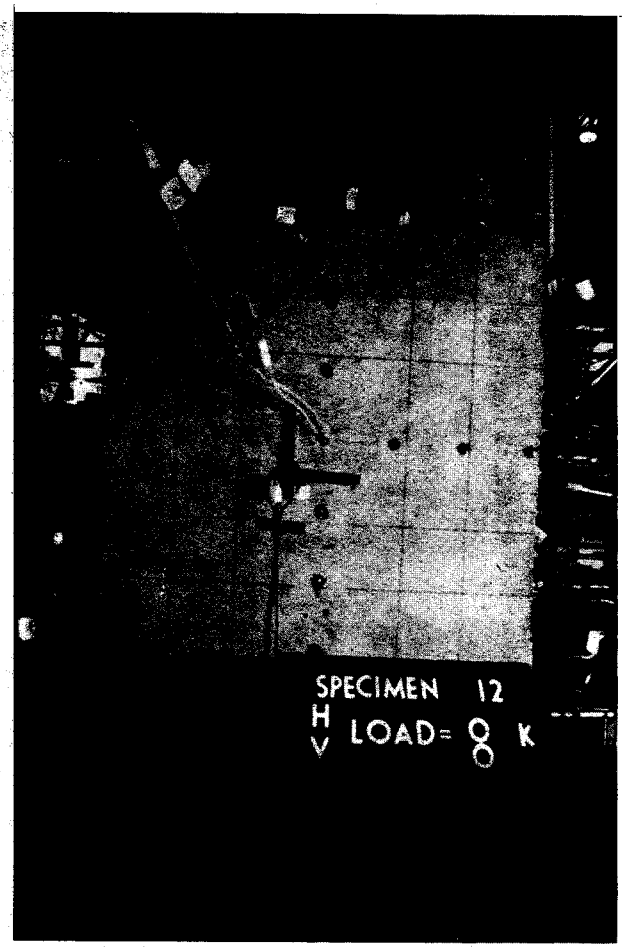

(b) Face B Before Loading

Figure 6.12.2 Development of Cracking in Segment 12

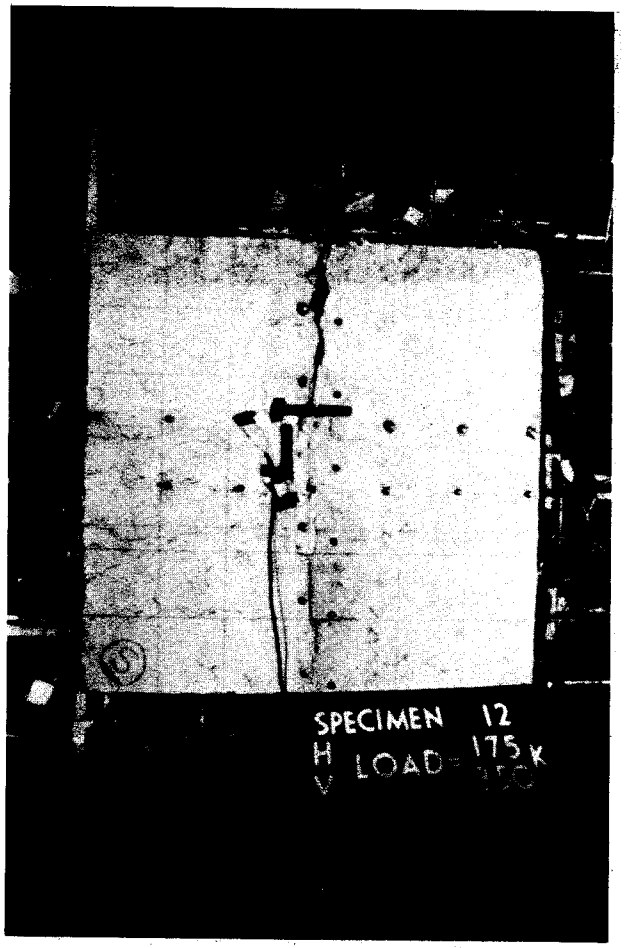

(c) Face A of Onset of Horizontal Cracking

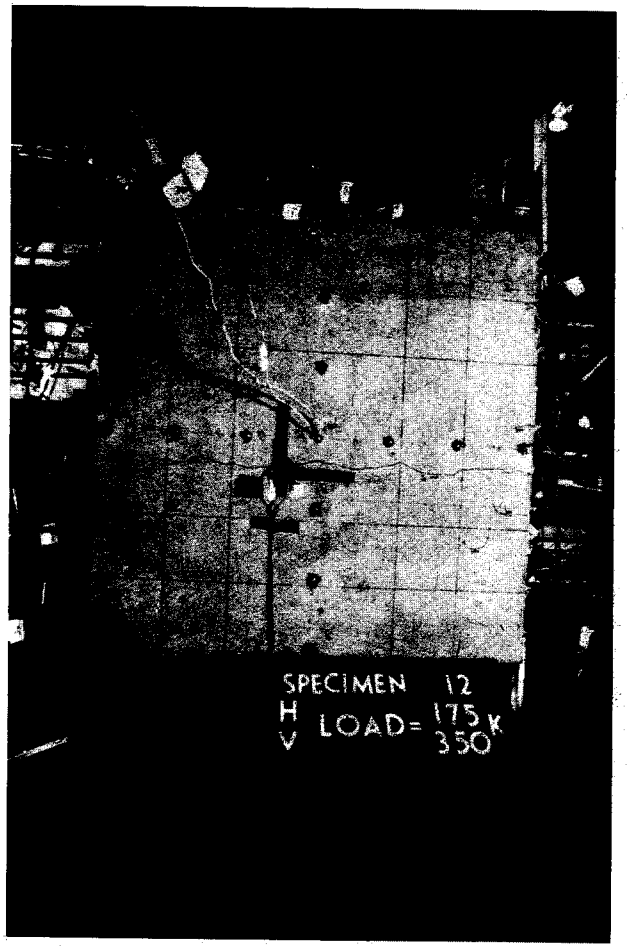

(d) Face B at Onset of Horizontal Cracking

Figure 6.12.2 Development of Cracking in Segment 12

(e) Face A at Onset of Vertical Cracking

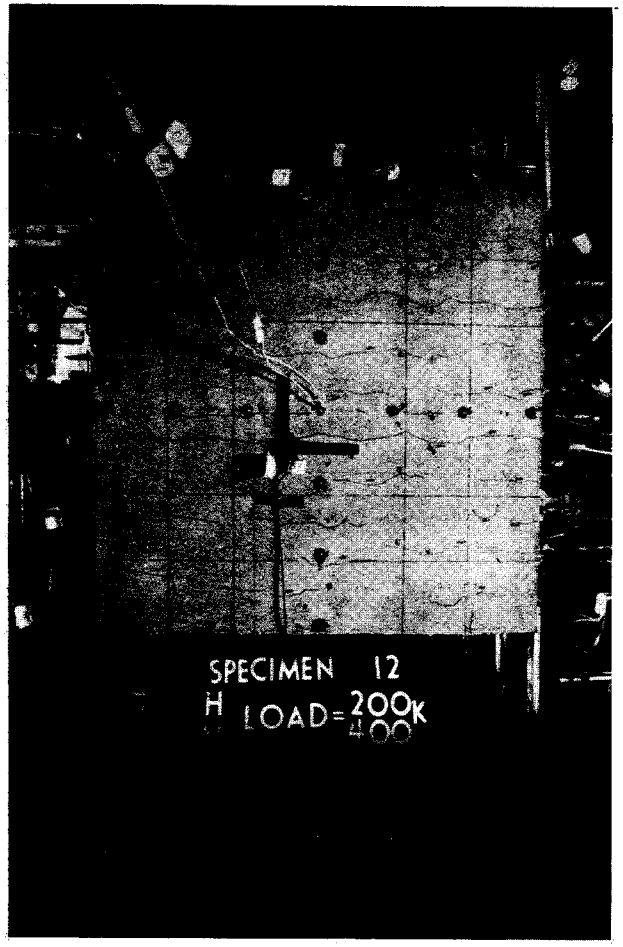

(f) Face B at Onset of Vertical Cracking

Figure 6.12.2 Development of Cracking in Segment 12

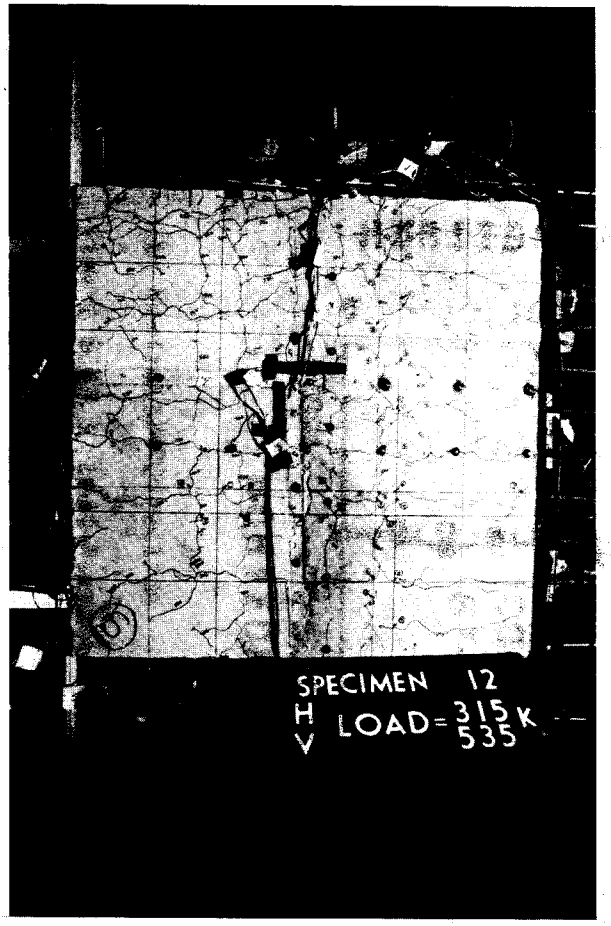

(g) Face A at End of Test

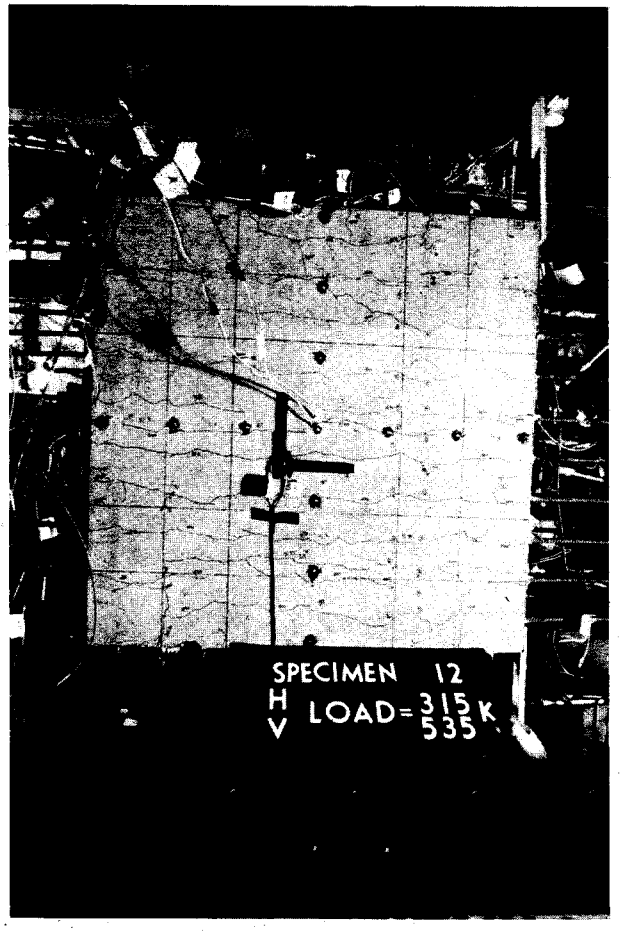

(h) Face B at End of Test

Figure 6.12.2 Development of Cracking in Segment 12

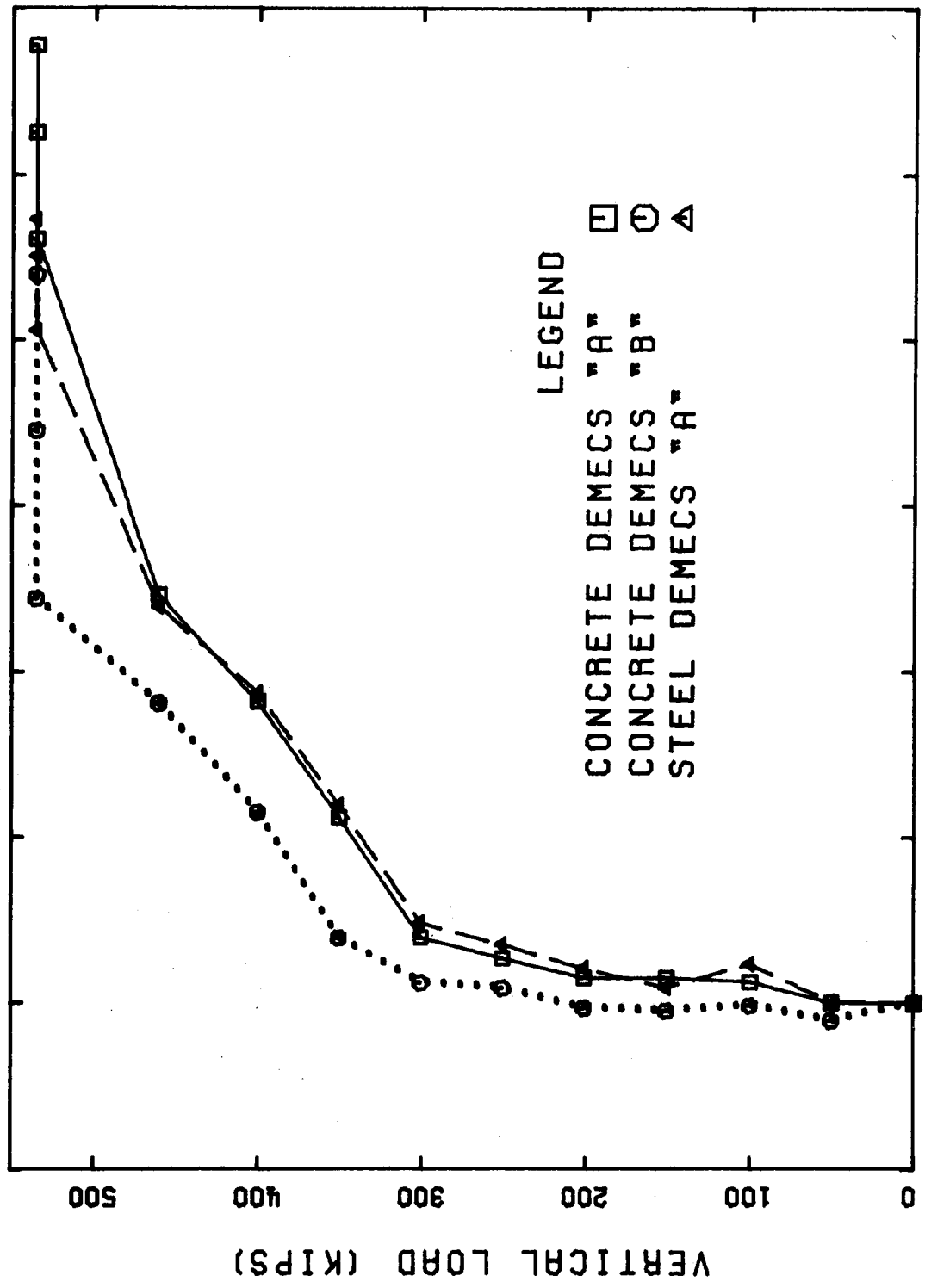

(a) Vertical Direction

Figure 6.12.3 Load-Average Strain Curves, Segment 12

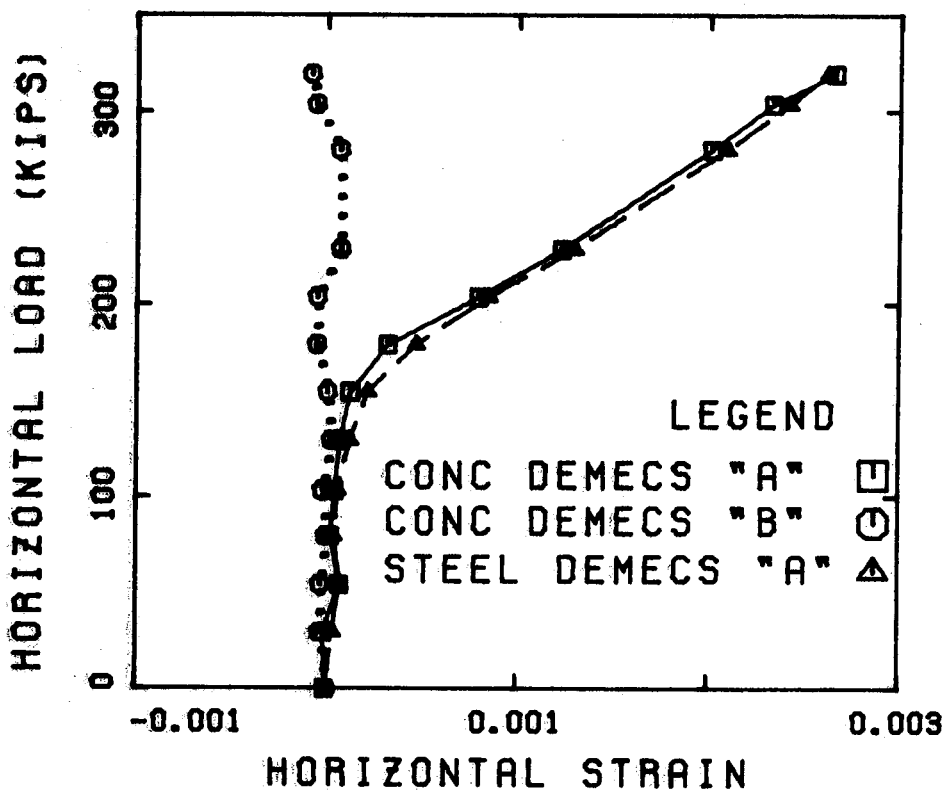

(b) Horizontal Direction

Figure 6.12.3 Load-Average Strain Curves, Segment 12

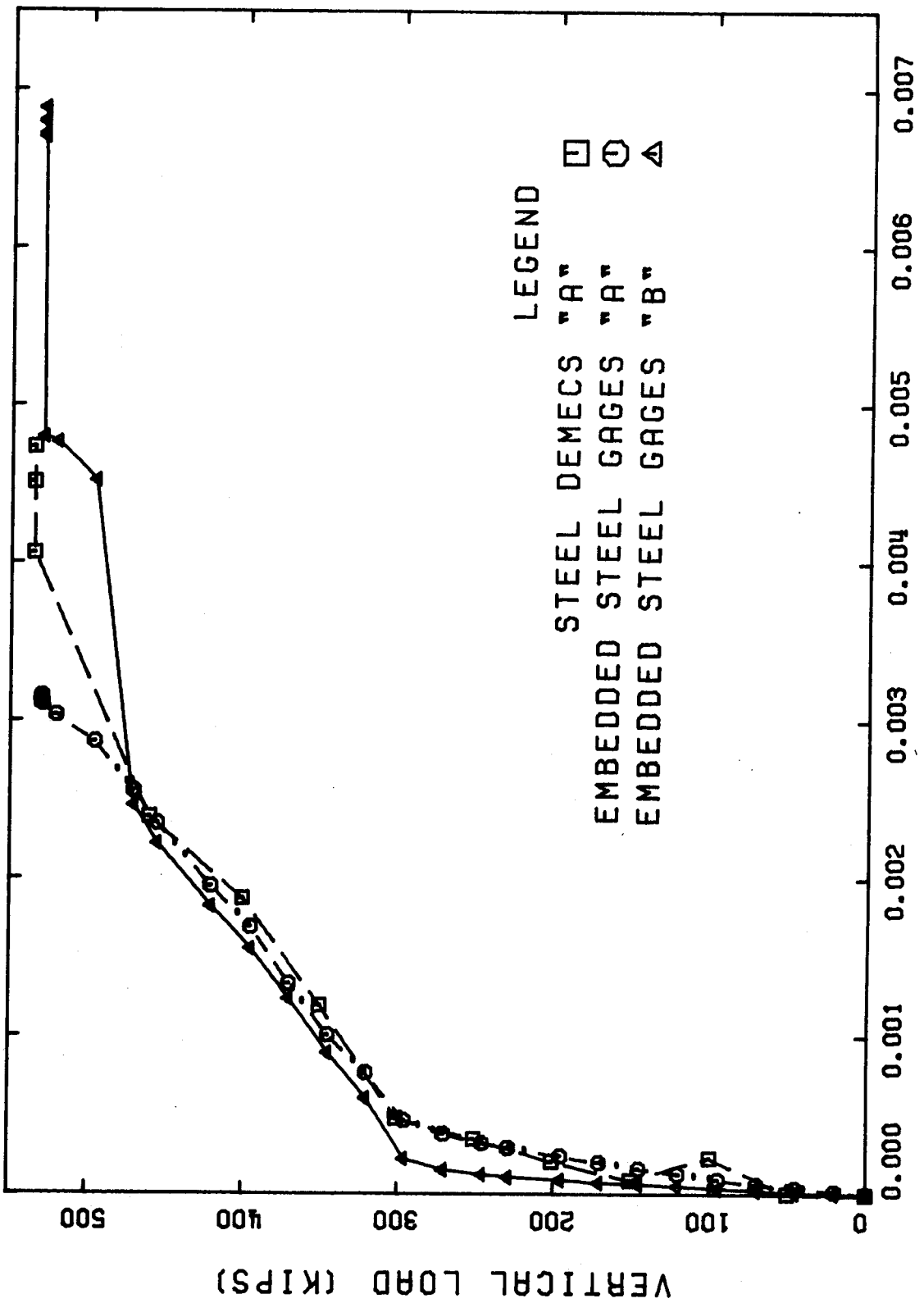

(a) Vertical Direction

Figure 6.12.4 Load-Average Steel Strain Curves, Segment 12

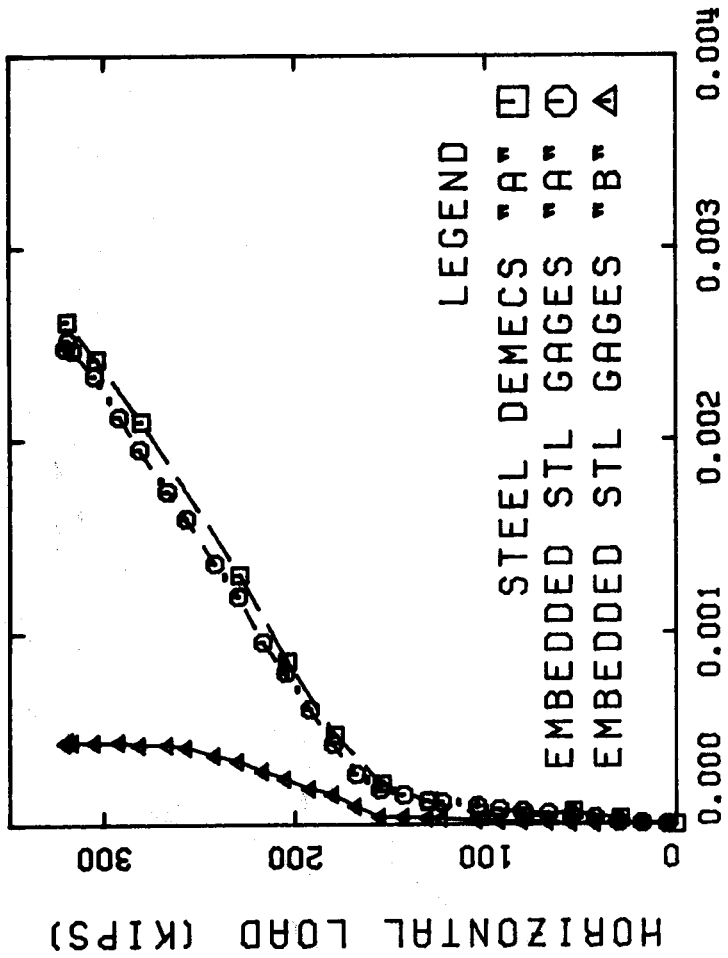

(b) Horizontal Direction

Figure 6.12.4 Load-Average Steel Strain Curves, Segment 12

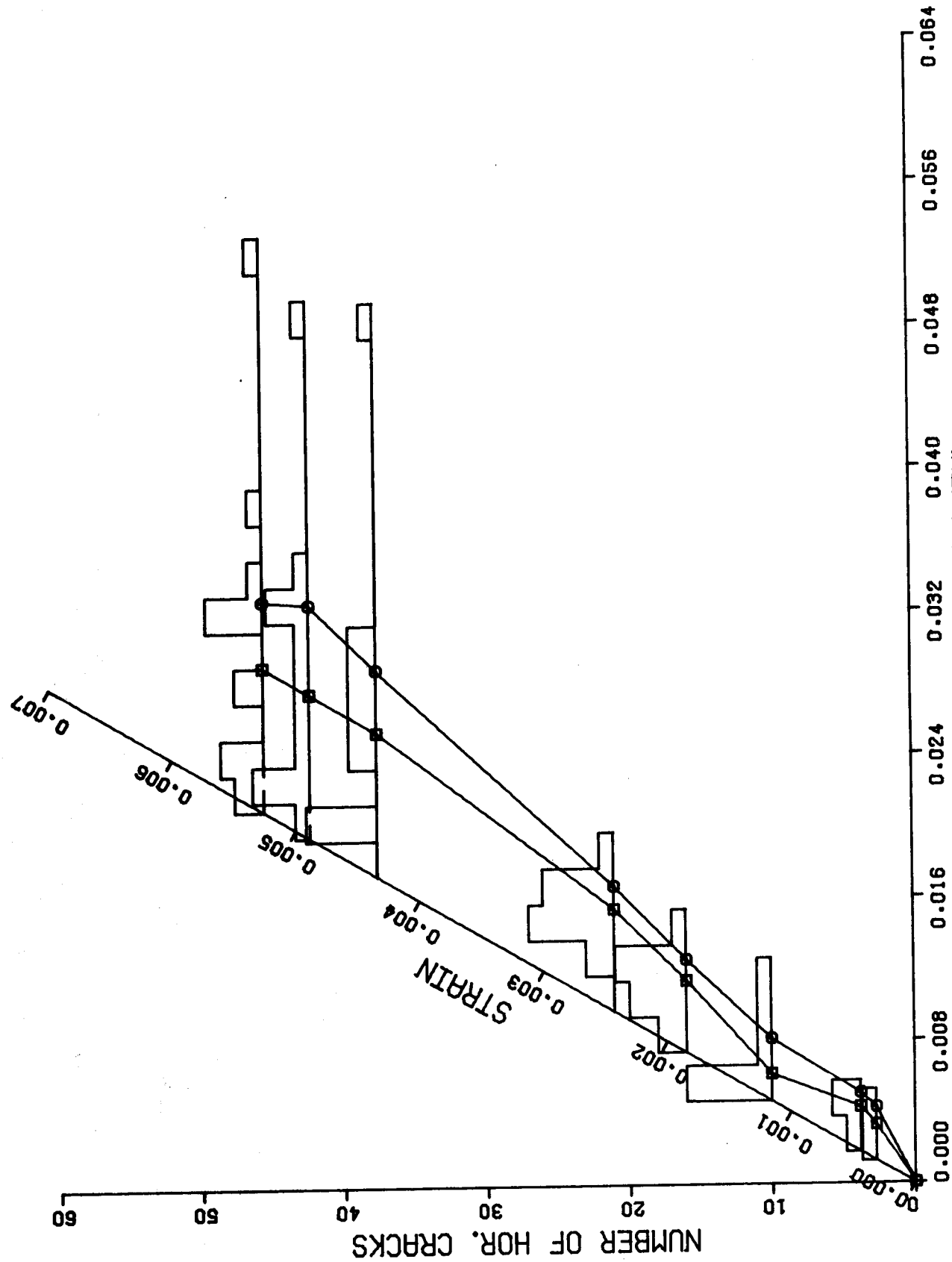

(a) Horizontal Cracks

Figure 6.12.5 Distribution of Crack Widths, Segment 12, Face A

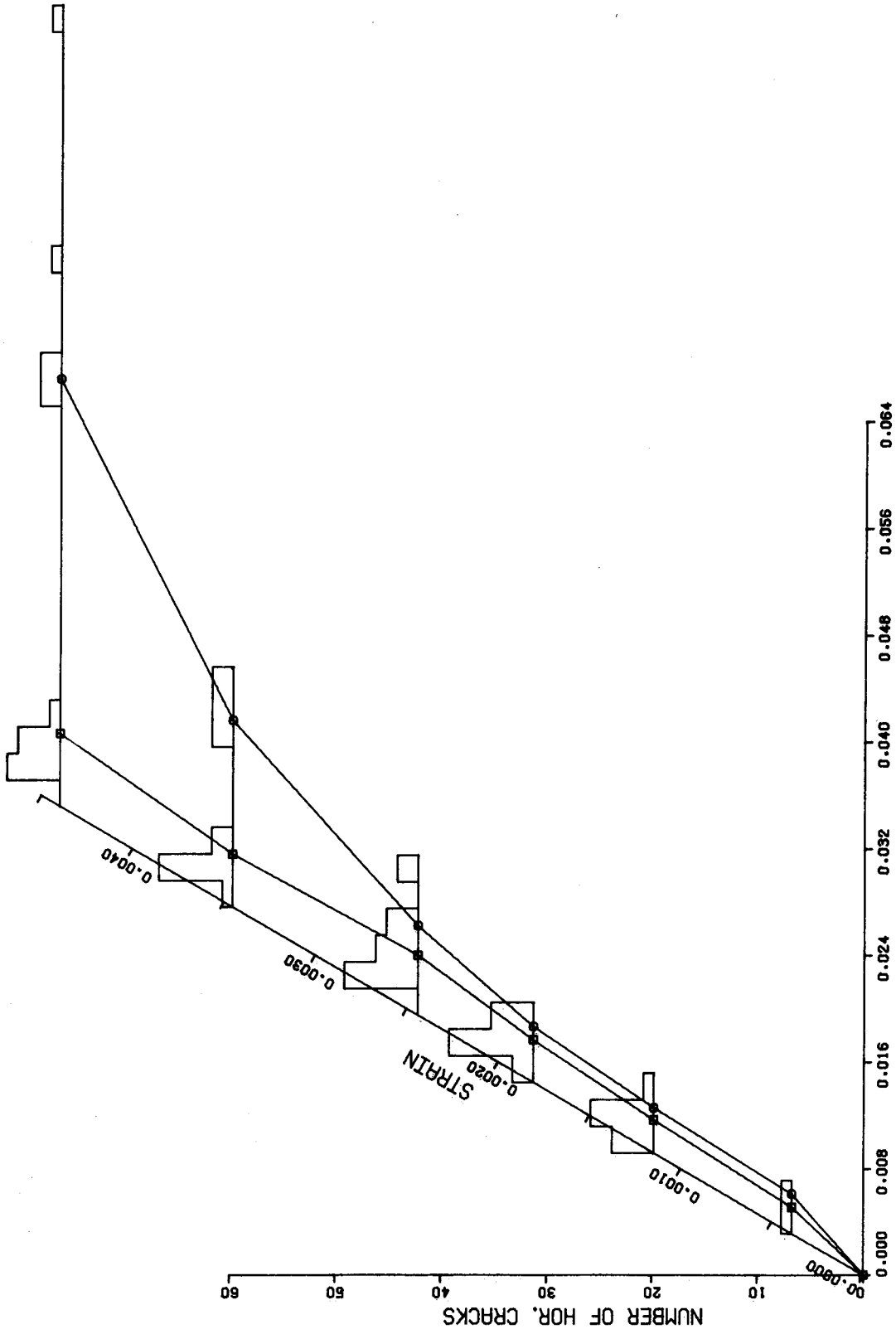

(b) Horizontal Cracks

Figure 6.12.5 Distribution of Crack Widths, Segment 12, Face B

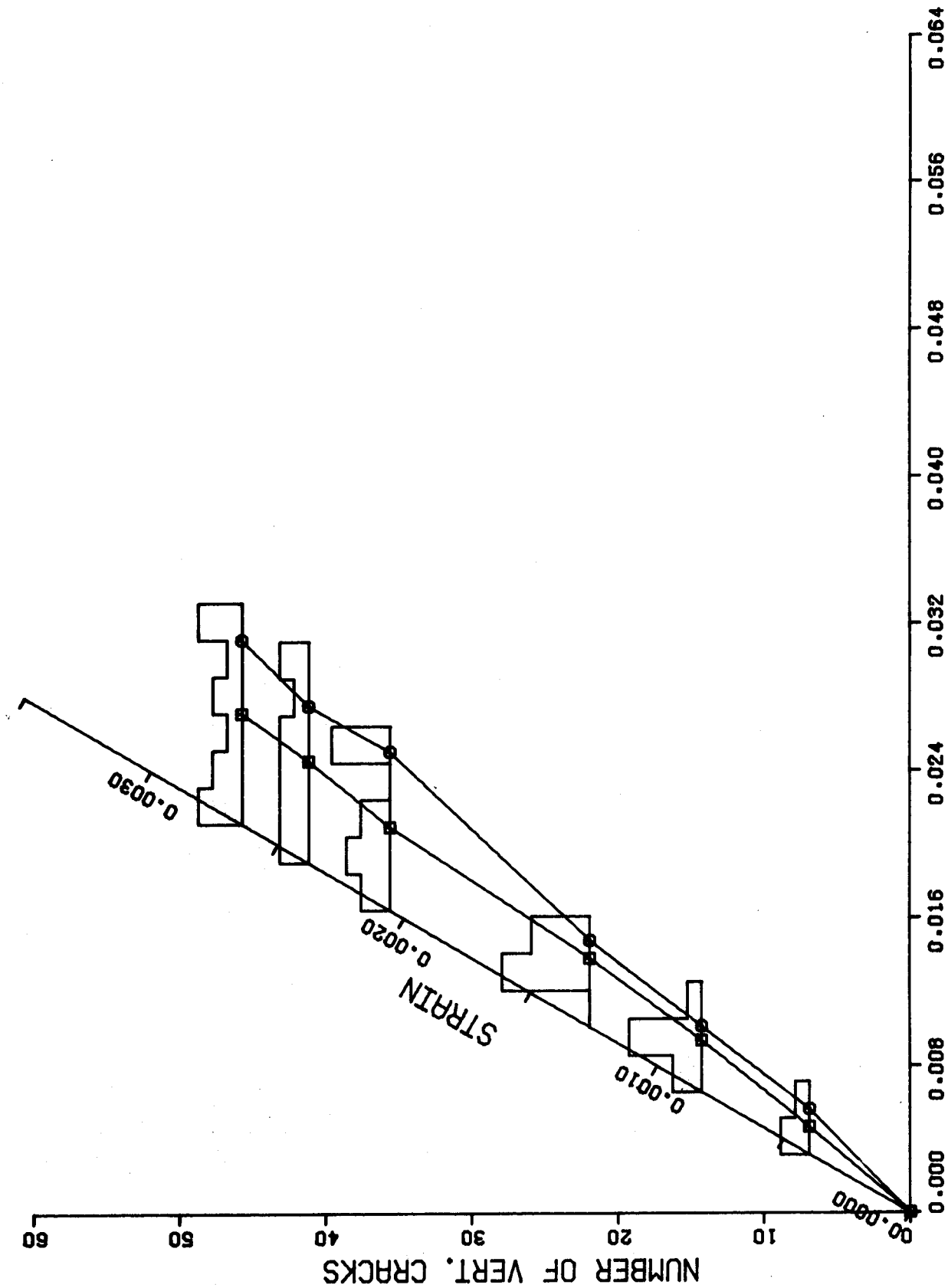

(c) Vertical Cracks

Figure 6.12.5 Distribution of Crack Widths, Segment 12, Face A

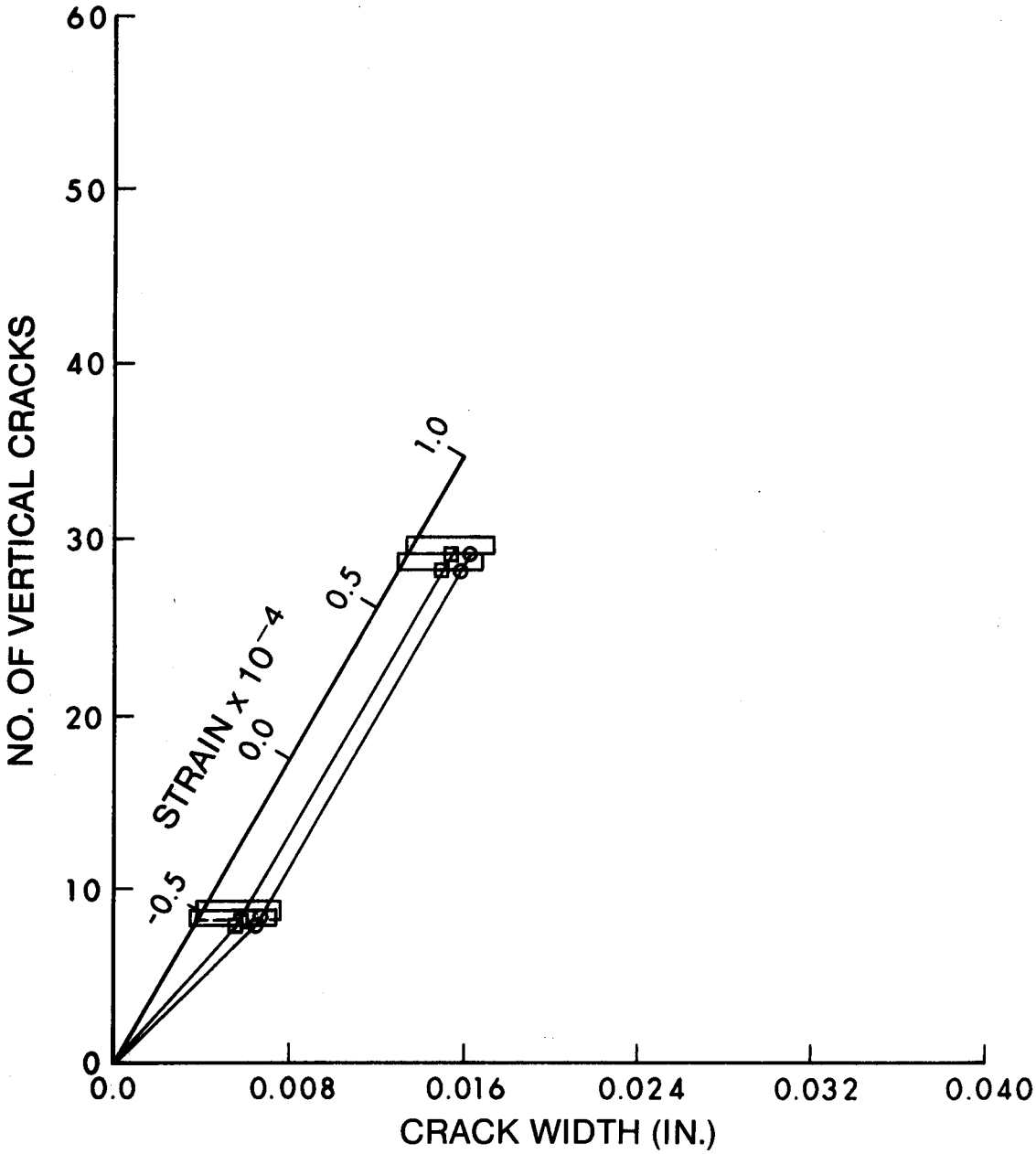

(d) Vertical Cracks

Figure 6.12.5 Distribution of Crack Widths, Segment 12, Face B

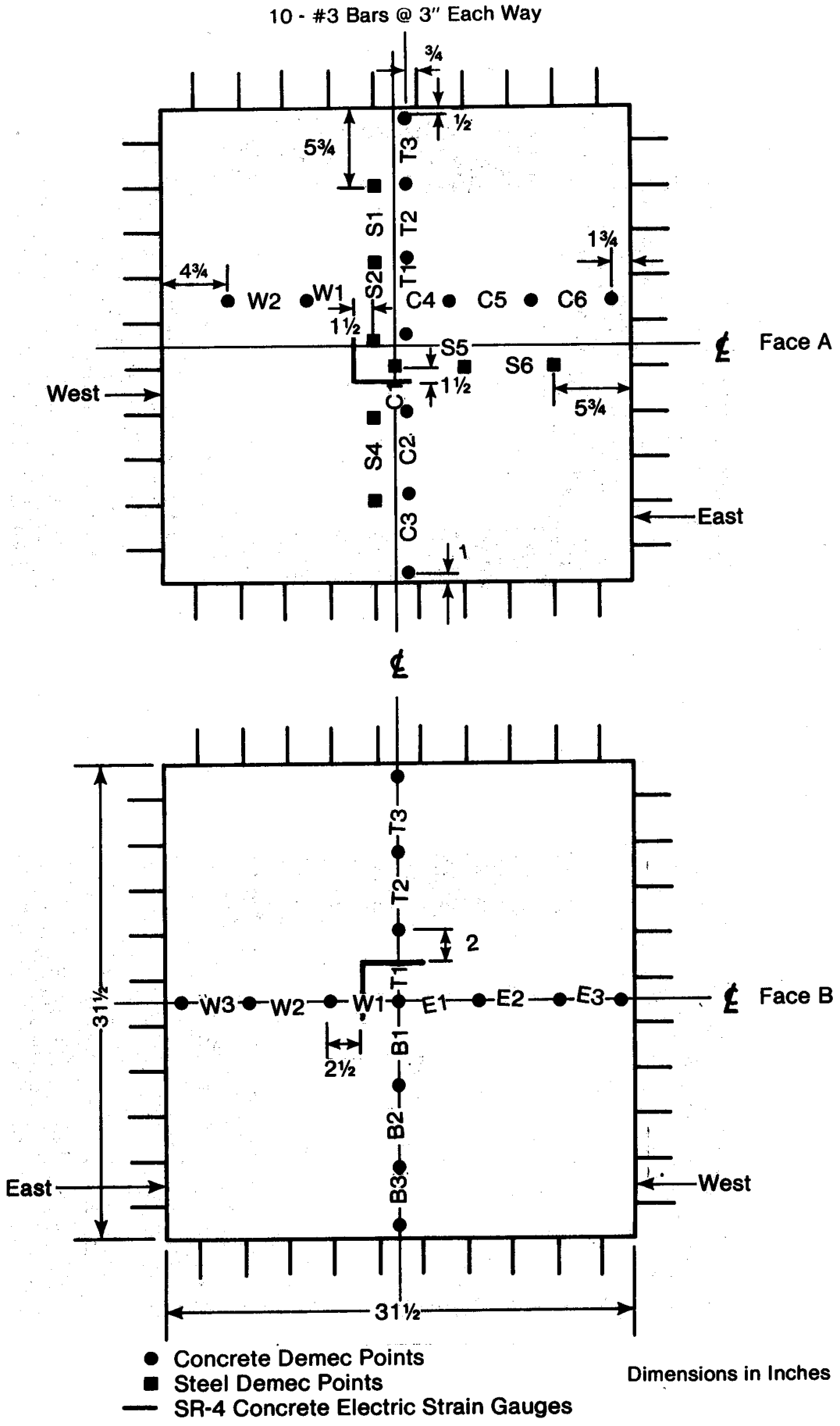

Location of Strain Measurements, Specimen 13

Figure 6.13.1 Location of Strain Measurements, Segment 13

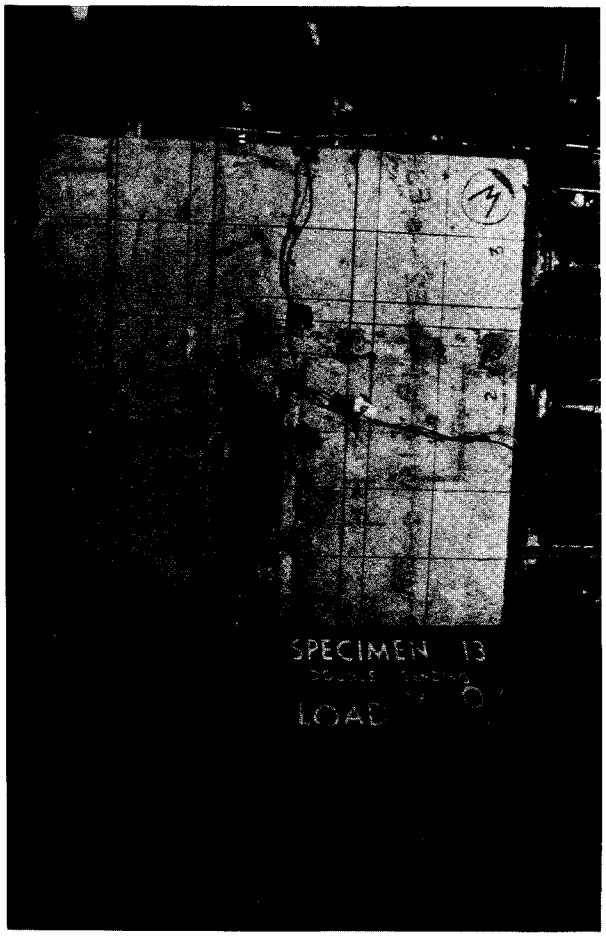

(a) Face A Before Loading

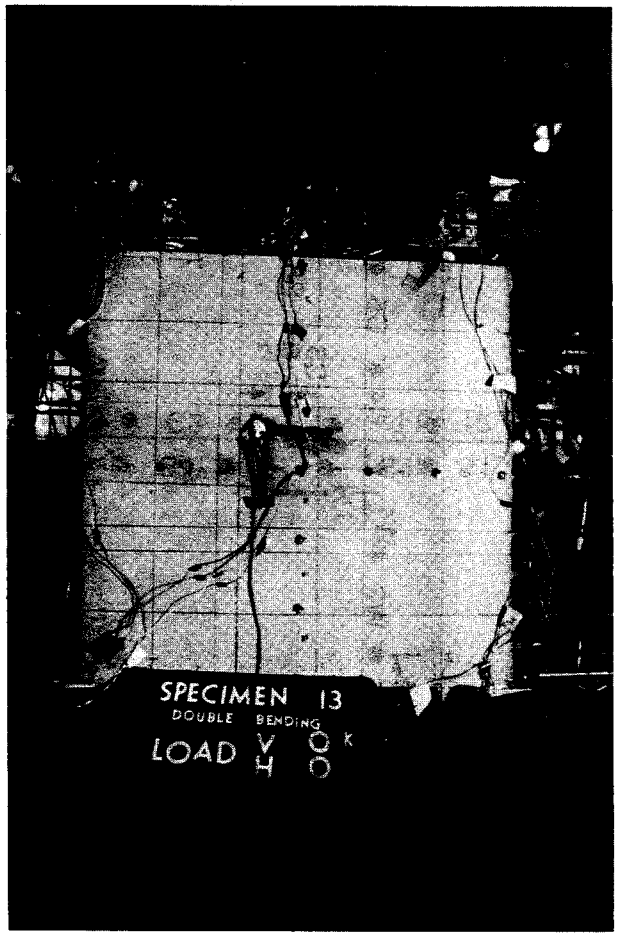

(b) Face B Before Loading

Figure 6.13.2 Development of Cracking in Segment 13

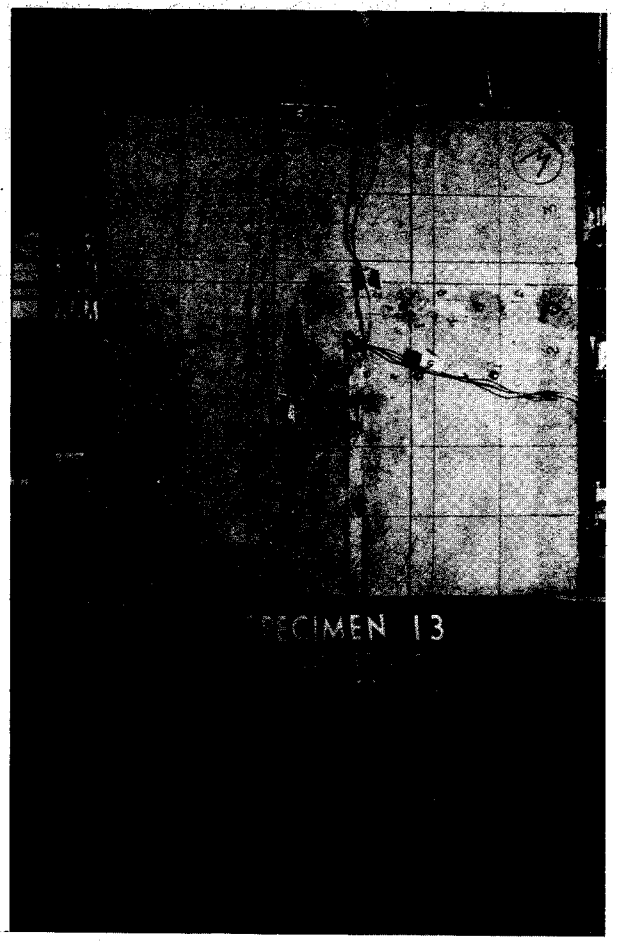

(c) Face A at Onset of Horizontal Cracking

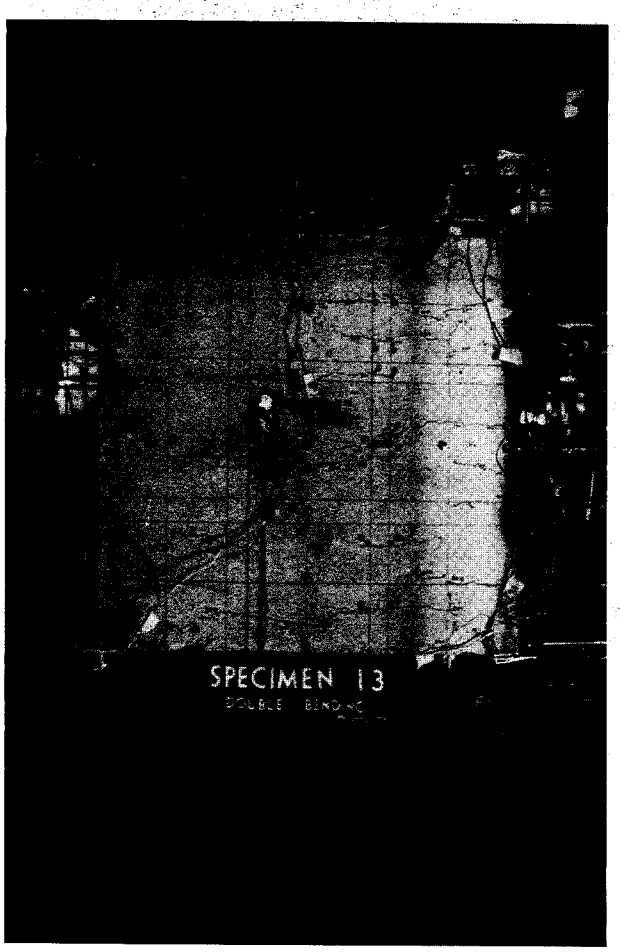

(d) Face B at Onset of Horizontal Cracking

Figure 6.13.2 Development of Cracking in Segment 13

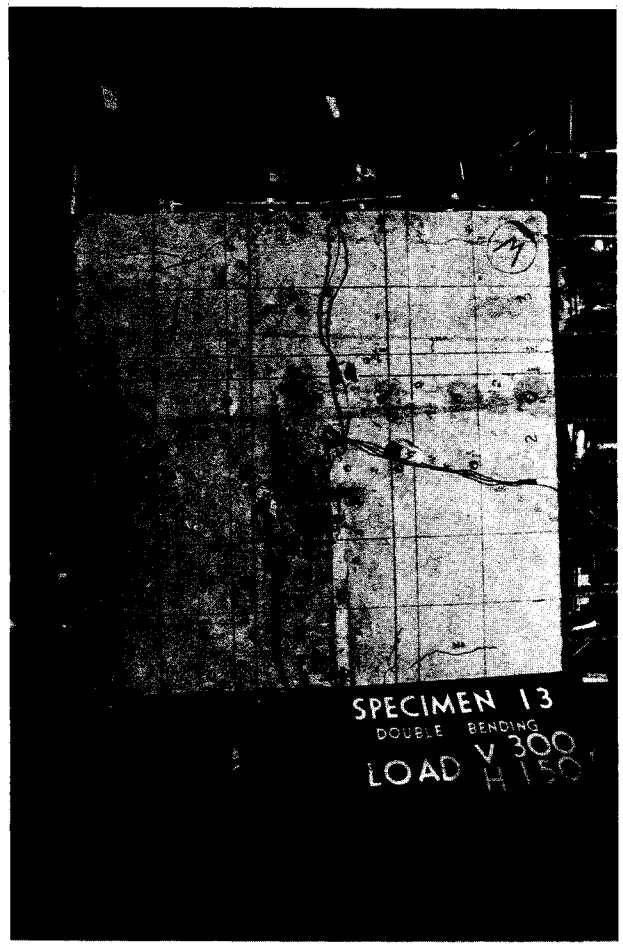

(e) Face A at Onset of Vertical Cracking

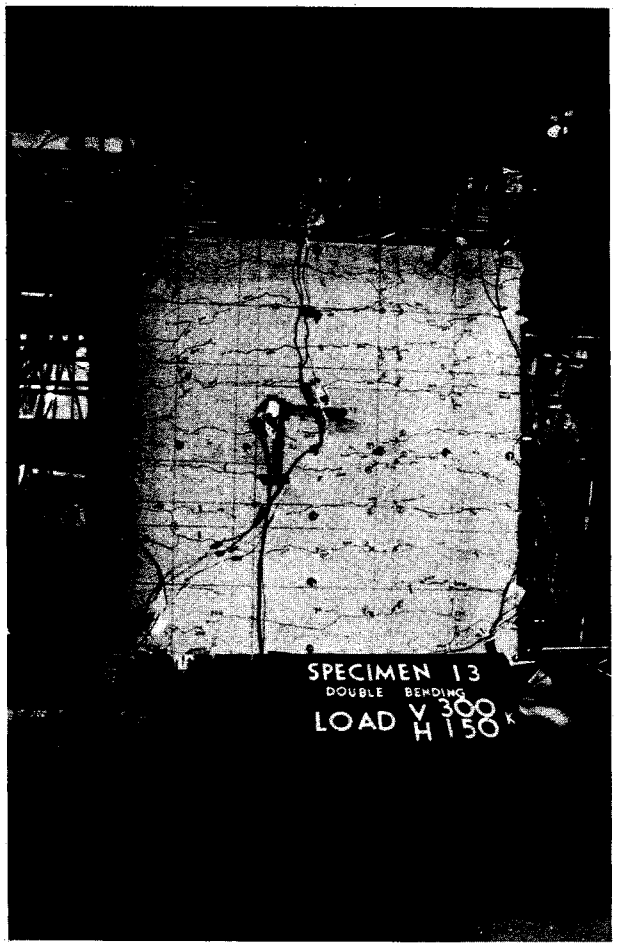

(f) Face B at Onset of Vertical Cracking

Figure 6.13.2 Development of Cracking in Segment 13

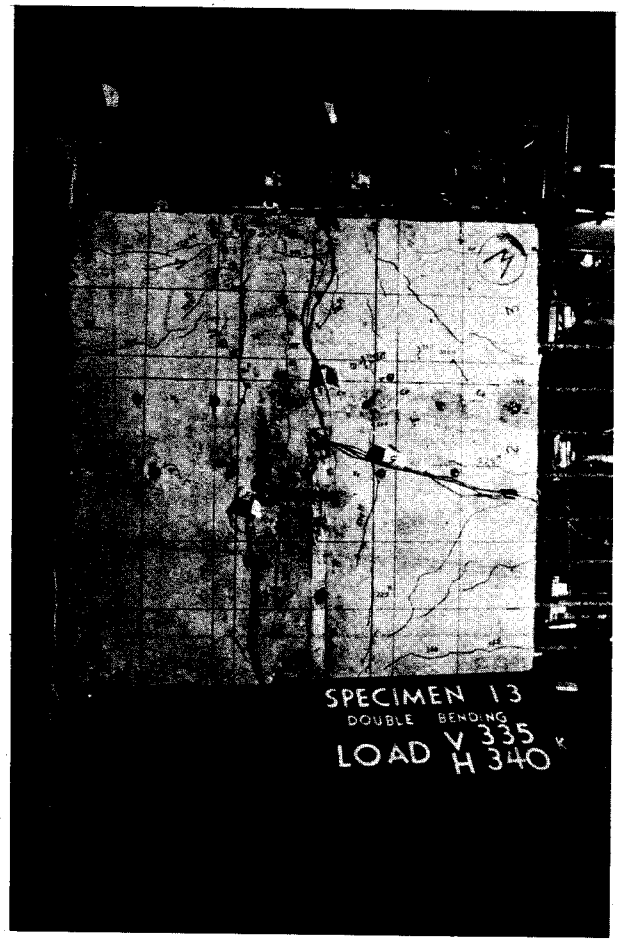

(g) Face A at End of Test

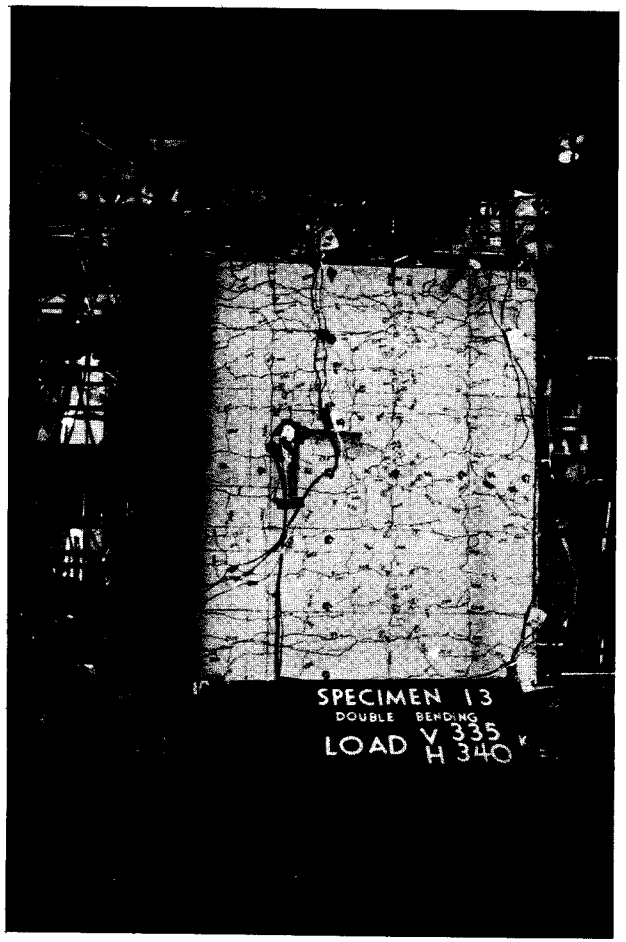

(h) Face B at End of Test

Figure 6.13.2 Development of Cracking in Segment 13

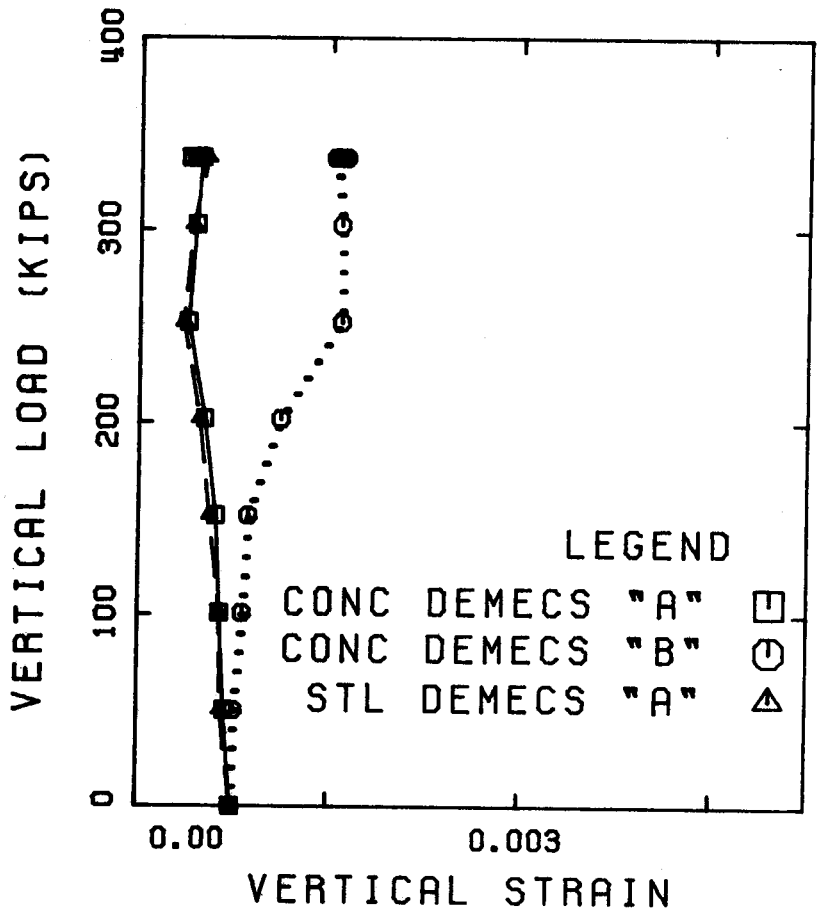

(a) Vertical Direction

Figure 6.13.3 Load-Average Strain Curves, Segment 13

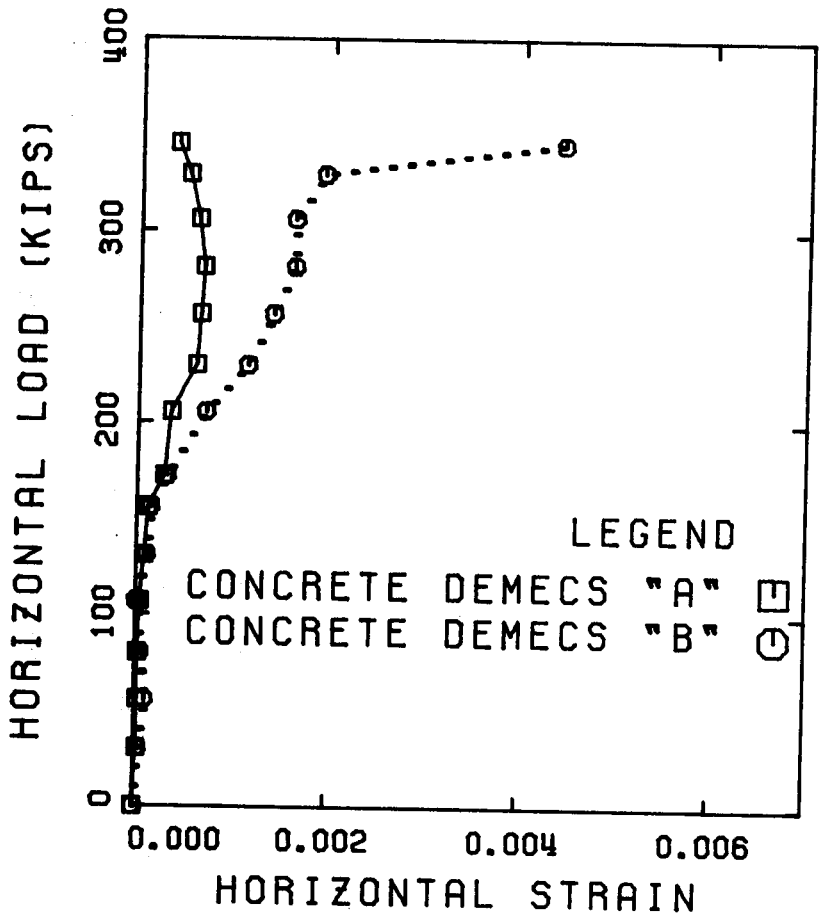

(b) Horizontal Direction

Figure 6.13.3 Load-Average Strain Curves, Segment 13

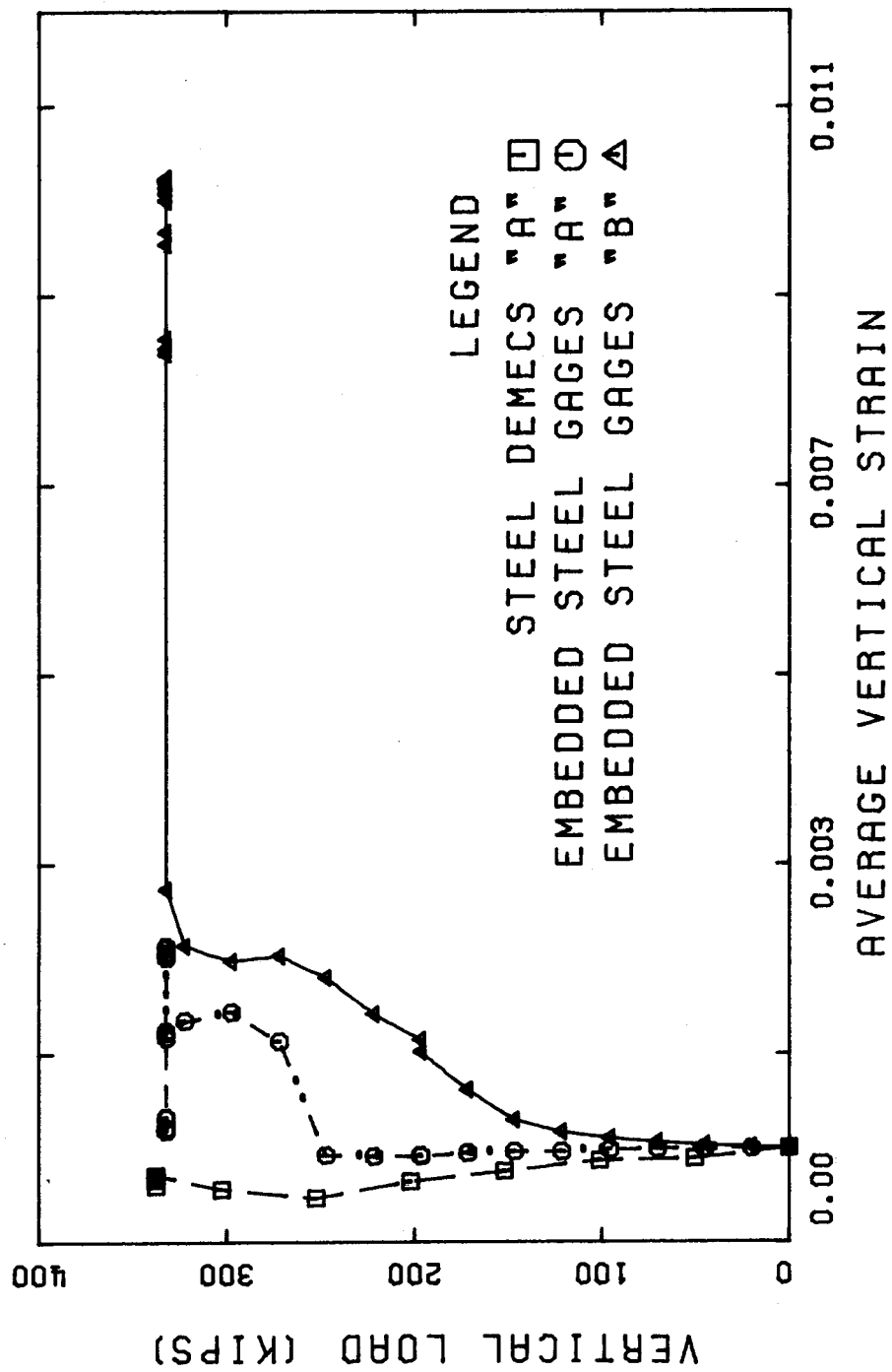

(a) Vertical Direction

Figure 6.13.4 Load-Average Steel Strain Curves, Segment 13

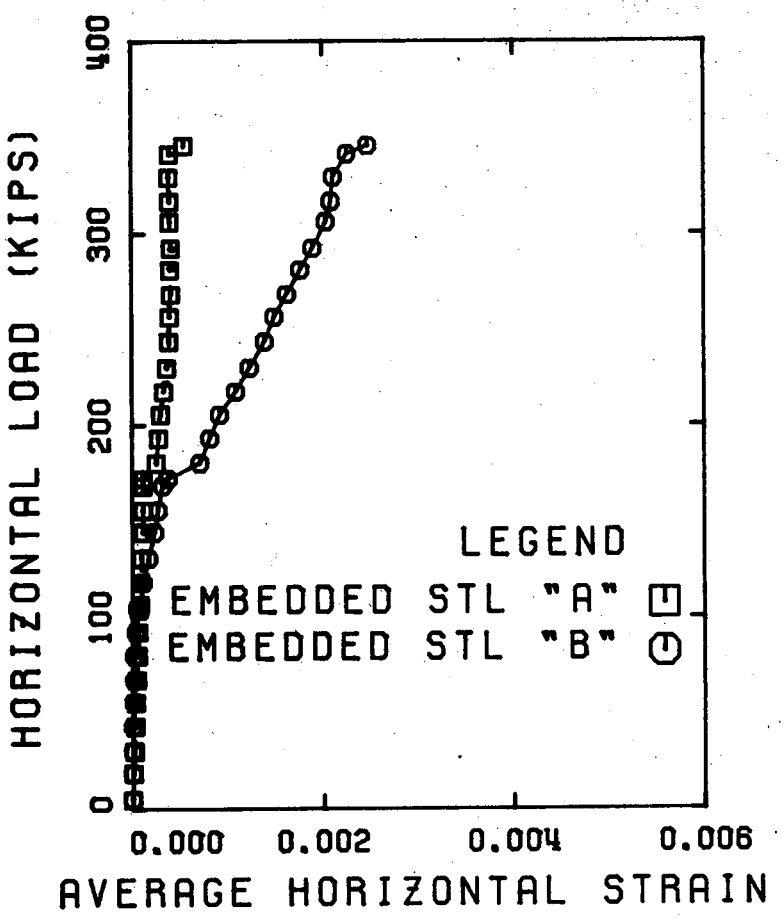

(b) Horizontal Direction

Figure 6.13.4 Load-Average Steel Strain Curves, Segment 13

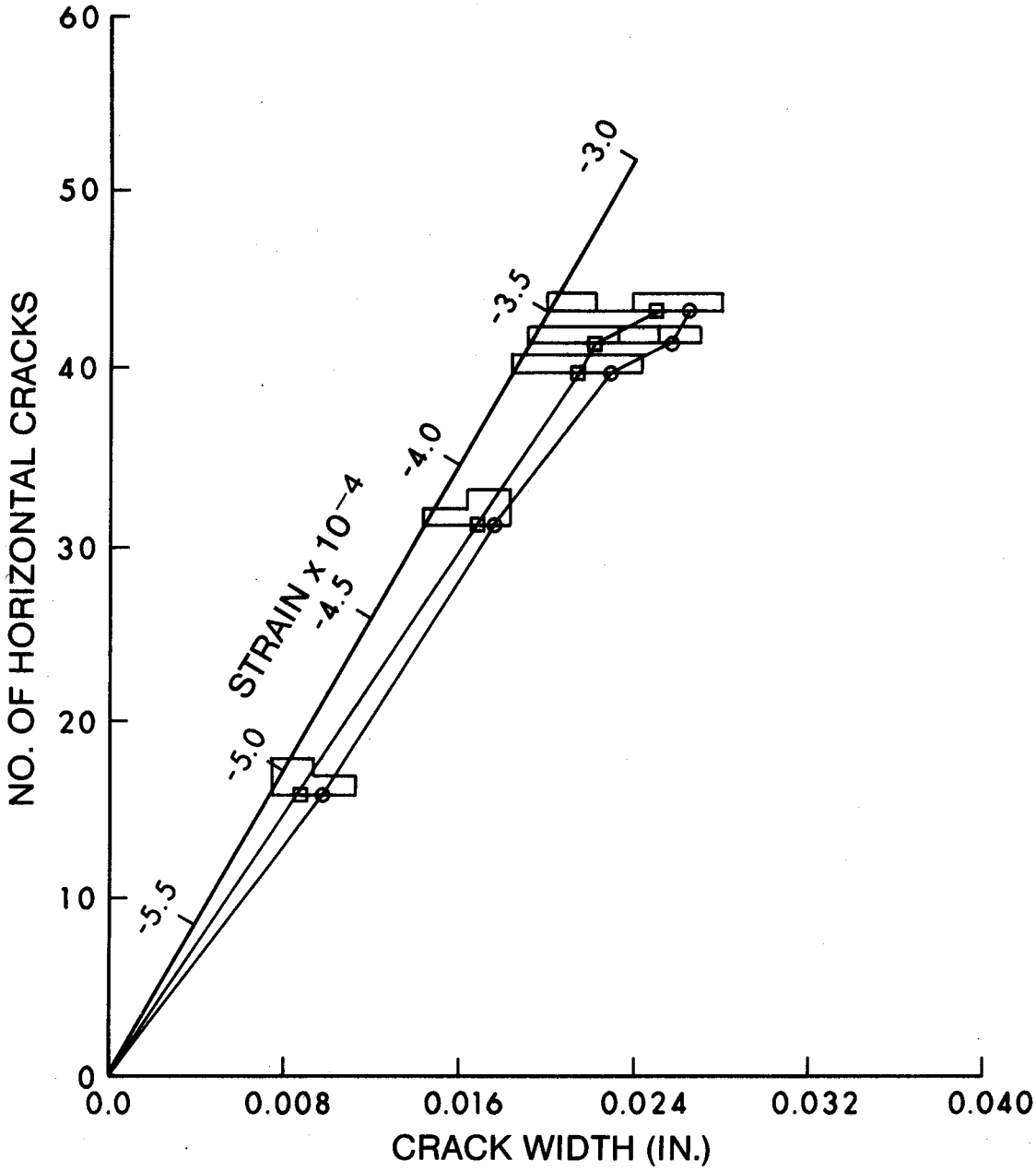

(a) Horizontal Cracks

Figure 6.13.5 Distribution of Crack Widths, Segment 13, Face A

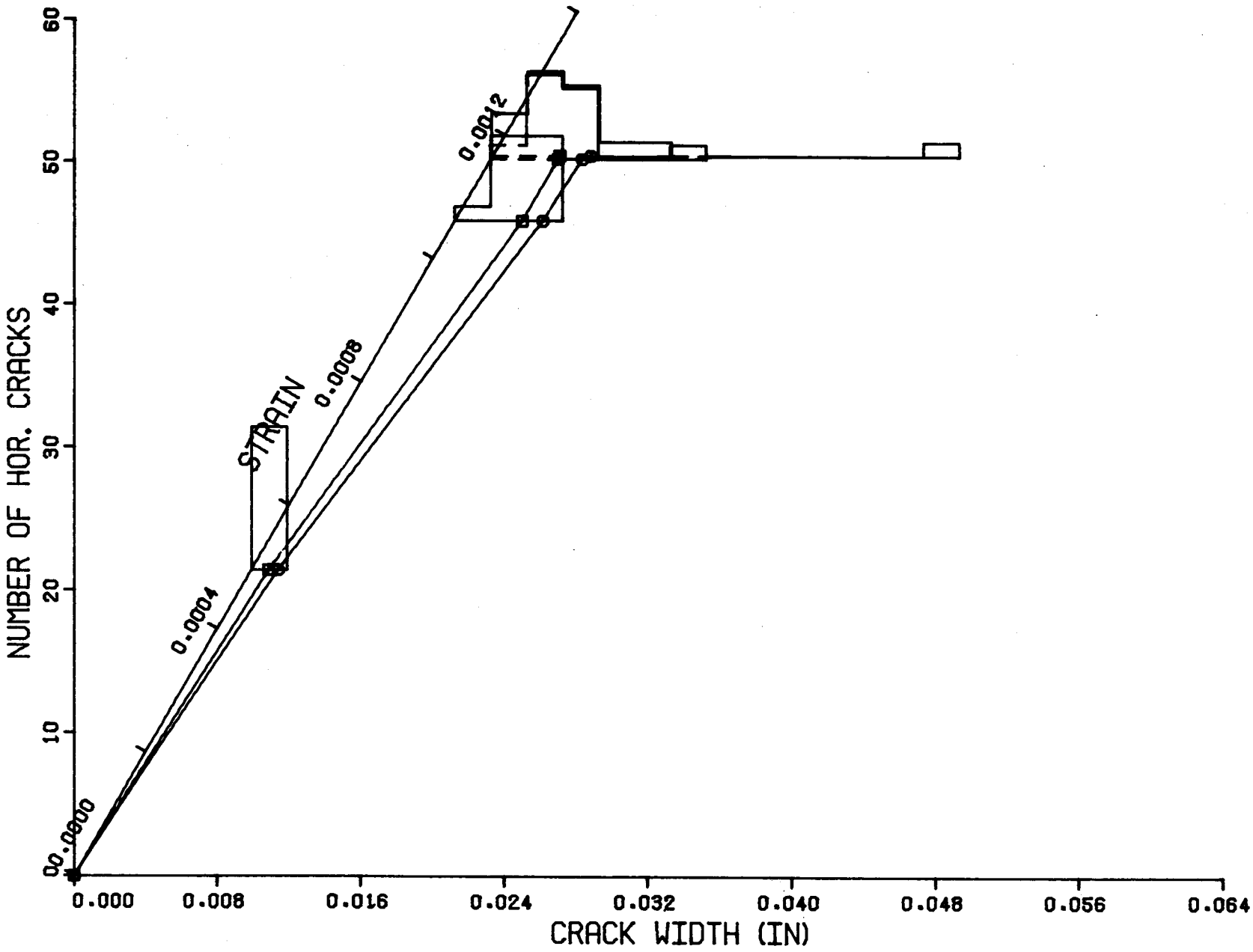

(b) Horizontal Cracks

Figure 6.13.5 Distribution of Crack Widths, Segment 13, Face B

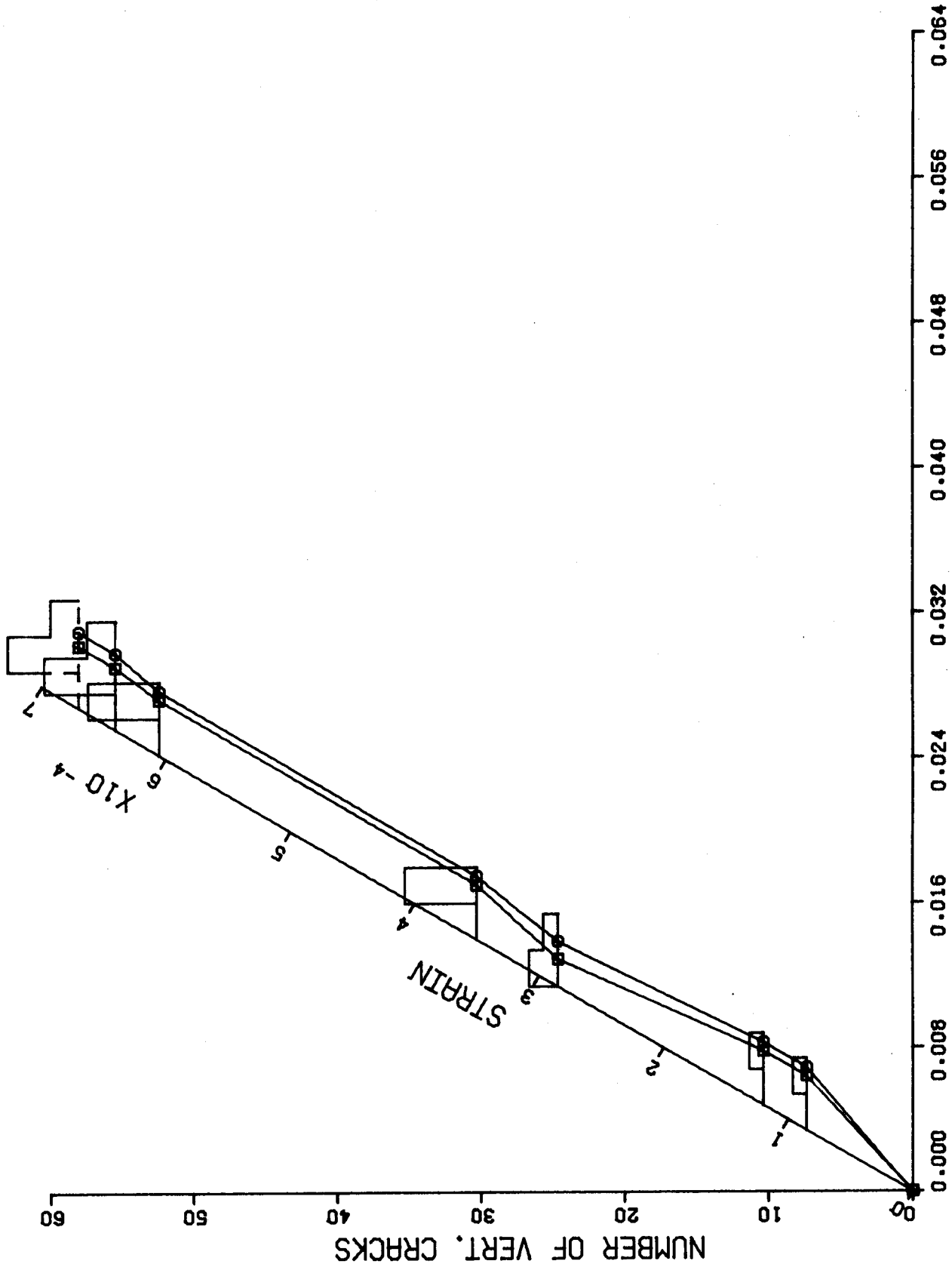

(c) Vertical Cracks

Figure 6.13.5 Distribution of Crack Widths, Segment 13, Face A

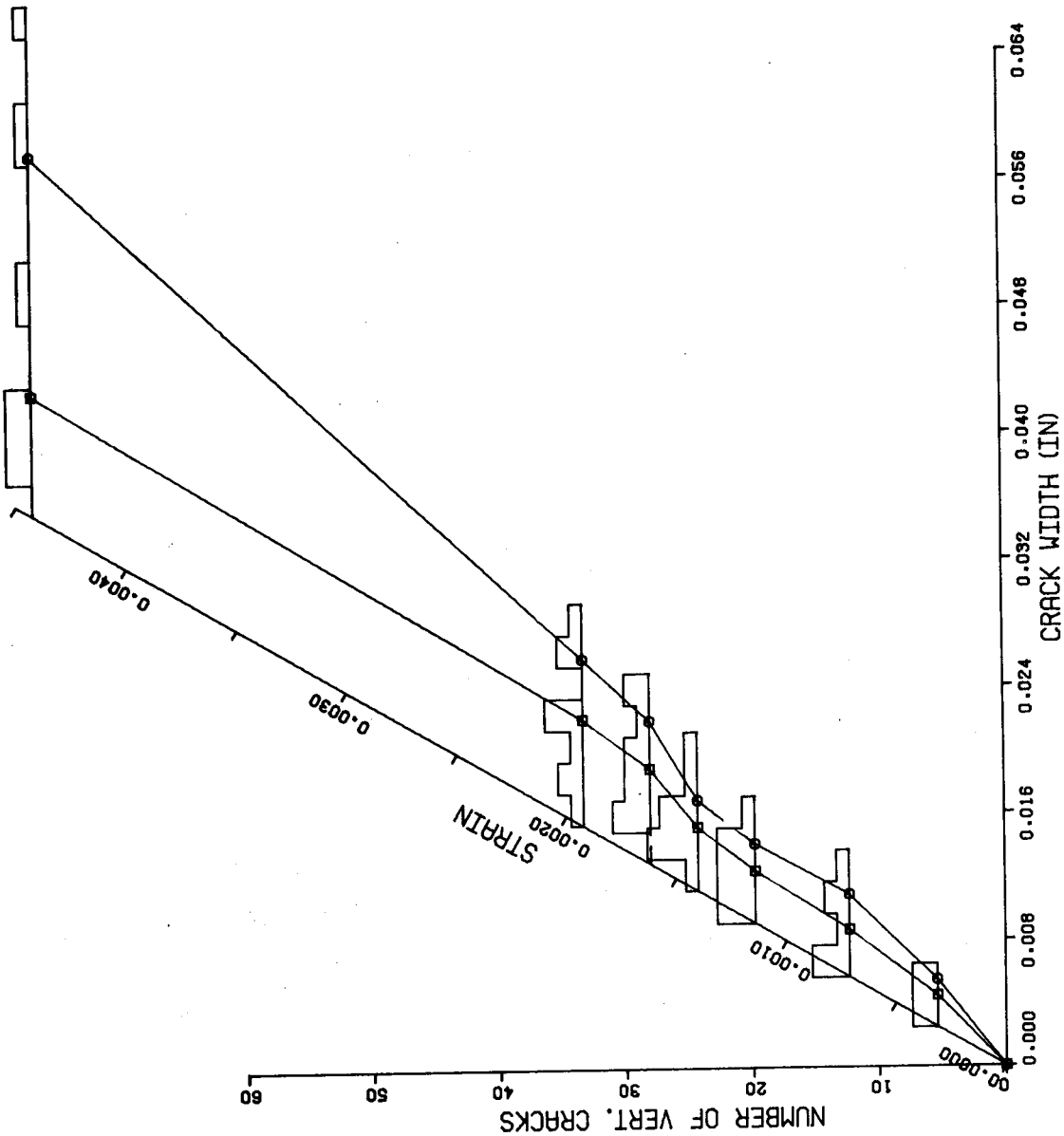

(d) Vertical Cracks

Figure 6.13.5 Distribution of Crack Widths, Segment 13, Face B

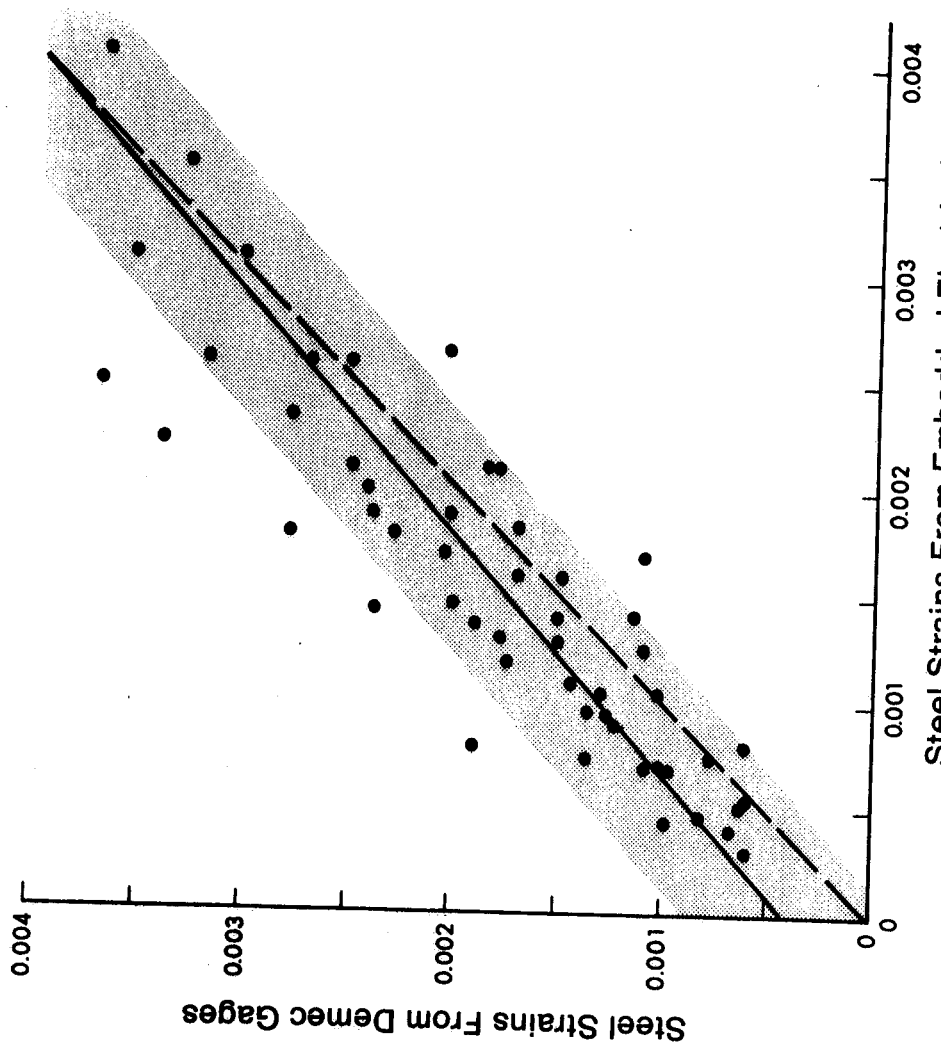

Figure 7.1 Relationship between Steel Strains from Demec Gages and Embedded Gages

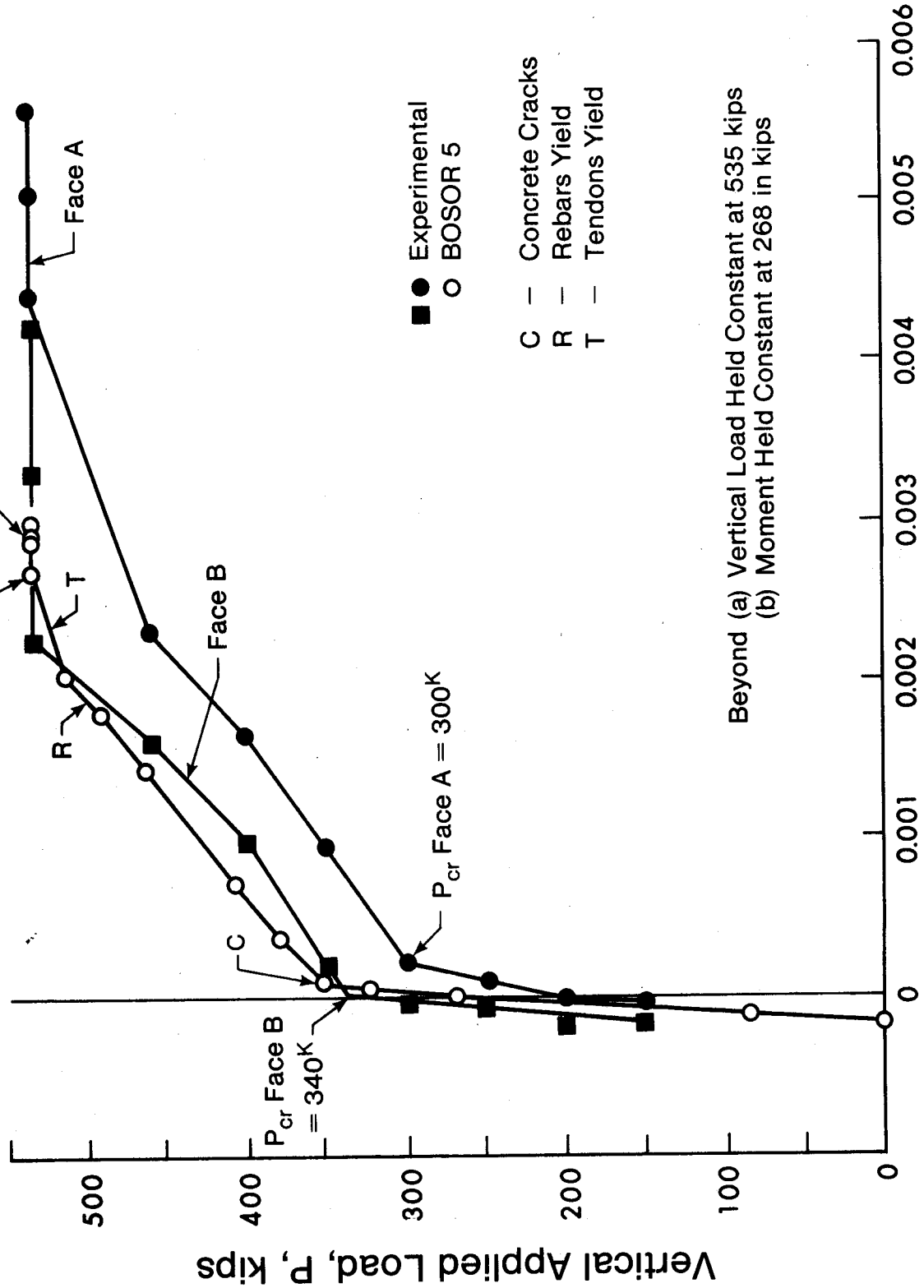

Figure 7.2 Comparison of Measured and Predicted Load Strain Response, Segment 12

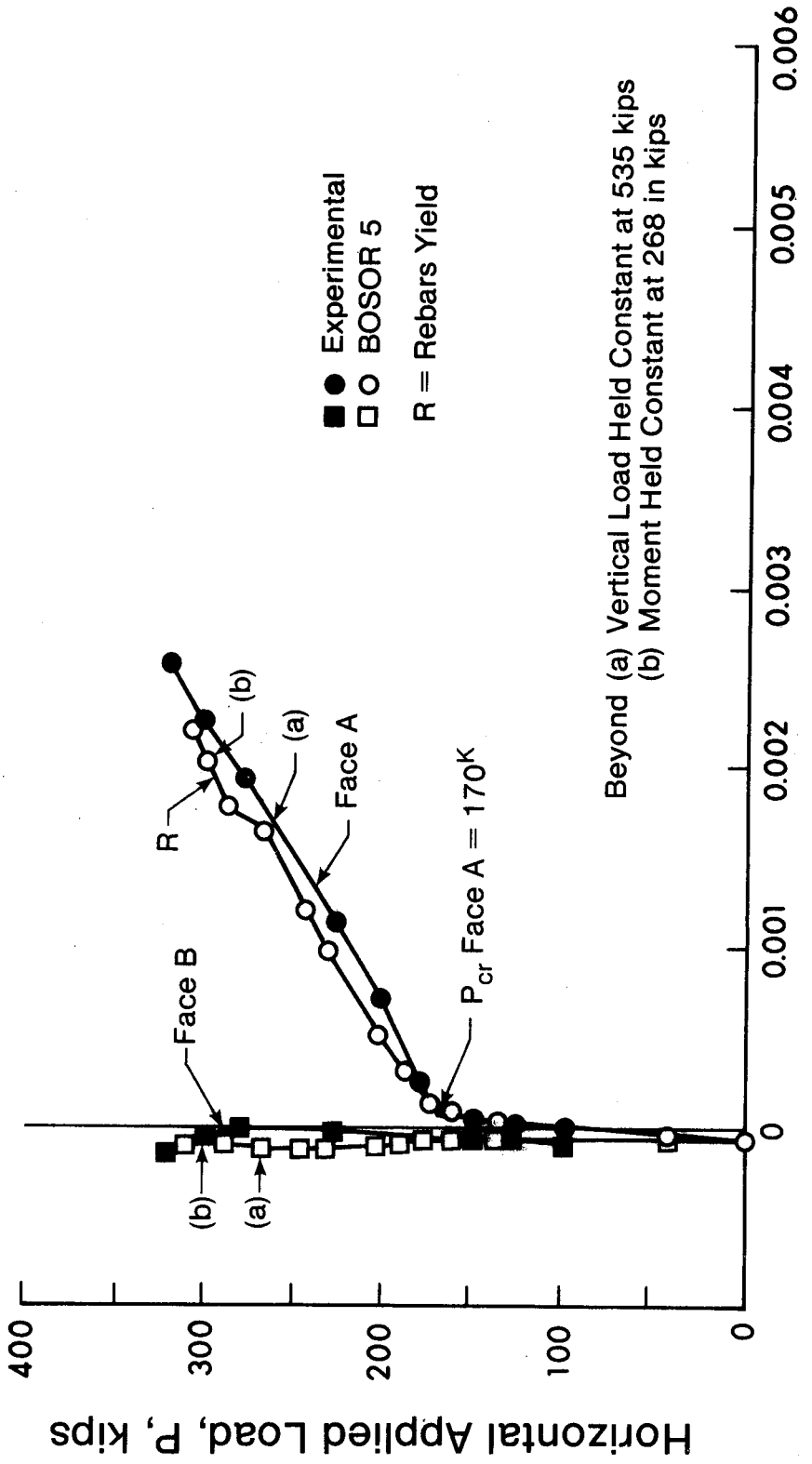

Figure 7.3 Comparison of Measured and Predicted Load Strain Response, Segment 12